The role of satellite cells in skeletal muscle plasticity

Thesis by

Louise Richardson

Submitted in accordance with the requirements for the degree of Doctor of Philosophy

The University of Leeds
Faculty of Biological Sciences
School of Molecular & Cellular Biology

September 2021

The candidate confirms that the work submitted is his/her own and that appropriate credit has been given where reference has been made to the work of others.

Acknowledgements

First and foremost, I would like to thank my supervisors, Michelle Peckham and Stuart Egginton, for their continued support and enthusiasm throughout the project. I am also grateful to the members of the Peckham lab, both current and those who have passed through, for the support and advice shared with me when I needed it most. I am of course indebted to the Biotechnology and Biological Sciences Research Council and the University of Leeds, for facilitating my research journey.

I would also like to extend thanks to Colin Johnson and Dapeng Wang, and the Next Generation Sequencing facilities at St. James's University Hospital, for collaborating with me on my RNAseq investigation. And to those belonging to the labs of Stuart Egginton and Anne-Gaelle Borycki, for helping me refine my surgical and fibre isolation techniques at the beginning of the project.

Finally, I would like to give special thanks to my little family: my partner Yasmin and our two mischievous cats, Bjorn and Salim. Thank you for keeping me sane and filled to the brim with nutritious food, escapism, perspective, and love.

Abstract

The regenerative capabilities of skeletal muscle allow it to grow in response to external stimulus such as load or injury. When stimulus is applied, muscle stem cells (satellite cells) proliferate and differentiate to build on existing muscle, causing hypertrophy. Many proteins are involved in facilitating this response and the role of MEGF10, a transmembrane protein involved in muscle myopathy, is still poorly understood.

An *in vivo* mouse overload model and complimentary *in vitro* culture experiments were used to better understand the role of satellite cells and MEGF10 in muscle hypertrophy. Experiments on control mice showed that after 10-days overload, skeletal muscle fibres showed optimum levels of muscle hypertrophy, myonuclear accretion, and expression of the myogenic transcription factors Pax7, MyoD and myogenin. Overloading mice that were either heterozygous ($Megf10^{+/-}$) or homozygous ($Megf10^{-/-}$) for a MEGF10 mutation demonstrated that loss of MEGF10 significantly impaired the hypertrophy process, and resulted in impairments to the diaphragm that may affect respiration. A separate analysis of Pax3-expressing C1F myoblasts demonstrated that these cells undergo the same myogenic expression pattern as Pax7-expressing C2C12 myoblasts, and undergo enhanced fusion and differentiation on soft polydimethylsiloxane (PDMS) surfaces of a stiffness similar to muscle *in vivo.*

In conclusion, this study has provided novel data regarding the importance of MEGF10 in hypertrophy, and highlighted its role in the expansion of muscle satellite cells that will then go on to fuse and differentiate. Additionally, a previously unreported effect on the diaphragm has been found that may serve in validating this MEGF10 knockout mouse as a translatable model of the MEGF10 myopathy, early onset myopathy, areflexia, respiratory distress and dysphagia (EMARDD). The importance of cell culture surface stiffness has also been highlighted by this study, as well as the importance of using *in vitro* systems to support *in vivo* analyses in muscle research.

Table of contents

List of Abbreviations

Avg	Average
.AVI	Audio video interleave
BdrU	Bromodeoxyuridine
bp	Base pair
BSA	Bovine serum albumin
CEE	Chick embryo extract
cDNA	Complentary DNA
CL	Contralateral
CSA	Cross-sectional area
°C	Degrees Celcius
DAPI	4’,6’- diamidino-2-phenylindole
DEG	Differentially expressed gene
DMD	Duchenne Muscular Dystrophy
DMEM	Dulbecco’s Modified Eagles Medium
DNA	Deoxyribonucleic Acid
ECM	Extracellular matrix
EDL	Extensor digitorum longus
EGF	Epidermal growth factor
EMARDD	Early-onset Myopathy, Areflexia, Respiratory Distress and Dysphagia
Emi	Emilin
FACS	Fluorescence-activated cell sorting
FBS	Fetal bovine serum
FITC	Fluorescein Isothiocyanate

FOV	Field of view
xg	Acceleration of gravity
ɣIFN	Gamma interferon
GC	Guanine-cytosine
GPa	Gigapascals
HBSS	Hank's Balanced Salt Solution
HC	Haematopoietic cells
HEPES	4-(2-Hydroxyethyl)piperazine-1-ethanesulfonic acid
Hrs	Hour(s)
HS	Horse serum
HTML	Hypertext Markup Language
ICC	Immunocytochemistry
ICD	Intracellular domain
KPa	Kilopascals
Lac	Lactose
LN2	Liquid nitrogen
Mdx	Muscular dystrophy X-linked
MEGF	Multiple Epidermal Growth Factor-like Domains Protein
min	Minute(s)
ml	Millilitre
mm	Millimetre
mM	Millimolar
µl	Microlitre
µm	Micrometre

µM	Micromolar
mRNA	Messenger RNA
NNA	Nearest neighbour analysis
No.	Number
OCT	Optimum cutting temperature
OL	Overloaded
Pax	Paired Box
PBS	Phosphate buffered saline
PBST	Triton X-100 in PBS
PCA	Principal component analysis
PCR	Polymerase chain reaction
PDMS	Polydimethylsiloxane
PE	R-phycoerythrin
PFA	Paraformaldehyde
pH	Potential hydrogen. Decimal logarithm of hydrogen ion
P/S	Penicillin Streptomycin
RNA	Ribonucleic acid
RPKM	Reads per Kilobase of transcript per Million
SCs	Satellite cells
S.D	Standard deviation
S.E.M	Standard error of the mean
Seq	Sequencing
TA	Tibialis anterior
3D	Three dimensional
TM	Transmembrane

TF	Transcription factor
TRITC	Tetramethylrhodamine B isothiocyanate
U	Units
UV	Ultraviolet
WT	Wild type

1 Introduction

1.1 Skeletal muscle regeneration

1.1.1 Skeletal muscle as a plastic organ

Skeletal muscle is an invaluable tissue of the body, comprising ~40% total body weight and facilitating a variety of bodily functions including movement, breathing and swallowing (Frontera et al., 2015). The contraction of skeletal muscle is largely mediated by voluntary stimulus, with signals from the brain initiating contraction at the neuromuscular junction (NMJ), which describes the space between the motorneurone and a muscle fibre. This space, whereby the diffusion of neurotransmitter occurs, is known as a synapse (Ferraro et al., 2012). Briefly, following signals from the brain actioning movement, an action potential propagates down a nerve axon, and when this action potential reaches the NMJ, the neurotransmitter acetylcholine (Ach) is released into the synapse. This Ach then travels across the synapse to reach nicotinic receptors on the skeletal muscle fibre membrane, known as the sarcolemma. On binding, the nicotinic receptors channels open to allow the entry of sodium ions (Na^+) into the cell. Entry and subsequent accumulation of Na^+ ions into the skeletal muscle cell leads to an increase in resting potential of the cell from around -95mV to -50mV, and when this occurs it triggers an action potential that then spreads through the muscle fibre. The action potential spreads across the muscle cell sarcolemma and interacts with a transverse tubule (T-tubule) system that allows the action potential to reach deep into the fibre. These are invaginations of the skeletal muscle plasma membrane, that maintain the store of calcium ions (Ca^{2+}) within the sarcoplasmic reticulum of skeletal muscle cells (Flucher et al., 1993). These calcium stores are tightly controlled by membrane depolarization, thus, when action potential reaches the sarcoplasmic reticulum, Ca^{2+} ions are expelled. The ions diffuse into thin, contractile rod-like structures

within muscle fibres known as myofibrils, causing a cascade that results in the shortening of small contractile units called sarcomeres, and subsequently contraction of the whole muscle tissue. This sequence of events, whereby an action potential in the sarcolemma facilitates the contraction of skeletal muscle, is known as excitation-contraction coupling. To turn off contraction and relax the muscle, Ca^{2+} ions are pumped back into the sarcoplasmic reticulum (Rebbeck et al., 2014).

Skeletal muscle is a plastic organ capable of regeneration. Each skeletal muscle in the body consists of hundreds of multinucleated muscle fibres, also known as myofibres. Each nucleus is responsible for the local environment of ~20-40μm^3, and accretion of these nuclei occurs in conjunction with growth and regeneration of the skeletal muscle (Ato and Ogasawara, 2021; Prasad and Millay, 2021). Satellite cells, quiescent muscle 'stem' cells, are associated with each muscle fibre and lie between the muscle cell membrane and the basal lamina. They provide a source of mononucleated myoblasts that can fuse with the existing muscle fibre. As muscle fibres lengthen during periods of growth from birth to adulthood, myoblasts fuse into existing muscle fibres, to maintain this relationship (Cossu and Biressi, 2005). Load bearing and resistance exercise induces muscle hypertrophy, a process which can include adding additional proteins to increase the number of myofibrils, combined with myoblast fusion (Konopka and Harber, 2014). The exact mechanisms that skeletal muscle fibres use to sense external stimuli and which subsequently drive the coordinated increase in surface area of the sarcolemma, cytoplasmic volume, number of nuclei and number of new fibres is still unclear. Each of these are integral to hypertrophy and the process is likely to involve satellite cell activation (Attwaters and Hughes, 2021). Skeletal muscle damage and disease activates satellite cells, resulting in new myoblasts to repair muscle (Shultz, 1989). Understanding the activation and contribution of satellite cells to muscle growth and repair is an area of active research.

Formation of new muscle fibres by myoblasts can be investigated using a tissue culture method, a popular approach to understanding this process. Animal models can

be used to determine how satellite cells are activated and contribute to the growth and repair of muscle *in vivo*. In the work reported here, I have used both approaches to better understand muscle fibre formation. My aim was to better understand muscle differentiation using cultured cells, and to better understand the contribution of satellite cells to muscle hypertrophy and the role of MEGF10 (multiple EGF like domains 10, known to cause skeletal muscle disease), using an animal model.

1.1.2 Myogenesis during development

Myogenesis is the formation of skeletal muscle tissue, which occurs at embryonic, neonatal and adult stages of life. It is characterised by rapid proliferation of skeletal muscle cell precursors (myoblasts), followed by activation of muscle-specific genes, which ultimately leads to the development of new contractile muscle fibres. These new muscle fibres build upon the existing skeletal muscle during ontogenetic growth allowing the overall composition, which is roughly 40% of total human body weight, to be maintained (Ato and Ogasawara, 2021).

Developmentally, myogenesis is categorised into primary and secondary phases. Primary (embryonic) myogenesis describes the process in which myoblasts undergo proliferation, and then exit the cell cycle in order to fuse together into myotubes. Secondary (fetal) myogenesis follows, and refers to the process in which several secondary myotubes form, building upon the surface of the primary myotubes that were formed in utero (Buckingham et al., 2003). At the neonatal stage, adult muscle fibres form and a distinct niche of muscle stem cells, known as satellite cells start to be established, residing underneath the newly formed basal lamina.

In the developing embryo, myogenesis is initiated in the somites, which are blocks of mesoderm situated either side of the neural tube, a primitive structure that eventually forms the central nervous system (Chal and Pouquie, 2017). Cells proliferate here, and migrate outwards to the structures that will eventually become the limbs (limb

buds), and at these sites, cells differentiate to form the skeletal muscle (Buckingham, 1992) (Fig. 1A). Expression of transcription factors throughout this process of proliferation and migration is key to development of the musculature (Fig. 1B). Within the somite, the first protein to trigger myogenesis is myogenic regulatory factor 5 (Myf5). Myf5 is a transcription factor belonging to a family of skeletal muscle specific proteins known as myogenic regulatory factors (Ott et al., 1991). Expression of Myf5 results in the downregulation of paired box 3 (Pax3), which is part of a wider family of pax genes that all have a critical role in the development of organs and tissues (Williams and Ordahl, 1994). Pax3 is necessary for myogenesis in that it specifies cells to adopt a myogenic fate upstream of Myf5*,* facilitates separation of the somites and thus proper body patterning, and forms the dermomyotome, a primitive combination of the parts of the developing embryo that will go on to become the skin and the muscle (Tajbakhsh et al., 1997; Tajbakhsh and Buckingham, 2000).

Members of the myocyte enhancer factor-2 (Mef2) family are another group of transcription factors with a role in the regulation of myogenic differentiation during embryonic development (Taylor and Hughes, 2017). Mef2d promotes the expression of myogenic genes downstream of key myogenic transcription factors, myoblast determination protein 1 (MyoD) and myogenin*,* by recruiting proteins that will then interact with promoters bound to MyoD, thus expediting the pro-myogenic activity of MyoD (Aziz et al., 2010). Mef2 family proteins are Ca^{2+} sensitive, and are activated by calcineurin, alongside many other Ca^{2+} signalling molecules (Huang et al., 2019).

Another important signalling pathway in embryonic myogenesis is Notch*.* While this pathway is also important in postnatal myogenesis, in the embryo skeletal muscle stem cells are maintained by the Notch ligand, Delta-like1 (Dll1), which is expressed by muscle fibres, and interacts with Notch receptors (Notch-1, Notch-2 and Notch-3) present in the satellite cell membrane. This interaction maintains the developing muscle progenitor cells in a state of proliferation, allowing adequate muscle cells to be populated for the formation of the demomyotome (Mourikis and Tajbakhsh, 2014).

Following the upregulation of Myf5 and the simultaneous downregulation of Pax3, Paired box 7 (Pax7) becomes activated. Pax7 is similar in function to Pax3, except it is necessary for the proliferation of foetal myoblasts, as opposed to embryonic. In addition, Pax7 has recently been found to be crucial in driving hypertrophy during pre-pubertal stages of development. Recent work has shown accretion of $Pax7^{+}$ nuclei surrounding myofibres in pre-pubertal mice (Bachman et al., 2018). Myoblast determination protein 1 (MyoD) is a basic helix-loop-helix muscle-specific transcription factor that causes some cells of the dermomyotome to commit to becoming skeletal muscle cells. As levels of MyoD rise, more cells within the dermomyotome exit the cell cycle, develop into immature skeletal muscle cells (myoblasts), and go on to fuse together forming myotubes (Buckingham, 2006). The next myogenic protein to be expressed in these developing cells is myogenin, which is another basic helix-loop-helix transcription factor that promotes maturation of the nascent myotubes through the process of cell differentiation. The final myogenic protein to be expressed in these cells is myogenic regulatory factor 4 (MRF4), which is expressed transiently during development of the somites, and also in the final stages of myogenic cell differentiation. The specific role of MRF4 is unclear, as MRF4 null mice are fully viable, which suggests a certain level of redundancy with the other members of the myogenic regulatory factor family during development (Hinitis et al., 2007). As myotubes begin to develop, myogenin is expressed, followed by myosin during development of the sarcomere (Agarwal et al., 2020).

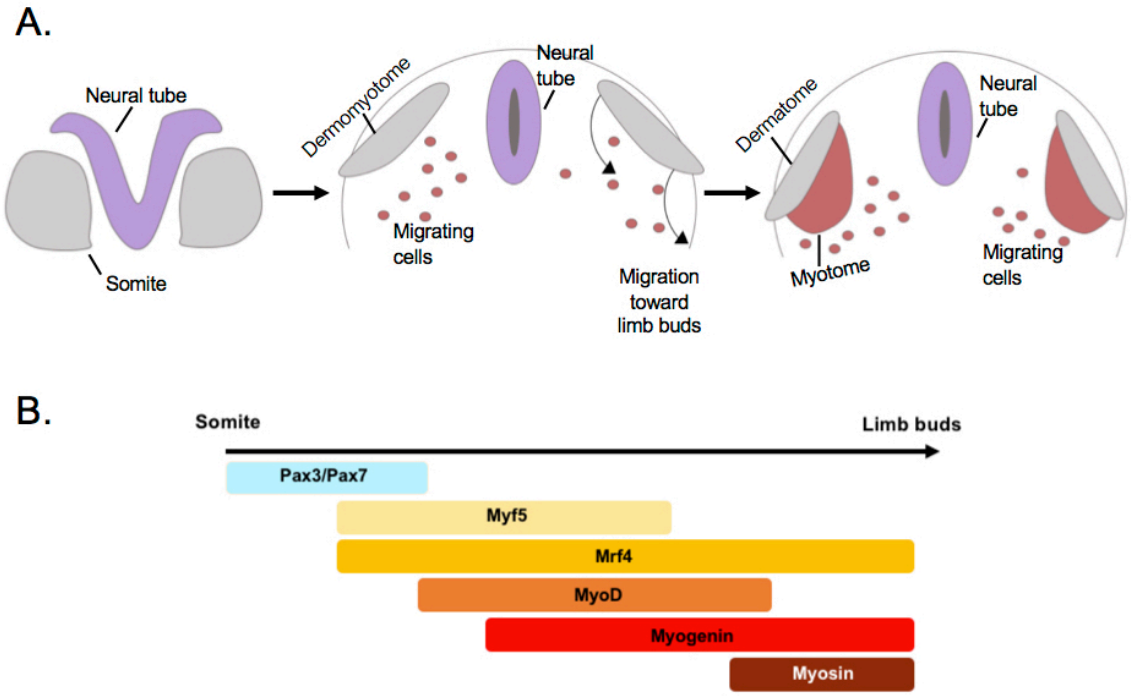

Figure 1. Myogenesis in development. A. Schematic showing the developing somite. Myogenic progenitor cells migrate from the somite, which later becomes the dermomyotome. Cells migrate towards the limb buds for development into skeletal muscle, and the dermomyotome separates into the dermatome and myotome. Adapted from *Buckingham, 1992.* **B.** Timeline of myogenic protein expression from the somite stage to muscle development in the limb buds. The length of coloured panels represents the relative duration of expression.

1.1.3 Myogenesis in adults

In the adult, myogenesis must still take place in order to respond to external stimuli such as injury or load bearing exercise, and this response is made possible by the satellite cells (Mauro, 1961). Satellite cells are a heterogenous stem cell niche that are present from birth, and reside between the basal lamina and sarcolemma of muscle fibres. Normally, they exist in a quiescent state. When activated, they can either produce daughter cells that will remain under the basal lamina and replenish the satellite cell niche, or daughter cells that will commit to the myogenic programme and grow into mature myotubes, building on existing muscle tissue (Kuang et al., 2008). Satellite cells provide a cellular reserve which the body can draw upon on an *ad-hoc* basis when muscle regeneration is necessary. The response of the satellite cells is specific, because other cells within the microenvironment such as muscle fibres, motor neurones, vascular and inflammatory cells offer protection to the satellite cells from other stimuli that do not directly necessitate repair of the skeletal muscle (Siegel et al., 2009).

There are multiple steps involved in myogenesis, each facilitated by key signalling pathways (Fig. 2). Activation of satellite cells allows them to proliferate to produce nascent myotubes, or to self-renew and replenish the satellite cell niche. The pathways that act during this time include Notch, Wnt and MAPK, and these continue to send signals that facilitate the proliferation of satellite cells after activation (Fu et al., 2015). As well as driving proliferation, Wnt signalling has been observed to restrain the process, ultimately preventing unregulated proliferation of satellite cells and myoblasts (Yin et al., 2013). Signalling pathways involving growth factors such as fibroblast growth factor (FGF), insulin-like growth factor (IGF) and hepatocyte growth factor (HGF) stimulate the activation of satellite cells by the activation and upregulation of Myf5 (Perez-Ruiz et al., 2007). These growth factors are present during skeletal muscle development, but their production is also stimulated by nitric oxide (NO) production after muscle injury (Wozniak and Anderson, 2007). During proliferation, there is some overlap in signalling with activation, although some new pathways come into play, such as Janus

kinase (JAK)-signal transducer and activator of transcription (STAT), bone morphogenic protein (BMP), cyclooxygenase-2 (COX-2) and nuclear factor kappa B NF-κB. JAK-STAT signalling promotes myoblast proliferation and acts as a checkpoint, preventing premature differentiation (Sun et al., 2007). BMP signalling also promotes proliferation, allowing expansion of satellite cells, before being inhibited by the inhibitor molecule Chordin, which allows myogenic daughter cells to differentiate (Fredrichs et al., 2011). Mechanical stretch of mature skeletal muscle fibres can trigger proliferation of satellite cells via the COX-2 pathway, a process that aids in regeneration of muscle in the adult (Otis et al., 2005). The fate of daughter cells following proliferation is dependent on transcription factor expression; those expressing MyoD will go on to develop into muscle cells and those lacking MyoD will return to the satellite cell niche. The NF-κB pathway is involved in both proliferation and the transition into differentiation; the canonical NF-κB acts to drive expansion and prevents precocious differentiation, however the non-canonical NF-κB pathway triggers the beginning of differentiation and promotes the fusion of myotubes (Straughn et al., 2019). MyoD and myogenin-expressing myoblasts then progress on the differentiation stage of myogenesis, whereby they move further towards becoming adult myotubes. Additional signalling pathways involved in this process include mammalian target of rapamycin (mTOR) and phosphatidylinositol-3-kinase (PI3K), which regulate differentiation through the control of IGF expression. The mTORC/PI3K pathway mediates this via a muscle-specific enhancer, and higher levels of IGF promote myogenic development (Honardoost et al., 2015). The cell-cell adhesion required for differentiation is facilitated by RhoA and p38 MAPK signalling, and this function persists in importance during fusion and myotube maturation (Lovett et al., 2006). The fusion of myoblasts is also facilitated by focal adhesion kinase signalling, which regulates the attachments of cells to one another, and to the ECM (Quach et al., 2009). The integrity and protrusion of the myoblast membrane during fusion is controlled by the cell division cycle 42 (Cdc42)/Rac pathway, which influences actin dynamics (Vasyutina et al., 2009). Additionally, the Wnt/β-Catenin pathway ensures adequate

fusion of myoblasts by promoting the expression of a renal protein nephrin, which has been found to be important in the myogenesis of all vertebrates (Suzuki et al., 2018). The maturation of myotubes is characterised by an increase in myosin heavy chain (MyHC) expression, and the formation of the muscle sarcomere. It involves signalling pathways that featured earlier in myogenesis, such as the JAK/STAT and PI3K pathways (Fu et al., 2015). Many genes are involved in the formation of the sarcomere, and the timing and level of this gene expression is controlled by the Hippo pathway, ensuring the development of new muscle fibres is tightly regulated (Kaya-Copur et al., 2021). The organisation of sarcomeric components within the maturing myotube is mediated by the small ubiquitin-like modifiers (SUMO pathway), which promotes the transcriptional activity of myogenic proteins insert fug by way of post-translational modifications (Nayak and Amrute-Nayak, 2020).

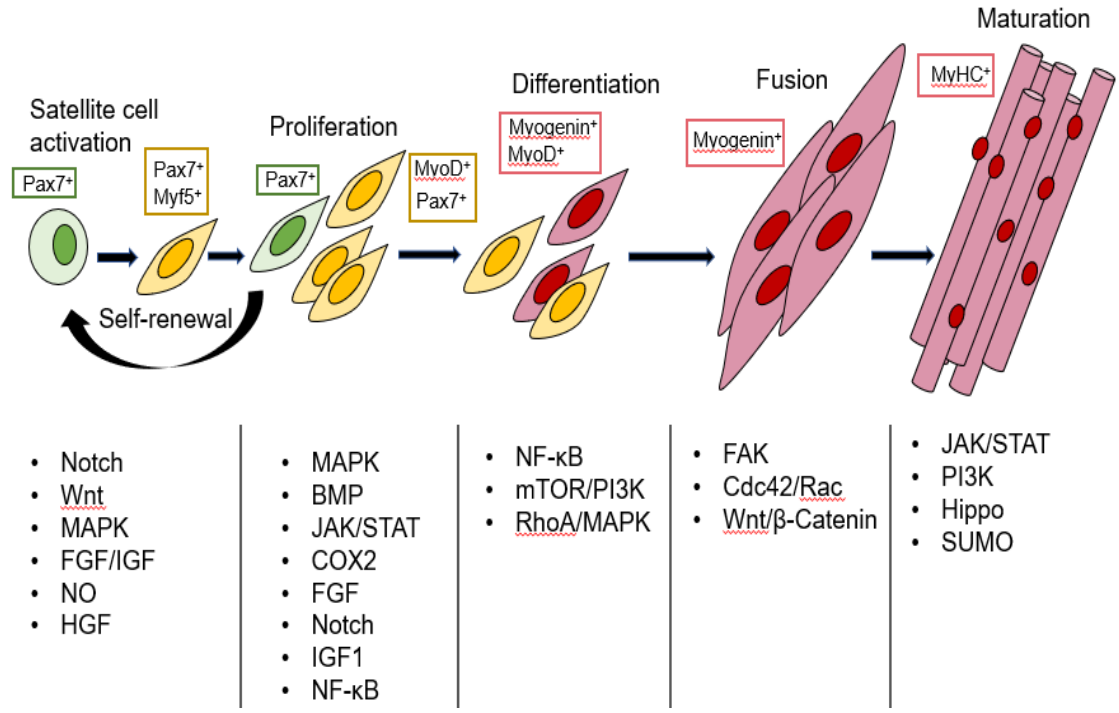

Figure 2. Series of events involved in myogenesis. Schematic of the activation and proliferation of satellite cells, followed by the subsequent myogenic specification, differentiation, fusion and maturation of myoblasts into adult myotubes. The associated transcription factors and key signalling pathways at each step are highlighted.

The molecular interactions that occur within the signalling pathways involved at each stage of myogenesis are crucial to the formation new muscle tissue during development and in response to stimulus. The Notch signalling pathway is considered to play a large part in mediating satellite cell activation, and is involved in regulating cell fate. Notch signalling also acts in adults to maintain skeletal muscle homeostasis (Mourikis and Tajbakhsh, 2014). It has also been found to promote self-renewal in response to external stimulus in the adult, through direct regulation of Pax7. Work exploring the effects of overexpressing the Notch intracellular domain (NICD) in adult satellite cells resulted in a shift in the favour of self-renewal, and decreased the amount of terminal differentiation (Wen et al., 2012). Under normal conditions, in response to stimuli such as injury, the Notch ligand Delta (released by neighbouring myoblasts and myotubes) binds to the Notch receptor, which resides in the membrane of the satellite cells. This causes the Notch intracellular domain to become cleaved and it is then incorporated into the nucleus, where it can trigger the Notch signalling cascade. This then switches on downstream genes involved in satellite cell proliferation (Ehebauer et al., 2007; Wen et al., 2012). Genes involved in myogenic commitment and subsequent differentiation are inhibited by Notch. Interaction at the receptors induces expression of a family of transcriptional repressors known as Hes-related repressor proteins (Herp) genes (Zhang et al., 2021). These genes are able to indirectly repress MyoD at its basic helix-loop-helix domain (Kopan et al., 1994, Iso et al., 2003).

In adult muscle, the majority of satellite cells are quiescent, only becoming activated in response to extrinsic signals from the environment. The state of quiescence is not merely a default state. Rather, satellite cells undergo active transcriptional activity in order to keep them quiescent, preserving energy and maintaining the stem cell niche until they are required for regeneration (Yusuf and Fruman, 2003). For example, recent work suggests that satellite cell quiescence is maintained by the cytokine oncostatin M (OSM), which allows reversible exit from the cell cycle. Experiments deleting OSM from satellite cells, and treating cells with OSM *in vitro*, has shown it to be necessary for

maintaining cell number and regenerative capacity following injury (Sampath et al., 2018). The quiescence of satellite cells is dependent on the correct extracellular niche, and this has led to great difficulty in studying these cells *in vivo*, as isolation methods can stimulate the cells and cause them to shift from a quiescent to an activated state (Dhawan and Rando, 2005).

When a satellite cell is in a quiescent state, it exists in one of two functional phases: G_0 or G_{Alert}. In response to external stimuli, satellite cells switch from G_0 to G_{Alert}, wherein cells have a greater regenerative capacity. From this point, satellite cells can then return to a 'reversible' G_0 state and resume quiescence, or an 'irreversible' G_{Alert} state whereby satellite cells proceed with myogenic differentiation (Fig. 3). Many key genes and pathways are involved in the reversible and irreversible transition between quiescent satellite cell states, and also in the transition to proliferative and differentiated states later in the myogenic process (summarised in Table 1). When in a G_{Alert} state, cells are able to respond to external stimuli without changing their position in the cell cycle or committing to a myogenic fate (Rodgers et al., 2014). (Fig. 3). In response to stimulation, satellite cells can then proliferate, producing non-myogenic daughter cells that replenish the satellite cell niche (Olguin and Olwin, 2004).

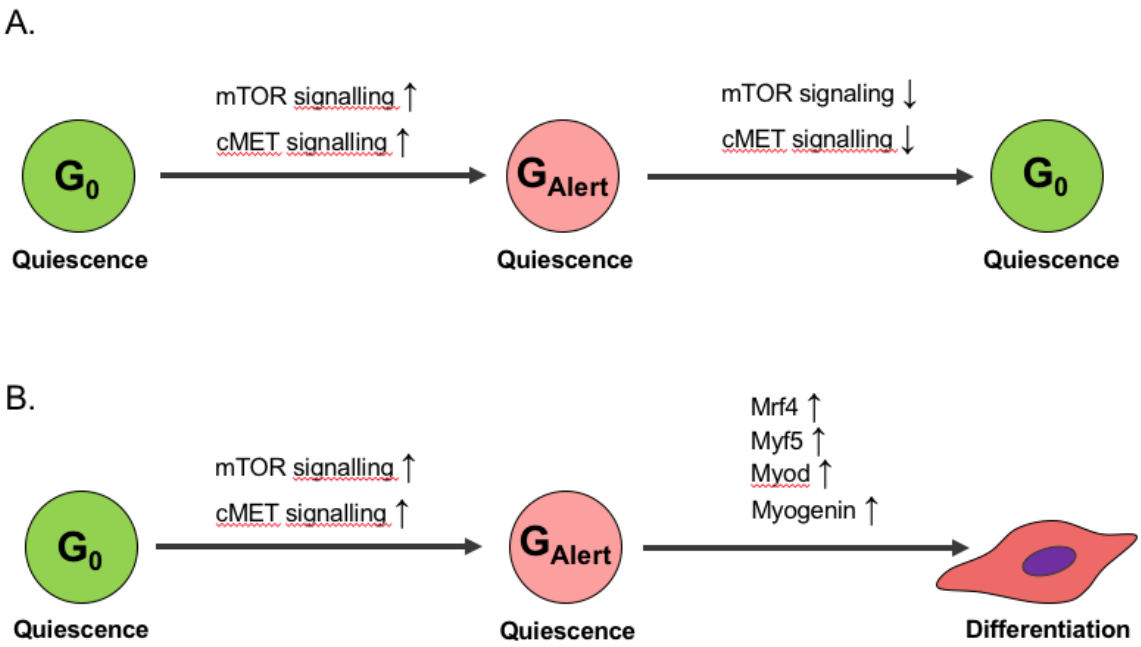

Figure 3. Reversible and irreversible transition from G_0 to G_{Alert}. A. Schematic of reversible transition showing the increased mechanistic target of rapamycin (mTOR) and mesenchymal epithelial transition factor (cMET) signalling that changes a quiescent satellite cell from G_0 to G_{Alert}, and the reduction of this signalling that returns the satellite cell to G_0. **B.** Schematic of irreversible transition showing the increased mTOR and cMET signaling that changes a quiescent satellite cell from G_0 to G_{Alert}, and the increase in myogenic regulatory factors (MRFs) that move the satellite cell to a committed state destined for myogenesis.

Process	Gene	Description
Quiescence	Oncostatin M (OSM)	Secreted niche factor that is a member of the interleukin-6 family of cytokines. Induces quiescence by inhibiting s-phase entry and preventing cell division (Sampath et al., 2018).
	Mechanistic target of rapamycin kinase (mTORC)	Regulates satellite cell proliferation and primes quiescent satellite cells for activation by switching from G_0 to G_{Alert} (Rodgers et al., 2014). KO experiments have shown mTORC as necessary for adequate expression of Pax7, Myf5, MyoD and myogenin later in myogenesis (Zhang et al., 2015).
	Mesenchymal epithelial transition factor (cMET)	Receptor tyrosine kinase that interacts with hepatocyte growth factor (HGF) to regulate satellite cell quiescence. Increased signaling facilitates transition from G_0 to G_{Alert} quiescent states (Rodgers et al., 2014).
	Syndecan-3 and Syndecan-4	Highly expressed in quiescent satellite cells with an irreversible myogenic fate. Involved in signal transduction of various growth factors e.g. fibroblast growth factor (FGF) and HGF. (Cornelison et al., 2001).
	Myostatin	Member of the transforming growth factor β family. Maintains quiescence through the negative regulation of cell division, by decreasing the activity of cyclin dependent kinase 2 (Cdk2) in satellite cells (McCroskery et al., 2003).
	Muscle cadherin (M-cadherin)	Ca^{2+} dependent cell adhesion molecule, involved in anchoring cells to one another (Wernig et al., 2004).
	Paired box 7 (Pax7)	Ubiquitous marker of satellite cells; found in most. Involved in activation and self-renewal of the niche (Olguin and Olwin, 2004; Zammit et al., 2006). The importance of Pax7 was apparent in work that found Pax7 knockout

		mice failed to thrive as a result of inadequate muscle formation in utero (Kuang et al., 2006).
	Paired box 3 (Pax3)	A transcription factor protein, overlapping in function with Pax7 but is primarily involved in the specification and maintenance of myogenic cells during embryogenesis (Messina and Cossu, 2009).
	Cluster of differentiation 34 (CD34)	Ubiquitous marker of satellite cells; found in most. Cell surface glycoprotein involved in cell-cell adhesion (Beauchamp et al., 2000).
	Calcitonin receptor (CALCR)	G-protein coupled receptor that negatively regulates the cell cycle to maintain quiescence (Fukada et al., 2009). A signalling cascade with Notch, collagen V and CALCR maintains quiescence in a cell-autonomous manner (Baghdadi et al., 2018).
	Multiple epidermal growth factor-like domains 10 (MEGF10)	Transmembrane protein expressed by both quiescent and activated satellite cells. Activates Notch signalling to inhibit myogenic differentiation and enhance self-renewal (Holterman et al., 2007).
	Notch1 and Notch2	Ligands that interact with Notch receptors on satellite cells to maintain cells in a quiescent state and also promote self-renewal as opposed to myogenic differentiation in activated satellite cells (Mourikis et al., 2011).
Activation	Myogenic factor 5 (Myf5)	Helix-loop-helix transcriptional activator. Accumulation of Myf5 in satellite cells causes exit from the cell cycle and progression to myogenesis (Crist et al., 2012).
	Myoblast determination protein 1 (MyoD)	Helix-loop-helix transcriptional activator. Upregulated in satellite cells committed to myogenesis, specifying them for terminal differentiation (Charge and Rudnicki, 2004).
	Phosphatidylinositol 3-kinase (PI3K)	Promotes quiescence exit and early activation by phosphorylating protein kinase B (Akt),

		which activates MyoD. (Kaliman et al., 1996; Briata et al., 2011)
	Jagged-1	Notch ligand that is induced upon satellite cell activation, leading to pro-proliferative Notch signaling (Gnocchi et al., 2009).
	Bone morphogenic protein (BMP)	Prevents precocious differentiation by inhibiting the upregulation of MRFs. BMP receptor proteins are expressed by activated satellite cells, and their interaction with BMP4 prevents E-proteins from binding to MyoD and myogenin (Ono et al., 2011; Weintraub and Benezram, 1992).
	Laminin α1 and α2	Proteins deposited by activated satellite cells into the basal lamina to remodel the ECM. Necessary for driving proliferation (Rayagiri et al., 2018).
Differentiation	Noggin	Binds to BMPs, preventing their interaction with BMP receptors on the satellite cells. Thus, interfering with the anti-differentiative effects of BMP. This then allows committed satellite cells to proceed with differentiation (Feng and Derynck, 2005; Ono et al., 2011)
	Myogenin	MRF that marks the onset of terminal differentiation. While Myf5 and MyoD have overlapping functions in driving satellite cell specification, myogenin is uniquely important for differentiation. Myogenin transcription is activated by increasing levels of MyoD (Andrs and Walsh, 1996).
Fusion	Vascular cell adhesion molecule 1 (VCAM1)	Facilitates fusion of myoblasts by the binding of very late antigen-4 to its receptor VCAM1 (Rosen et al., 1992)

Table 1. Genes involved in satellite cell maintenance and regeneration. Genes that play a part in the quiescence, activation, differentiation of satellite cells and their fusion with other myogenic cells to facilitate muscle regeneration.

1.1.4 Migration of satellite cells during myogenesis

Migration of the satellite cells along the length of the myofibre is vital to the regeneration process, as this precedes the fusion with other satellite cells, or with the myofibre. Satellite cells use a method of movement known as amoeboid migration, a primitive form of movement used by rounded single cells, exhibiting the same locomotion mechanisms as used by the protist amoeba (*Dictyostelium discoideum*) (Friedl, 2004; Yamada and Sixt, 2019). This type of migration takes the form of actin polymerisation or hydrostatic membrane blebbing (Lämmermann and Sixt, 2009). Using amoeboid locomotion, satellite cells exhibit a crawling movement along the fibre, facilitated by a continuous series of weak, short lived attachments to the fibre membrane, via β1 integrins (Worthylake et al., 2001).

Amoeboid movement facilitated by actin polymerisation allows effective movement via protrusions known as lamellipodia and filopodia, generated by rapidly polymerising actin filaments. When lamellipodia or filopodia form, filamentous actin pushes against the leading edge of the protrusion, moving the whole cell forward. This mechanism is relatively fast, and is considered the primary driving force for movement of cells such as satellite cells (Yoshida and Soldati, 2006).

Hydrostatic blebbing, another feature of amoeboid migration, describes the small protrusion of plasma membrane that occurs when the interaction between the plasma membrane and the actin cortex is disrupted. This causes the small area that temporarily lacks actin to be pushed outwards by the internal hydrostatic pressure of the cell. These small protrusions are often referred to as ‘false feet’. Subsequent retraction of the blebs is facilitated by RhoA/ROCK signalling, whereby RhoA activates the effector kinase Rho-associated kinase (ROCK), which then phosphorylates myosin light chain. This then stimulates contraction of the actomyosin cytoskeleton, and the bleb protrusion is retracted (Fackler and Grosse, 2008). Blebbing and rapid actin polymerisation are independent mechanisms of locomotion in the satellite cell that are both integral to its movement along the skeletal muscle fibre. During the course of migration, movement via

actin-rich protrusions (lamellipodia/filopodia) alternates with movement via blebbing (Paluch and Raz, 2013).

Cues that guide the amoeboid movement of satellite cells along fibres were explored in earlier work that investigated ‘pathfinding’ cues. Using 3D timelapse, it was found that satellite cells are much faster than other cells such as myoblasts, and that movement on the fibre is influenced by a multitude of different cues. These include exogenous cytokines such as hepatocyte growth factor (HGF) and fibroblast growth factor (FGF), and signalling molecules such as semaphorins, plexins, netrins, Ephs and ephrins (Siegel et al., 2009).

1.1.5 Muscle hypertrophy

The regenerative capability of muscle means that in response to load-bearing work, muscles gradually adapt and increase in mass, in a process known as hypertrophy. During this process, muscle fibre size and myonuclear accretion of fibres increases. Satellite cells have a role in hypertrophy, because in response to the stimulus caused by increased load, they proliferate and fuse with existing muscle fibres, ultimately increasing the overall muscle mass (Modd and LeBlond, 1971).

Muscle hypertrophy occurs providing that the levels of skeletal muscle protein synthesis exceeds the levels of protein breakdown (Damas et al., 2018). The upstream signalling pathways that mediate hypertrophic protein signalling are still not fully understood, although the IGF/Akt dependent activation of mTOR pathway is strongly implicated in hypertrophy. mTOR is a serine/threonine protein kinase that is able to adopt forms: mTOR1 and mTOR2. mTOR1 primarily mediates protein synthesis in hypertrophy, and mTOR2 phosphorylates, and subsequently activates the protein kinase Akt, regulating the survival and proliferation of satellite cells during hypertrophy (Saxton et al., 2017). Growth factors such as insulin and IGF1 activate mTORC1 via Akt, inducing muscle hypertrophy. The relationship between insulin and IGF1 in this pathway is exemplified by the ability of both growth factors to activate the other’s respective

receptors (Griffeth and Bianda, 2014). The overexpression of individual components of this pathway, Akt and IGF1 have resulted in muscle hypertrophy, further consolidating the IGF/Akt/mTOR signalling as a primary driver of protein synthesis during hypertrophy (Musaro et al., 2001; Bodine et al., 2001). Alongside increased protein synthesis, myonuclear accretion as a result of satellite cell hypertrophy contributes to muscle hypertrophy, although the necessity of satellite cells in the hypertrophy process is a topic of debate (Bamman and Roberts, 2018). Previous work has reported impaired hypertrophy and reduced myofiber size in mouse models of hypertrophy when satellite cells are depleted (McCarthy et al., 2011; Egner et al., 2016). However, it was later revealed that impairments in hypertrophy occur when satellite cells are depleted in young mice, not adult, suggesting a greater role for satellite cell driven myonuclear accretion in the hypertrophy of developing bodies (Murach et al., 2017). Regardless of satellite cells being more critical to hypertrophy earlier in life, several studies have found myonuclear accretion to be important for the maintenance of long-term hypertrophy (Moriya and Miyazaki, 2018; Egner et al., 2016; Fry et al., 2014; Goh et al., 2019), The differential requirements for satellite cells to drive hypertrophy based on age may be due to the skeletal muscle fibres of older mice containing myonuclei with a greater reserve capacity to drive myogenic transcription in the absence of satellite cells (Kirby et al., 2016). The growth of the long bones in younger mice may mark a period of skeletal muscle development that is more reliant on satellite cells (Ferguson et al., 2003). Beyond this critical developmental period, whereby satellite cells may be especially primed to drive hypertrophy, the myonuclear domain of muscle fibres may expand to facilitate hypertrophy in the absence of satellite cell activity (Kirby et al., 2016).

A well-established model to study hypertrophy is compensatory hypertrophy of the extensor digitorum longus (EDL), induced by removal of the synergistic tibialis anterior (TA) in the hind legs of young rats and mice (James, 1973; Egginton et al., 2011). The procedure causes an additional load to be placed on the EDL on the operated side, and as such, simulates the act of undertaking load-bearing exercise. As a result of the

increased load on the EDL, the sarcomere length increases and mild hypertrophy of the muscle is observed (Sciaffino et al., 1976; Egginton et al., 2011). Previously, overload of the EDL muscle has been carried out for between 7 and 30 days, justifying further exploration of overload between these time points to identify the time-point of maximal hypertrophy. Studies have not only identified increases in muscle size, but also changes in the vascular supply to the EDL and changes in fibre cross sectional area (Armstrong et al., 1979; Rosenblatt and Parry, 1992; Johnson, 1988).

Early experiments were carried out to track satellite cell behaviour during this compensatory hypertrophy. By administering ^{3}H-thymidine to rats 24, 48 and 72hrs after overload surgery, satellite cell fate could be tracked. In animals killed immediately after the final injection of ^{3}H-thymidine, ^{3}H labelled nuclei belonging to both satellite cells and adult myofibres could be detected. When animals were killed 4 weeks after the last injection, the only ^{3}H labelled nuclei that could be detected were those within adult myofibres. This provided further evidence that satellite cells contribute to muscle hypertrophy by fusing with pre-existing muscle fibres (Schiaffino et al., 1976).

Accompanying the increase in skeletal muscle mass, compensatory hypertrophy simultaneously drives angiogenesis within the muscle. Overload-induced angiogenesis is a graded response, which is influenced by the intensity of the overload, i.e. how long the mouse is left to be ambulant before the muscle is harvested for analysis. Angiogenesis is determined by the upregulation of pro-angiogenic factors such as vascular endothelial growth factor (VEGF) and its receptors (Egginton et al., 2011). The capillary network must be densely distributed throughout the muscle in order for the tissue to obtain enough oxygen to meet its high energy demands. This distribution allows for constant communication between capillaries and satellite cells, and it has been found that muscle with a higher capillary density undergoes an enhanced hypertrophic response (Hendrickse and Degens, 2019). The function of satellite cells in the process of driving hypertrophy is dependent on the delivery of factors such as cytokines and growth factors through the capillaries.

1.2 Heterogeneity within the satellite cell population

1.2.1 Heterogeneity based on protein expression

Satellite cells exist as part of a heterogenous population, able to produce daughter cells of stem cell or myogenic fate, depending on the protein expression of the parent satellite cell (Fig.4). In adults, when growth is complete, quiescent satellite cells are able to be stimulated when repair is needed, via signals that are sent when the basal lamina is disturbed (Hardy et al., 2016). Early experiments that used autoradiographic labelling to trace the movement of satellite cells established that upon stimulation, some satellite cells divide to produce quiescent daughter cells that replenish the existing niche (Snow, 1977). Other daughter satellite cells will commit to a myogenic fate, transforming into myoblasts that will eventually fuse together and differentiate into myofibres (Kann et al., 2016).

Satellite cells ubiquitously express Pax7 and as such, a good method to identify satellite cells is to stain for $Pax7^+$ cells that reside underneath the basal lamina of skeletal muscle fibres (Buckingham and Relaix, 2015). Regardless of whether they are in a quiescent or activated state, satellite cells also express high levels of muscle cadherin (M-cadherin) (Irintchev et al., 1994), α7-integrin (Gnocchi et al., 2009) CD34 (Beauchamp et al., 2000) and multiple epidermal growth factor-like domains 10 (MEGF10) (Holterman et al., 2007), however expression of each of these is not ubiquitous amongst all satellite cells, further establishing the heterogeneity of these cells.

As satellite cells change state from quiescence, they express additional myogenic transcription factors which allow them to become activated, proliferate or differentiate (Fig. 4). When satellite cells become initially committed to a myogenic cell fate, Myf5 begins to be expressed by $Pax7^+$ satellite cells. Further expression of Myf5, accompanied by MyoD expression marks the transition of satellite cells into nascent myoblasts. Myogenin expression occurs in the later stages of myogenic activity, whereby myoblasts fuse to each other and to the pre-existing muscle fibres to drive regeneration

(Tierney and Sacco, 2016). The majority of satellite cells in the body express Myf5 and are committed to a myogenic cell fate (around 90%). The remaining cells in the niche are $Pax7^{+}/Myf5^{-}$ and are destined to be quiescent or self-renewing. Previous work used a Cre-LoxP system to tag satellite cells that expressed Myf5 with yellow fluorescent protein (YFP). The Cre-LoxP system worked by generating heterozygous mice that carried a Myf5-Cre allele, and breeding these with mice that had a YFP reporter knocked in at the locus of a ubiquitously expressed gene (ROSA26). Thus, in the offspring, any satellite cells that had expressed Myf5 at any point, would also express YFP, allowing for identification. Subsequent immunofluorescent analysis found that $Pax7^{+}/YFP^{-}$ satellite cells were committed to self-renewal, and in contrast, $Pax7^{+}/YFP^{+}$ cells went on to become myoblasts (Kuang et al., 2007).

Heterogeneity within the satellite cell population is observed regardless of whether the skeletal muscle is from the same or different developmental origin. Differences in the capacity for self-renewal were observed between satellite cells derived from cranial mesoderm and those derived from the somite (Sambasivan et al., 2011a; Sambasivan et al., 2009). Contrastingly, different fusion and proliferation capacities were found within the same population of extracted satellite cells in experiments using β-galactosidase labelled satellite cells from the same muscle source (Rouger et al., 2004).

Amongst the satellite cell population, other cells that cannot be classified as satellite cells (not initially expressing Pax7) are able to contribute to the formation of myocytes alongside satellite cells, via fusion with myogenic cells. These include muscle-associated angiogenic cells such as pericytes. In previous work using *mdx* mice, transplanted pericytes were found to colonise the host tissue, forming additional skeletal muscle fibres that were able to differentiate to maturity and express the expected range of myogenic markers (Myf5, MyoD, myogenin etc.) (Dellavalle et al., 2007). The co-existence of satellite cells and the other cells that surround them, further adds to the rich heterogeneity of the satellite cell niche.

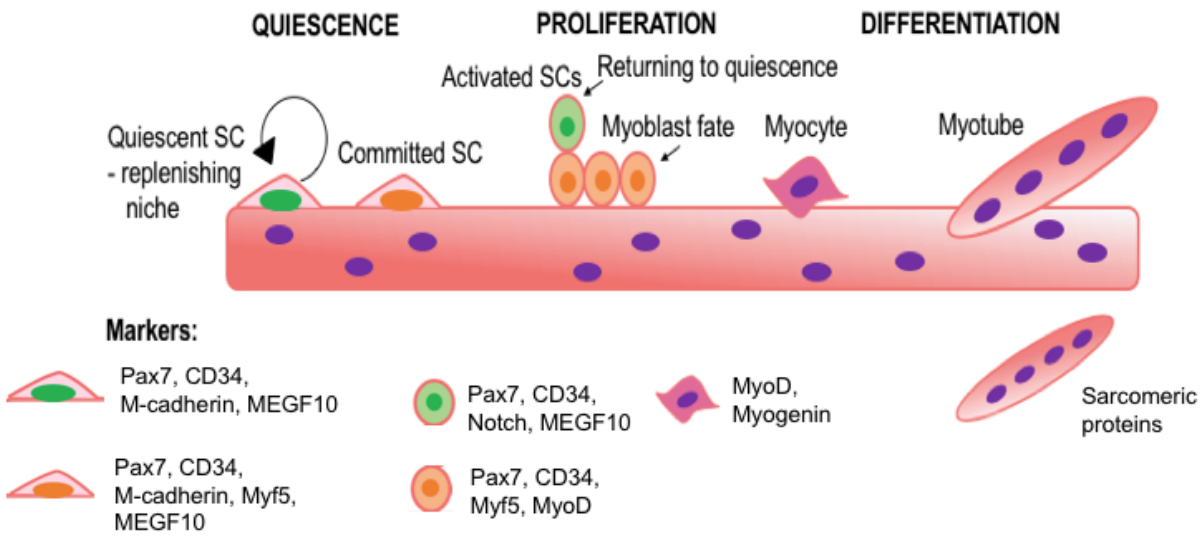

Figure 4. Differential expression of transcription factors by satellite cells on the muscle fibre. Schematic showing the heterogeneity of satellite cells on a single muscle fibre. Cells marked in green express markers that indicate they will return to quiescence within the niche, and cell marked in orange express markers that will facilitate myogenic development.

1.2.2 Asymmetric vs symmetric satellite cell division

Renewal capacity and cell fate is also dependent on the orientation of satellite cell division. The two types of division are categorised as asymmetric division (where the mitotic spindle of the dividing cell is perpendicular to the myofibre axis) and symmetric division (planar division where both resultant daughter cells remain in contact with the sarcolemma of the myofibre) (Kuang et al., 2004) (Fig. 5). Typically, asymmetric divisions yield one daughter cell that is committed to myogenesis ($Myf5^{+}$), and one daughter cell that retains stemness and will return to the satellite cell niche ($Myf5^{-}$). Symmetric divisions on the other hand, give rise to two daughter cells of the same fate. Satellite cells that lack myogenic specification will give rise to two daughter cells that retain stem cell properties that go on to replenish the stem cell niche. Symmetric division of satellite cells that have already adopted myogenic specification results in daughter cells that also have a myogenic fate (Fig. 5) (Cossu and Tajbakhsh, 2007).

Division type is influenced by cell polarity and orientation of spindle fibres in relation to the basal lamina. To establish polarity that leads to asymmetric division, the structural protein dystrophin interacts with microtubule affinity regulating kinase 2 (Mark2), a serine/threonine protein kinase involved in the control of cell polarity and microtubule stability. When this interaction is compromised, the number of asymmetric divisions within the satellite cell population is significantly reduced (Dumont et al., 2015). Planar cell polarity, which results in symmetric divisions and self-renewal, is established by the upregulation of the Wnt7a protein in satellite cells. Wnt7a signalling facilitates the expression of the planar cell polarity protein Vangl2, and when this signalling process is impeded, expansion of the satellite cell pool is significantly reduced (Le Grand et al., 2009). Thus, it is clear that both types of division are essential for adequate regeneration of muscle through proliferation of self-renewing satellite cells and differentiation of committed myogenic satellite cells.

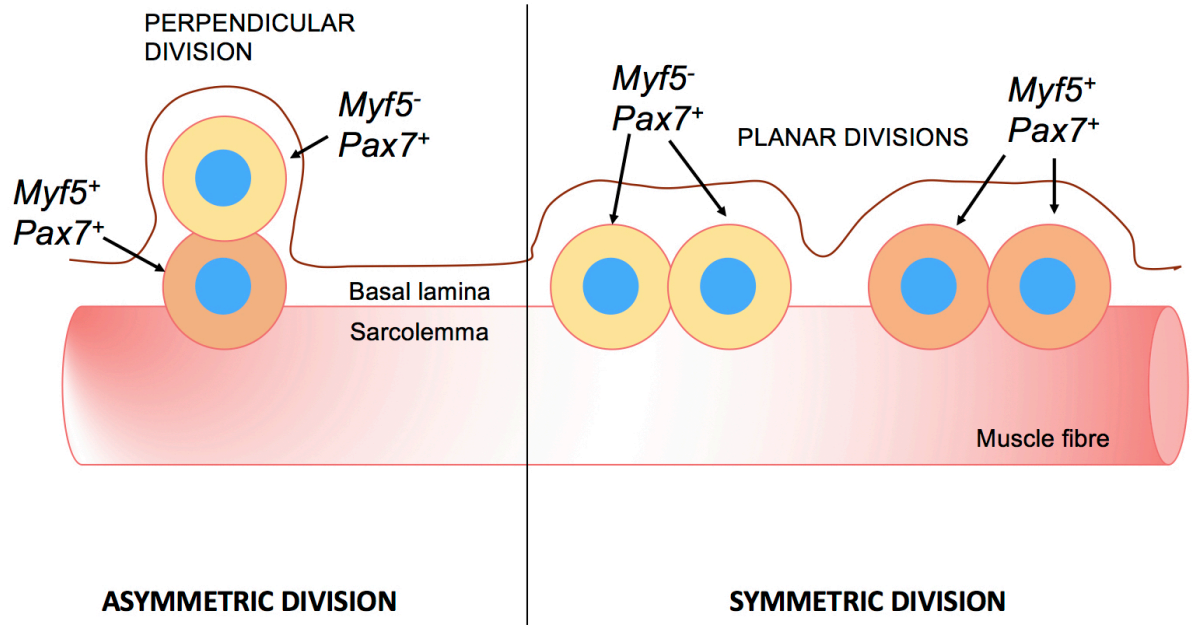

Figure 5. Asymmetric and symmetric satellite cell divisions. The left panel shows asymmetric perpendicular division with one daughter cell remaining in contact with the myofibre (orange) that will adopt a myogenic fate, and one daughter cell in contact with the basal lamina to the outside of the myofibre (yellow) that will self-renew. The right panel shows two symmetric planar divisions, with all cells remaining in contact with the myofibre. Resultant daughter cells may be myogenic (orange) or self-renewing (yellow).

1.3 The role of the skeletal muscle extracellular matrix

1.3.1 Function of the ECM

In vivo, part of the satellite cell is enclosed by the extracellular matrix (ECM) of the basal lamina and part is in close contact with the skeletal muscle cell membrane. This generates a complex environment consisting of molecules that influence cell polarity, architecture and behaviour through constant exchange of biochemical and mechanical signals (Thomas et al., 2014). The basal lamina is connected to the sarcolemma, a thin membrane that sheaths individual muscle fibres, via transmembrane receptors such as integrins and dystroglycan (Han et al., 2009). The ECM is a complex mesh that is made up of several components, each conferring vital structural and functional properties that assist in generation of mechanical force, maintenance of satellite cells and regeneration of adult muscle. Similarly, the satellite cells and mature myofibres use a variety of proteins that allow them to interact with the ECM (Table 2, Fig. 6).

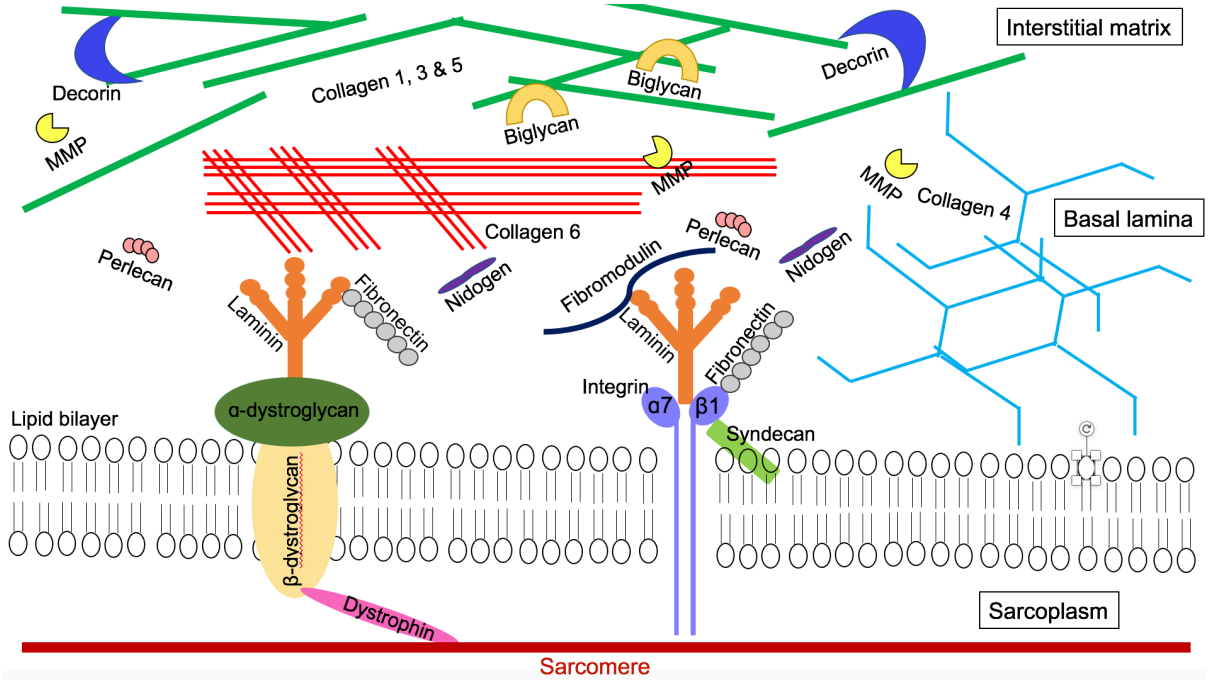

Figure 6. Schematic showing components of the skeletal muscle ECM. Adapted from Csapo *et al. 2020.*

Group	Component	Function
Collagens	Type 1	Present mainly in the perimysium (connective tissue surrounding each bundle of muscle fibres) of skeletal muscle, but also can be found in the epi- and endomysium (Light and Champion, 1984). Alongside type 3, type 1 is the most common collagen isoform in muscle. Confers mechanical strength and stiffness to muscle (McKee et al., 2019).
	Type 3	Evenly distributed between the perimysium and epimysium (connective tissue surrounding several bundles of muscle fibres) of skeletal muscle (Light and Champion, 1984). Presents as a loose meshwork that confers elastic and fatigue-resistant properties to skeletal muscle (Kovanen, 2002).
	Type 4	Helical collagen that is the primary constituent of the basement membrane. It provides a large network of meshed scaffold that integrates other components of the ECM (Poschi et al., 2004).
	Type 5	Critical for maintaining satellite cells in a quiescent state. A signalling cascade that occurs when collagen 5 interacts with Notch and calcitonin receptor (CALCR) allows satellite cells to autonomously avoid entering the cell cycle (Baghdadi et al., 2018).
	Type 6	A key component of the satellite cell niche. Knockout studies have shown it critical for self-renewal in response to muscle injury (Urcuiolo et al., 2013). Mutations in this collagen result in muscular dystrophies that involve

		impaired connective tissue and muscle development e.g. Ullrich congenital muscular dystrophy and Bethlem myopathy (Baker et al., 2005).
	Type 9	Important during early development, acts a bridge between fibrils and other components of the ECM (Khaleduzzaman et al., 1997).
	Type 12	A fibril-associated collagen important in maintaining integrity of the muscle tissue. Has an interrupted triple helix structure (Jakobsen et al., 2007).
	Type 14	Another member of the triple-helix collagen family, and important for aiding muscle metabolism (Jakobsen et al., 2007).
	Type 15	Provides structural stability to the muscle and associated microvasculature. Found exclusively within the basement membrane (Eklund et al., 2001).
	Type 18	Capable of binding with growth factors and links the basement membrane to other constituents of the basement membrane such as glycoproteins (Heljasvaara et al., 2017).
Glycoproteins	Laminin 211	Major component of the basement membrane and present in the basal lamina of skeletal muscle. Provides a structural link between the basement membrane and the cytoskeleton. Involved in cell-cell adhesion, satellite cell proliferation, differentiation and migration. Composed of one α2 chain, one β1 chain and one ɣ1 chain. The α2 chain is referred to as Lama2 and mutations in

		Lama2 can lead to muscular dystrophy (Holmberg and Durbeej, 2013).
	Fibronectin	Form a mesh of branching fibrils throughout the ECM. Involved in cell-cell adhesion, collagen recruitment and vascular stimulation in response to muscle contraction (Wood et al., 2021; Hocking et al., 2007). High expression of fibronectin activates Wnt7a signalling to facilitate increased symmetric division of satellite cells (Bentzinger et al., 2013).
	Nidogen	Key component of the basal membrane that helps specify satellite cells for myogenic differentiation and promotes the adhesion of mature myotubes. Duchenne muscular dystrophy (DMD) patients have been found to be deficient in nidogen (Zhou et al., 2021).
Proteoglycans and glycosaminoglycans	Decorin	The most abundant proteoglycan in the perimysium. It regulates the growth of collagen fibrils and has been found to reduce scarring after muscle injury repair (Li et al., 2007). Decorin binds to TGFβ1, an inhibitor of proliferation and differentiation. This sequesters binding sites on TGFβ1, reducing interactions between TGFβ1 and satellite cells, and thereby promotes increased proliferation and differentiation (Li et al., 2008).
	Biglycan	Less abundant than decorin but acts in the same way competing for TGFβ1 binding sites. Highly upregulated when nascent myotubes begin to form (Casar et al., 2004).
	Perlecan	Binds with histone H1 (distributed throughout the ECM) and in doing so

		stimulates proliferation of myoblasts (Henriquez et al, 2002).
	Fibromodulin	Regulates the expression of collagen type 1 α1 and integral membrane protein 2a – both of which are important for the maintenance of skeletal muscle calcium channels. Enhanced activation of these calcium channels by fibromodulin helps aid regeneration (Lee et al., 2018).
	Syndecans	Family of cell surface transmembrane heparin sulphate proteoglycans. Syndecans 1, 3 and 4 are expressed in developing skeletal muscle but 3 and 4 are restricted to the ECM of adult tissue. They have regulatory roles in the activation, proliferation and differentiation of satellite cells, with expression by cells present for at least 96hrs post-activation (Cornelison et al., 2001). Syndecan 4 is involved in the transduction of force by working with integrins to connect the ECM to the actin cytoskeleton. This mechanism relies on a conformation change in the cytoplasm as a result of tension upon syndecan 4, which then triggers the kindlin-integrin-RhoA pathway (Chronopolous et al., 2020).
Matrix remodelling enzymes	Matrix metalloproteinases (MMPs)	Family of enzymes that digest the ECM. Different MMPs specifically digest different parts of the ECM e.g. collagens. This process facilitates the migration of satellite cells after activation, and remodelling of skeletal muscle tissue after injury (Chen and Li, 2009).
Glycoproteins	α-dystroglycan	Extracellular peripheral protein that forms a complex with β-dystroglycan, allowing a

		strong connection between the ECM and cell cytoskeleton. α-dystroglycan binds to laminin 211 with high affinity (Winder, 2001).
	β-dystroglycan	Transmembrane protein that forms a complex with α-dystroglycan. The intracellular domain of β-dystroglycan binds to the large structural protein, dystrophin (Winder, 2001).
	Integrin α7β1	Integrins are transmembrane receptors that connect cells to components of the ECM and interact with short amino acid sequences specific to different molecules. Integrin α7β1 is an integrin complex on the surface of satellite cells and myoblasts that acts as a laminin receptor. Binds laminin 211 in the ECM to the actin cytoskeleton of skeletal muscle cells and promotes the proliferation and adhesion of satellite cells (Liu et al., 2008). This integrin complex is one of two distinct ways that muscle fibres attach to laminin.
Structural proteins	Dystrophin	Actin-binding protein on the surface of the sarcolemma that stabilises the plasma membrane by attaching the actin cytoskeleton to the ECM. This protects cells from damage as a result of muscle contraction (Gao and McNally, 2015). Dystrophin is downregulated or absent in many muscular dystrophies (Matsumara et al., 1992). The dystrophin-glycoprotein complex is one of two distinct ways that muscle fibres attach to laminin.

Table 2. List of the proteins that comprise the skeletal muscle ECM, and proteins that allow skeletal muscle cells to interact with the surrounding ECM.

1.3.2 ECM related skeletal muscle diseases

The integrity of the connection between the ECM and skeletal muscle cells is important in maintaining the function of the tissue. As well as providing physical anchorage, these proteins and their associated signalling molecules provide chemical cues that allow the skeletal muscle cells to interact with the extracellular environment (Kim et al., 2011) (Fig. 7). The protein network linking the ECM to the cell membrane includes adhesion complexes composed of integrins, and receptor complexes that interact with specific components of the ECM. Examples of these receptor complexes include Discoidin Domain receptors (DDRs) that interact with fibrillar collagen and elastin protein binding receptors (EBPRs) that interact with elastin (Hastings et al., 2018). The constant feedback between the ECM and skeletal muscle allows information to be exchanged on the stiffness and composition of the extracellular environment. Interactions at receptor sites trigger signalling pathways that send information regarding the microenvironment, to the cell nucleus. This induces transcriptional activity in the nucleus that modifies cell behaviour based on the interactions with the ECM. The signalling pathways that are triggered by these interactions include PI3K/Akt, extracellular-signal regulated kinase (ERK) and MAPK, and these influence cell behaviours such as proliferation, survival and deposition of ECM proteins (Yue, 2014).

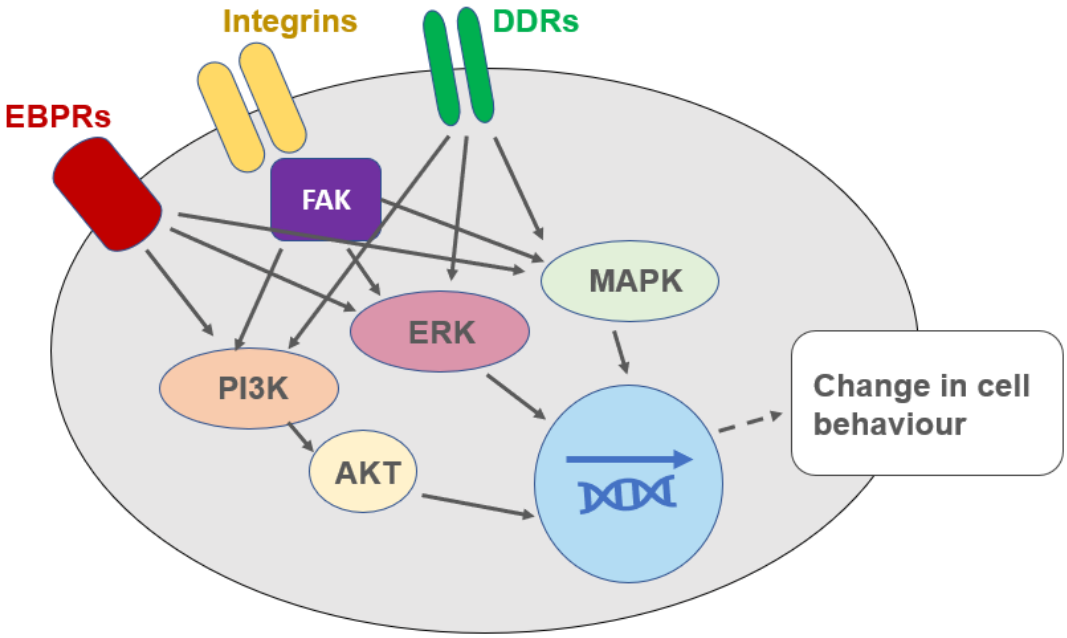

Figure 7. Schematic showing protein network and signalling processes that take information from the ECM to the cell nucleus.

When the communication between the ECM and skeletal muscle cells is disturbed, diseases of the skeletal muscle can occur. Muscular dystrophy includes a group of heterogenous, inherited myopathies that are pathologically similar in that they are each characterized by progressive muscle weakness (Mercuni and Muntoni, 2013). Depending on the specific kind of muscular dystrophy, prognosis, severity, and affected muscle groups may differ. Alongside clinical presentation, muscular dystrophies are classified based on the affected gene associated with the disease. Well-known variants are Duchenne and Becker muscular dystrophy, both of which involve mutations in the DMD gene which codes for the dystrophin protein. Dystrophin acts as a 'shock absorber' within the muscle fibre and confers overall structural stability, forming a connection between the sarcolemma of the muscle fibre and the ECM. When dystrophin fails to be transcribed, dystroglycan, which binds to Lama2, is lost. This results in a loss of connection between the sarcolemma and the ECM, resulting in skeletal muscle that lacks elasticity and cannot act as a 'shock absorber' in the way that normal muscle tissue can. Thus, muscle cannot fully repair after damage (Dowling et al., 2021). In dystrophic patients, the integrity of the muscle fibre membrane is compromised following contraction. This is the result of micro-lesions caused by mechanical stress (particularly during lengthening contractions, such as during downhill walking or running) and unreglated Ca^{2+} entry (Houang et al., 2018) The weakening of skeletal muscle fibres results in the loss of ambulation that blights Duchenne muscular dystrophy patients, typically before they reach teenage years (Landfeldt, 2016). Additionally, loss of dystrophin results in a reduced number of asymmetric divisions, which normally give rise to myogenic daughter cells (Dumont et al., 2015). Thus, in dystrophin-associated muscular dystrophies, muscle wastage does not just occur due to fragile adult muscle fibres, there is also a failure of regeneration at the stem cell level.

Mutations in genes that encode type 6 collagen (ColVI) result in a type of muscular dystrophy known as Ulrich congenital muscular dystrophy (UCMD). ColVI is needed to provide a structural link between the components of the basement membrane;

other collagens, biglycan and decorin (Bidanset et al., 1992; Bonaldo et al., 1990). In UCMD, lack of ColVI results in reduced muscle tissue integrity, and impaired migration and survival of myogenic cells. The disease presents in patients as pronounced scoliosis, joint hyperlaxity and respiration difficulties. Many mutations in the ColVI gene have been identified, meaning that this disease can present with a broad spectrum of severity. Milder cases of this disease are referred to as Bethlem myopathy (Allamand et al., 2011).

Early onset myopathy, areflexia, respiratory distress and dysphagia (EMARDD), an autosomal recessive disease, is another form of muscular dystrophy. Symptoms of this condition present during infancy and include weakness of the limbs, in the facial muscles affecting facial expressions, difficulty swallowing (dysphagia) and respiratory distress due to paralysis of the diaphragm muscle. It is this respiratory distress that leads to the incredibly poor prognosis of EMARDD patients, with all sufferers eventually becoming reliant on ventilators to breathe. Currently, care available for EMARDD patients is largely palliative with a focus on managing symptoms. The nerve conduction speeds of patients with EMARDD have been found to be within normal range, suggesting that the muscle weakness is not of neurological origin (Logan et al., 2011). The disease is extremely rare, affecting less than one in one million people worldwide (Orpha, 2021). EMARDD is caused by mutations in the gene encoding the multiple epidermal growth factor-like protein 10 (MEGF10). Patients with EMARDD have retarded neurological reflexes and severe difficulty swallowing, alongside generally poor muscle strength (Fig. 6A). This is due to poor myofiber assembly and/or maintenance; biopsies from these patients show significantly reduced muscle fibre diameter and fibre nucleation compared to normal patients (Fig. 6B) (Logan et al., 2011). EMARDD is an autosomal recessive disease caused by a compound homozygous or heterozygous mutation in the MEGF10 gene on chromosome 5q23. Cases typically describe asymptomatic (often consanguineous) parents who are heterozygous for a mutation on exon an of the MEGF10 gene. Children of these individuals who inherit a homozygous mutation display

the symptoms of EMARDD (Pierson et al., 2012). There is also at least one reported case of EMARDD in a child who was found to have heterozygous missense and frameshift mutations in the MEGF10 gene. The severity of the EMARDD phenotype has been found to vary depending on the specific type of MEGF10 mutation (Logan et al., 2011).

The mutated protein in EMARDD, MEGF10, is a transmembrane protein containing an N-terminal cysteine-rich domain known as an EMI domain, and 17 EGF-like domains. It belongs to the multiple epidermal growth factor protein family, in which other members include MEGF8, involved in right-left patterning and limb formation, and MEGF11, which has a role in regulating the spacing of retinal neurones (Engelhard et al., 2013, Chiu et al., 2020). The MEGF10 protein acts as a regulator of myogenesis in satellite cells, and interacts with the Notch1 protein in myoblasts (Li et al., 2021, Holterman et al., 2007). MEGF10 has additional roles outside of skeletal muscle, with high expression in the central nervous system where it mediates the phagocytosis of apoptotic cells and amyloid-beta peptides by acting as an 'engulfment receptor' (Iram et al., 2016). Alongside MEGF11, MEGF10 also has a role in retinal neuron arrangement (Kay et al., 2012), Previous work using mice with a mutated copy of the MEGF10 gene, thereby preventing MEGF10 signalling, found that they failed to make and maintain the same amount of neuronal connections as wild-type mice. This was linked to a failure of astrocytes to engulf excess excitatory and inhibitory neurones, which is a critical developmental process known as synaptic pruning. Although the mice in this study contained mutations in MEGF10 related to EMARDD, the effect on the skeletal muscle was not explored. (Iram et al., 2016 Chung et al., 2013). Non-mammalian orthologs of MEGF10, including the *C.elegans* ortholog Ced-1 and the *drosophila* ortholog Draper have provided additional information on the functions of MEGF10. Ced-1 has been shown to aid in the innate immune response, cytoskeletal rearrangement and phosphatidyliserine (PS) binding, which is a key process in apoptosis. Draper also mediates apoptosis through binding to PS, however in mammals, apoptosis has been

found to occur via the interaction between MEGF10 and ATP-binding cassette transporter (ABCA1) (Hamon et al., 2006). Although MEGF10 has a clear role in promoting proliferation of satellite cells and regulating the differentiation of myoblasts, the specific molecular mechanisms by which it does this is still unclear. The relationship with the Notch signalling pathway is likely to be influential, as previous studies have found that Notch proteins decrease in tandem with diminished MEGF10 levels (Holterman et al., 2007).

Structurally, the MEGF10 protein is a type-1 single-pass transmembrane receptor composed of a signal peptide, EMI domain and 17 EGF-like domains. The EMI domain is composed of 7 cysteine residues that function by forming cross-links between other cysteine residues, alongside other proteins. It is necessary for cell adhesion and facilitates the extracellular interactions of MEGF10 (Doliana et al., 2000). The 17 EGF-like domains are split into two groups: the EGF-like domains, and EGF-laminin domains which are larger. Like the EMI domains, the EGF-like domains also form bonds between cysteine residues. They are involved in facilitating signal transduction through the cytoplasm and facilitate protein-protein interactions via the binding of Ca^{2+} which has a stabilising effect (Benitez and Komivez, 2000; Rao et al., 1995). MEGF10 also contains a single intracellular domain (ICD), which contains 13 tyrosine residues, facilitating receptor tyrosine kinase activity and downstream signalling that allows the phagocytotic and myogenic activity of MEGF10 (Pawson and Scott, 1997) (Fig. 8). MEGF10 proteins can be detected in the plasma membrane and in intracellular vesicles within the cytoplasm, and it is thus able to bind to ligands in both locations. MEGF10 has been reported to interact with Notch, a transmembrane protein that also has a composition of EGF domains. Both Notch receptor proteins and MEGF10 can be activated by the Notch ligands e.g. Delta and Serrate. The MEGF10 protein exists in different isoforms; to this date, two isoforms have been reported. The first isoform has been described here, and in comparison, the second isoform is truncated, lacking several 3’ exons and has a

different C-terminal sequence. There are currently little data regarding the differential expression of MEGF10 isoforms (Hughes, 2016).

There are many reported mutations in the MEGF10 gene (Table 3, Fig.9) that lead to the Mendelian condition, EMARDD. Alongside EMARDD, mutations of MEGF10 can also lead to multi-minicore disease, a myopathy that presents similarly to EMARDD, but with additional scoliosis and joint hyperlaxity. In addition, onset of respiratory distress occurs later in life than EMARDD (Liewluck et al., 2016; Boyden et al., 2021b). A group of neuromusclular conditions akin to EMARDD, but with mutations occurring out with the MEGF10 gene, are spinal muscular atrophy with respiratory distress (SMARD). Patients with SMARD present during infancy with respiratory distress due to diaphragmatic paralysis and suffer general muscle atrophy (Grohmann et al., 2001, Guenther et al., 2007).

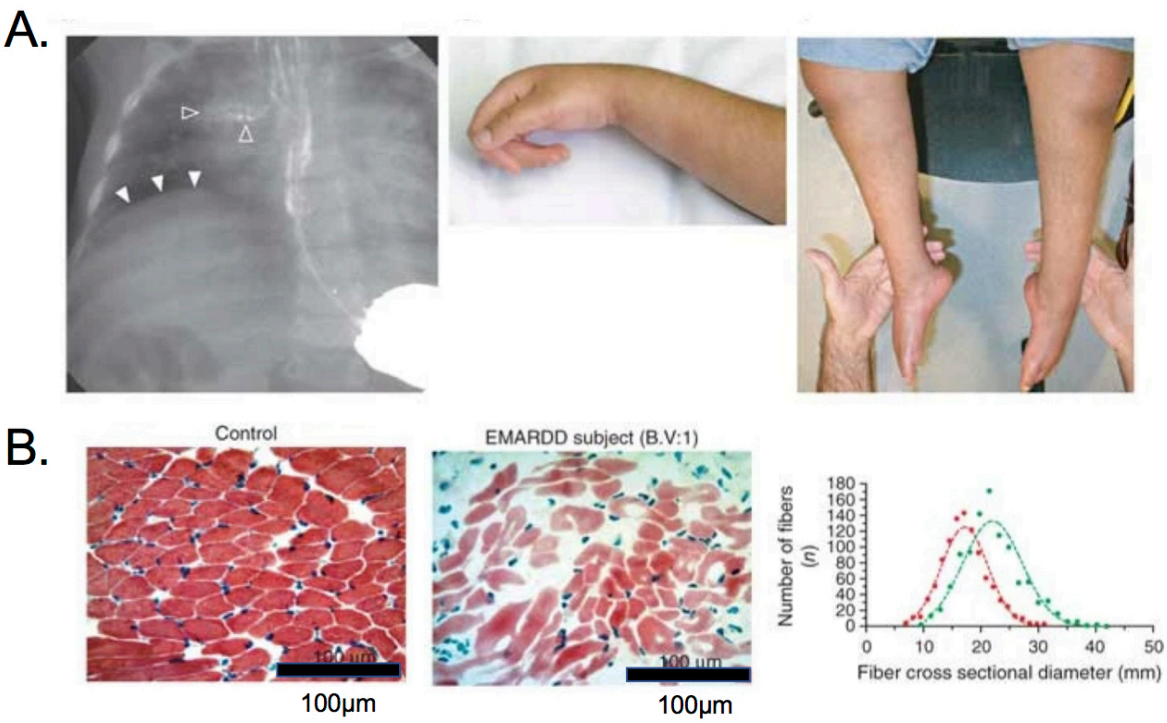

Figure 8. Physiological effects of EMARDD. A. Clinical presentation of a patient with EMARDD. Aspiration in the lung, indicating dysphagia, weakness of the hand and muscle wastage in the calves. **B.** Histological sections showing reduced diameter of muscle fibres in the EMARDD patient. Graph shows the EMARDD patient in red and the control in green, and consolidates the significantly reduced fibre diameter as a result of EMARDD (Logan et al., 2011).

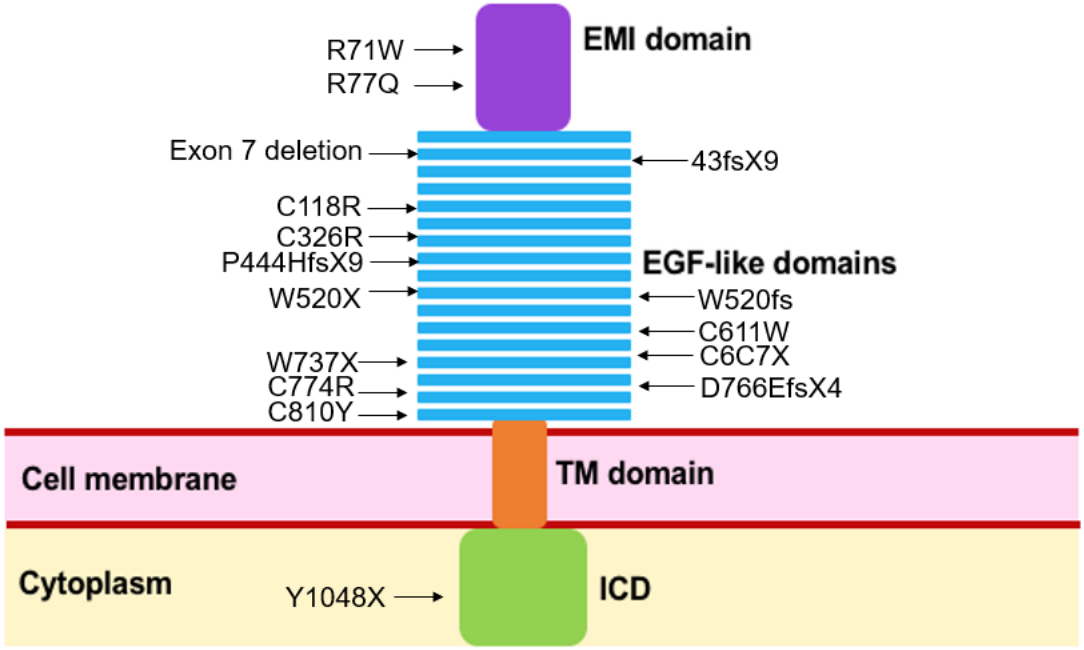

Figure 9. MEGF10 structure and known mutations. ICD (intracellular domain) is shown in green, TM (transmembrane) domain in orange, 17 EGF-like domains in blue and the EMI domain is in purple. The relative locations of MEGF10 mutations are indicated with arrows.

MEGF10 mutation	Mutation type	Disease caused by mutation	Source
R71W	Missense	Multi-minicore disease	(Boyden et al., 2012)
R77Q	Missense	Multi-minicore disease	(Boyden et al., 2012)
C118R	Missense	Muscular dystrophy, limb girdle	(Harris et al., 2017)
C326R	Missense	Multi-minicore disease	(Boyden et al., 2012)
P442HfsX9	Nonsense	EMARDD	(Logan et al., 2011)
W520X	Nonsense	EMARDD	(Logan et al., 2011)
W520fs	Frameshift	EMARDD	(Posey et al., 2017)
C611W	Missense	Multi-minicore disease	(Boyden et al., 2012)
W737X	Nonsense	Muscle weakness	(Wu et al., 2018)
D766EfsX4	Frameshift	EMARDD	(Logan et al., 2011)
C767X	Nonsense	EMARDD	(Logan et al., 2011)
C774R	Missense	EMARDD	(Logan et al., 2011)
C810Y	Missense	EMARDD	(Takayama et al., 2016)
Y1048X	Nonsense	EMARDD	(Logan et al., 2011)
Exon 7 deletion	Frameshift	EMARDD	(Pierson et al., 2012)
43 fsX9	Frameshift	EMARDD	(Takayama et al., 2014)

Table 3. MEGF10 mutations. A summary of MEGF10 mutations, alongside mutation type, associated disease and the study that first reported the mutation. (In addition, 2 splicing mutations, 4 small deletions. 2 small insertions and one gross deletion have been reported).

Previous work in the Peckham involved an investigation into the role of MEGF10 in skeletal muscle myopathy, to thereby also elucidate further its role in myogenesis. This work demonstrated that while MEGF10 is expressed at low levels in cultured myoblasts, introducing a MEGF10 mutation into the myoblasts and driving its overexpression results in impaired cell fusion and motility. In addition, MEGF10 was detected in satellite cells on fibres isolated from a mouse model of hyperplasia. The proposed role of MEGF10 in cell adherence was supported by this investigation, as purification of the MEGF10 ECD allowed myoblasts to attach to a non-adherent surface (Hughes, 2016). The presence of MEGF10 in satellite cells in this hyperplasia model, and its involvement in the fusion, motility and adherence of myoblasts, leads to the hypothesis that MEGF10 plays a key role in the satellite cell response to external stimulus. It is also hypothesised that in the event of MEGF10 becoming non-functional through mutation, the regeneration process will become impaired, with reduced muscle hypertrophy and muscle atrophy.

1.4 Skeletal muscle cells in culture

1.4.1 Mammalian cell lines

Mammalian cell lines in culture are commonly used to explore myogenesis *in vitro,* to replicate the processes that occur in muscle tissue *in vivo*. A popular cell line for this purpose is the C2C12 line (Blau et al., 1985), which is a subclone derived from C2 myoblasts (Yaffe and Saxel, 1977). These myoblasts were originally obtained by harvesting cells from a CH3 mouse following leg-crush injury, and were subsequently spontaneously immortalized in culture. As a result, C2C12 cells grow readily in culture and under the appropriate conditions, will fuse together to form myotubes which have a protein expression profile similar to myotubes that form skeletal muscle *in vivo* (Blau et al., 1985). At the myoblast stage, C2C12 cell behave in a way that is comparable to satellite cells in an activated state, making them a good model for satellite cell research

(Buratti et al., 2004). However, the disadvantage of using these cells to study myogenesis is that the timing of differentiation cannot be well controlled. Differentiation is typically initiated by reducing serum levels within the culture medium, however many cells continue to proliferate at this stage, and as a result, the differentiation process as a whole is impeded, with myogenesis failing to achieve the level of maturity observed *in vivo.* In addition, if C2C12 cells are injected into muscle in animals, they form tumours (Morgan et al., 1992).

An alternative to C2C12 cells that allows a much greater degree of control over the switch from proliferation to differentiation are satellite cells derived from the H2K^{b}-tsA58 immortomouse (Morgan et al., 1994). These cells are distinctive in that they are maintained in a proliferative state by a temperature-sensitive mutant of T-antigen, tsA58, derived from the SV40 virus T-antigen gene. Transcription of the tsA58 gene is regulated by an upstream H2K^{b} promoter, which is active in the presence of ɣ-interferon. Thus, when H2K^{b}-tsA58 cells are grown at 33°C in the presence of ɣ-interferon, they remain in a proliferative state. When the incubation temperature is raised to 37°C and the ɣ-interferon removed from the media, cells exit the cell cycle and begin to differentiate. The removal of ɣ-interferon prevents transcription of the tsA58 gene, and any remaining T-antigen is degraded as a result of the increase in temperature (Morgan et al., 1994). As well as this enhanced control over the timing of myogenesis, C1F cells are favourably used in place of C2C12 cells because they are capable of forming myotubes that reach greater levels of maturation before detaching from the cell culture surface, and they do not form tumours when injected into mice (La Framboise et al., 2003; Morgan et al., 2002).

Primary myoblasts are also studied *in vitro*. These cells are typically generated by isolating satellite cells from muscle using enzymatic digestion (Musaro and Barberi, 2010). The resultant pool of cells is heterogenous, containing many non-myogenic cells that must be removed via purification. Methods to enrich the satellite cell population include pre-plating cells, differential centrifugation and fluorescence-activated cell

sorting (FACS) (Musaro and Barberi, 2010). Once purified, satellite cells can be grown in culture much in the same way as the myoblast cell lines.

Satellite cells *in vitro* can also be studied by isolating skeletal muscle fibres and visualising the satellite cells *in situ* (Moyle and Zammit, 2014). Although fibre isolation is somewhat limited in that it removes the fibres from their natural environment, satellite cells can still be observed on the fibre and fibres can be cultured for a period of time before they expire. The advantage of this approach is that it more closely resembles an *in vivo* environment in which satellite cells remain in position underneath the basal lamina (Collins and Zammit, 2009).

1.4.2 The importance of stiffness

Typically, primary myoblasts and myogenic cell lines such as C2C12 cells are cultured on glass coverslips coated with gelatin, or an ECM protein such as laminin or collagen. However, the stiffness of glass (or plastic) is much higher (elastic modulus of ~50-60GPa) (Monclus et al., 2010) than that of muscle tissue *in vivo* (elastic modulus of ~12kPa) (Engler et al., 2004a), and thus does not well replicate the *in vivo* niche these cells are normally exposed to. On surfaces of very high stiffness, actin and myosin within growing myoblasts form an excess of contractile bundles known as stress fibres, resulting in atypical fibre contraction. Additionally, integrin proteins cluster together on the cells to form multiple focal adhesions (Engler et al., 2004b). Focal adhesions are a necessary structural and chemical connection between the skeletal muscle cell and the extracellular matrix, however the surplus focal adhesions observed on stiff surfaces may not be representative of the focal adhesions present on cells *in vivo* (Griffin et al., 2004). In contrast, when skeletal muscle cells are grown on softer surfaces, with a similar elastic modulus to that *in vivo*, they differentiate into myofibres with more prominent actomyosin striations compared to cells grown on surfaces of higher elastic modulus (Engler et al., 2004a).

Satellite cells have a range of mechanisms that allow them to sense the stiffness of their surrounding substrate and neighbouring cells, both *in vivo* and *in vitro*. This helps to explain why small differences in elastic modulus can drive large alterations in cell behaviour. For example, focal adhesions, which are connected to the actomyosin cytoskeleton, respond to a stiffer environment by enlarging and recruiting additional cytoskeletal proteins, a process regulated by RhoA/ROCK signalling (Chrzanowska and Burridge, 1996). The activity of metalloproteinases (and their inhibitors), enzymes that can remodel the ECM, is decreased on stiffer surfaces, meaning that normal myogenic processes such as satellite cell migration may be impaired in harder surfaces (Tian et al., 2019). An important transcriptional activator in satellite cells involved in detection of substrate stiffness is yes-associated protein (YAP) and its cofactor, transcriptional coactivator with PDZ-binding motif (TAZ). Forces fed back from the environment travel through focal adhesions to the nucleus, increasing the size of nuclear pores and thereby allowing the entry of more YAP and TAZ into the satellite cell nucleus (Elosegui-Artola et al., 2017). YAP and TAZ are phosphorylated when the Hippo pathway is activated, and this phosphorylation inhibits YAP and TAZ. However, it has been found that YAP and TAZ are able to operate independent of this pathway, instead relying on RhoA activity and forces generated through the actomyosin cytoskeleton (Dupont et al., 2011). Recent work exploring mechnosensitive ion channels found Piezo Type mechanosensitive ion channel component 1 (Piezo1) to be important in driving differentiation of myoblasts in culture (Bosutti et al., 2021). Piezo1 works by concerting mechanical pressure exerted upon the cell membrane into electrical intracellular signals that influence the Hippo pathway. The Ca^{2+} influx caused by Piezo1 activation leads to RhoA/Rho-associated protein kinase (ROCK) dependent assembly of the sarcomere. (Ridone et al., 2019).

In order to trigger these signalling pathways, cells exert traction forces via the focal adhesions which creates a pushing/pulling motion capable of deforming the ECM (Engler et al., 2004). The extent to which the ECM can be deformed directly relates to

its stiffness as dictated by Young's Modulus of Elasticity, and a proportional amount of tyrosine phosphorylation is then carried out in the cell in response (Grzelkowska-Kowalczyk, 2016).

1.5 Hypothesis and Aims

The effect of substrate stiffness

Although stiffness is known to have a strong influence on muscle differentiation, and many stiffness-sensitive genes have been identified, we still lack an understanding of how it affects myoblast behaviour to favour differentiation (Darnell et al., 2018). Although a previous RNASeq study was performed for C2C12 cells cultured on patterned hydrogels with a stiffness that promoted myogenesis (Denes et al., 2019), a detailed study into changes in gene expression pattern that help to explain the enhanced differentiation on soft surfaces was not performed. An RNASeq analysis of H2k^{b}-tsA58 myoblasts has also not been performed. Thus, my first aim was to compare differentiation of C1F cells (a clone of H2K^{b}-tsA58) on soft and hard surfaces, and to use RNAseq to determine differences in gene expression for these cells cultured on the two different surfaces during differentiation. In parallel, I analysed fusion, terminal differentiation and expression of specific proteins in fixed cells differentiated on these two types of surfaces by immunostaining and analysis, to confirm the changes in RNA levels observed by RNAseq.

Hypertrophy and the role of MEGF10 in the satellite cell response

MEGF10 has been suggested to be important to satellite cell behaviour (Li et al., 2021; Saha et al., 2017; Holterman et al., 2007; Logan et al., 2011). In humans, lack of MEGF10 reduced the size of myofibres, and the muscle additionally lacked Pax7^{+} nuclei, suggesting that lack of MEGF10 affected satellite cell number. In adult mice MEGF10 was reported to be primarily expressed in the pectoralis major muscles of

the diaphragm (Logan et al., 2011). Additionally, siRNA mediated knockdown of MEGF10 depleted the self-renewing satellite cell pool (Holterman et al. 2007). However, a previous study using a gene trap mediated approach to knockout MEGF10 in skeletal muscle (Megf10$^{tm1c(KOMP)Jrs}$ mouse), only showed a mild phenotype (Saha et al., 2017). Only when the MEGF10$^{-/-}$ mouse was crossed with the *mdx* mouse (which lacks dystrophin) was a strong phenotype observed (Saha et al., 2017). Moreover, most studies that investigate satellite cell behaviour *in vivo* use a technique that ablates the skeletal muscle, by injection of toxins into the muscle (Murach et al., 2021). A more physiological approach is to study the behaviour of satellite cells in response to overload, which leads to muscle hypertrophy, although this approach is less often used, perhaps as it requires surgery (Murach et al., 2021).

Thus, in the second part of this thesis I implemented an established model of inducing hypertrophy, overload of EDL by unilateral extirpation of the TA in the mouse. I used this model to explore changes in sequential myogenic transcription factor expression, capillarisation and tissue hypertrophy after overload (Egginton et al., 1998; Egginton et al., 2011) to determine when the peak in the myogenic response would occur at some point from 6-14 days overload, establishing baseline conditions for further experiments.

I was then able to investigate how this response was impacted when MEGF10 was reduced using a MEGF10 knockout mouse model. I used a different knockout model to the previous study (Saha et al., 2017), in which exons 1 to 24 were deleted (Megf10$^{tm1(KOMP)Vlcg}$), and which has only previously been used to demonstrate a brain phenotype (Iram et al., 2016; Chung et al., 2013). Based on earlier work (Holterman et al., 2007; Li et al., 2021), I expected loss of MEGF10 to impair satellite cell proliferation and migration and thus the muscle response to overload. I tested this idea by comparing hypertrophy and satellite cell activation between wild-type, MEGF10$^{+/-}$ and MEGF10$^{-/-}$ mice using a range of immunofluorescent analyses.

I further explored the satellite cell response in wild-type, Megf10$^{+/-}$ and Megf10$^{-/-}$ mice using *in vitro* cell culture of isolated muscle fibres. I compared myogenic transcription factor expression of mouse muscle fibres kept in culture, for wild-type, Megf10$^{+/-}$ and Megf10$^{-/-}$ mice to determine if the activation of satellite cells in culture was affected. Trends were observed to understand if transcription factor expression of satellite cells in culture was similar to expression when exposed to hypertrophy stimulus.

2 Expression of Myogenic Markers by Muscle Cell Lines

2.1 Introduction

Myoblasts, derived from striated muscle satellite cells, will recapitulate the process of muscle differentiation in culture into multinucleated myotubes (Snow, 1978). Satellite cells are the stem cells of skeletal muscle that reside underneath the basal lamina of the muscle fibre. When stimulated, they can transition from a quiescent to an activated state (Kuang et al., 2008). They then proliferate to form new daughter satellite cells that will replenish the stem cell niche, or differentiate into myoblasts (Kuang et al., 2008). Myoblasts *in vitro* are typically cultured on stiff glass surfaces (~100kPa), pre-coated with gelatin and/or extracellular matrix (ECM) materials (Irianto et al., 2016). Early experiments tested different ECM components and found collagen and laminin to be particularly effective in promoting myoblast adhesion, growth and differentiation into myotubes (Ehrmann and Gey, 1956; Kleinman et al., 1981; Clark et al., 1997).

Quiescent and newly activated satellite cells in the basal lamina of skeletal muscle fibres express the paired homeobox gene Pax3 or Pax7. Pax7 is expressed in all quiescent satellite cells. Expression of Pax3 is more variable, and is not expressed in most hindlimb muscles (Buckingham and Relaix, 2015). These two genes are redundant, and required for satellite cell function in adult muscle (Wardle, 2019). On activation of satellite cells, four specific myogenic regulatory transcription factors are involved in directing muscle differentiation (Wardle, 2019). These myogenic factors all share a similar structure (basic helix-loop-helix). The first to be activated is myogenic factor 5 (Myf5), although this transcription factor has also been shown to be expressed in quiescent satellite cells (Beauchamp et al., 2000). Myogenic regulatory factor 4 (Mrf4, also called Myf6) along with Pax3/7 and Myf5f, triggers the activation of myogenic determination gene number 1 (MyoD) (Berkes and Tapscott, 2005). Like Pax7 and Pax3, Myf5 can also be expressed in quiescent satellite cells and/or throughout differentiation (Cornelison and Wold, 1997). Myf5, Mrf4 and MyoD are required to activate the fourth

myogenic factor, myogenin, which is required for fusion of myoblasts and formation of multi-nucleated myotubes (Wright et al., 1989). The relationship between these different factors is complex. For example, normal skeletal muscle development can occur in the absence of Myf5 and MyoD, as long as Mrf4 is present (Rhodes and Konnieczny, 1989). Also important are the Mef2 family of genes (Mef2a, b, c and d), which encode myogenic transcription factors that belong to the MADS family of transcription factors (Shore and Sharrocks, 1995). Mef2c can act synergistically with MyoD and myogenin to promote myogenesis, while Mef2a and d can act synergistically with MyoD, and this is mediated through direct interaction of the two proteins (Molkentin et al., 1995). Mef2c has also been shown to be important for the maintenance of sarcomere integrity, by regulating transcription of the sarcomeric gene myomesin (Pothoff et al., 2007). The process of myogenesis is regulated by the transmembrane protein, multiple EGF-like domains 10 (MEGF10). MEGF10 has been suggested to interact with Notch1 to promote satellite cell proliferation, therefore it may be important for muscle regeneration (Holterman et al., 2007).

Alongside the changing expression of myogenic transcription factors, sarcomeric genes increase in expression over the course of skeletal muscle cell differentiation. The organisation of contractile proteins into sarcomeres involves the polymerisation of actin and myosin into thin and thick filaments (Craig and Padron, 1994). As differentiation progresses, there is also a switch in expression from embryonic (Myh3) to fetal (Myh4) to slow myosin heavy chain (Myh7) *in vivo* and *in vitro* (Peltzer at al., 2008; Silberstein et al., 1986). Early work which carried out RNA analysis on myoblasts derived from the C2 cell line to investigate transcription of actin and myosin genes found distinct patterns of genetic up and downregulation during differentiation (Cox et al., 1990). Certain proteins are required to maintain the structural integrity of the sarcomere, such as titin (Ttn), a giant protein that stabilises actin and myosin filaments and confers elastic properties to the muscle (Labeit et al., 1997). Sarcomere assembly is directed by telethonin (Tcap), and during this process, the length of thin filaments is regulated by another giant protein

called nebulin (neb) (Ruilin et al., 2009; Littlefield and Fowler, 2008). Sarcomere length is additionally governed by myosin binding protein C (mybpc), via its actin and myosin filaments, altering their positions in relation to one another (Li et al., 2016). The folding of myosin is facilitated by a specific striated muscle chaperone, uncoordinated mutant number-45 myosin chaperone b (Unc45b). It acts as a template for the assembly of myosin within the sarcomere, informing on the correct regularity and geometry of filaments (Salimi et al., 2019).

Recently, tissue stiffness has been suggested to play an important role in cellular differentiation, including that of myoblasts (Discher et al., 2013) and this stiffness is important for their phenotype (Engler et al., 2004). Experiments using the C2C12 cell myogenic line showed that while fusion was not affected by the surface stiffness, differentiation was much better on surfaces with a stiffness close to that which the cells would experience *in vivo (*~12 kPa*)* (Gilbert et al., 2010). The striated appearance of muscle specific actin and myosin was only found to develop in myotubes cultured on a surface with a similar stiffness to muscle tissue *in vivo*.

An alternative to using C2C12 cells is to use conditionally immortal skeletal muscle myoblasts derived from the *H-2K^b* tsA58 'immorto' mouse (Jat et al., 1991). Our laboratory has isolated several clones of satellite cells from this mouse, one of which is the C1F clone (Peltzer et al., 2008). These cells contain the temperature sensitive mutant of the SV40 large T-antigen (tsA58) under the control of an inducible promoter (*H-2k^b*). At a temperature of 33°C and in the presence of interferon-ɣ (ɣIFN), this drives transcription of the tsA58 gene, and promotes cell proliferation. When the temperature is increased to 37-39°C, and ɣIFN is removed, no further T-antigen is expressed, and the remaining T-antigen is rapidly degraded, with the half-life for degradation sitting between 3.3 and 5hrs (Roy and Fiers, 1983). This allows the myoblasts to exit the cell cycle and differentiate (Jat et al., 1991). Unlike C2C12 cells, *H-2K^b* tsA58 derived cells do not form tumours when transplanted into mice (Morgan et al., 1994). The choice of C1F myoblasts was further supported by their tendency to form a

greater number of thick myotubes with more defined striations. Compared to C2C12 cells, C1F cells display higher levels of fusion and are able to adhere to the cell culture surface for longer, allowing more advanced maturation of myotubes (Parker et al., 2016).

In this study, the C1F clone was used to compare expression of RNA during differentiation on optimised silicone surfaces with an elastic modulus similar to that of skeletal muscle tissue *in vivo* (12kPa) compared to differentiation on standard hard surfaces. This RNAseq analysis was used to characterise the changes in gene expression over the course of 7 days of myogenic differentiation, and was complemented by immunocytochemistry (ICC). As it is already known that the cells should better differentiate on the softer surface, we expected to observe changes at the mRNA level that would support this, such as higher increases in levels of RNA for myogenic and sarcomeric proteins.

2.2 Methods

2.2.1 General procedures

All media, glassware, plastic and surgical tools were sterilised before use, either by autoclaving at 121°C for 15 min or washing thoroughly with 70% ethanol in H_2O.

2.2.2 Mammalian cell culture

All cell culture media and reagents were obtained from Gibco (Thermo Fisher Scientific). All reagents and materials were used in a class II biological safety cabinet under sterile conditions. All media was heated to 37°C prior to use.

2.2.3 Recovery of cells from liquid nitrogen storage

Cells were recovered from liquid nitrogen storage and then immediately went under a rapid thaw process, by heating vials at 37°C. 1ml of this thawed solution was then diluted

in 10ml warmed media in a ventilated T75 flask. The flask was then transferred to a carbon dioxide controlled and humidified incubator.

2.2.4 C2C12 myoblasts

C2C12 cells are a myogenic cell line that is derived from the C2 cell line, cells which were originally obtained from CH3 mice following crush injury (Blau et al., 1983). C2C12 myoblasts proliferate in high serum conditions at a temperature of 37°C, 5% CO_2 and begin to differentiate when the serum level is reduced. Myoblast media was composed of DMEM supplemented with 20% FBS, 1% P/S and 2% CEE, and lower serum differentiation media was composed of DMEM supplemented with 4% HS and 1% CEE. Cells were left in myoblast media for 1-2 days until reaching ~70% confluence. They were then incubated in differentiation media for 3-7 days allowing myoblasts to join together and form myotubes.

2.2.5 C1F myoblasts

C1F cells provide an alternative to C2C12 cells, which also allows observation of proliferation and differentiation but additionally allows for superior control over the timing of the switch from one state to the other. C1F cells were kept in a proliferative state whilst in the presence of ɣIFN (20 U/ml), due to the presence of a thermolabile T-antigen gene (tsA58), which is derived from the SV40 virus. C1F cells were left to incubate in myoblast media for 1-2 days until they reached a confluency of ~70%.

2.2.5.1 Differentiation of C1F myoblasts

C1F cells exit the cell cycle and begin to differentiate when the serum content of the media is reduced, ɣIFN removed, and incubation settings changed. Differentiation media was composed of DMEM, 4% HS and 1% CEE. Incubation was set to 37°C, 5% CO_2

and cells were left to incubate in these conditions for 3-7 days until myoblasts had fused with one another forming multinucleated myotubes. Media was changed on a daily basis.

2.2.6 Passaging cells

Following recovery from LN_2 and seeding into a T75 flask, cells were left to proliferate until reaching ~70% confluency. At this point, they are ready to be transferred to a fresh flask. At this point, spent media was aspirated from the flask and 2ml TrypLE was added to detach the cells. TrypLE was evenly spread over the layer of cells by gently moving the flask from side to side, and the flask was then returned to the incubator for ~5 mins. 8ml media was then added to the flask to recover the cells. 10µl of this cell suspension was then sampled and dispensed to a haemocytometer (Hawksley BS.748) for cell counting. New cell solutions were seeded onto fresh flasks at a density of ~$5x10^4$ cells/ml and were passaged once more before seeding onto coverslips.

2.2.7 Storage of cells

Cells at a low passage number (below 10) were harvested for storage to allow for future use. These cells were detached with TrypLE, then pelleted by centrifuging at 1000 x *g* for 5 mins. Cells were resuspended at a density of ~$1x10^6$ cells/ml. To allow for protection against the formation of intracellular and extracellular crystals during the freezing process, growth media was supplemented with 10% dimethyl sulfoxide (DMSO). 1ml of this cell suspension was then transferred to labelled cryovials (Nunc), contained within a polystyrene box, and left at -80°C overnight. The following day, vials were placed into long-term LN_2 storage. This slow-freezing process is carried out to allow adequate efflux of water, reducing the likelihood of ice formation which can damage cells.

2.2.8 Preparation of coverslips

Prior to seeding cells onto glass coverslips, coverslips had to be acid-washed to smoothen their surface, allowing optimum attachment of cells. Coverslips were washed with a solution of 37% hydrochloric acid (Acros Organics) in water, and were then rinsed with MilliQ purified water, before storage in 70% ethanol until use.

2.2.9 Seeding cells onto coverslips

Prepared coverslips were removed from storage in 70% ethanol and allowed to air dry before cells were seeded. They were then carefully transferred to the wells of 24-well plates. Coverslips were either coated in gelatin or PDMS to allow a 'hard' vs 'soft' comparison. For the gelatin coating, 50µl of 0.1% gelatin was dispensed onto each coverslip and these were then incubated at 37°C for ~20 min. Excess gelatin was then aspirated. A layer of collagen was then added by incubating coverslips in a solution of collagen from calf skin (Sigma) mixed 1 in 10 with water overnight, and then aspirating the next day. For the PDMS coating, 50µl sterile PDMS was dispensed onto each coverslip and allowed to set at room temperature for ~2 days. Before adding the collagen solution, these surfaces had to be treated a UV-activated crosslinker (Sulfo-SANPAH, Pierce). When surfaces were ready, 100µl of cell suspension was added at a density of $1x10^5$ cells/ml. Cells were incubated at the required temperature for 30min to allow cells to attach to the surface, and then ~400µl additional growth media was added. Cells were allowed to proliferate and later differentiate on coverslips.

2.2.10 Preparation of PDMS surfaces

Synthetic culture surfaces were fabricated using Sylgard 184 (Dow Corning, US) elastomer and curing agent. When combined, the elastomer and curing agent form a silicone-based organic polymer known as polydimethylsiloxane (PDMS) (Oschner et al., 2007). PDMS was selected over other polymers for a multitude of reasons: low optical

transparency allowing good microscopic visualisation of cells, low autofluorescence, tight adherence to glass, high gas permeability, ease of moulding and relatively low cost (Elveflow, 2021). By using a curing agent to elastomer ratio of 1:50, an elastic modulus of ~12kPa was obtained. Using a w/w ratio, components were weighed into separate glass beakers and autoclaved. Elastomer and curing agent were then mixed together thoroughly with a sterile metal spatula before transfer to a 15ml falcon tube. The PDMS mixture was centrifuged at 1000 *xg* for 2 mins to degas, and a snipped pipette tip was then used to dispense 1ml of the mixture onto the surface of a 60mm diameter Nunc™ petri dish. The PDMS was carefully smoothed across the entirety of the surface with a sterile metal spatula and left to set at room temperature for 48hrs.

2.2.11 Crosslinking collagen to surfaces

To improve the adherence, fusion and differentiation of cells cultured on the PDMS surfaces, collagen was crosslinked onto the surface (Oschner et al., 2007). Collagen was selected over other ECM proteins because it is the most abundant component of the skeletal muscle ECM and forms a very thin layer that would not alter the elasticity of the PDMS (Gillies and Lieber, 2011). Other ECM coatings such as Matrigel™ form a much thicker layer than would introduce a new component of elasticity. Collagen solution was prepared by mixing 0.1% solution type 1 collagen from calf skin (Sigma) diluted 1 in 10 with sterile water, and a hetero-bifunctional crosslinking agent, N-sulphosuccinimidyl-6-(4′-azido- 2′-nitrophenylamino) hexanoate (Sulfo-SANPAH) (Pierce, cat no. 2324-50) was prepared in a 0.5mg/ml solution with 50mM HEPES buffer at pH 8.5. 3ml Sulfo-SANPAH solution was added to each coated petri dish, to cover the surface. Dishes were then irradiated with a UV source for 8 mins, activating the crosslinker. After exposure, spent Sulfo-SANPAH was aspirated and wells washed with HEPES solution. Another 3ml Sulfo-SANPAH was added to each dish and the previous step repeated. 3ml collagen solution was then applied to each surface and allowed to adhere for 4hrs

at room temperature, before being washed 3 times with PBS (Wong, 1993). For standard petri dishes that were not coated with PDMS, a crosslinker was not necessary and collagen was applied using the same process, omitting the Sulfo-SANPAH treatment.

2.2.12 Isolation of RNA from cultured cells

To determine levels of gene expression on standard versus PDMS surfaces, RNA was isolated from C1F cells at different stages of differentiation. C1F myoblasts were originally isolated from the hindlimb muscles of neonatal (1 day old) 'immorto' mice (Morgan et al., 1994) and shown to differentiate into myotubes (Peltzer et al., 2008). C1F myoblasts were proliferated in medium composed of DMEM 1X + GlutaMAX supplemented with 20% heat inactivated foetal bovine serum (FBS, Gibco), 2% chick embryo extract (CEE, E.G.G. Technologies), 1% (v/v) Penicillin/Streptomycin (P/S, Gibco) and were incubated at 33°C with 10% CO2. The growth medium was supplemented with 20 U/ml gamma interferon (γFN, Life Technologies) (Morgan et al., 1994). Cells were switched to differentiate by exchanging the cells into differentiation medium, removing the γFN and raising the incubation temperature to 37°C with 5% CO2. Differentiation medium was composed of 1X DMEM + GlutaMAX (Gibco) supplemented with 4% horse serum (Gibco), 1% CEE and 1% (v/v) P/S. Cells at passage 3 were seeded onto standard or PDMS coated 60mm Nunc™ petri dishes at a density of $2x10^5$ cells/ml.

Cells were harvested as undifferentiated cells (UD), and at days 1, 3, and 7 of differentiation. Sampling undifferentiated cells allowed observation of gene expression in proliferating myoblasts, at day 1 observation of fusing myoblasts, at day 3 observation of myotubes early in the differentiation process, and at day 7, myotubes that are more mature with more developed sarcomeres. Cells on the softer surfaces were additionally harvested at day 5 of differentiation to capture any additional changes in gene expression

as myotubes mature. At each time point, they were lysed directly with TRIzol™ (Invitrogen) reagent, by adding 1ml TRIzol™ to each dish, and using a cell scraper to remove the adherent cells into solution. The resulting cell lysate was mixed thoroughly by pipette, placed into labelled Eppendorf tubes and mixed further by vortex. The lysed cell suspensions were stored at -80°C until they were sent for processing.

2.2.13 Sample processing

Processing of C1F samples was carried out at the Leeds Institute of Medical Research at St James's University Hospital, using their standard genomics workflow (Dembo and Wang, 1999). Briefly, RNA samples were treated with a TURBO DNA-free™ Kit (Ambion Inc.) using conditions recommended by the manufacturers, and then cleaned with an RNA Clean & Concentrator™-5 spin column (Zymo Research Corp.) RNA was tested for quality and yield using a NanoDrop 1000 spectrophotometer and an Agilent 2100 Bioanalyzer.

To minimize bubble PCR artefacts, we used 100 ng of purified total RNA in library preparation, following the "TruSeq" Illumina protocol. In brief, RNA was polyA-selected, chemically fragmented to about 200 nt in size, and cDNA synthesized using random hexamer primers. Each individual library received a unique Illumina barcode. RNA-seq was performed on an Illumina HiSeq 2000 or HiSeq2500 instrument with six or eight libraries multiplexed per flow-cell lane using 151 bp paired-end reads.

2.2.14 Bioinformatic analysis

To generate differential gene expression data from the raw reads, files were processed through a standard bioinformatics workflow pipeline (Fig. 10). When sample sequencing runs were completed, the Tapestation stored read sequences and the corresponding quality score in a text-based format known as FASTQ files. Quality control of the FASTQ files was carried out using FastQC, a programme designed to spot potential problems

(such as poor base sequence quality or unusual distribution of GC content) in high throughput sequencing datasets (Illumina, 2014). FastQC software can be downloaded at www.illumina.com and requires Java to operate. Following import of the data to the programme, a summary was generated flagging up any problematic areas within the data. Summary graphs and tables were also produced, allowing quick assessment of the data. FASTQ file results were then exported to an HTML based permanent report.

Adaptor sequences were then trimmed from the FASTQ files using the command line tool Cutadapt (Andrews, 2014). Reads containing an adaptor were either trimmed or completely discarded, and if reads were still outside of a specified length after the trimming process, these were also discarded. Cutadapt was also used to minimise the number of random hits, through the specification of a minimum amount of overlap between the read and the adaptor.

Reads were then trimmed or filtered according to their quality score using the open-source application PRINSEQ (Martin, 2011). The source code was obtained from http://prinseq.sourceforge.net/. PRINSEQ generated graphical information regarding the length, guanine-cytosine (GC) content, quality score and distribution of 'sequence complexity'. 'Sequence complexity' refers to sequence duplication, contamination, artifacts and ambiguous bases. The removal of duplicate sequences is necessary as their presence can result in false measures of differential expression downstream. Contamination within the read sequences can include unremoved tag sequences. Their removal with PRINSEQ allows for more precise read assembly. Ambiguous bases present as the letter "N" for positions that could not be identified as a particular base. This is indicative of a low-quality sequence, and may cause issues for downstream analysis. The percentage of 'N's in a dataset is a good indicator of the overall sequence quality (Schmieder and Edwards, 2011). Analysis was carried out online and data was then exported for subsequent offline analysis.

Raw reads were aligned to the mouse (*Mus Musculus*) full genome (GRCm38, UCSC mm10) using Spliced Transcripts Alignment to a Reference (STAR) software, a

splice-aware aligner (Huse et al., 2007). GTF transcript annotation files were downloaded from Ensembl. Transcripts were assembled using STAR, which aligned sequences to the reference mouse genome using two major steps; the seed searching step and the clustering, stitching and scoring step. The seed searching step locates splice junctions within the read sequence, without the need for prior knowledge of the splice junction's location or properties. In this step, STAR is also able to identify mismatches and indels within the sequence. Indels are intermediate long insertions or deletions, longer than 2 bases and shorter than the sequence reads. The presence of indels can cause significant issues with read alignment (Dobin et al., 2013). The clustering, stitching and scoring step of the read alignment involves gathering the 'seeds' identified in the first phase, clustering and stitching them together to build the alignment of the entire read sequence. This process is guided by a user-defined scoring system that considers matches, mismatches, insertions, deletions and splice junction gaps. The scoring system applies 'penalties', allowing a quantitative report on the quality and success of the alignment process.

The aligned reads were then processed using SAMtools, a set of utilities that can be accessed at http://samtools.sourceforge.net (Sun et al., 2017). SAMtools stored the aligned reads and carried out manipulation of the alignments, including filtering out unmatched reads. SAM files consist of a tab-delimited text file that contains sequence alignment data. At this stage, sequence alignment map (SAM) files were converted to binary alignment map (BAM) files, which saves on storage space since BAM files are stored as a binary representation of SAM data. In the BAM format, the files are also easier to manipulate.

Estimates of raw gene counts was then carried out using the featurecounts function of the Rsubread package (Li et al., 2009). Reads were inputted in BAM format, counted and summarised. Only uniquely mapped reads were counted by featurecounts, and overlapping reads were disregarded. As a result, pairs of reads that could be

mapped to two or more locations were not counted. This avoided the inaccurate detection of genes that were not truly up or downregulated at the RNA level.

Differential gene expression (DEG) was performed using DESeq2 with statistical significance expressed as a p-value adjusted for a false discovery rate of 0.05 using Benjamini-Hochberg correction for multiple-testing (Liao et al., 2019). Deseq2 can be accessed at http://www.bioconductor.org/packages/release/bioc/html/DESeq2.html (Love et al., 2014). The package utilises negative binomial generalised linear model (GLM) filling. Negative binomial GLM is a regression model whereby the dependent variable is a count of the number of times an event occurs. This can then estimate the dispersion and logarithmic fold changes of genes within the sample (Ander et al., 2010). The package applies the Wald test to the data in order to assess whether fold change is statistically significant or not. After running the data through the Deseq2 package, results tables were generated for experimental comparisons listed in Table 4. Alongside the relative fold change, the Reads per Kilobase of transcript per Million (RPKM) for selected sarcomeric genes at each individual time point was calculated and values for both surfaces plotted together for comparison.

T2 (standard): UD vs D1	T3 (PDMS): UD vs D1	UD: T2 (standard) vs T3 (PDMS)
T2 (standard): UD vs D3	T3 (PDMS): UD vs D3	D1: T2 (standard) vs T3 (PDMS)
T2 (standard): UD vs D7	T3 (PDMS): UD vs D5	D3: T2 (standard) vs T3 (PDMS)
	T3 (PDMS): UD vs D7	D7: T2 (standard) vs T3 (PDMS)

Table 4. Experimental group comparisons.

The results contained a list of gene symbols for all genes detected in the process, and information was arranged into categories listed in Table 5.

Column in results table generated by Deseq	Information provided by the column
basemean	Average of the normalized counts taken over all samples
Log2FoldChange	log2 fold change between the groups
lfcSE	Standard error of the log2FoldChange estimate
stat	Wald statistic
pvalue	Wald test p-value
padj	Benjamini-Hochberg adjusted p-value

Table 5. Report categories generated by Deseq2.

Spreadsheets of results were generated by the Leeds Institute for Data Analytics, and were subsequently analysed to investigate changes in gene expression and read count throughout the differentiation process on standard versus PDMS surfaces.

The FASTQ files for each of the 28 RNA-Seq samples have been successfully submitted to Sequence Read Archive (SRA) with the accession number: PRJNA682314.The DEG reports were used to compare expression in downstream analysis, using a cutoff of padj <0.05, and a fold change of >1 or <-1. WebGestalt (WEB-based Gene SeT AnaLysis Toolkit) was used for Over-representation/gene clustering analyses (Ren and Kuan, 2020; Liao et al., 2019). Additionally, we used Degpatterns to perform a gene clustering analysis using 5478 genes that were differentially expressed across time points for T2 and 8042 for T3 (cutoff of padj < 0.001). Values of RPKM (Reads per kilo base per million mapped reads) were used to compare expression levels for specific transcripts of interest.

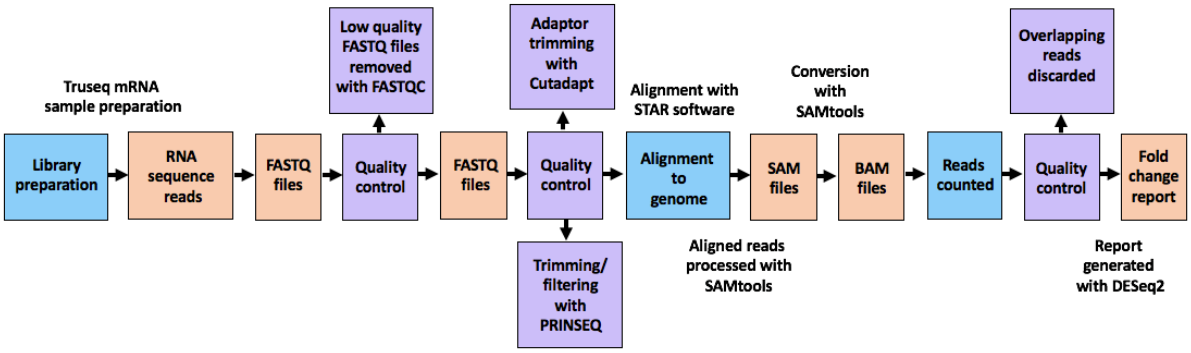

Figure 10. Standard bioinformatics workflow pipeline. Overall RNAseq workflow for read alignment, quality control and generation of final report on differential gene expression.

2.2.15 RNAseq data analysis

Changes in expression were ranked by sorting the Log2FC column from smallest to largest, using the 'Sort and Filter' tab in Excel. This listed genes in an order that placed most downregulated genes at the top, and most upregulated genes at the bottom. Fold change was classed as being large enough for consideration if it was less than -1 or greater than 1, so the formula, "=IF(OR(C2>1,C2<-1), "sig", "nonsig")" was applied to values in the Log2FC column. Fold change was deemed significant if the padj value was below 0.05, so the formula, "=IF(H2<0.05), "sig", "nonsig")" was applied to the values in the padj column. By applying this organisational strategy to all spreadsheets for all experimental time points, the top 20 up and downregulated genes at each day differentiation could be easily obtained.

This list of 20 genes was then pasted into the online gene set analysis toolkit, WebGestalt (WEB-based Gene SeT AnaLysis Toolkit : http://www.webgestalt.org) (Zhang et al., 2005). After pasting the list of gene names directly into the appropriate box, an analysis was performed using a set of parameters (Tables 6 & 7).

RNAseq analysis was performed for plastic (hard: T2) and PDMS (soft: T3) as triplicate biological repeats at each time point. However, data for one of the hard surface repeats was later excluded as the read length (101bp) was shorter than in later experiments (151bp) and a principal component analysis (PCA) plot showed that this earlier dataset failed to cluster with those from later experiments.

Webgestalt homepage option	Appropriate selection
Organism of interest	Mus musculus
Method of interest	Over-representation analysis (ORA)
Functional database	Geneontology (selecting either "cellular component", "biological process" or "molecular function" from the additional dropdown menu)
Select gene ID type	Gene symbol
Select reference set	Genome protein-coding

Table 6. WebGestalt Basic Analysis Parameters.

The advanced parameters are described in Table 4.

Webgestalt homepage option	Appropriate selection
Minimum number of genes for a category	5
Maximum number of genes for a category	2000
Multiple test adjustment	BH
Significance level	FDR 0.05
Number of categories expected from set cover	10
Number of categories visualised in the report	40
Colour in DAG	Continuous

Table 7. WebGestalt Advanced Analysis Parameters.

2.2.16 Immunocytochemistry

Immunocytochemistry was performed on C1F cells to visualise expression of myogenic transcription factors and sarcomeric myosin on standard versus PDMS cell culture surfaces. Standard surfaces were prepared by dispensing 50µl 0.01% gelatin in sterile water onto 13mm diameter round glass coverslips and allowing this to set at 37°C. Excess gelatin was then aspirated and the glass surfaces were coated with collagen from calf skin (Sigma), using the same dilution as described previously. Collagen from

calf skin (Sigma) was mixed 1 in 10 with sterile water and left to adhere for 4hrs at room temperature before excess was aspirated. Coverslips were coated with PDMS by preparing the curing agent and polymer as described previously, then 50µl PDMS was dispensed onto each coverslip and spread carefully with a sterile metal spatula. As before, PDMS was left to set for 48hrs and the surfaces were treated with sulfo-SANPAH to allow the adherence of collagen.

Cells at passage 3 were seeded onto coverslips at a density of $2x10^5$ cells/ml and as described previously, cells were harvested at UD, D1, and D3. Cells were fixed with 4% paraformaldehyde in phosphate-buffered saline (PBS) and washed 3x with PBS before being transferred to a staining board. To permeabilise cells, coverslips were treated with 50µl of permeabilization solution: 0.1% Triton X-100 diluted in PBS containing 1% bovine serum albumin (BSA) (Thermo Fisher Scientific), for 5 minutes prior to staining. Primary antibody was diluted in wash buffer (1% BSA in PBS) using the dilution described (Table 8). This was applied to coverslips, followed by incubation for 1hr at room temperature in a dark moist chamber. Primary antibody was then removed and coverslips washed 5 times with wash buffer. Secondary antibody was diluted in wash buffer using dilution as described (Table 8), and then applied to coverslips with an incubation time of 1hr. Following removal of the secondary antibody, coverslips were washed 5 times with wash buffer and once with PBS, before being mounted onto glass slides with Prolong® Gold anti-fade mountant (Invitrogen). Slides were left to dry at room temperature in the dark overnight and stored at 4°C before imaging.

Antibody	Dilution	Species	Catalogue no.
Pax7 (DSHB hybridoma)	1:20	Mouse	N/A
Pax3 (DSHB hybridoma)	1:20	Mouse	N/A
MyoD (Invitrogen)	1:100	Mouse	MA1-41017
Myogenin (Invitrogen)	1:50	Mouse	MA511486
A4.1025	1:10	Mouse	Peckham lab (Silberstein et al., 1986)
Alexa 546 anti-mouse (Invitrogen)	1:400	Goat	A-11030
Alexa 488 anti-mouse (Invitrogen)	1:400	Goat	A28175
DAPI	1:500	N/A	40043

Table 8. Antibodies and their dilutions. Primary and secondary antibodies used and their dilutions. DSHB: Developmental Studies hybridoma bank.

2.2.17 Fusion index

Cells were visualised using the upright LSM880 confocal microscope (Zeiss) and fluorescent images were obtained using excitation/emission filters in the DAPI and FITC (or TRITC) channels using a 40x objective lens (N.A 1.4).

To estimate the fusion index, cells were stained with the primary antibody A4.1025 (diluted at 1 in 10) to stain up skeletal muscle myosin (all isoforms) (Jat et al., 1991) and DAPI (4'6-diaminidino-2-phenylindole) to stain DNA (1/500 dilution), followed by anti-mouse Alexa-Fluor 488 or Alexa-Fluor 546 secondary antibody (1/400 dilution). Images of the cells were captured using a Delta Vision Widefield Deconvolution Microscope (Delta Vision, USA) using a 40x objective lens (N.A. 1.4). Three biological repeats were performed, and cell images were taken from 10 random fields of view for each repeat. The fusion index was determined by dividing the total number of nuclei found within myotubes (identified by their positive staining for skeletal myosin (using A4.1025)) by the total number of nuclei in the field of view (Millay et al., 2013). Cells were additionally imaged using an LSM880 confocal microscope (Zeiss) and 40x objective lens (N.A 1.4) to visualise differentiation.

2.2.18 Myotube analysis

High magnification images of C1F cells stained for skeletal myosin were obtained on an LSM880 confocal microscope and 40x objective lens, allowing visualisation of the sarcomere on differentiated myotubes. Images from three biological repeats were analysed using Image J processing software (NIH). To obtain measurements of myotube width, 20 myotubes per repeat were selected at random and the width of each measured using the software. Similarly, the total number of nuclei within myotubes were counted and recorded from 20 randomly selected myotubes. Level of striation was assessed by assigning 20 randomly selected myotubes into one of three categories: “fully striated”, “partially striated” or “no striations”. This analysis was carried out on myotubes grown on hard (T2) and PDMS (T3), and values compared.

2.2.19 Statistical analyses

Statistical tests were performed and graphs generated using GraphPad Prism version 8 for Mac (GraphPad Software, La Jolla California, USA, www.graphpad.com). Graphs show mean ± standard deviation (S.D) for each observation. Unpaired t-tests with Welch’s correction and one-way and two-way ANOVAs were carried out to test for any statistically significant differences between conditions. The level of statistical significance is indicated by the number of asterisks displayed above graphs: **** represents a P value <0.0001. *** represents a p value <0.001. ** represents a P value <0.01. * represents a p value <0.05.

2.3 Results

2.3.1 Mapping and alignment of reads was successful

The quality and success of the read alignment was assessed by accessing the report generated by the differentially expressed genes (DEG) analysis. Within each batch, there were a very high number of raw reads, number of clean reads, percentage mapping,

percentage uniquely mapped reads and percentage successfully aligned fragments. Results for both batches were combined to give an overall percentage for each sample time point (Table 9). The consistently high percentages of mapping and alignment at each sample day suggests that the sample processing was successful. As such, results generated from these samples could be trusted as being uniquely mapped reads.

Sample day	Avg mapping %	Avg % mapping rate	Avg % successfully aligned fragments
UD	99.22	92.73	49.15
D1	99.06	93.11	48.65
D3	99.11	92.00	48.13
D5	99.49	93.59	43.60
D7	98.86	90.81	47.90

Table 9. Average percentages of mapping and successful alignment of reads at each time point, for both sample batches.

2.3.2 Overall gene expression is affected by the culture surface

At each time-point, a list of up and downregulated genes on hard surfaces compared to soft was generated, and the top 100 up and downregulated genes for each condition are listed in Annex 1 for reference. At UD, 312 genes were upregulated and 905 genes were downregulated At D1, 1122 genes were upregulated and 2019 genes were downregulated. At D3, 376 genes were upregulated and 453 genes were downregulated. At D5, 602 genes were upregulated and 350 genes were downregulated The PCA analysis (Fig. 11) shows that the RNA data for samples on hard (T2) or for soft (T3) surfaces tend to cluster together for each day of sampling. This indicates that gene expression patterns within each sample are highly correlated. Samples for the two different treatments tend to cluster into different groups, suggesting that gene expression is affected by the surface on which the cells were grown. Repeats for the same conditions do not completely overlap, as there will be some variation in the data, from sequencing lanes or sample variation/experimental set up. Hierarchical analysis (Fig. 12) also shows that samples within each treatment (hard (T2) vs soft (T3) cluster

together but samples from different treatments are less closely linked. The overall analysis of gene expression shows a marked difference between cells grown on standard plastic surfaces (T2: hard) compared to PDMS (T3: soft) surfaces.

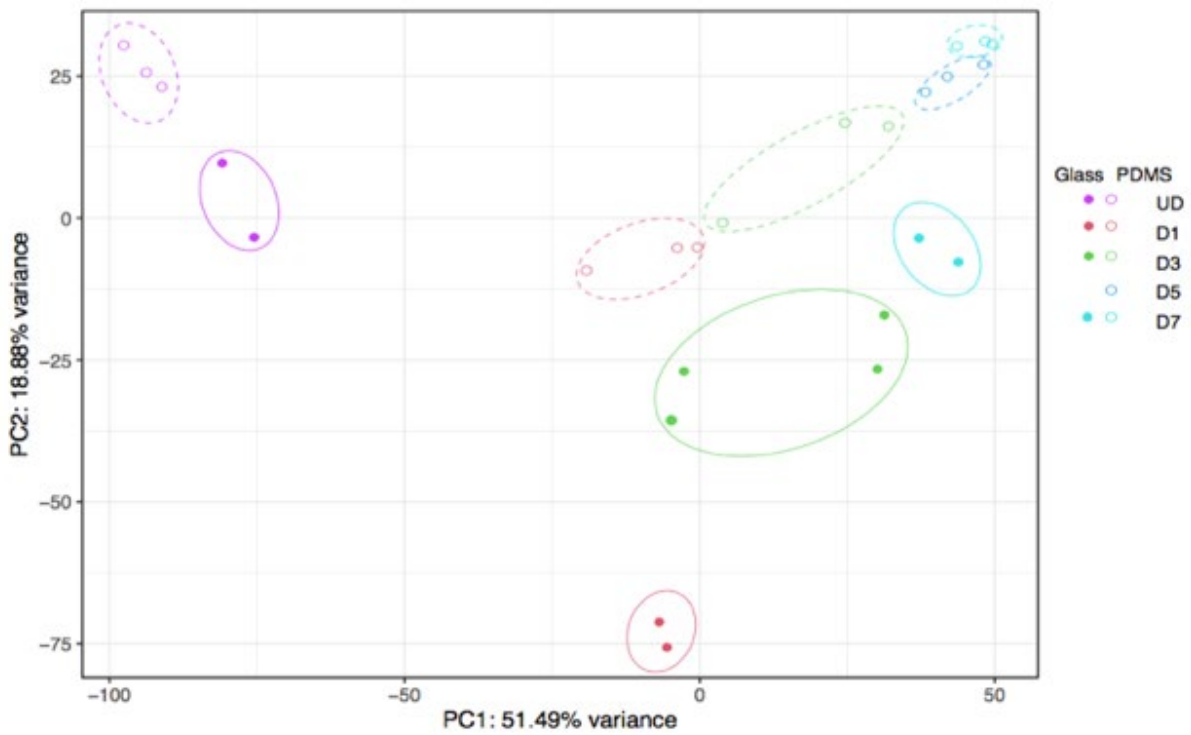

Figure 11. PCA plot for cells differentiating on either hard or soft surfaces. Principal component analysis (PCA) for each set of samples at each time point. The 'hard' surface (~60GPa stiffness) are the results for cells grown and differentiated on plastic. The 'soft' surface (~12kPa) are the results for cells grown and differentiated on PDMS. At each time point, the values for samples on hard surfaces and PDMS surfaces are shown. Dashed coloured lines: T3 (soft surface) and solid-coloured lines T2 (hard surface).

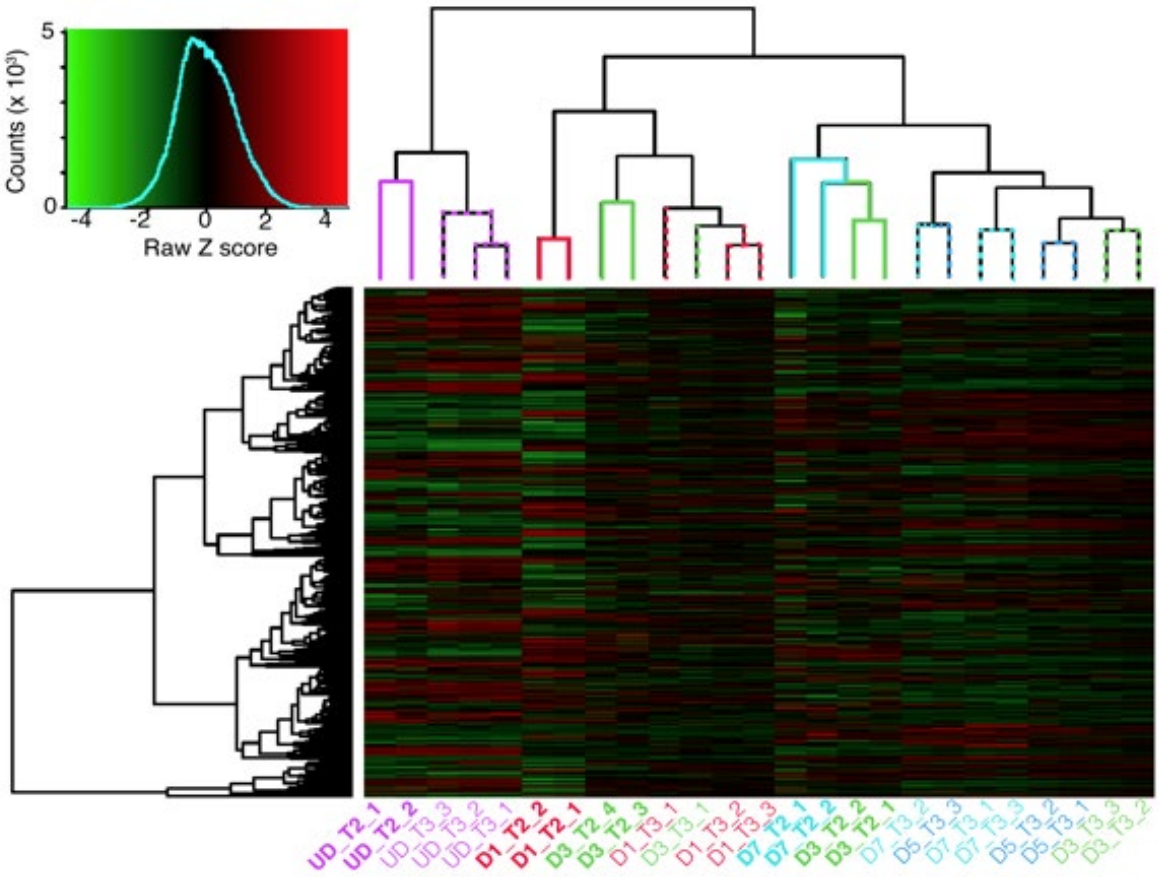

Figure 12. Dendogram for cells differentiating on either hard or soft surfaces. Hierarchical clustering of gene expression for cells grown on hard or soft surfaces at different each time point. The branch length at the top of the figures indicates the level of dissimilarity between sample clusters (those with shorter branches have a higher degree of similarity). Each individual branch represents a group of related genes expressed within the corresponding sample labelled underneath. Bold font: T2 (hard surface) and Light font: T3 (soft surface). UD: magenta, D1: red, D3: green, D5 (T3 only): blue and D7: cyan.

2.3.3 Comparison of overall gene expression between hard and soft surfaces over time revealed distinct clusters of genes

Cluster analysis was carried out to reveal patterns of gene expression. On both surfaces, changes in gene expression over the seven-day differentiation period were found to have different patterns. Cluster patterns that are similar on hard and soft surfaces were compared to identify genes that overlapped in expression on both surfaces, and genes that were exclusively expressed by cells grown on one or the other surface. This analysis revealed that although similar patterns of expression were observed on hard and soft surfaces, within each of these patterns, only a proportion of expressed genes were the same on both surfaces. Ultimately this affirms that there are many genes present in the soft dataset that are not present in the hard dataset and vice versa.

2.3.4 Enrichment analysis revealed upregulated genes involved in specific processes

Enrichment analysis determined two major categories of genes that were upregulated on softer surfaces compared to hard; genes involved in muscle cell development and sarcomerogenesis. Analysis of these gene lists in Webgestalt returned associated Gene Ontology (GO) terms that were related to these clusters. Ultimately, allowing us to see the biological processes that are enhanced on PDMS surfaces.

Within each of these clusters, the fold change of all associated genes within the cluster was observed (Fig. 13)Differences in expression levels are consistently observed between the two surfaces, with greater overall fold changes being observed on PDMS for both clusters. The genes that were listed within each cluster associated with biological processes of interest informed the choice of individual genes that would later be explored and compared between conditions. Alongside these genes that were flagged by the Webgestalt analysis, key myogenic transcription factor genes, and genes involved in

sarcomerigenesis were prioritised for individual comparison in order to reveal how the surface stiffness affects myogenesis.

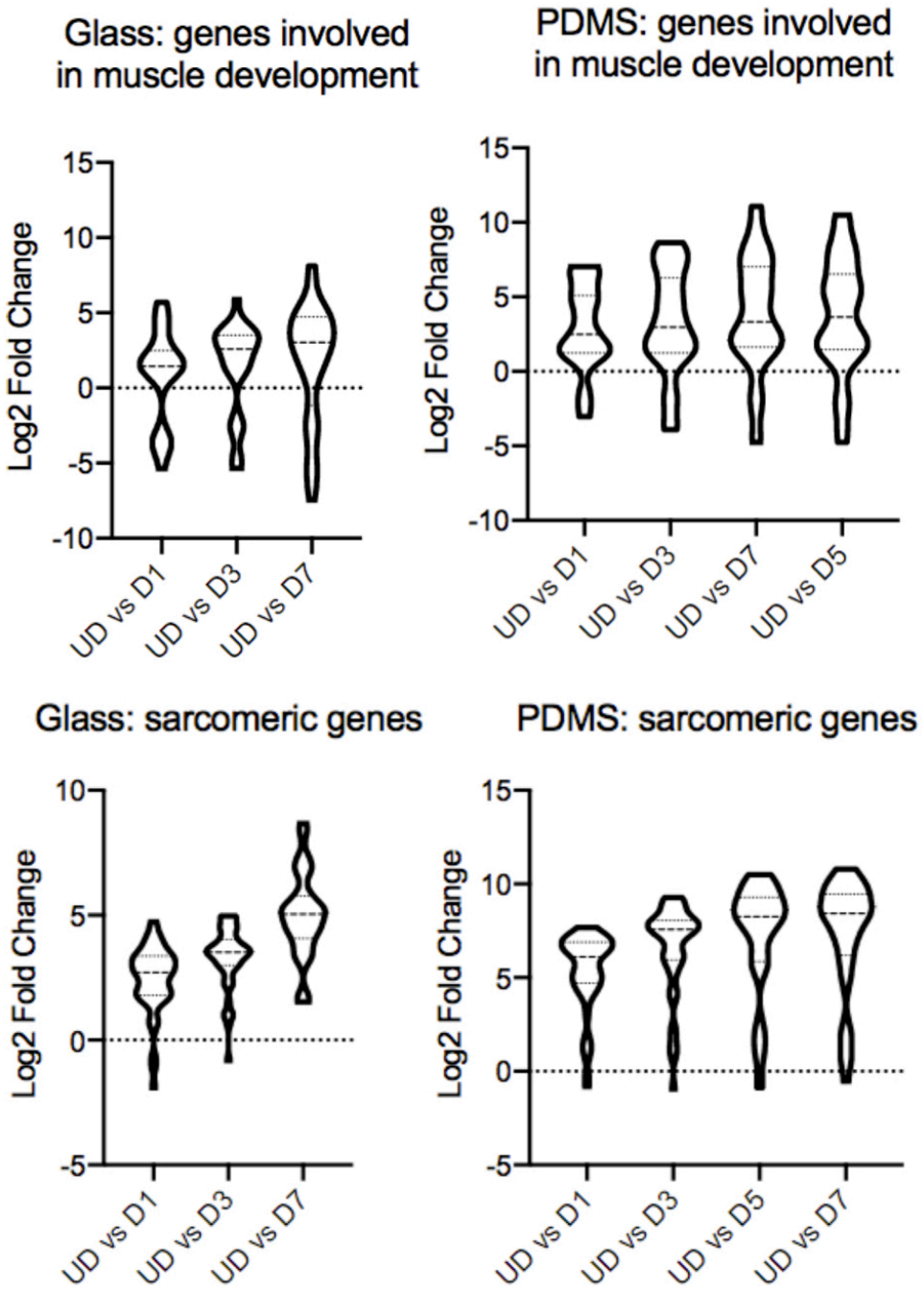

Figure 13. Fold change of genes within clusters. Violin plots showing entire distribution of fold change of genes within each cluster on hard and soft surfaces at each time point.

Additionally, Webgestalt analysis of genes expressed at >1 fold higher (log2fold change) on hard surfaces than on soft surfaces (padj <0.05) revealed that RNA expression for genes associated with the extracellular matrix (ECM) were higher on hard surfaces (Fig. 14). The ECM genes that changed the most within the ECM GO category were the collagen genes, of which the majority showed higher expression on hard surfaces compared to soft, with a peak at D1 differentiation. Subverting the general trend within this GO category, Col8a2 showed increased expression on soft surfaces compared to hard. Genes encoding ECM structural constituent, ECM binding and growth factor binding were enriched for cells cultured on hard surfaces across the time course (Fig. 14). Genes identified within these GO categories included laminins (Lama2, Lama5, Lamb1, Lamb2), integrins (Itga5, Itga7, Itgb1) and Nidogen (Nid1). Like the collagen genes, genes within these GO categories showed highest expression at D1 on hard surfaces. Thus, growing cells on hard surfaces increases gene expression for a range of range of ECM and associated proteins, as well as the receptors that bind these proteins.

A global analysis of the change in expression levels across genes that show a significant change (pAdj<0.05; log2fold change is < or >1), showed that the largest difference in gene expression occurred at day 1 (D1) of differentiation. This is consistent with the switch to terminal differentiation into myotubes at D1.

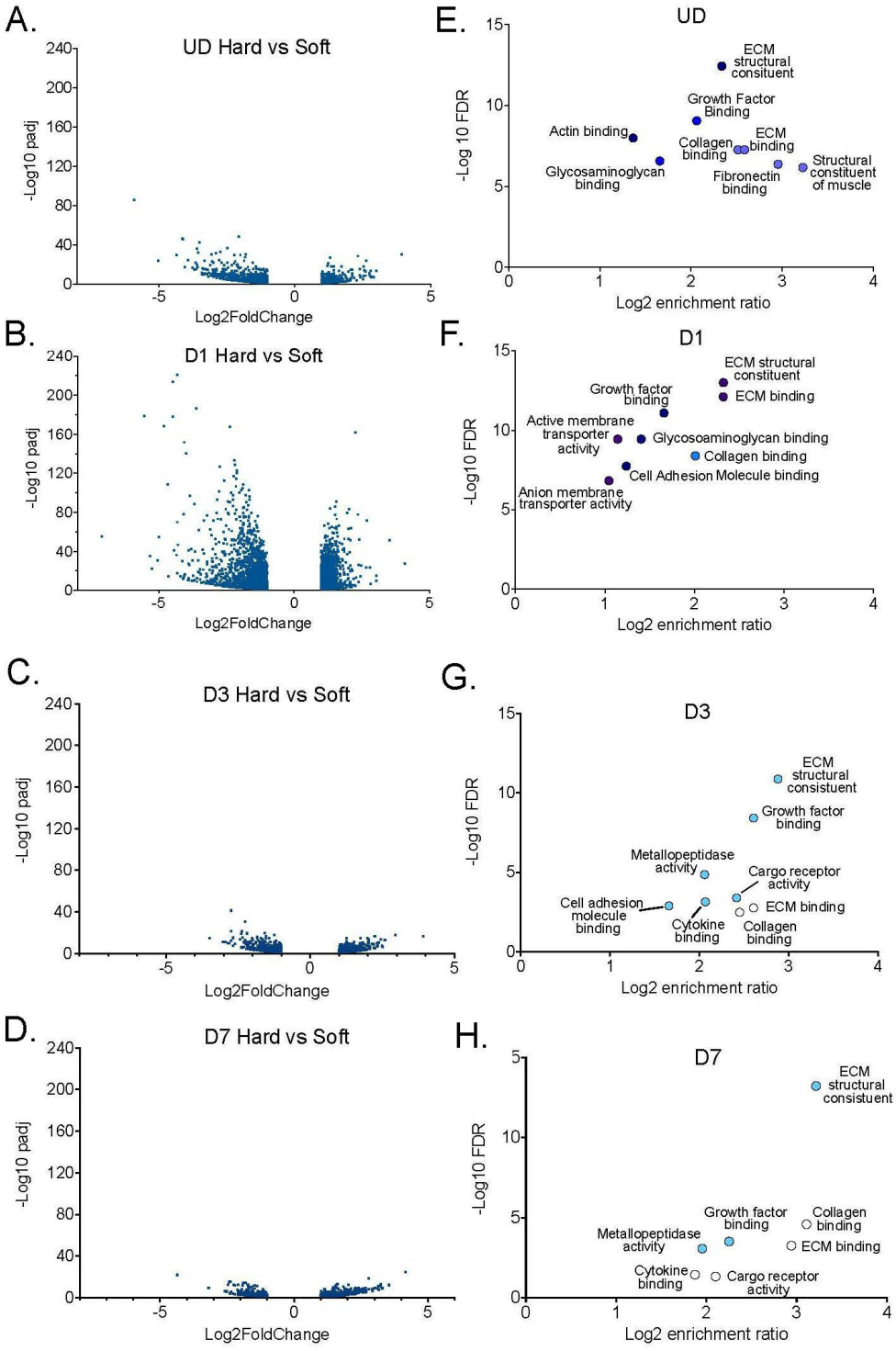

Figure 14. Global comparison of changes in gene expression levels at each time point between soft and hard surfaces. A-D. Volcano plots for gene expression where the fold change is either >1 or <-1, and where the padj is <0.05. **E-H.** Results from a Webgestalt analysis for enriched gene sets (molecular function) at each time point, for a comparison of T2 with T3, down-regulated genes (e.g lower expression in T3). The log10 false discovery rates (FDR) are shown for those with a p value of <0.05. The symbol colour for each gene set is related to the number of enriched genes within each gene set from dark blue (>100) to white (<20).

2.3.5 C1F differentiation is improved on soft surfaces

Pax3 and Pax7 were used in the analysis as markers of myogenic cells. The RNAseq data demonstrated that undifferentiated (UD) C1F cells on soft and hard surfaces express Pax3 (Fig. 15A) and that these levels decreased as the cells differentiated, as expected (Fig. 15A). RPKM levels were analysed as a means of observing the absolute number of reads mapped to a gene, to supplement the information on relative fold change from one condition to another. A differential gene (DEG) analysis showed that levels of Pax3 were significantly lower at each day (D1-D7) of differentiation compared to UD cells (Fig. 15A, B) on soft surfaces. Levels did not significantly decrease on soft surfaces compared to UD until D7 on hard surfaces. Directly comparing Pax3 levels between cells on soft and hard surfaces showed a small but increase in expression of Pax3 in D1 cells on soft surfaces (Fig. 15C), suggesting that soft surfaces might promote higher levels of Pax3 expression.

In contrast, levels of Pax7 in cells cultured on soft surfaces were very low (Fig. 15D). A differential gene (DEG) analysis of Pax7 comparing expression levels at D1-7 with those in UD cells did not show any significant changes on soft surfaces (Fig. 15E). Expression of Pax7 appears to be higher for cells grown on hard surfaces and appears to increase from UD to D1 and D3 (Fig. 15D). However, a differential gene analysis shows no significant change in expression from between UD cells and D1-7 cells (Fig. 15E). A direct comparison of Pax7 expression between soft and hard surfaces (Fig. 15C) does show a significant difference in expression at each time point. This is likely due to the very low expression levels of Pax7 in cells on soft surfaces. Additionally, no Pax7 was detected in C1F cells that were stained for it using immunofluorescence, but Pax3 staining was present in cells grown on both surfaces. The RNAseq and immunofluorescence data taken together suggests that C1F cells predominantly express Pax3 and not Pax7. This difference is particularly apparent when cells are cultured on softer surfaces closer in stiffness to that of natural muscle. The increase in Pax7

expression on stiffer surfaces is suggestive of the C1F cells operating in a state that is further from their behaviour *in vivo*.

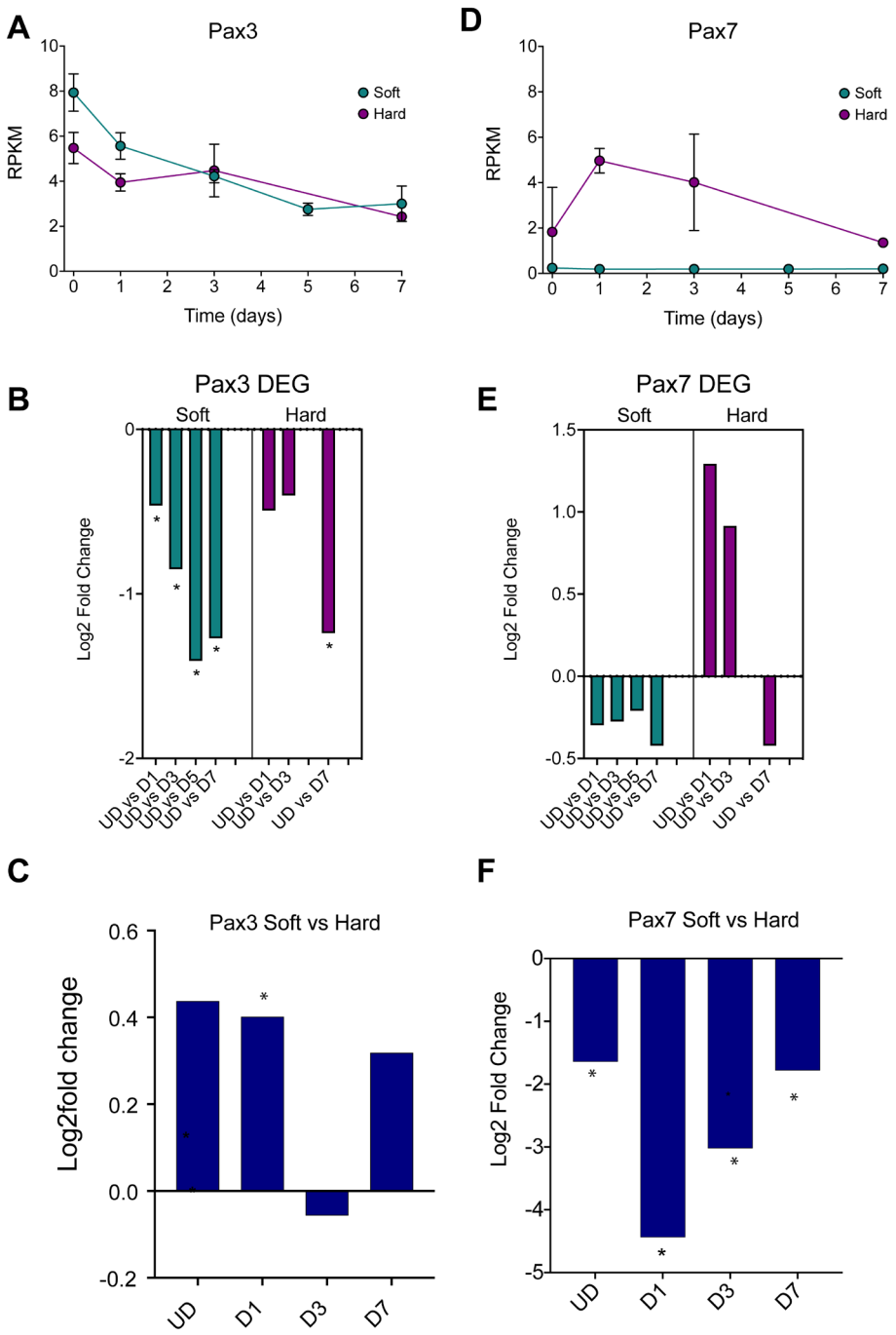

Figure 15. Comparison of Pax3 and Pax7 expression profiles on soft and hard surfaces for C1F cells. A, D. RPKM values for each time point samples for soft and hard surfaces, from undifferentiated cells (UD) to Day 7 of differentiation (D7). Error bars show the standard deviation (S.D.). **B, E.** Differential gene analysis (DEG) for Pax3 and Pax7, comparing UD with D1, D3, D5 and/or D7 on soft and hard surfaces * indicates padj <0.05. all other results are not significantly different. **C, F.** Results for DEG comparing T2 with T3 from UD to D7, * indicates padj <0.05.

Next, the expression patterns of the 4 myogenic regulatory factors Myf5, MyoD, myogenin and MRF4 (Myf6) belonging to the helix-loop-helix family of transcription factors, were investigated (Hernandez-Hernandez et al., 2017; Zammit, 2017). Expression levels of Myf5 were decreased significantly in differentiating cells at D1 to D7 compared to UD cells, for cells grown on soft surfaces (Fig. 16A, B) showing a similar change in expression to Pax3. Levels also decrease significantly for cells grown on hard surfaces (Fig. 16A, B). As the levels of Pax3 and Myf5 decrease, the levels of MyoD increased (Fig. 16A). A differential gene analysis showed that the expression levels of MyoD were increased significantly at D1-D3 compared to UD cells on both soft and hard surfaces and is also increased significantly at D5 and D7 compared to UD on soft surfaces. Myogenin expression is increased significantly in cells at D1-D7 compared to undifferentiated cells (Fig. 16A, B). Myf6 expression is significantly increased at later time points, from D3 onwards, compared to UD cells (Fig. 16A, B). Levels of Mef2a,c and d increased significantly from UD cells to D1-7 cells on both hard and soft surfaces and the magnitude of the log2fold change was higher on soft surfaces (Fig. 16A, B).

Directly comparing gene expression for all these transcription factors at D1 showed expression is significantly higher for cells on soft, compared to hard surfaces, with the exception of Myf6 (Mrf4) (Fig. 16C). Strikingly, the increase in expression levels for myogenin between UD and D1 was much higher for cells on soft surfaces compared to those on hard surfaces (Fig. 16C). At this time point, fusion of myoblasts would ordinarily be occurring, a process driven by myomixer. As myogenin is a master regulator of differentiation, this indicates that the cells on soft surfaces may fuse earlier and thereby begin differentiating into mature myotubes at a faster rate than those on hard surfaces.

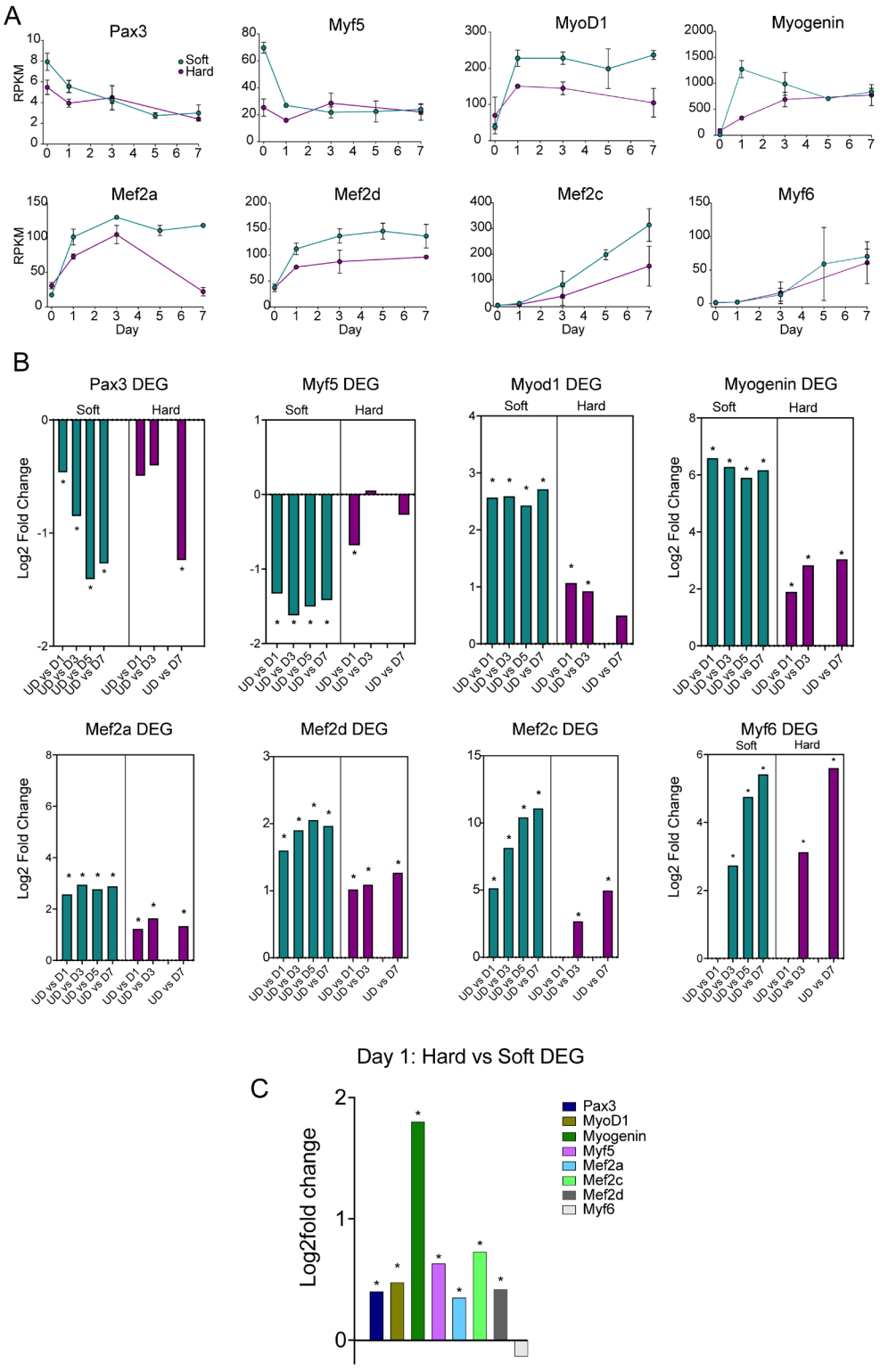

Figure 16. Expression of myogenic factors on soft and hard surfaces in C1F cells. A. RPKM values for each time point samples for soft and hard surfaces, from undifferentiated cells (UD) to Day 7 of differentiation (D7). Error bars show the standard deviation (S.D.). **B.** Differential gene analysis (DEG) for each of the myogenic factors over time, comparing UD with D1 etc, for soft and hard surfaces, * indicates padj <0.05. **C.** Results for a DEG comparing T2 with T3 at day 1, where the main changes in myogenic factors are observed, * indicates padj <0.05.

The general trend for expression of a selection of sarcomeric proteins was investigated next, with a focus on key structural proteins, such as skeletal (Acta1) and cardiac actin (Actc1), actinin-2 (ACTN2: found in the z-disc), myosin heavy chain genes (Myh3 – embryonic, Myh8 – perinatal, and Myh7 – slow/β-cardiac), titin (Ttn), nebulin (Neb), t-cap, myosin binding protein-C (Mybpc) and Unc45b, a specific striated muscle chaperone, important for the folding of myosin. As myoblasts begin to fuse, α-cardiac actin, α-skeletal actin, myosin light chain 1, myosin light chain 3 and embryonic myosin light chain genes are upregulated. As myotubes mature, there is a shift from predominantly α-cardiac actin to predominantly α-skeletal actin. Interestingly, a transition from embryonic to adult myosin light chains was not observed. Changes in differential expression of these sarcomeric genes were consistent both *in vivo* and *in vitro*. The changes in RNA for all of these genes shows a general increase in levels as the cells differentiate, consistent with the myogenic nature of the C1F clone (Fig. 17). However, changes were more marked for cells cultured on soft surfaces (Fig. 17A, B). Directly comparing soft with hard surfaces (Fig. 17C) shows that RNA expression levels for many sarcomeric genes are lower on soft than for hard surfaces in undifferentiated cells. This suggests that growth on soft surfaces might tend to inhibit differentiation. This difference in expression quickly reverses on day 1 for many of these genes, with expression levels significantly higher in cells cultured on soft surfaces, concomitant with the increase in myogenin levels (Fig. 16) as cells switch to differentiation.

In addition to the sarcomeric genes, the expression pattern for two key genes that encode membrane proteins myomixer (Gm7325) and myomerger (Tmem8c) was investigated. The expression of both genes is increased significantly from D1-7 on both soft and hard surfaces, compared to undifferentiated cells (Fig. 17A, B). Expression of myomixer is increased significantly at D1 on soft surfaces compared to hard surfaces (Fig. 17C). Expression of Notch1 increases significantly between UD and D1 of differentiation on both hard and soft surfaces (Fig. 17A, B). Moreover, there is a

significantly higher level of expression of Notch1 in cells cultured on hard surfaces at D1 (Fig. 17C). This is interesting, as we might have expected Notch1 to decrease at D1, as the cells cease proliferating and start differentiating. MEGF10 has been suggested to interact with Notch1 and to be significantly downregulated when C2C12 cells were induced to differentiate by serum withdrawal (Holterman et al., 2007). We found that expression levels of MEGF10 increased significantly between undifferentiated cells and D1 on both soft and hard surfaces. However, on soft surfaces, MEGF10 levels remain significantly elevated at D3-7 compared to UD cells, while on hard surfaces, MEGF10 levels do not. MEGF10 levels are significantly increased for cells cultured on hard surfaces at D1 (Fig. 17C) and then significantly increased for cells cultured on soft surfaces at D7.

Overall, this analysis of gene expression demonstrates that Pax3 positive C1F cells express a range of markers for myogenic differentiation, with a pattern consistent with differentiation of myoblasts into multinucleated myotubes.

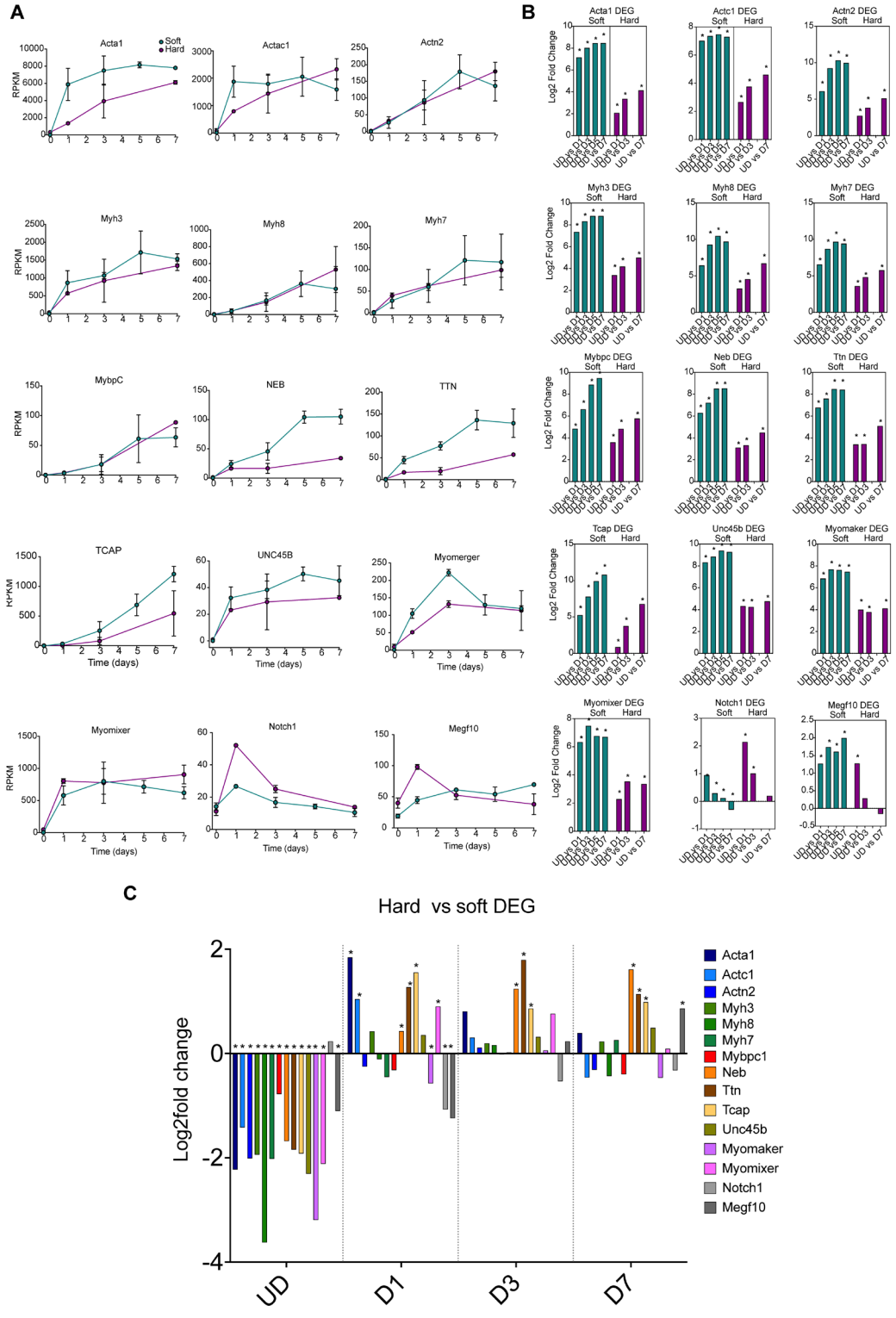

Figure 17. Expression of sarcomeric genes on soft and hard surfaces in C1F cells. A. RPKM values for each time point samples for soft and hard surfaces, from undifferentiated cells (UD) to Day 7 of differentiation (D7). Error bars show the standard deviation (S.D.). **B.** Differential gene analysis (DEG) for each of the genes over time, comparing UD with D1 etc, for soft and hard surfaces, * indicates padj <0.05. C shows the results for a DEG comparing T2 with T3 at each day from UD to D7, * indicates padj <0.05.

2.3.6 Differential gene expression of collagen genes is different on hard and soft surfaces

Next, the expression of collagen (COL) genes found in the ECM structural constituent category between hard and soft surfaces at each time point was analysed. This analysis focused on genes with the highest RPKM values and known to be associated with skeletal muscle ECM (Csapo et al., 2020). Almost all the COL genes analysed showed a high early peak in RNA expression at D1 in cells cultured and a generally higher overall RNA expression of collagen genes (Fig. 18A) on hard surfaces. A differential gene analysis (DEG) that compared expression levels at each day of differentiation with that in undifferentiated cells grown on the same type of surface showed similar trends for collagen expression for most collagen genes (both Col1 genes, Col3a1, Col5a1 and 2, both Col8 genes, Col12a1, Col16a1 and Col18a1 (Fig. 18B). A differential expression analysis comparing expression at each time point between soft and hard surfaces, showed higher levels of collagen in cells cultured on hard surfaces (Fig. 18C).

While the general trend in differential expression of collagen genes was similar, some differences were observed. The RNA expression profiles of COL4 genes (Collagen IV: Col4A1, 4A2 and 4A5) between cells cultured on soft and hard surfaces. On hard surfaces, the RNA expression levels for Col4 peaked at day 1, and levels were higher than that found for cells cultured on soft surfaces. A differential gene analysis showed RNA levels from D1-D7 were lower than in UD cells for cells cultured on soft surfaces (Fig. 18B). In contrast RNA levels increased at D1 for cells cultured on hard surfaces before then decreasing from D3-D7, but levels remained higher than in UD cells. A direct comparison between soft and hard surfaces showed that Col4 RNA levels for each of these three isoforms were higher in undifferentiated cells on soft surfaces compared to those on hard surfaces (Fig. 18C). Also of note is that there is an expression peak of Col8a2 on soft surfaces, but not on hard surfaces, the reverse of the general trend.

Finally, Col25a1 continues to increase from UD to D7 on soft surfaces but after increasing at D1, it stays about the same on hard surfaces.

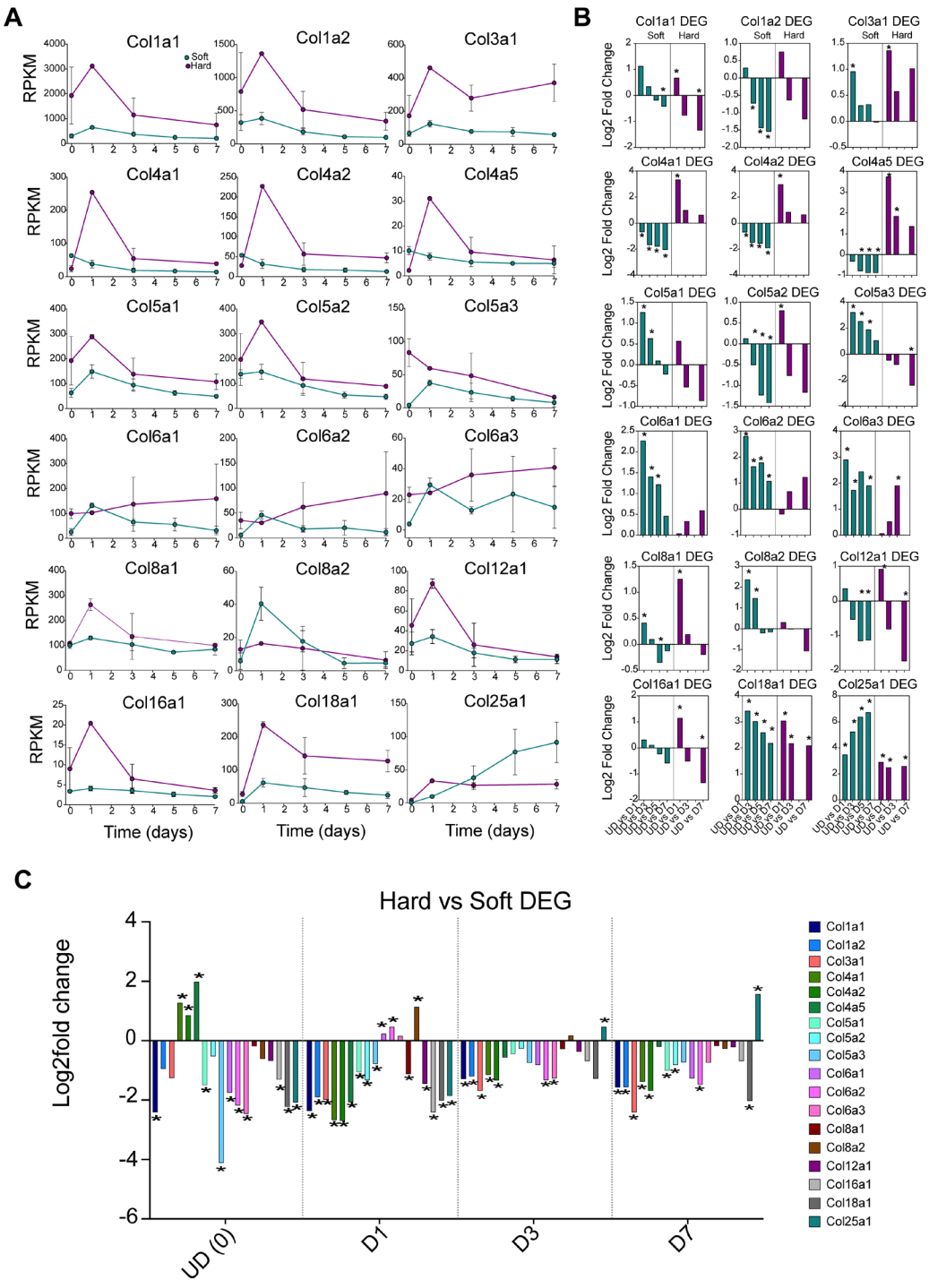

Figure 18. Comparison of gene expression for collagens important in muscle on hard and soft surfaces over time. A. RPKM plots for hard (magenta) and soft (green) surfaces for each of the collagens, over time. Day 0 (D0) represents undifferentiated cells (UD). Days 1-7 represent the time course of differentiation. **B.** Differential gene analysis for each day of differentiation (D1-7) to undifferentiated cells (UD) for cells cultured on hard and on soft surfaces, *indicates significant change in Log2fold expression (padj value <0.05). **C.** Differential gene analysis for expression levels of each collagen isoform between hard and soft surfaces, at each day (from UD to D7), * indicates significant change in Log2fold expression (padj value <0.05)

2.3.7 Differential gene expression analysis of laminin, nidogen and integrin genes was different on hard and soft surfaces

Differential gene expression analysis was carried out on laminins and other proteins found in the ECM. Laminins (Lama2, Lama5, Lamb1, Lamb2) also show a clear peak in expression at day 1 on hard surfaces (Fig. 19A) consistent with the idea that the cells on hard surfaces are stimulated more strongly to create their own ECM niche. Nidogen (Nid1) also showed a higher peak of expression at day 1 on harder surfaces (Fig. 19A). Of the integrin genes with the highest levels of RNA (as judged by RPKM levels) integrins α5 (Itga5), α7 (Itga7) and β1 (Itgb1) had a peak of expression at day 1 on hard surfaces, which was higher than that on soft surfaces (Fig. 19A, C). A differential gene analysis over time, on hard and on soft surfaces showed a general decrease in expression for the majority of these genes.

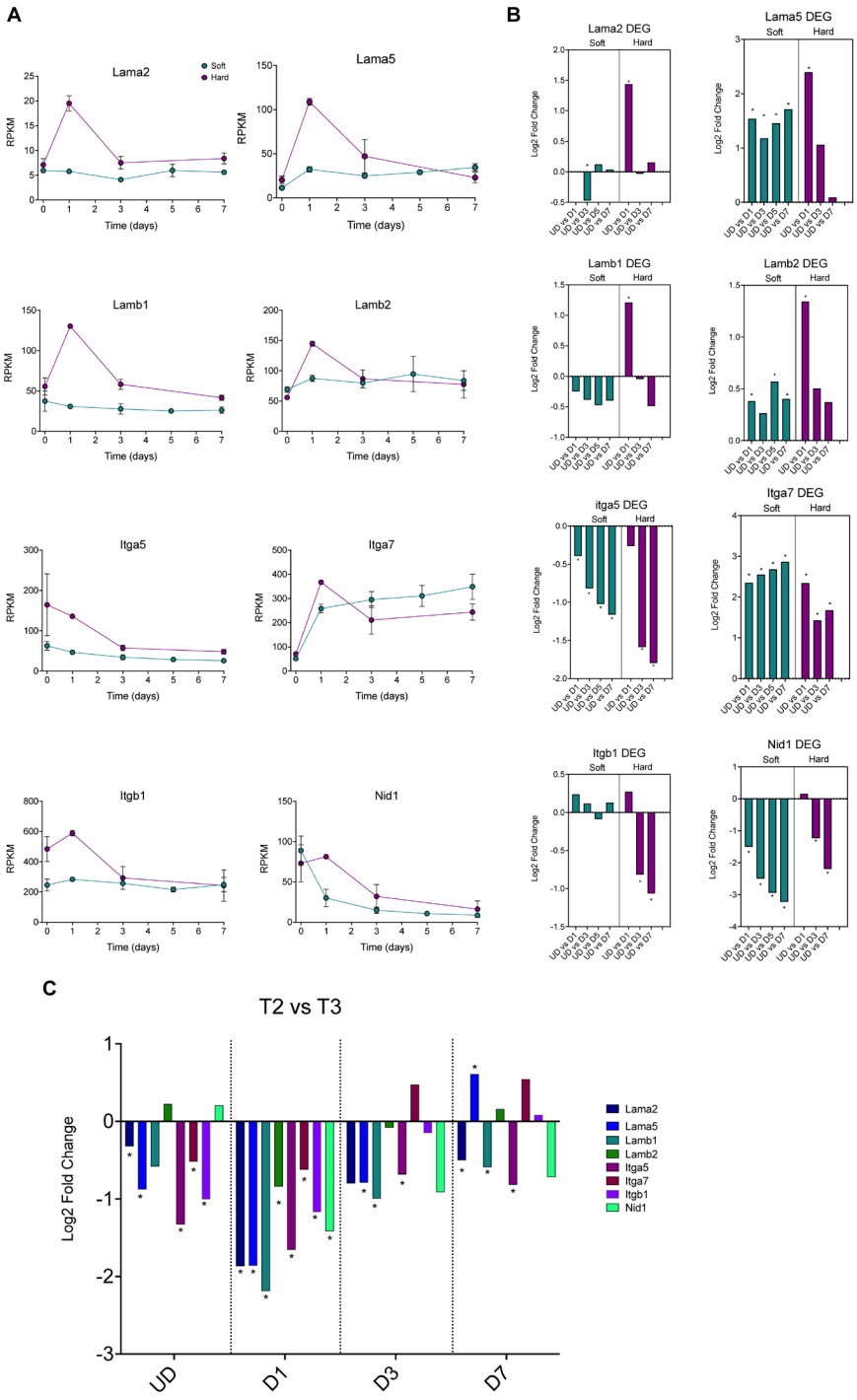

Figure 19. Comparison of gene expression for laminins, integrins and Nid1 (nidogen) on hard and soft surfaces over time. A. RPKM plots for hard (magenta) and soft (green) surfaces for each of the genes of interest, over time. Day 0 (D0) represents undifferentiated cells (UD). Days 1-7 represent the time course of differentiation. **B.** Differential gene analysis comparing each day of differentiation (D1-7) to undifferentiated cells (UD) for cells cultured on hard and on soft surfaces, *indicates significant change in Log2fold expression (padj value <0.05). **C.** Differential gene analysis for expression levels of each collagen isoform between hard and soft surfaces, at each day (from UD to D7), * indicates significant change in Log2fold expression (padj value <0.05)

2.3.8 Improved myoblast fusion and myofibrillogenesis occurred on soft surfaces

To supplement the RNAseq analysis exploring changes in gene expression during differentiation, percentage fusion on both surfaces was measured (Fig. 20). The percentage fusion was greater for T3 at D1, D3 and D5 differentiation, until a plateau was reached at D7 whereby % fusion was not significantly different. The greatest difference in fusion between the surfaces was at D1, when average fusion was 52% for T2 and 87% for T3. Staining for skeletal myosin and DAPI revealed that for T3, myotubes appeared thicker and had more well-defined sarcomeric striations (Fig. 21A, B). The average diameter of myotubes grown on PDMS surfaces (T3) was 29μm, compared to only 19μm on hard surfaces (T2), a difference that was found to be significant (Fig. 22A). When striation organisation was compared between cells grown on the two surfaces, a significantly greater proportion of myotubes were fully straited for T3, compared to T2 (Fig. 22B). Both had a similar proportion of myotubes that were partially straited, and while cells grown on PDMS had less myotubes that completely lacked striation, this difference was not found to be significant (Fig. 22B). The differences observed through myosin staining suggests that soft, PDMS surfaces offer an optimised environment for the fusion and subsequent differentiation of cultured myoblasts.

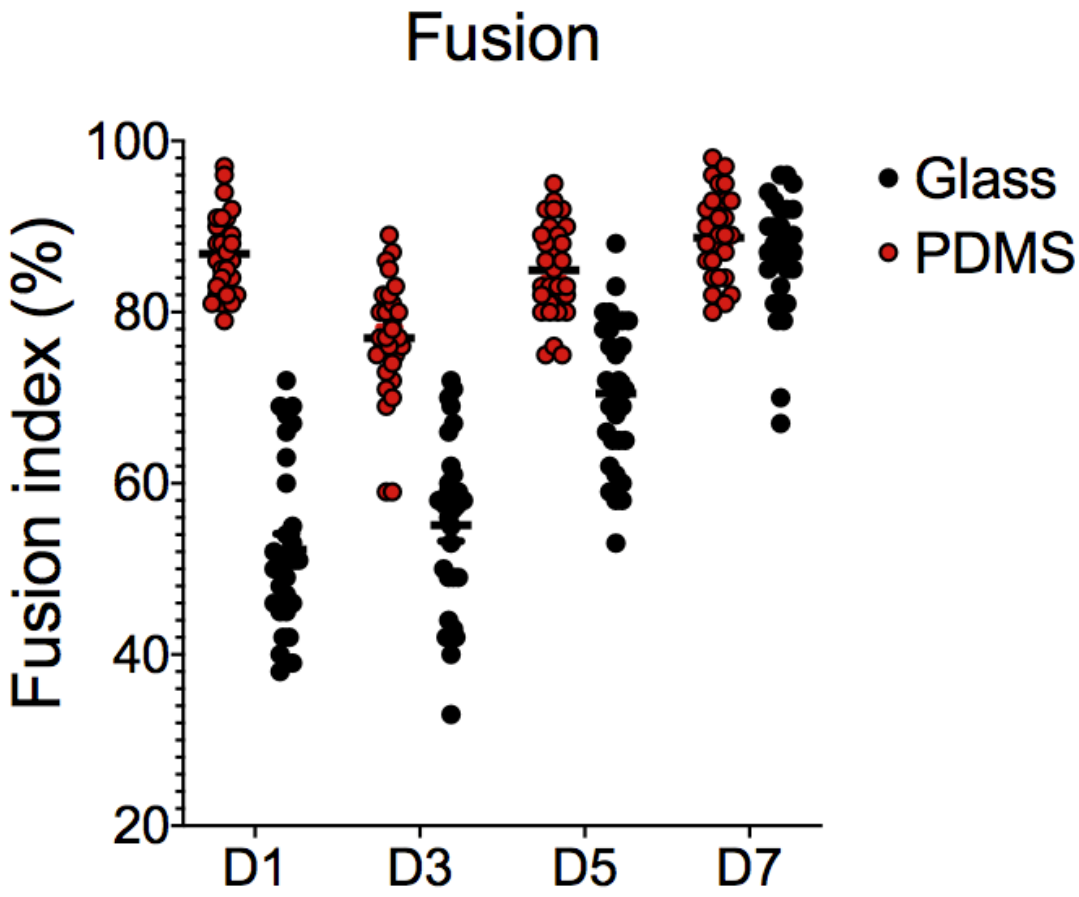

Figure 20. Fusion index analysis to determine fusion of myoblasts on hard and soft surfaces. A. Percentage of fused myoblasts averaged over 10 fields of view. n=3 experiments.

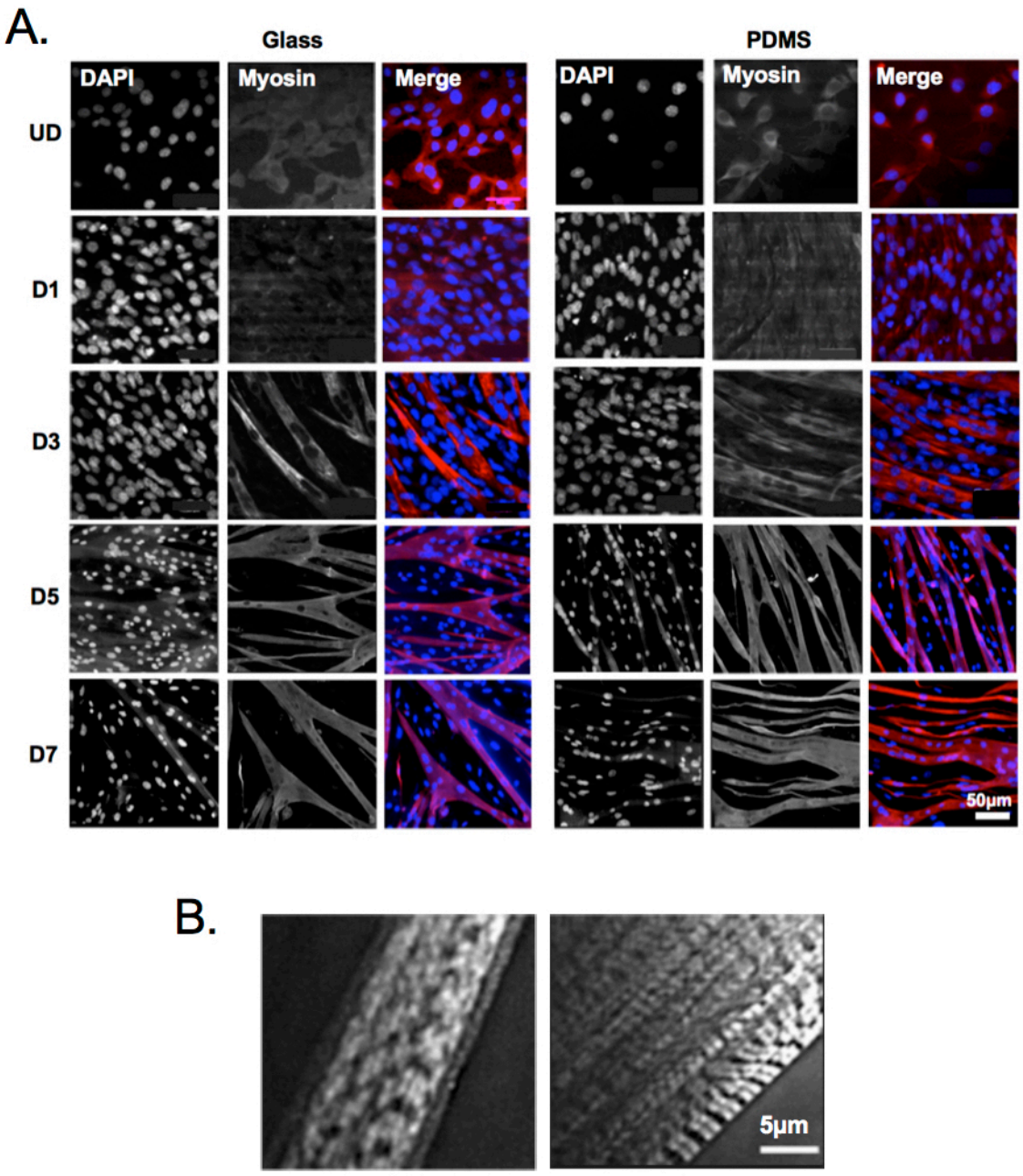

Figure 21. Immunofluorescent staining of C1F cells on glass and PDMS. A. Representative images of C1F cells stained for skeletal muscle myosin, (shown in red in the merged image), and the nucleus (DAPI, shown in blue in the merged image) from days 1-7 (D1-7). **B.** Striations along the sarcomere of a D7 differentiated myotube cultured on glass and PDMS.

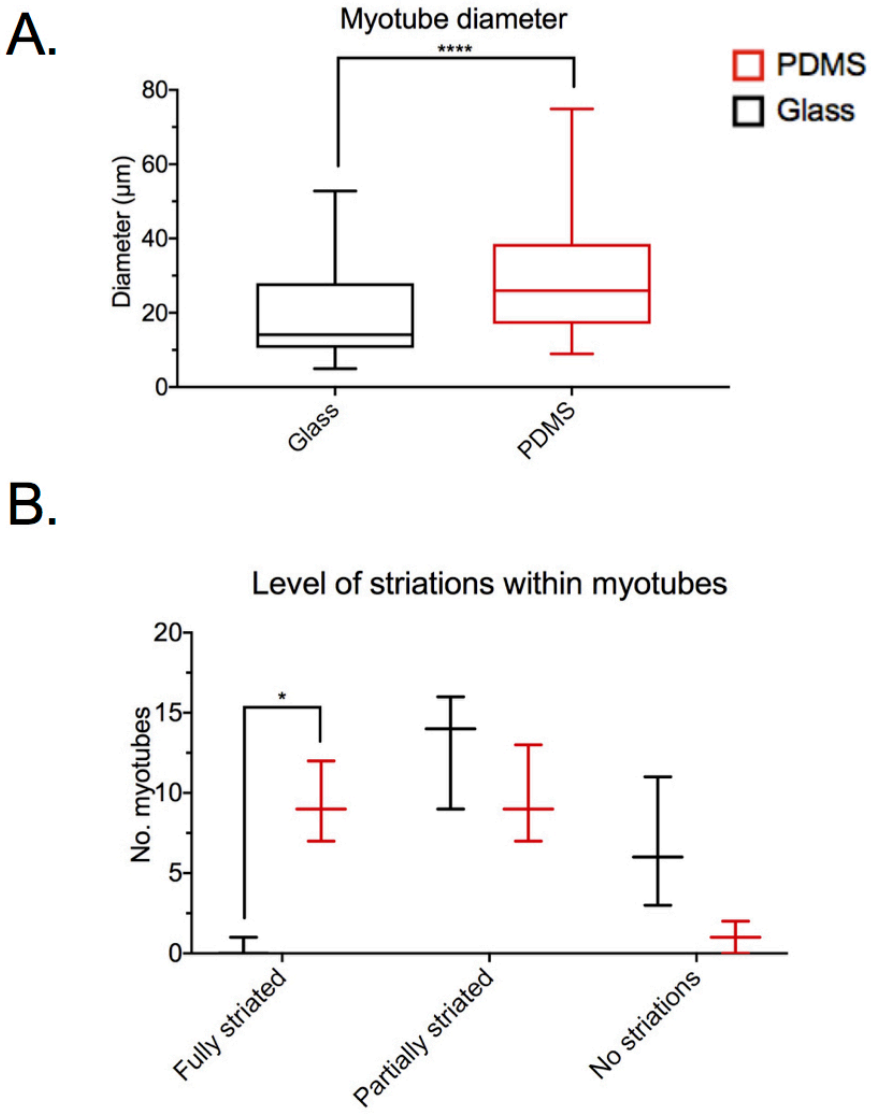

Figure 22. Comparison of myotube development. A. Box plots showing the diameter of myotubes for T2 vs T3. **B**. Box plots showing the degree of striation achieved by myotubes for T2 vs T3. Box plots show minimum, first quartile, median, third quartile and maximum values in each graph. Error bars represent S.D. ** p <0.01, **** p <0.0001.

2.3.9 Differences in myogenic transcription factor expression for soft vs hard surfaces

Immunostaining and quantification of transcription factors (Pax3, MyoD and myogenin) at each time point, C1F cells were stained for Pax3, MyoD and myogenin showed changes in expression similar to that observed by RNASeq (Fig. 23, 24, 25). Quantification of transcription factor staining revealed differences in expression of each TF, on soft surfaces compared to hard. During proliferation (UD) and at D1 of differentiation, when Pax3 is most highly expressed, expression was significantly greater on T3 (Fig. 26A). In proliferating cells, the average number of myoblasts expressing Pax3 was only 27% for T2, compared to 44% for T3, suggesting that these surfaces promote enhanced proliferation in addition to fusion. Changes in MyoD expression were similar, with significantly greater expression for T3 at all stages of differentiation (Fig. 26B). Similar to the findings in the RNAseq analysis, a spike of MyoD was observed at D1 on T3, whereas the peak on T2 occurred at D3 of differentiation. The same trend was observed when C1Fs were stained for myogenin, with a spike in expression at D1 for T3, compared to a D3 peak for T2 (Fig. 26C). Expression was significantly lower for T2 at both D1 and D3 differentiation, but the largest difference in expression was at D1, with an average of 9% myogenin^{+} nuclei for T2 and 80% for T3. Ultimately, the results of the ICC analysis support the trends of TF expression, and differences between surfaces, observed in the RNAseq analysis.

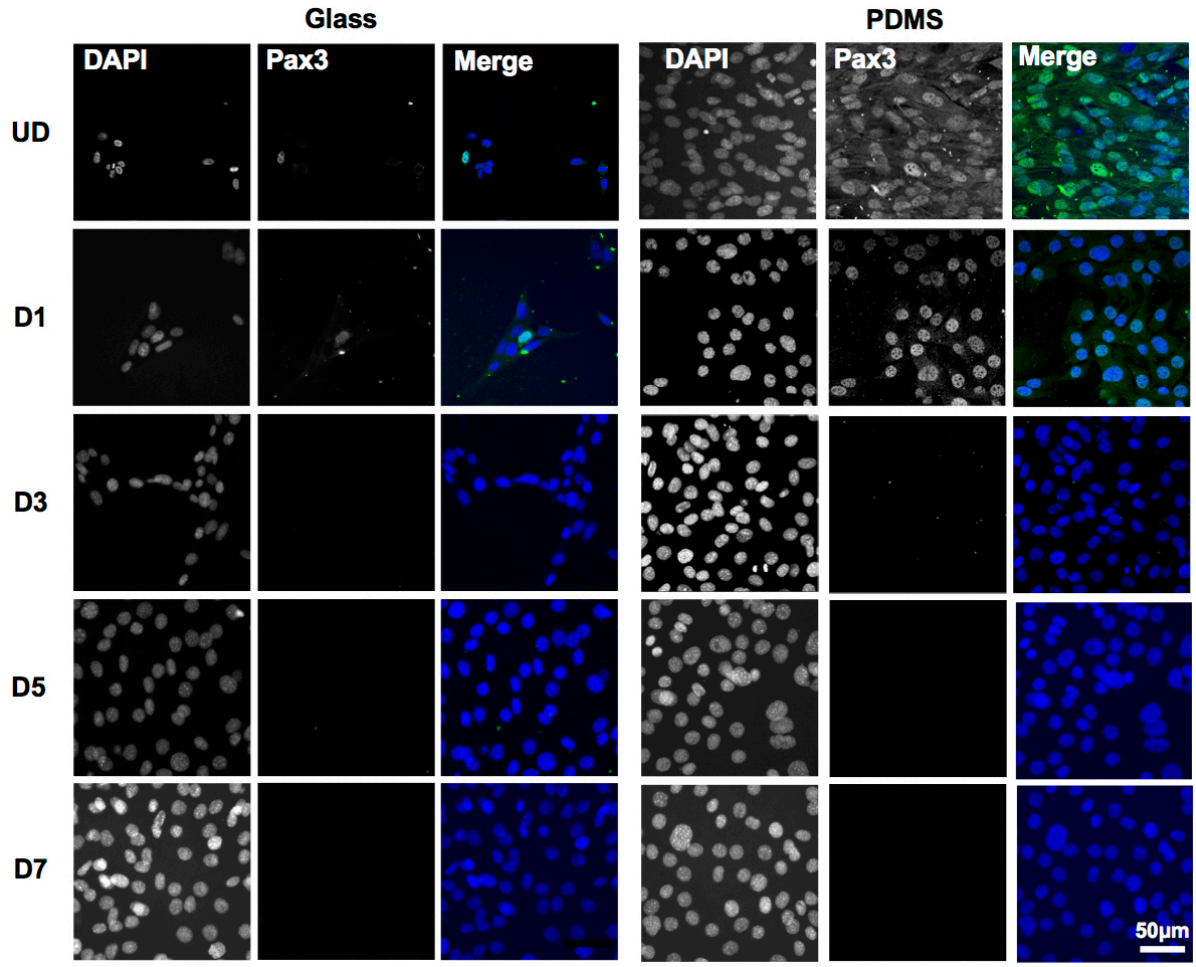

Figure 23. Immunofluorescent staining of Pax3 for C1F cells on glass and PDMS. Representative images of C1F cells stained for Pax3 (shown in green in the merged image), and the nucleus (DAPI, shown in blue in the merged image) from days 1-7 (D1-7).

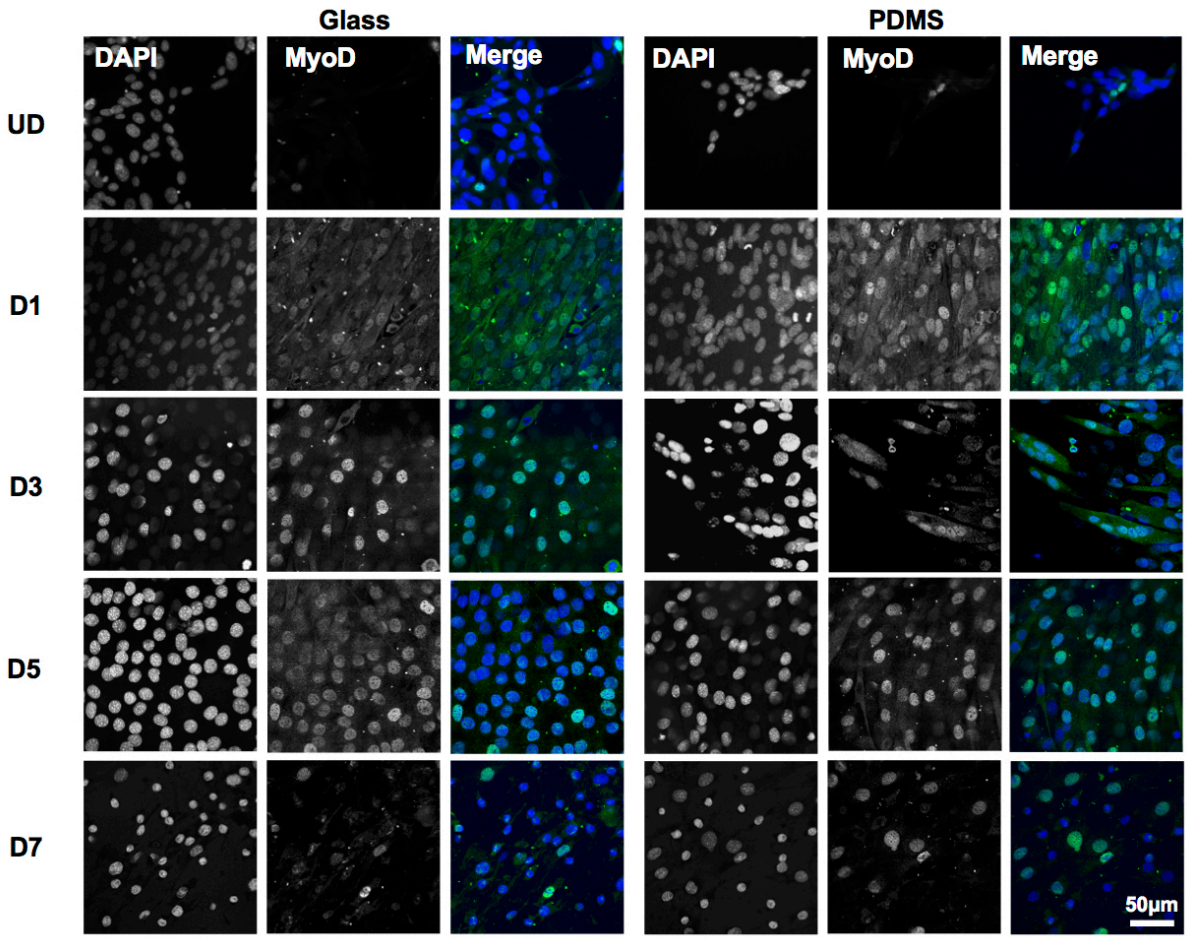

Figure 24. Immunofluorescent staining of MyoD for C1F cells on glass and PDMS. Representative images of C1F cells stained for MyoD (shown in green in the merged image), and the nucleus (DAPI, shown in blue in the merged image) from days 1-7 (D1-7).

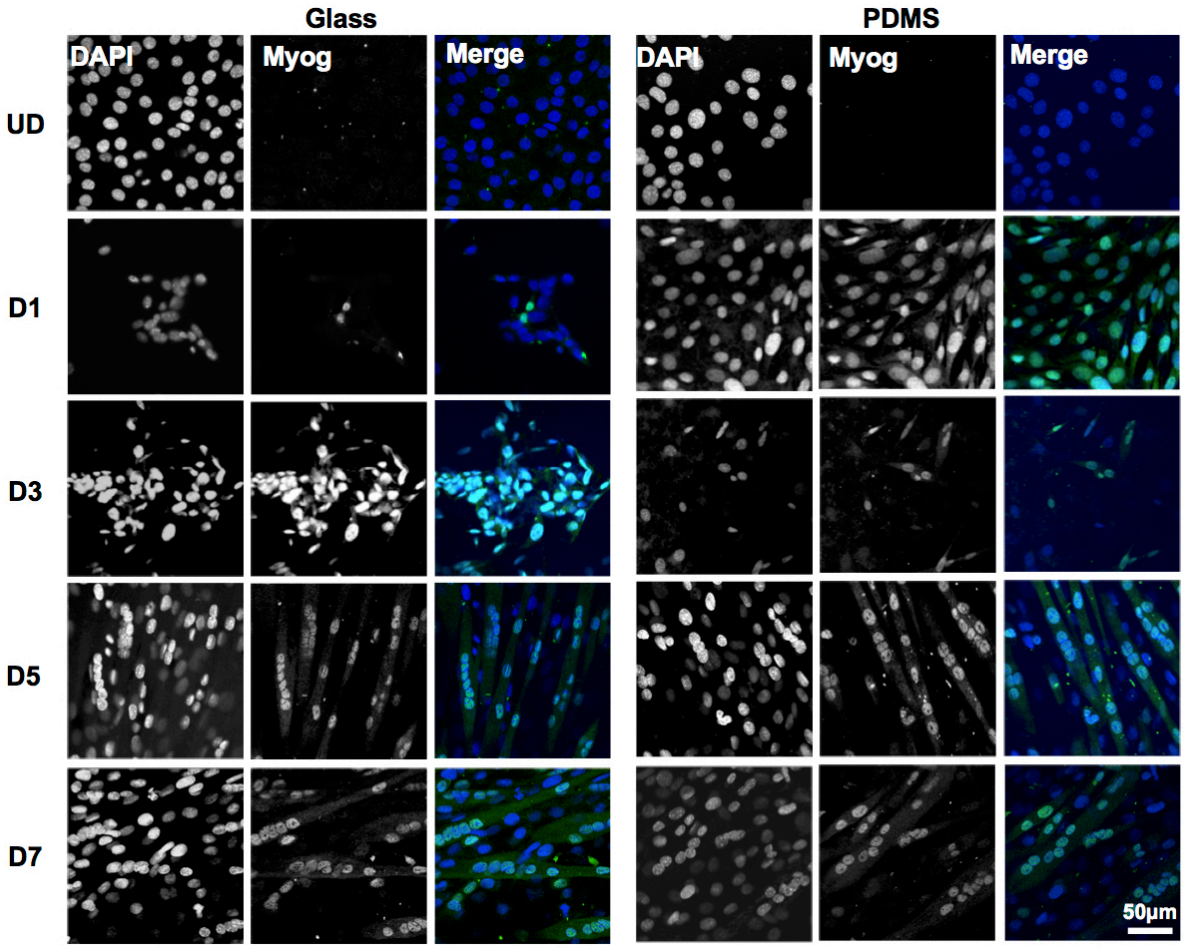

Figure 25. Immunofluorescent staining of myogenin for C1F cells on glass and PDMS. Representative images of C1F cells stained for myogenin (shown in green in the merged image), and the nucleus (DAPI, shown in blue in the merged image) from days 1-7 (D1-7).

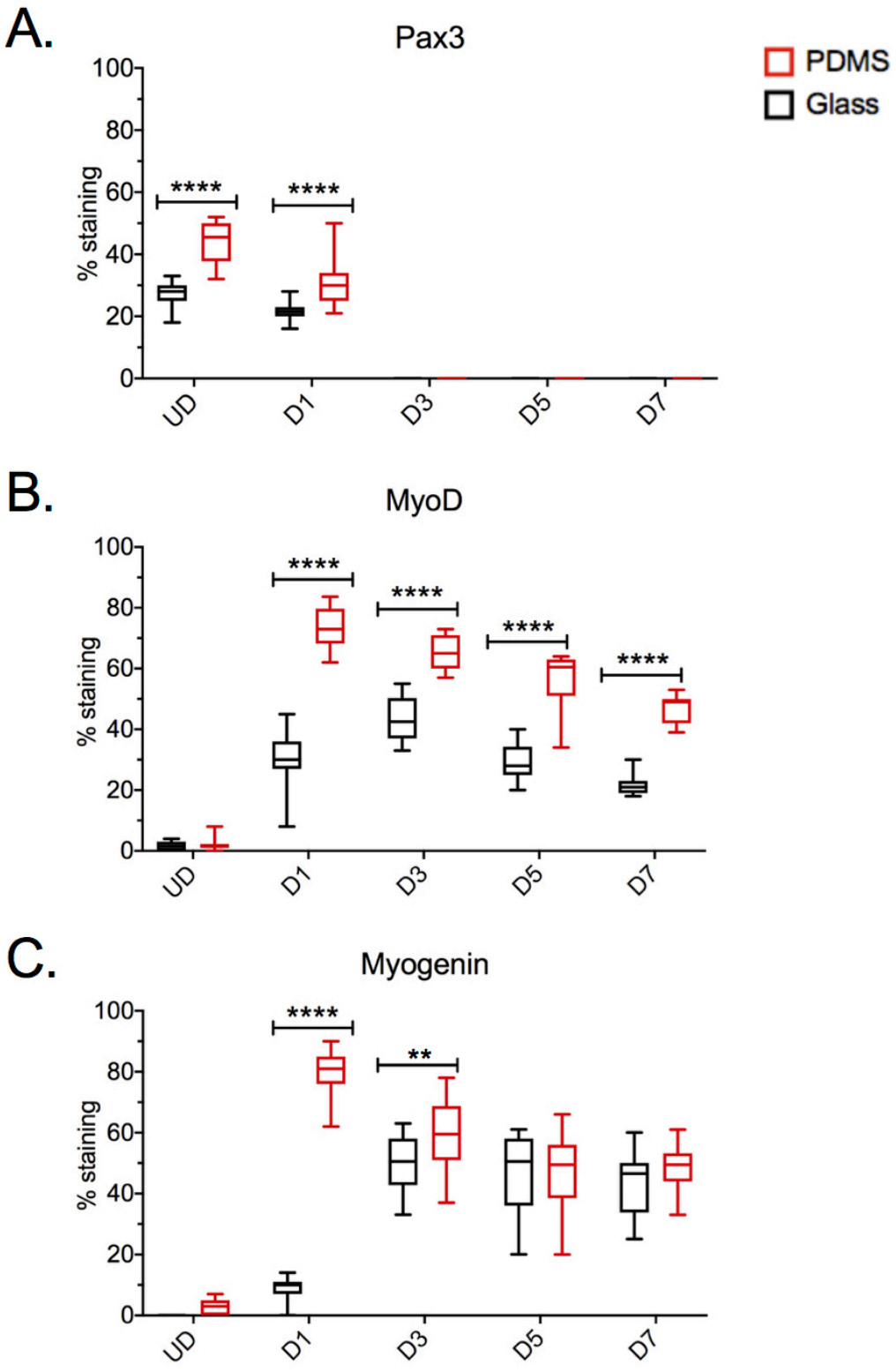

Figure 26. Percentage of nuclei stained positively for Pax3, MyoD and Myogenin. A. Box plots showing the % nuclei stained positively for Pax3 within a field of view on hard and soft surfaces. B. Box plots showing the % nuclei stained positively for MyoD within a field of view on hard and soft surfaces. Box plots showing the % nuclei stained positively for myogenin within a field of view on hard and soft surfaces. Box plots show minimum, first quartile, median, third quartile and maximum values in each graph. Error bars represent S.D. ** p <0.01, **** p <0.0001.

2.4 Discussion

These data show that a clonal cell line of myoblasts derived from the immortal mouse differentiate better on softer (~12kPa) surfaces than on hard, in agreement with previous work on C2C12 cells. These cells express Pax3 and not Pax7, and yet follow the same differentiation pathway observed for Pax7 expressing cells such as C2C12 cells. The PCA analysis of the overall RNAseq data showed that the results for cells grown on PDMS clustered together, and were different to those grown on hard surfaces, which formed separate clusters, at each time point. A key difference we discovered for myogenic factors was the early high-level expression of MyoD and myogenin on the softer surface compared to cells cultured on hard. Generally, expression of most genes was higher on PDMS than on harder surfaces.

In the immortal mouse myogenic clone used here (C1Fs), Pax3 and not Pax7 was detected in proliferating cells, and its levels reduced during differentiation. Expression levels of Pax7 mRNA were not significant. The majority of satellite cells and the C2C12 myoblasts express Pax7 rather than Pax3 (Kuang et al., 2006). Despite this difference, the Pax3 expressing cells appear to undergo the same myogenic pathway in culture as reported for Pax7 positive C2C12 cells. Our findings thus support the evidence that despite the differences in roles of these two genes, Pax3 and Pax7 are capable of triggering a myogenic programme that follows the same transcriptional pattern leading to muscle maturation (Relaix et al., 2006).

Expression levels of MyoD rise earlier and faster on PDMS than on hard surfaces at day 1. This agrees with previous reports of a precocious rise in MyoD on soft surfaces, alongside overall greater expression by cells (Denes et al., 2016). Since MyoD activation is necessary for the specification of terminal differentiation and triggers myogenin activation, the entire myogenic process is expedited. Not surprisingly then, we also find an earlier peak in the rise of myogenin on softer surfaces. The increased levels of these two myogenic transcription factors are likely to result in the

increased fusion and expression of sarcomeric genes reported here. One reason for the precocious expression of myogenic transcription factors and subsequent enhanced myogenic maturation may be because the elasticity of the optimised PDMS surface provides an environment that better encourages sustained adhesion of cells to the culture surface, expediting the complex signalling between cells and the ECM. The relationship between cells and the external environment has been shown to influence cell polarity, architecture and behaviour so there are undoubtedly some effects on downstream signalling, some of which may be involved in maturation of the cultured cells (Engler et al., 2009).

The stiffness of the surface clearly has an influence on myogenesis throughout all time points, and both proliferation and differentiation are expedited on the softer surfaces. Myoblast proliferation following adherence to culture surface occurred in the time between points UD and D1, as evidenced by the highest levels of Pax3 expression observed at this time. At both time points, Pax3 RPKM and fold change was higher on soft surfaces, suggesting that this surface has a positive effect on proliferation. Levels on both surfaces level out after D1, which ties in with the end of the proliferative phase, when Pax3 expression drops to facilitate the progression of the myogenic programme (Relaix et al., 2006). Although Pax7 expression was low (especially on softer surfaces), a spike in expression was still observed on harder surfaces between UD and D1, further confirming this time period as the proliferative phase for myoblasts. Increases in Pax3 trigger an increase in Myf5 expression to mark the onset of myogenic specification followed by fusion and differentiation, as detailed in previous work that used a Pax3 retroviral expression model in C2C12 cells (Collins et al, 2009). This relationship was observed in our RNAseq results, with the highest levels of Myf5 observed between UD and D1. Notably, Myf5 expression in myoblasts grown on soft surfaces were roughly triple that of those grown on harder surfaces. This high expression of Myf5 in proliferating myoblasts will likely have facilitated the precocious differentiation observed in C1F cells grown on soft surfaces, since more $Myf5^{+}$ cells will result in more MyoD expression. Myf5

and MyoD have overlapping roles in triggering the onset of differentiation, but MyoD is crucial in that it is far more effective in activating the expression of growth phase target genes that promote myogenesis such as L-myc, m-cadherin, Runx1, Spp1, Six1, IGFB5 and Chrnβ1 (Ishibasi et al., 2005). As predicted, levels of MyoD were higher around D1, followed by higher levels of myogenin, and then sarcomeric genes as myotubes mature.

The differences in expression of several collagens between surfaces further suggests that stiffness manipulates the behaviour of the ECM. Collagen IV is part of the basement membrane, a thin sheath of connective material that surrounds skeletal muscle, and other cell types (Pozzi et al., 2017). A heterotrimer composed of two α1 (Col4a) and one α2 molecules is found in many types of basement membranes, including that of muscle (Thomas et al., 2015). The increased expression of Col4 genes in cells cultured on hard surfaces at day 1 of differentiation suggests that the hard surface is promoting basal lamina formation more strongly than the soft surface, possibly to counteract the hardness of the culture surface. The reasons for differences in expression profiles for Col8a1 and Col25a1 are unclear. Integrin α5, β1, binds to fibronectin (FN1), and its levels decrease as myoblast fusion and differentiation progress, as reported previously (Karalaki et al., 2009). There was a general decrease over time for integrin genes, on both surfaces. Integrin α7, β1 is the main laminin receptor on myoblasts and myotubes and has been shown to be important for myoblast fusion (McClure et al., 2019). Thus, growing cells on hard surfaces increases gene expression for a range of ECM and ECM associated proteins, as well as the receptors that bind these proteins. This raises the possibility that the cells cultured on hard surfaces attempt to form their own niche, through expression of ECM proteins, to enable them to differentiate on hard surfaces, and could help to explain the delay in expression of myogenic genes.

Other key genes of interest were revealed by the RNAseq analysis, that were not selected for investigation prior. Vascular cell adhesion molecule 1 (VCAM1) was upregulated on soft surfaces compared to hard at D1 differentiation, which is consistent with the precocious myogenesis observed on these surfaces. VCAM1 is an

adhesion protein that aligns myoblasts for fusion into myotubes via the interaction with the integrin VLA-4 and has previously been found to rise in expression from D3-D14 differentiation in C2C12 myoblasts grown on standard surfaces (Rosen et al., 1992, Przewozniak et al., 2013). In satellite cells, VCAM1 is upregulated during skeletal muscle regeneration and previous work has shown that regeneration is impaired when VCAM1 is deleted by knockout mutation (Choo et al., 2017). This suggests a similar role for VCAM1 *in vivo.* Another gene of interest that was found to be upregulated early in the differentiation process on soft surfaces was cytochrome c oxidase subunit 6B1 (COX6B). This is the final enzyme in the electron transport chain which drives oxidative phosphorylation, therefore it has a vital role in cell metabolism during myogenesis (Little et al., 2018). The importance of this gene in maintaining skeletal muscle was highlighted in previous work that used a laminin α2 deficient mouse model of muscular dystrophy. Proteomic analysis found that COX6B was downregulated in these mice compared to WT, suggesting that breakdown of the basement membrane and ECM can negatively impact on metabolic processes involved in regeneration (Menezes de Oliviera et al., 2014). It follows that conversely, providing an extracellular environment that better replicates the *in vivo* surroundings can increase the expression of genes associated with an intact and functional ECM. To conclude, this study has highlighted limitations of widely used hard surfaces (i.e. glass or plastic) in skeletal muscle cell culture. We have shown the magnitude of the transcriptomic differences in cells grown on different cell culture surfaces, and demonstrated the benefits of using surfaces that have been fine-tuned to exhibit elasticity that mimics that of skeletal muscle *in vivo*. Continued work to further support the case for optimized cell culture surfaces will hopefully expedite the transition to a standardized, improved surface that will be used across skeletal muscle research labs, ultimately aiding the research of a multitude of muscle diseases.

3 Muscle Hypertrophy Model

3.1 Introduction

Myopathies, diseases of skeletal muscle, can impair the ability of a muscle to regenerate in response to damage, either directly affecting myocyte activity or indirectly through effects on muscle stem (satellite) cells. One example is Duchenne muscular dystrophy (DMD), in which the lack of dystrophin (a subsarcolemmal protein) prevents the formation of a vital scaffold that links cytoskeletal actin filaments to dystrophin and the dystrophin associated glycoprotein complex in the sarcolemma, and then to extracellular proteins in the extracellular matrix (Ciciliot and Schiaffino, 2010). This weakens the sarcolemma and prevents the repair of damaged muscle with contractile elements, thus further propagating fibre damage and progressive muscle weakness. In addition, satellite cells from DMD patients appear to lack normal proliferative capacity, impeding the regeneration process (Allen et al., 2016; Duan et al., 2021). Most recently, this has been linked to a lack of dystrophin in the satellite cells. Dystrophin functions in activated satellite cells to establish cell polarity via its interaction with the serine threonine kinase Mark2. When dystrophin is absent, Mark2 is downregulated and cannot establish satellite cell polarity (Dumont et al, 2015). This disrupts the balance between symmetric division (which generates two new satellite cells) and asymmetric division (which generates one new satellite cell and a myoblast) (Chang et al., 2016). In the absence of Mark2, the polarity regulator Pard3 cannot be localized at the opposite side of the satellite cell, so the number of asymmetric divisions becomes greatly reduced (Dumont et al., 2015). The consequence of this is that activated satellite cells fail to generate enough new myoblasts to effectively repair the muscle tissue. This leads to atrophy and fibrosis, and eventually, often fatal muscle wastage. Fatalities in DMD patients usually occur when damage to the diaphragm and respiratory muscles occur, leading to respiratory arrest (Duan et al., 2021).

A second example of a myopathy, in which the ability of muscle to regenerate is impaired, is EMARDD (early myopathy, areflexia, respiratory distress and dysphagia). Fibres in skeletal muscle of EMARDD patients have a reduced diameter and fewer nuclei per fibre. This disease is caused by mutations in MEGF10 (multiple epidermal growth factor-like domains 10), a membrane protein likely important in the interaction of satellite cells with the extracellular matrix. MEGF10 has also been suggested to be important in promoting satellite cell proliferation, whilst regulating myogenic differentiation (Holterman et al., 2007). Mutations in MEGF10 have been suggested to reduce proliferation of activated satellite cells, resulting in less myogenic cells that are able to eventually fuse together to form new adult myofibres (Li et al., 2021)).

In addition to their role in muscle repair, satellite cells may contribute to skeletal muscle hypertrophy. Muscle hypertrophy is the increase in diameter of fibres in response to hormonal, endocrine or mechanical stimulus, resulting in increased girth of the muscle. Although increases in strength are not linear with hypertrophy, the process can lead to improvements in strength (Vigotsy et al., 2018). The number of skeletal muscle fibres may also increase in a process known as hyperplasia, however this process is less well understood and does not always occur alongside hypertrophy (Gonyea and Antonio, 1993). Muscle hypertrophy is a common adaptive change that occurs in response to activities such as resistance training, whereby progressive overload is applied to the muscle, causing microtrauma to the fibres. (Charge and Rudnicki, 2004). There are generally two kinds of hypertrophy: myofibrillar and sarcoplasmic. The former involves an increase in sarcomeric proteins such as actin and myosin within the fibres, resulting in a relatively modest hypertrophy but enhancement of force-generative capability of the muscle. Sarcoplasmic hypertrophy results in greater glycogen storage and hypertrophy, but less upregulation of sarcomeric proteins, and thereby poorer improvements in strength (Kraemer and Zatsiorsky, 2006). Irradiating overloaded EDL muscle, which blocks satellite cell activation, inhibits hypertrophy in mice and rats, demonstrating that satellite cell activity may contribute to this process. When satellite

cells are not inhibited, overloaded EDL muscle continues to hypertrophy up to about 30 days with a peak change in hypertrophy at day 7 (Rosenblatt and Parry, 1993). Despite their supporting role in muscle hypertrophy, satellite cells are not required for muscle hypertrophy in the adult (McCarthy et al., 2011). This was demonstrated by previous work using mice, whereby satellite cell function was impaired by tamoxifen treatment. Following overload surgery and compared to untreated controls, satellite cell mediated myonuclear accretion and hyperplasia of fibres was reduced. However, muscle fibre size was still able to increase in adult mice, resulting in overload hypertrophy. Notably, muscle hypertrophy of younger mice was impaired by the tamoxifen treatment, suggesting a need for $Pax7^{+}$ satellite cells to aid hypertrophy earlier during development (Murach et al., 2017). Additionally, functional analysis of fibres isolated from the muscle of satellite cell-depleted mice revealed that a loss of $Pax7^{+}$ does not negatively impact on force, Ca^{2+} sensitivity or rate of cross-bridging (McCarthy et al., 2011). Thus, the hypertrophic response is not reliant on the activity of satellite cells.

A major signalling pathway that regulates hypertrophy is the the IGF/Akt/mTOR pathway. This drives protein synthesis in response to growth factors such as insulin (Musaro et al., 2001; Bodine et al., 2001). There is evidence that mTOR can become activated to drive hypertrophy in a separate signalling process that does not involve Akt, and this activation may be via MAPK/Erk kinase (MEK) phosphorylation of tuberous sclerosis complex 2 (TSC2). This activation of TSC2 can facilitate independent activation of mTOR before the phosphorylation of Akt has occurred (Miyazaki and Moriya, 2020). Another activator of mTOR and thus an important molecular player in hypertrophy, is Ras homolog enriched in the brain (Rheb), as indicated by its overexpression in mice driving hypertrophy of the TA via the PI3-Akt pathway (Goodman et al., 2010). Amino acids are also capable of activating mTOR, with leucine previously being found to promote hypertrophy via the inhibition of the mTOR negative regulator, Sestrin2 (Saxton and Sabatini, 2017). In addition to the protein synthesis driven by mTOR activation, hypertrophy is supplemented by myonuclear accretion driven by satellite cell activation.

In a muscle exposed to hypertrophy stimulus, satellite cells transition to an activated state from a quiescent state. Notch signalling is of great importance during regeneration as it promotes activation and proliferation of satellite cells when exposed to hypertrophy stimulus. In response to overload the Notch pathway is activated, facilitating the release of Notch ligands (e.g. Delta and Serrate) by muscle fibres and their subsequent binding to Notch receptors on the surface of satellite cells. This results in transcription of Recombination signal binding protein for immunoglobulin kappa J (RBPJ) and satellite cells adopt an activated, pro-proliferative state (Sultan et al., 2021; Brack et al., 2008). The propagation of satellite cells in this process allows additional myonuclei to be added to the muscle fibre, remodelling the muscle tissue. The MEGF10 protein has been closely linked to Notch and may have a similar role in muscle hypertrophy via myonuclear accretion, so further research on the role of MEGF10 in satellite cells and muscle regeneration is warranted (Holterman et al., 2007; Saha et al., 2017).

Muscle hypertrophy is impeded by the age-related loss of muscle mass and strength known as sarcopenia. Many factors are at play in sarcopenia; specific atrophy of fast type fibres (slow fibres tend to be maintained into old age), loss of motor units and reduced satellite cell number (or reduced responsiveness of satellite cells). All of these contribute to the loss of muscle strength and mass (Logan et al., 2011). Strength training can ameliorate the effects of sarcopenia, in part due to increased vascularisation within the muscle, providing satellite cells with a denser capillary network (Narici and Maffulli, 2010; Snijders and Gianni 2017). The proximity of satellite cells to neighbouring capillaries has been found to be important, as they are able to reciprocally activate one another via the exchange of growth factors. The closer satellite cells are to capillaries, the more likely they are to exist in an activated state (Egginton et al., 1998). Thus, undertaking load-bearing exercise, which promotes angiogenesis within the tissue, is effective in providing muscle with a greater regenerative capacity at the stem cell level.

Engineering muscle overload in rodents, using surgery, is a good model for the hypertrophy and hyperplasia that occurs during load-bearing exercise (such as strength

training with weights) in humans (Murach et al., 2017). One type of overload model involves surgery to remove the tibialis anterior (TA) muscle from one leg, which forces the synergistic extensor digitorum longus (EDL) to undergo sustained stretch and thereby work harder when the animal is ambulant (Egginton et al., 2011). It results in a mild hypertrophy, and larger fast type 2a and 2b fibres, compared to unloaded muscle (Hendrickse and Degens, 2019). This type of muscle perturbation is more physiological than inducing acute muscle damage by injecting toxins (Mahdy, 2019). When hypertrophy is induced by injury e,g, with cardiotoxin (CTX) an acute inflammatory response is initiated whereby neutrophils diapedesis disrupts the basement membrane, ultimately impeding and delaying the regeneration process (Nishimura et al., 2015). The inflammatory processes that occur in response to muscle injury with CTX may not well replicate the inflammatory processes that occur in human muscle regeneration, whereby injury is unlikely to occur by toxin. The muscle extirpation hypertrophy model introduces a stimulus in the form of increased load on the EDL, which better replicates a normal physiological event in humans. As well as exploring hypertrophy as a result of weight-bearing activity, the muscle overload model is also useful in determining how disease states may affect muscle hypertrophy. Previous work using the *mdx* mouse, which is a model for DMD, has shown that overloaded EDL muscle is unable to withstand the added strain resulting from TA extirpation, and undergoes accelerated deterioration (Farrell et al., 1999). Transplantation of satellite cells alleviated this deterioration and improved contractile strength, fibre size and capillarisation (Dick and Vrobva, 1993).

Here I utilised the muscle overload model of muscle hypertrophy, to determine how it affects the behaviour of satellite cells in response to external mechanical stimulus. I then used this model to determine how satellite cells respond to overload in a mouse model for EMARDD, in which MEGF10 is deleted.

3.2 Methods

3.2.1 General procedures

All media, glassware, plastic and surgical tools were sterilised before use, either by autoclaving at 121°C for 15 min or washing thoroughly with 70% ethanol in H_2O.

3.2.2 Animals

Male and female adult C57BL/6Tac (bred in-house at the University of Leeds) and Megf10$^{tm1(KOMP)Vlcg}$ mice (age approx.. 6 weeks, final body mass approx. 25g) were used in this study. Fully mature mice were deliberately chosen and the age of the mice was kept consistent throughout the study to control for the differences in the hypertrophic response of muscle observed between developing and adult mice. All experimental procedures and sacrifice were conducted with approval of the local animal welfare and ethics committee, under Home Office project licences 70/8674 and PP1775021. Mice were housed in groups in a temperature-controlled environment with access to food and water *ad-libitum*. Cages underwent light/dark cycles. Originally, I planned to exclusively use male mice in this study. However, to reduce unnecessary wastage of animals, females born from breeding pairs were used for additional analyses. Breeding was carried out under service licence PP0237211, with two breeding cages of C57BL/6Tac x heterozygous Megf10$^{tm1(KOMP)Vlcg}$, and one breeding cage of heterozygous Megf10$^{tm1(KOMP)Vlcg}$ x heterozygous Megf10$^{tm1(KOMP)Vlcg}$. Mice were stunned by concussion and killed by cervical dislocation.

The Megf10 $^{tm1(KOMP)Vlcg}$ mice (RRID: MMRRC_048576-UCD, MGI ID: 4454190, background: C57BL/6Tac, intragenic targeted knockout deletion, gene ID: 70417) were obtained from the Mary Lyon Centre at the MRC Harwell Institute and exported to our laboratory to establish breeding colonies. Briefly, the model was generated by replacing exons 1-24 of mouse Megf10 by homologous recombination with an expression selection cassette

as detailed by the Knockout Mouse Project (KOMP, University of California Davis, Davis, CA: https://www.komp.org/geneinfo.php?geneid=68051). The Megf10$^{tm1(KOMP)Vlcg}$ mice harbour the Velocigene cassette ZEN-Ub1 inserted into the MEGF10 gene between positions 57340143 and 57372060 on chromosome 18, generating a 31918bp deletion that deletes exons 1-24 of MEGF10 (Fig. 27). The mouse line was rederived in the Harwell facility after its original generation at Regeneron Pharmaceuticals. qPCR has shown no mRNA for MEGF10 expressed in the cerebellum in homozygote animals (Mouse Genomics Informatics) (Velocigene, 2008; Iram et al., 2016). Megf10$^{-/-}$ (homozygous knockout) mice were generated on a C57BL/6NTac background. Megf10$^{-/-}$, Megf10$^{+/-}$ (heterozygous), and wild-type animals used in the experiments were generated by breeding Megf10$^{+/-}$ together. The Megf10$^{tm1(KOMP)Vlcg}$ model is likely superior to another previous MEGF10 knockout model used to explore the effects on myogenic behaviour (Megf10 $^{tm1c(KOMP)Jrs}$) because this previously reported mutant construct only deletes exons 3-4 of the MEGF10 gene, and the Megf10$^{tm1(KOMP)Vlcg}$ construct destroys a much larger area of the gene with the deletion of exons 1-24. It is hypothesised that this larger deletion will result in a more severe muscle phenotype in the knockout mice, improving on the results obtained with the Megf10 $^{tm1c(KOMP)Jrs}$ mouse, whereby the muscle phenotype was very mild (Saha et al., 2017).

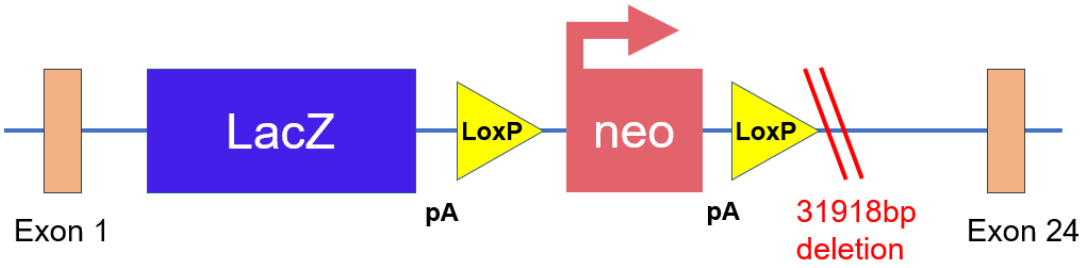

Figure 27. Megf10$^{tm1(KOMP)Vlcg}$ mutant construct. Schematic showing the KO construct that deletes exons1-24 on the MEGF10 gene, composed of a neomycin resistance cassette flanked by LoxP sites, polyadnylation sites and a LacZ sequence.

3.2.3 Genotyping

To accurately determine the genotype for each mouse, ear biopsies were collected by unit staff at Central Biomedical Services (CBS), University of Leeds. Biopsies were placed into 96-well plates, sealed, and shipped to Transnetyx for genotyping (Transnetyx Inc. Cordova, TN) via FedEx courier. A bespoke PCR assay to determine genotype was designed by the Genetic Services team at Transnetyx based on information provided by KOMP (Knockout Mouse Project) mouse repository (Fig. 28). Results were obtained within 72 hours of sending the samples.

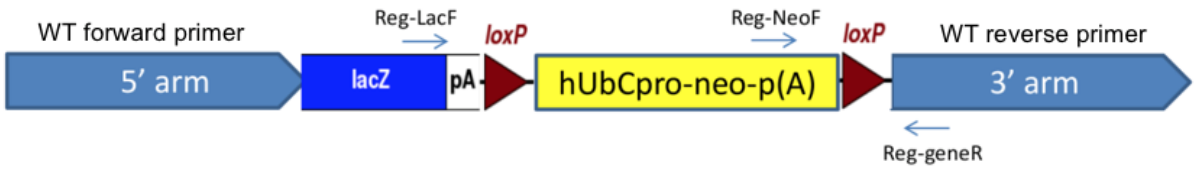

Figure 28. Primer strategy for TaqMan assay. Schematic showing forward and reverse primer, human ubiquitin C gene promoter (hUbCpro-neo-p(A)) selection cassette flanked by loxP sites and lacZ sequence within the mutant (tm1) allele. Primers used in genotyping used sequence from lacZ (Reg-LacF) and the neomycin selection cassette (tm1a allele: Reg Neo-F), the reverse primer Reg-geneR. The readout of LAC Z+ WT+ = heterozygous, LAC Z+ WT- = homozygous, and LAC Z- WT+ = wild-type.

Sequences of the genotype primers were:

LAC-Z

Forward primer: CGATCGTAATCACCCGAGTGT

Reverse primer: CCGTGGCCTGACTCATTCC

Reporter 1: CCAGCGACCAGATGAT

Reporter 2: N/A

MEGF10-1 WT

Forward primer: CTACCGGACAGCCTACCG

Reverse primer: CTTTCATAAAATCCTGGGCAACACT

Reporter 1: TATAGACGCAAATCCC

Reporter 2: N/A

Mendelian ratio was calculated by dividing the number of mice in each genotype group by the number in the smallest group (homozygous, in which there were 6 mice). If the ratio value was a decimal, numbers were rounded down. We did not obtain the expected Mendelian ratio of 1:2:1 and relative numbers of homozygotes were lower than anticipated. (Table 10).

	WT	Heterozygous	Homozygous
Total	13	20	6
Ratio	2	3	1

Table 10. Genotypic ratio of mice born from Megf10+/- matings. Total number of WT, heterozygous and homozygous mice and corresponding ratio.

3.2.4 Hypertrophy model surgery

Unilateral extirpation (removal) of tibialis anterior (TA) muscle was performed under aseptic conditions and the mice were anaesthetised using isoflurane. All instruments were sterilised and work carried out under a dissection microscope. Mice were first anaesthetised with 5% isofluorane in 2Lmin-1 (O2). The left leg was then shaved and wiped with ethanol to sterilize the area and remove surface bacteria. For the remainder of the operation, mice were maintained under anaesthetic at 2% isoflurane in 2L/min O2.

A single incision was made on the hindleg to expose the TA (Fig. 29A). Tweezers were used to lift the superficial distal tendon of the TA, and the TA was then removed by making incisions at proximal and distal points of attachment, using a scalpel. The TA cut end was then held over the wound area for approx. 10s to allow the release of chemokines to aid repair and blood clotting (Fig. 29B). The TA was then discarded and 1-2 drops of 2.5% Baytril® (Bayer AG) was applied to the wound for antiseptic protection. The area was swabbed with a cotton bud to remove blood and then the incision was sutured with MERSILK™ (Ethicon Inc.) braided silk suture, size 5.0. Sutures were intermittent and double-knotted to reduce the chance of mice unravelling them post-operatively. 1-2 more drops of Baytril® were applied to the closed wound and swabbed with sterile cotton buds, to remove dried blood that may lead to irritation. Using a 1ml syringe and a 26G brown needle (Terumo AGANI), 0.1ml 10% Vetergesic (Ceva Animal Health, Ltd) was administered to the scruff of the neck to provide post-operative analgesia. Mice were placed in a heated cage without sawdust for approx. 10 minutes to recover from anaesthetic, before being placed back into their original cage. Mice were observed to be normally ambulant, thus overloading the extensor digitorum longus (EDL), for a pre-determined length of time before sampling.

A.

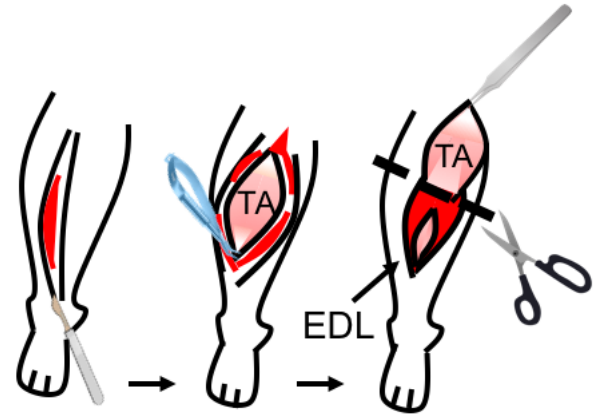

B.

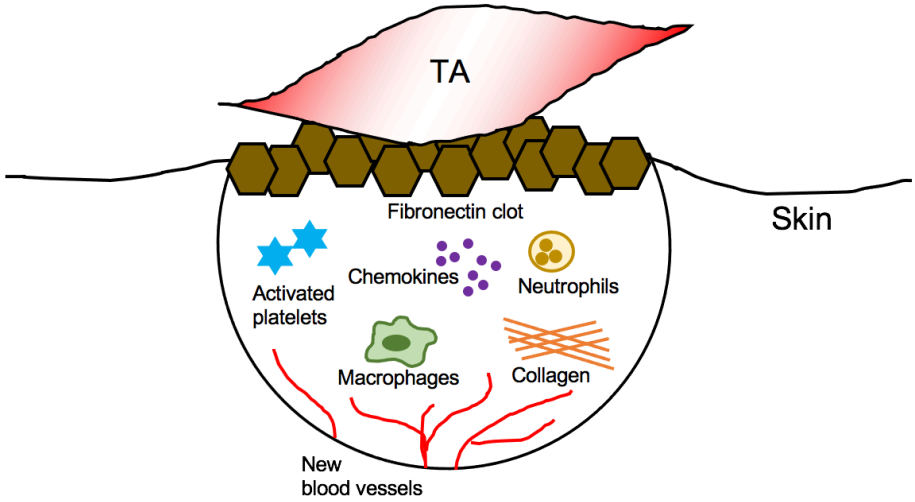

Figure 29. EDL overload surgery. A. Schematic illustration of the muscle extirpation process. An incision is made on the hind leg, and TA isolated and removed. During surgery, the wound is then sutured back. The EDL is subsequently removed for analysis. **B. Schematic illustration of wound repair**. When the TA is held against the open wound it encourages the activation of platelets, release of inflammatory chemokines, macrophages, neutrophils, vascularisation, collagen deposition and the formation of a fibronectin clot.

3.2.5 Sample isolation

EDL:

Changes in EDL muscle phenotype were assessed in control animals (no overload), as well as animals overloaded for 6, 7, 10 and 14 days, to observe changes in the muscle at each time-point. Mice were killed by Schedule 1 (concussion followed by cervical dislocation). Muscle was removed as quickly as possible to avoid the biochemical changes that occur prior to the onset of rigor mortis. The leg of a freshly killed mouse was shaven and dabbed with ethanol to promote cutaneous vasoconstriction. A small incision was made from just lateral to the knee, down to the beginning of the hindfoot. Blunt dissection using scissors and forceps was carried out to break through the layer of fascia atop the muscle. On the unoperated (contralateral) leg, the TA was first removed to access the EDL underneath. Forceps were used to slip underneath the tendon of the TA, and a scalpel used to release it at the base. The base of the TA was gripped using serrated forceps, the TA muscle was lifted up and severed at the top with a scalpel. The EDL was then accessed and removed in the same way as the TA. On the ipsilateral (overloaded) leg, the EDL was simply removed as described. The EDL, and the whole mouse, were both weighed to determine the EDL mass as a percentage of total body mass.

Gastrocnemius:

For additional analysis, the gastrocnemius muscle from both legs was removed from each mouse. Tweezers were used to pinch the skin at the incision site made to dissect out the EDL, and the skin was then pulled back to expose all of the underlying musculature. Dissection scissors were used to cut and remove the fascia covering the muscles. Forceps were used to lift up the distal tendon of the gastrocnemius and an incision was then made at this point. Using tweezers, the muscle was pulled back and another incision was made at the proximal tendon, releasing the muscle.

3.2.6 Sample storage

Samples of skeletal muscle were taken from control mice, and mice in which the EDL muscle had been overloaded for 6, 7, 10 or 14 days to observe changes in the muscle at each time-point. Mice were culled and sampled as described above. Muscles were either harvested for the purpose of single fibre isolation, cryosectioning or immediately snap frozen in liquid nitrogen and stored at a temperature of -80°C for protein extraction and subsequent analysis. EDL muscles used for single fibre isolation were transferred to vials for digestion. Those being used for cryosectioning were mounted (as described below) and then snap frozen for subsequent storage at -80°C.

3.2.7 Single muscle fibre isolation

Freshly isolated muscles were transferred to individual vials containing DMEM supplemented with 1% P/S (10,000U/ml), into which sterile-filtered collagenase type I (*Clostridium histolyticum* (Sigma)) had been diluted to a concentration of 2mg/ml. Muscles were digested for 1 hr 15 min at a temperature of 37°C in a cell culture incubator.

While muscles were being digested, 60mm petri dishes (Nunc) were coated with sterile filtered 5% BSA diluted in PBS and then filled with 6ml isolation medium (DMEM + 1% P/S). Two dishes were prepared for each muscle.

Following digestion, the muscle was transferred from the vial containing collagenase, to a dish filled with isolation media, using a fire polished wide-bore pipette, coated with 5% BSA. Under a stereomicroscope, which allowed the individual fibres to be observed, the muscle was flushed with medium using the wide-bore pipette. Care was taken not to make contact with the muscle, although the smoothened edges of fire-polished pipette minimised damage to the fibres if contact did occur. Flushing caused individual muscle fibres to separate from the muscle bulk and was carried out until the majority of fibres had been released. Finally, straight, transparent fibres were picked out

and transferred to the second dish of isolation media using a fire-polished, narrow-bore pipette coated with 5% BSA.

3.2.8 Cryosectioning of muscle samples

To prepare freshly dissected EDL muscle for cryosectioning and subsequent immunohistochemical analysis, a rapid freezing process was carried out. An isopentane-liquid nitrogen system was set up: a plastic cup was filled with isopentane (2-methylbutane), leaving ~2cm at the top and a wooden stand was used to suspend the cup in a small canister of liquid nitrogen, submerging the cup ¾ of the way in. A wooden pencil was then used to rapidly stir the isopentane until it became cloudy and viscous. EDL muscle was removed as previously described and the top and tail of the muscle were cut off with a razorblade, to create a cylindrical shape that did not taper at each end. The EDL was then bathed in optimum cutting temperature compound (OCT) (Agar Scientific), picked up gently with forceps, then propped up against a metal skewer that was secured into the middle of a labelled cork disk. When the EDL was aligned with the skewer, the entire construct was inverted and placed into the isopentane for ~20s. Submerging the muscle in isopentane at this point allows it to freeze more evenly and protects against tissue damage, compared to simply snap-freezing in liquid nitrogen (LN_2). Forceps were then used to remove the construct from the isopentane, and the metal skewer was removed from the cork, leaving muscle secured independently on the cork and positioned for sectioning. Samples were then dropped into LN_2 before being wrapped in tin foil and stored at -80°C.

Diaphragm muscle was also prepared for cryosectioning. The diaphragm was removed from mice by making an initial incision level with the hip to pierce the skin, and then carefully cutting upwards towards the sternum taking care not to pierce the gut. Skin was carefully peeled back to expose the abdominal musculature. Scissors were used to cut through the musculature and partially snip out the ribs allowing them to be pulled outwards with forceps. The diaphragm could then be identified and carefully released by

cutting around it, underneath the ribcage with dissection scissors. A strip of diaphragm was then carefully mounted onto a cork using OCT and LN_2, in the same process as with the EDL muscles used for cryosectioning.

Prior to sectioning, a cryostat (Leica) was cooled to -20°C for ~30mins and samples were placed inside the cryostat chamber to ensure they were at the same temperature as the apparatus. After sufficient cooling, samples were attached to a metal chuck using OCT to 'glue' them on, and then loaded in a position that was 90º to the cryostat blade. The sample was moved to just in front of the blade and the machinery was set to cut 30µm sections. The rotor was moved continuously until tissue began being shaved off by the blade. When 3-4 muscle sections had been cut, the rotor was locked and a fresh glass microscope slide was held above the tissue, and the difference in electrostatic attraction caused the tissue to lift up and adhere to the slide. An inverted Olympus CK 2 microscope with a 10x lens was used to inspect the sample, checking that the tissue sections were undamaged and complete without pores. 30µm sections continued to be cut until the tissue sections were undamaged and contained intact cross-sections of fibres. At this point, settings were changed to cut 10µm sections. Tissue was cut to allow 3-4 muscle sections linked together, then a few of these were placed onto each labelled glass slide. Slides were stored at -20°C until ready to fix and stain.

3.2.9 Fixation, staining and analysis of fibres

Selected fibres were transferred to a 2ml Eppendorf tube using the 5% BSA coated narrow-bore pipette and allowed to settle for ~5 min. Excess media was removed using the same pipette, taking care not to disturb the fibres. Fibres were then fixed with 400µl 4% PFA in PBS for 20 min at room temperature. Following this, fibres were washed three times with 700µl PBS (allowing fibres to settle for ~5 min between washes). Fibres were stored at 4ºC in 700µl PBS prior to staining.

Fibres were stained by first permeabilising their membranes with 500µl 0.5% Triton X-100 in PBS (PBST) for 10 min at room temperature, and then washing three

times with 700µl PBS. Fibres were then incubated with 500µl blocking solution (20% horse serum in PBS) for 30 min at room temperature to reduce non-specific antibody binding. Primary antibody solutions were prepared in PBS as listed (Table 11). Fibres were incubated in 500µl antibody solution at 4ºC overnight on a rocker. Primary antibody was then removed, and fibres washed three times with 700µl 0.025% Tween in PBS. Secondary antibody solutions were prepared in PBS according to dilutions as listed (Table 12). Fibres were incubated in 500µl antibody solution at room temperature for 1 hr 30 min on a rocker. Secondary antibody was then removed, and fibres washed three times in 700µl 0.025% Tween in PBS, and a final wash with 700µl PBS. Fibres were then carefully extracted using a narrow-bore 5% BSA coated pipette and transferred onto a clean glass microscope slide. The pipette was used to remove excess PBS from around the fibres, and the slide was allowed to air dry for a couple of minutes. Two drops of ProLong Gold antifade mountant was then added to the slide, and a 20mm x 40mm glass coverslip was placed on top. Slides were left overnight at room temperature in the dark, and then stored at 4ºC.

Antibody	Dilution	Species	Catalogue no.
Pax7 (DSHB hybridoma)	1:20	Mouse	N/A
MyoD (Invitrogen)	1:100	Mouse	MA1-41017
Myogenin (Invitrogen)	1:50	Mouse	MA511486
CD34 (BD Pharminogen)	1:50	Rat	553731
BAD5 (DSHB hybridoma)	1:50	Mouse	N/A
Laminin (Sigma)	1:30	Rabbit	L9393

Table 11. Primary antibodies used and their dilutions.

Antibody	Dilution	Species	Catalogue no.
DAPI (Sigma)	1:500	N/A	40043
Alexa 546 anti-mouse (Invitrogen)	1:400	Goat	A-11030
Alexa 488 anti-mouse (Invitrogen)	1:400	Goat	A-11029
Alexa 488 anti-rat (Invitrogen)	1:400	Donkey	A21208
Alexa 647 anti-rabbit (Invitrogen)	1:400	Goat	A21245
Griffonia (Bandeiraea) Simplicifolia Lectin I (GSL I, BSL I) Fluorescin	1:400	N/A	FL-1101

Table 12. Secondary antibodies used and their dilutions.

Cells were imaged on an LSM880 upright confocal microscope (Zeiss) using a 40x, N.A. 1.4, objective.

3.2.10 Measuring myonuclear accretion

Images were taken on a widefield Olympus IX-70 microscope, using a 40x lens. Images were taken of 15 muscle fibres from overloaded EDL muscle at each time point: D0, D6, D10 and D14. The number of myonuclei, nuclei attached to the periphery and spanning the length of myofibres, were positively stained for DAPI and counted for 1mm sections using ImageJ.

3.2.11 Quantification of transcription factor expression

The number of nuclei positively stained for a transcription factor (Pax7, MyoD or myogenin) per 50 myonuclei along the fibre was estimated by imaging three fibres per mouse, stained for DAPI and the transcription factor, using a 40x lens on the Olympus microscope. The numbers of positive nuclei per fibre were expressed as a percentage of 50 myonuclei, and the number per fibre was averaged.

3.2.12 Fixation, staining and analysis of cryosections

Slides were left at room temperature for ~10 mins to dissipate condensation. A hydrophobic barrier pen was then used to draw around each segment of 3-4 sections

joined together. Within the confines of the hydrophobic barriers, tissue was fixed by applying 100-200µl ice-cold 100% methanol and incubating at room temperature for 10 mins. Sections were then washed three times with PBS. Non-specific antibody binding was reduced by incubating with 5% BSA at room temperature for 30 min. Primary antibodies were diluted in PBS according to dilutions stated in Table 2 and were applied to tissue sections following removal of the blocking solution. Slides were incubated with the primary antibody overnight at 4°C. Primary antibody was then removed and sections were washed three times with wash buffer (1% BSA in PBS). Secondary antibodies were diluted in PBS according to dilutions stated in Table 3 and were applied to tissue sections, being left to incubate for 1hr at room temperature. Secondary antibody was then removed and sectioned were washed three times with wash buffer, before a final wash with PBS. Two drops of ProLong Gold antifade mountant was then added to the slide, and a 20mm x 40mm glass coverslip was placed on top. Slides were left overnight at room temperature in the dark overnight, and then stored at 4°C. Sections were imaged on a LSM880 upright confocal microscope (Zeiss) using a 40x objective.

3.2.13 Measurement of cross-sectional area

Cross-sectional area of individual muscle fibres was determined using ImageJ processing software (NIH). Outlines of each individual fibre were drawn around on each image using the freehand selection tool, and area in μm^2 was automatically calculated.

3.2.14 Quantification of fibre type

Slow fibre type distribution was determined using cross-sections stained with the BAD5 antibody and DAPI. Five fields of view were obtained from each mouse and 20 fibres in total were counted. From these 20 fibres, the % slow fibre content was calculated, and this data then averaged to each mouse.

3.2.15 Nearest neighbour analysis

The distribution of satellite cells and capillaries in relation to one another was established using nearest neighbour analysis on stained cryosections. Within each FOV, one $Pax7^{+}$ cell was randomly selected and the distance, in µm, between this cell and all its immediate $lectin^{+}$ neighbours were measured. Measurements were taken using ImageJ processing software (NIH), and this data then averaged to each mouse, to assess whether overload increased or decreased proximity of satellite cells to endothelial cells.

3.2.16 Measurement of laminin thickness

The width of the basement membrane between fibres in stained diaphragm cross sections was measured using ImageJ processing software (NIH). The 'straight line' tool was used to take orthogonal measurements of laminin (visualised with Alexa Fluor 488) normal to the sarcolemma, and this value recorded. Five measurements were taken per fibre, and five fibres were measured for 3 WT and 3 $Megf10^{+/-}$ mice.

3.2.17 Statistical analyses

Figure legends inform on number of biological repeats (n=) and this study has endeavoured to obtain a minimum of n=3 for all experiments. No statistical method was used to predetermine sample size and the experiments were not randomised. Statistical tests were performed and graphs generated using GraphPad Prism version 8 for Mac (GraphPad Software, La Jolla California, USA, www.graphpad.com). Graphs show mean ± standard deviation (S.D) for each observation. Unpaired t-tests with Welch's correction and one-way and two-way ANOVAs were carried out to test for any statistically significant differences between conditions. The level of statistical significance is indicated by the number of asterisks displayed above graphs: **** represents a P value <0.0001. *** represents a p value <0.001. ** represents a P value <0.01. * represents a p value <0.05.

3.3 Results

3.3.1 Overload had the largest effect at day 10 in WT mice

The relative mass of the overloaded EDL muscles was increased at each of the three time points sampled: D6, 10 and 14 (Fig. 27A). In contrast, the relative mass of the contralateral EDL muscles was unchanged, with no significant difference between contralateral tissue at all time points compared to D0 EDL (Fig. 30A). Expressing the change in weight as % hypertrophy (Fig. 30B) shows that there was ~40% hypertrophy of the overloaded muscles at D6-14, a significant increase compared to D0. The average percentage increase in EDL mass after 10-day overload was 41.4%, compared to the lower hypertrophy seen at D6, which increased by 35.5% on average. An apparent plateau was observed at D14, with an average increase in EDL mass of 41.7%, similar to that observed after D10 overload.

Counting the numbers of nuclei showed that the numbers of nuclei per mm also significantly increased in the overloaded compared to contralateral muscle fibres at D10 and D14. The percentage increase in nuclei per mm in overloaded fibres was significantly increased compared to D0 (Fig. 30C, D) by 56% at D6, 68% at D10, and 66% at D14. No significant differences were found when number of nuclei on contralateral fibres were compared between time points, or to D0 fibres. The increase in numbers of nuclei shows a similar trend to the increase in EDL mass following overload. As the largest effects of overload were observed at D10, this time point was used in subsequent experiments.

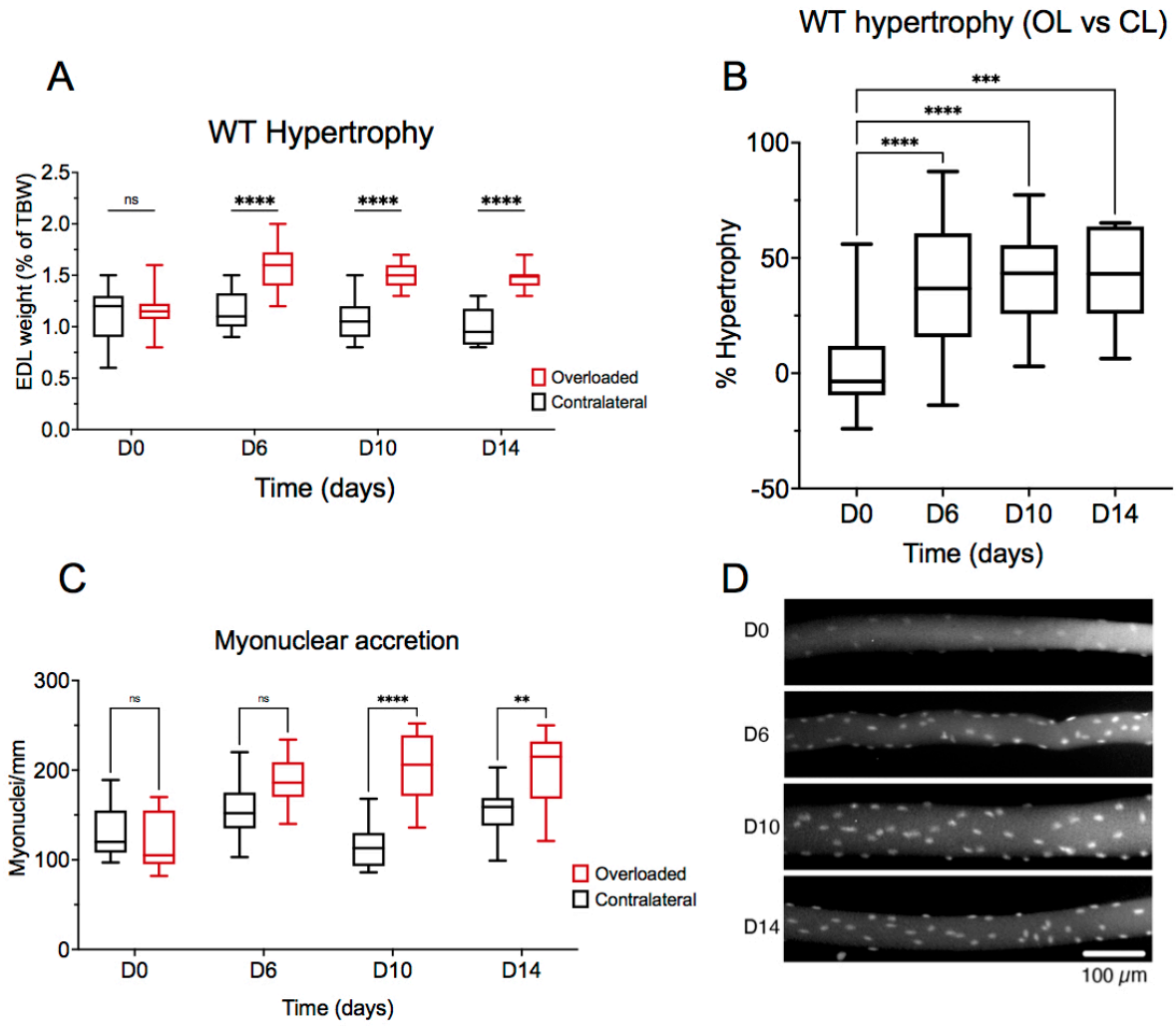

Figure 30. Effects of overload on EDL hypertrophy and number of myonuclei. A. The relative weight (EDL muscle weight as a proportion of the total mouse body weight) is shown (mean values +/- S.D) at each time point for unloaded (contralateral) and overloaded EDL. **B.** The % increase or decrease in weight of overloaded EDL compared to unoperated contralateral EDL represented by box plots. **C.** Box plots of the myonuclei per 1mm of fibre from overloaded and contralateral EDL muscle. Box plots show minimum, first quartile, median, third quartile and maximum values. **** p<0.0001. *** p <0.001. ** p <0.01. * p <0.05. **D.** Representative mages of overloaded muscle fibres. Nuclei stained with DAPI. 10x magnification.

3.3.2 The hypertrophy response to overload is reduced in Megf10$^{+/-}$ and Megf10$^{-/-}$ mice

At D10 overload, EDL muscle from Megf10$^{+/-}$ and Megf10$^{-/-}$ mice showed a significantly lower level of hypertrophy than that of WT mice as measured by % weight of the overloaded muscles compared to that at D0 (Fig. 31A). Comparing EDL muscle weights between contralateral and overloaded muscle, also showed that overload did not result in any significant hypertrophy of EDL in Megf10$^{-/-}$ mice, but did result in significant hypertrophy of overloaded EDL in WT and Megf10$^{+/-}$ mice (Fig.31B). No changes in EDL muscle weight were observed for WT, Megf10$^{+/-}$ and Megf10$^{-/-}$ mice for muscle not exposed to overload (D0) (Fig. 31D, E). Similarly, muscles from sham-operated mice did not show any hypertrophy in either WT or Megf10$^{+/-}$ mice when EDL from the sham-operated leg was compared to the contralateral EDL (Fig. 31G, H). Megf10$^{-/-}$ mice were not tested in the sham-operated experiments. Significant myonuclear accretion occurred in all genotypes after 10-day overload, but Megf10$^{-/-}$ mice showed a reduced response compared to WT and Megf10$^{+/-}$. On average, there were 24% less nuclei after overload in Megf10$^{-/-}$ fibres compared to WT, and 19% less nuclei compared to Megf10$^{+/-}$ fibres (Fig. 31C, J). No myonuclear accretion was observed when the left leg was compared to the right leg in D0 and sham operated EDL (Fig. 31F, I).

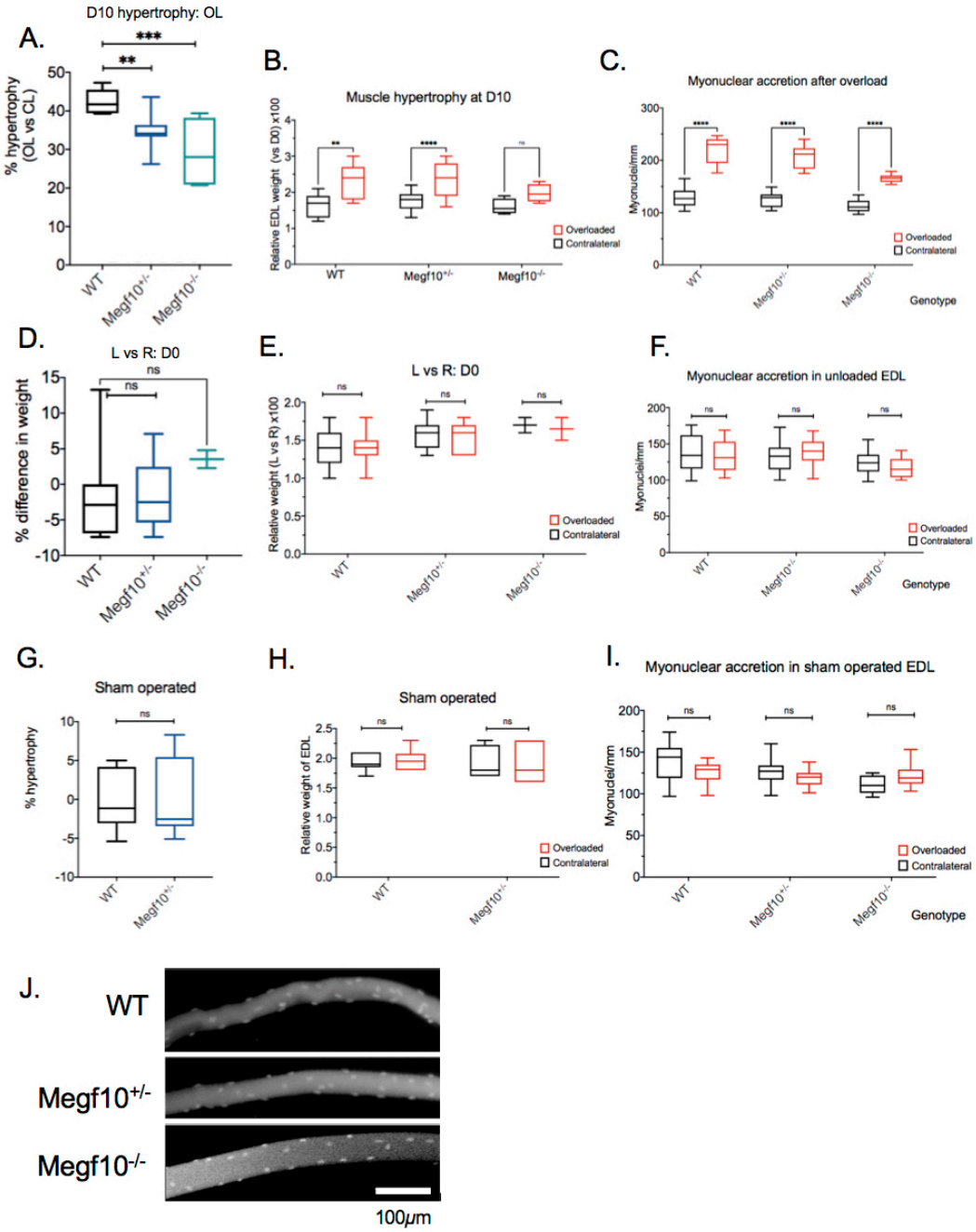

Figure 31. Megf10$^{+/-}$ and Megf10$^{-/-}$ mice show reduced EDL hypertrophy following muscle overload. A. Relative hypertrophy (%) following 10 days of overload. **B.** The relative mass for CL and OL EDL. **C.** Box plots of the myonuclei per 1mm of fibre from D10 OL and CL EDL muscle. **D.** The % increase or decrease in mass of left EDL compared to right EDL in D0 control. **E.** The relative mass for right and left EDL in D0 control. **F.** Box plots of the myonuclei per 1mm of fibre from right and left D0 EDL muscle. **G.** The % increase or decrease in weight of left EDL compared to right EDL in sham op control. **H.** The relative mass for right and left EDL in sham op control. **I.** Box plots of the myonuclei per 1mm of fibre from right and left sham op EDL muscle. **J.** Representative images of D10 overloaded muscle fibres. Nuclei stained with DAPI. X 10 objective. Box plots show minimum, first quartile, median, third quartile and maximum values in each graph. Error bars represent S.D. ** p <0.01, **** p <0.0001.

3.3.3 Lack of a clear change in cross-sectional area following overload

At D10, the mean fibre cross-sectional area (CSA) of individual OL fibres was significantly increased compared to CL fibres for WT and Megf10$^{+/-}$ mice but decreased for Megf10$^{-/-}$ mice (Fig. 32C). The mean fibre CSA averaged per mouse, showed the same trend, but the mean values were not significantly different (Fig. 32B). Average fibre CSA values for overloaded muscles were not significantly different between WT, Megf10$^{+/-}$ and Megf10$^{-/-}$ mice. The lack of statistical significance when values were averaged per mouse despite large differences in CSA was likely the result of a small sample size. Comparing individual values of CSA allowed the full range of data to be observed, and allowed biological significance to be understood in the absence of statistical significance. Images of stained cryosections showed that muscle fibres of Megf10$^{-/-}$ mice had large variation in CSA in both OL and CL EDL, and muscle sections often had fewer fibres per unit area due to their larger size (Fig. 32A).

However, at D0, there was an unexpected significant difference in fibre CSA between the right and left EDL muscles for Megf10$^{+/-}$ mice (Fig. 32E) and for the CSA measurements averaged per mouse (Fig. 32D). A significant difference between left and right EDL CSA for distribution of individual fibre measurements was also observed for WT mice. In sham operated controls, no significant differences were found (Fig. 32F and Fig. 32G). These differences in CSA between left and right EDL muscle fibres in controls make it challenging to interpret the data after overload.

A direct comparison of fibre CSA between D0 and D10 for WT, Megf10$^{+/-}$ and Megf10$^{-/-}$ mice showed that CSA significantly decreased after 10-day overload in WT and Megf10$^{-/-}$ mice but increased in Megf10$^{+/-}$ mice (Fig. 29I). The CSA of contralateral muscle fibres in WT or Megf10$^{+/-}$ did not change after overload, but there was a significant increase in CSA for Megf10$^{-/-}$ fibres. Fibre size in the contralateral tissue was highly variable when comparisons were made between genotypes (Fig. 32H).

The considerable variability in CSA measurements, with the greatest variation in muscle from Megf10$^{-/-}$ mice, makes it difficult to conclude that overload increases fibre CSA, or that genotype of the mouse affects the response.

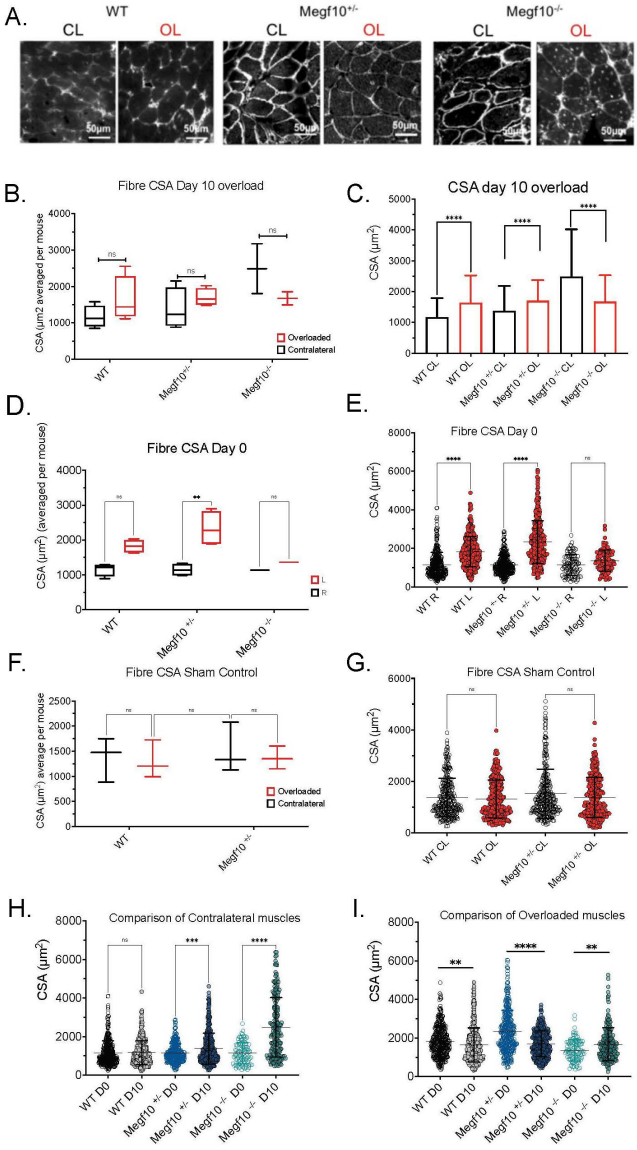

Figure 32. Changes to fibre cross-sectional area (CSA) in 10-day overloaded, unloaded (D0) and sham operated EDL. A. Representative images of D10 overloaded muscle fibre cross sections stained for laminin to show the fibre outlines. **B.** Mean ± S.D CSA for CL and OL EDL muscle fibres after 10-day overload, averaged per mouse (n=4 for WT and Megf10$^{+/-}$, n=2 for Megf10$^{-/-}$). **C.** Histogram showingfibre CSA measurements for CL and OL muscles. **D.** Mean ± S.D CSA, averaged per mouse, for unloaded EDL muscle (n=4 for WT and Megf10$^{+/-}$, n=1 for Megf10$^{-/-}$). **E.** Scatter plot showing each individual fibre measurement from all mice at D0 for left and right EDL muscles. **F.** Mean ± S.D CSA, averaged per mouse, in sham operated EDL muscle (n=3 for WT and Megf10$^{+/-}$). **G.** Scatter plot showing individual fibre CSA measurements for left and right EDL following sham operation on the left leg. **H.** Scatter plot showing direct comparisons of individual fibre measurements from D0 and D10 CL EDL muscles. **I.** Scatter plot showing direct comparisons of individual fibre measurements from D0 and D10 OL EDL muscles. 5 FOV analysed per mouse, 20 fibres measured per FOV. Black: CL, red: overloaded. **** p <0.0001. *** p <0.001. ** p <0.01. * p <0.05.

3.3.4 Fibres from Megf10$^{+/-}$ and Megf10$^{-/-}$ mice have lower numbers of Pax7^{+} satellite cell nuclei

Loss of Megf10 expression in humans has been linked to lower numbers of Pax7^{+} satellite cells (Logan et al., 2011). A change in numbers of Pax7^{+} satellite cells could be linked to the reduced hypertrophic response observed here for Megf10$^{-/-}$ (Fig. 31). To evaluate this, fibres were stained for the transcription factors Pax7, MyoD and myogenin, which are sequentially expressed as the cells become activated and then differentiate (Fig. 33).

At D0, the proportion of satellite cell nuclei that stained positive for Pax7 was significantly reduced between WT and Megf10$^{+/-}$ muscle fibres, and between WT and Megf10$^{-/-}$ fibres (Fig. 34D). These differences were observed for muscle fibres taken from both left and right legs, and measurements from right and left legs were consistent with each other (Fig. 34D).

3.3.5 Increase in numbers of TF+ satellite cell number as a result of overload is reduced in Megf10$^{+/-}$ and Megf10$^{-/-}$ mice

At D10, the proportion of satellite cell nuclei that stained positive for Pax7 was significantly lower in OL EDL muscle from Megf10$^{+/-}$ and Megf10$^{-/-}$ mice compared to WT, and significantly lower in EDL muscle from Megf10$^{-/-}$ compared to Megf10$^{+/-}$ mice (Fig. 33, Fig. 34A). In addition, the proportion of nuclei positive for Pax7 was significantly increased in OL muscle compared to CL muscle for WT and Megf10$^{+/-}$, but not for Megf10$^{-/-}$. Similarly, at D10 of overload, the number of satellite cell nuclei that were MyoD^{+} or myogenin^{+} were decreased for Megf10$^{+/-}$ and further decreased for Megf10$^{-/-}$ compared to WT, although this decrease was not significant for MyoD when comparing WT with Megf10$^{+/-}$ (Fig 34B, C).

For both WT and Megf10$^{+/-}$ mice, there were significant differences in Pax7 expression between right and left legs following sham operation (Fig. 34G). Levels

of MyoD and myogenin were not significantly different between muscles or between WT and Megf10$^{+/-}$ (Fig 34H, I). No significant differences in expression were observed for D0 mice, apart from a small increase in myogenin expression in the left leg of WT mice (Fig. 34D, E, F). Values for myogenin expression in sham operated mice were not significantly different from D0 mice. Thus, the change in myogenin expression is likely a result of overload (Fig. 34J). However, significant differences in Pax7 and MyoD expression between D0 and sham operated controls suggest that changes in the expression of these TFs may not be solely due to the overload (Fig. 34J).

Directly comparing the number of Pax7 positive nuclei between D0 and D10 EDL WT muscle showed there was a significant increase in Pax7 positive nuclei for OL (an increase of 12 nuclei, on average) but not control CL muscles (Fig. 34K). There was a small increase in TF staining on CL fibres compared to control, for MyoD and myogenin but a much more prononced increase in OL (an increase of 18 nuclei for MyoD and 31 for myogenin, on average). Megf10$^{+/-}$ showed a similar response(an increase of 34 nuclei for MyoD and 14 for myogenin, on average). The change in Pax7^{+} nuclei was not significantly increased after overload at D10. Additionally, MyoD expression on Megf10$^{+/-}$ D10 CL tissue was slightly higher than the control. In Megf10$^{-/-}$ mice, again a similar trend was observed, but, the response was much lower (an increase of 7 nuclei for MyoD and 12 for myogenin, on average). There was no observed increase in Pax7 expression at D10, compared to control (Fig. 34K). Thus, in the Megf10$^{-/-}$ mouse, muscle overload does not have any major effect on numbers of TF^{+} cells, consistent with the reduced hypertrophic response.

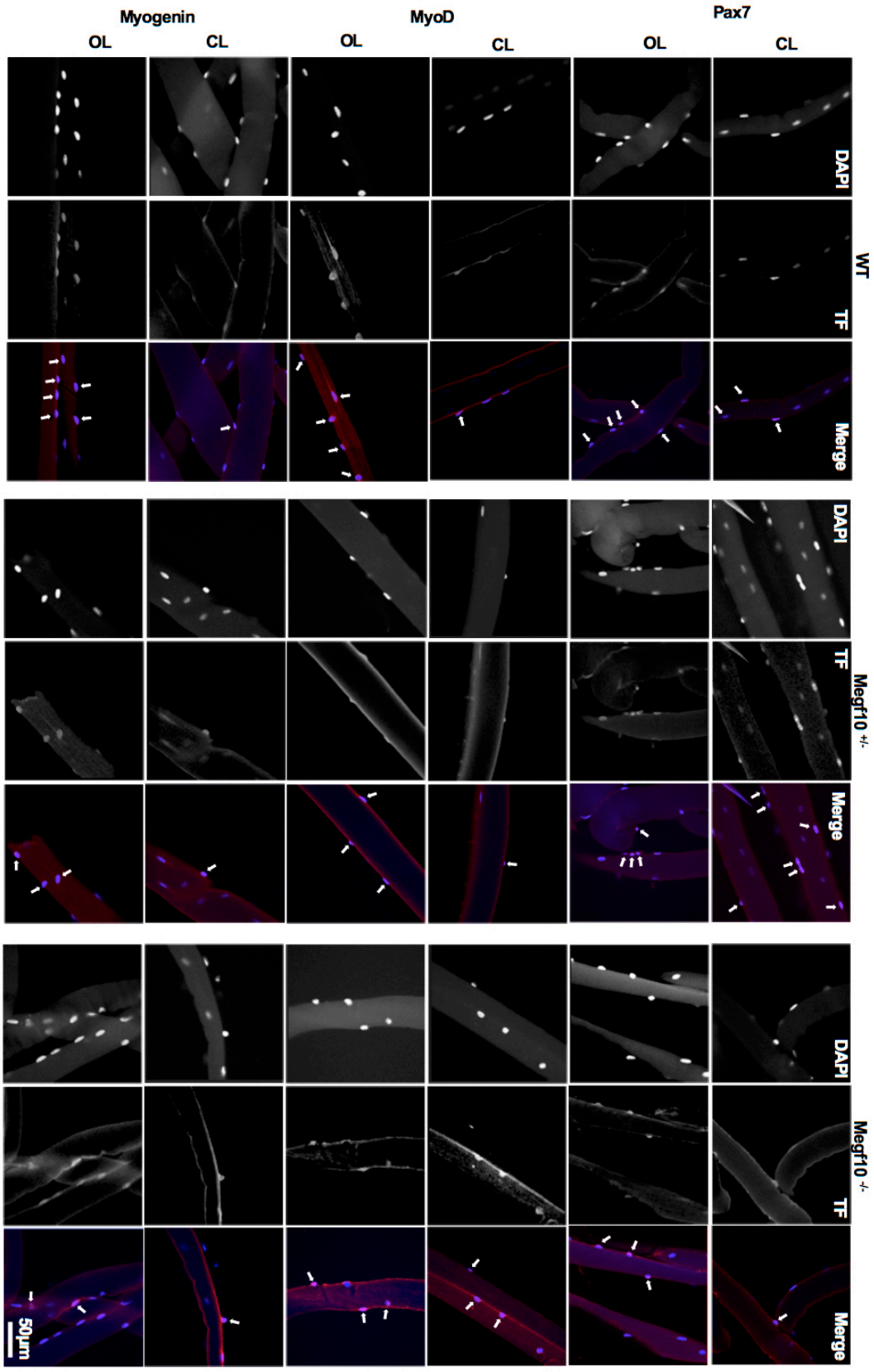

Figure 33. Immunofluorescent staining of satellite cells on isolated fibres. Single isolated fibres from contralateral and 10-day overloaded EDL muscle stained for Pax7, MyoD and myogenin in red and DAPI in blue.

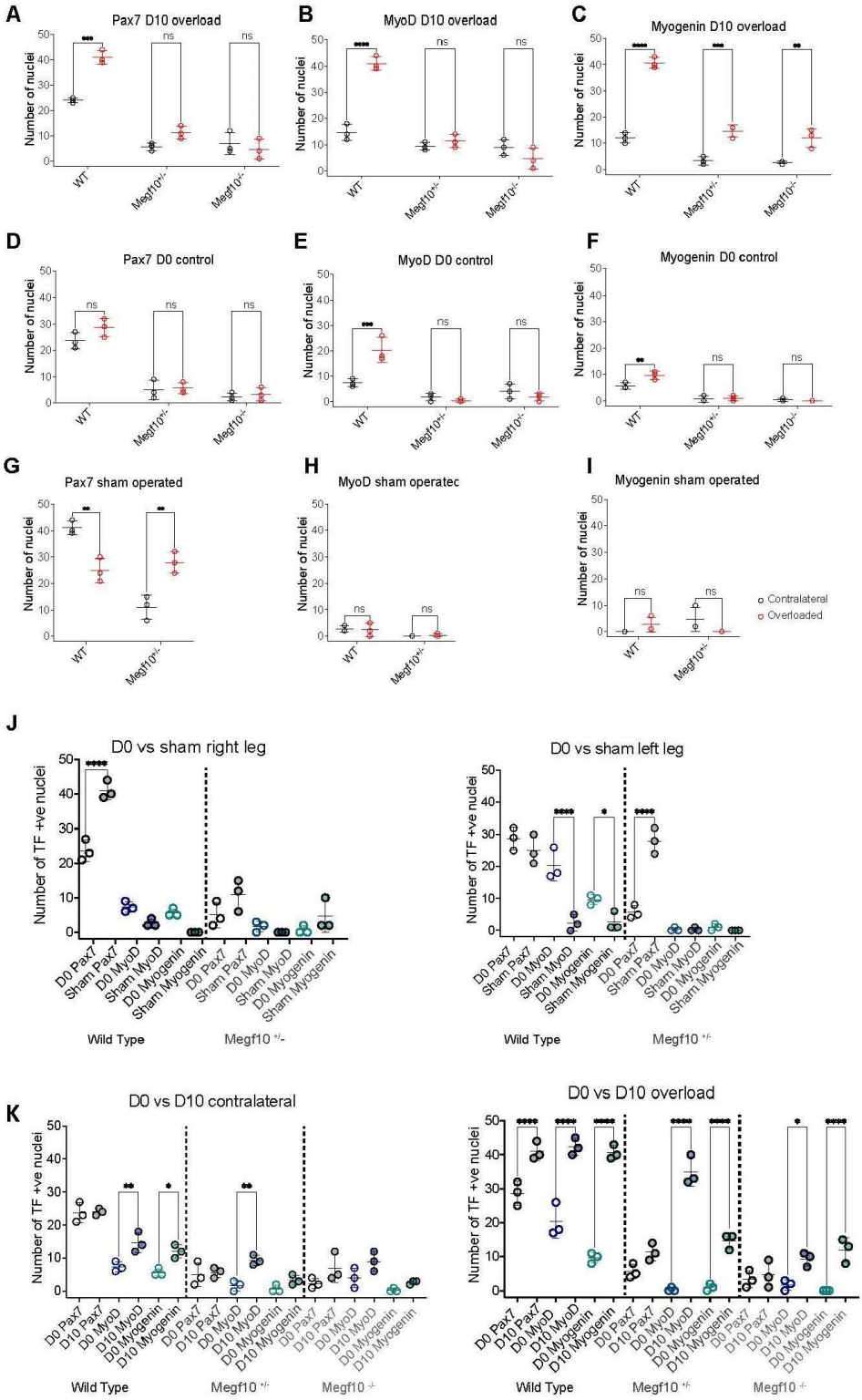

Figure 34. TF expression by satellite cells on fibres from WT, Megf10$^{+/-}$ and Megf10$^{-/-}$ mice. **A-I.** Comparisons shown between genotype for each TF. Black: CL, red: overloaded; or black: right leg, red: left leg if D0. **J.** Direct comparisons of TF staining on D0 and sham operated EDL fibres. **K.** Direct comparisons of TF staining on D0 and D10 overloaded EDL fibres. Error bars represent S.D. **** represents a P value <0.0001. *** represents a p value <0.001. ** represents a P value <0.01. * represents a p value <0.05.

3.3.6 Distribution of slow type 1 fibres in the EDL muscle was unaltered by loss of the MEGF10 gene

After 10-day overload in WT and Megf10$^{-/-}$ mice, no significant differences were found in the number of slow fibres before and after overload(Fig. 35A, C). While the change in proportion in slow fibres following overload was not significant, a wide range of percentages was observed for each genotype. In WT, slow fibre % ranged from 9-22%, in Megf10$^{+/-}$ it ranged from 8-18% and in Megf10$^{-/-}$ it ranged from 4-17%. There was no significant difference in the % of slow fibres in EDL muscles from WT, Megf10$^{+/-}$ and Megf10$^{-/-}$ in control, untreated mice. Muscles from each genotype contained ~ 5-10% slow muscle fibre types (Fig. 35B, D). Additionally, a direct comparison between D0 and D10 overloaded EDL showed no significant differences in percentage slow fibre type, in either the OL or CL tissue (Fig. 35E).

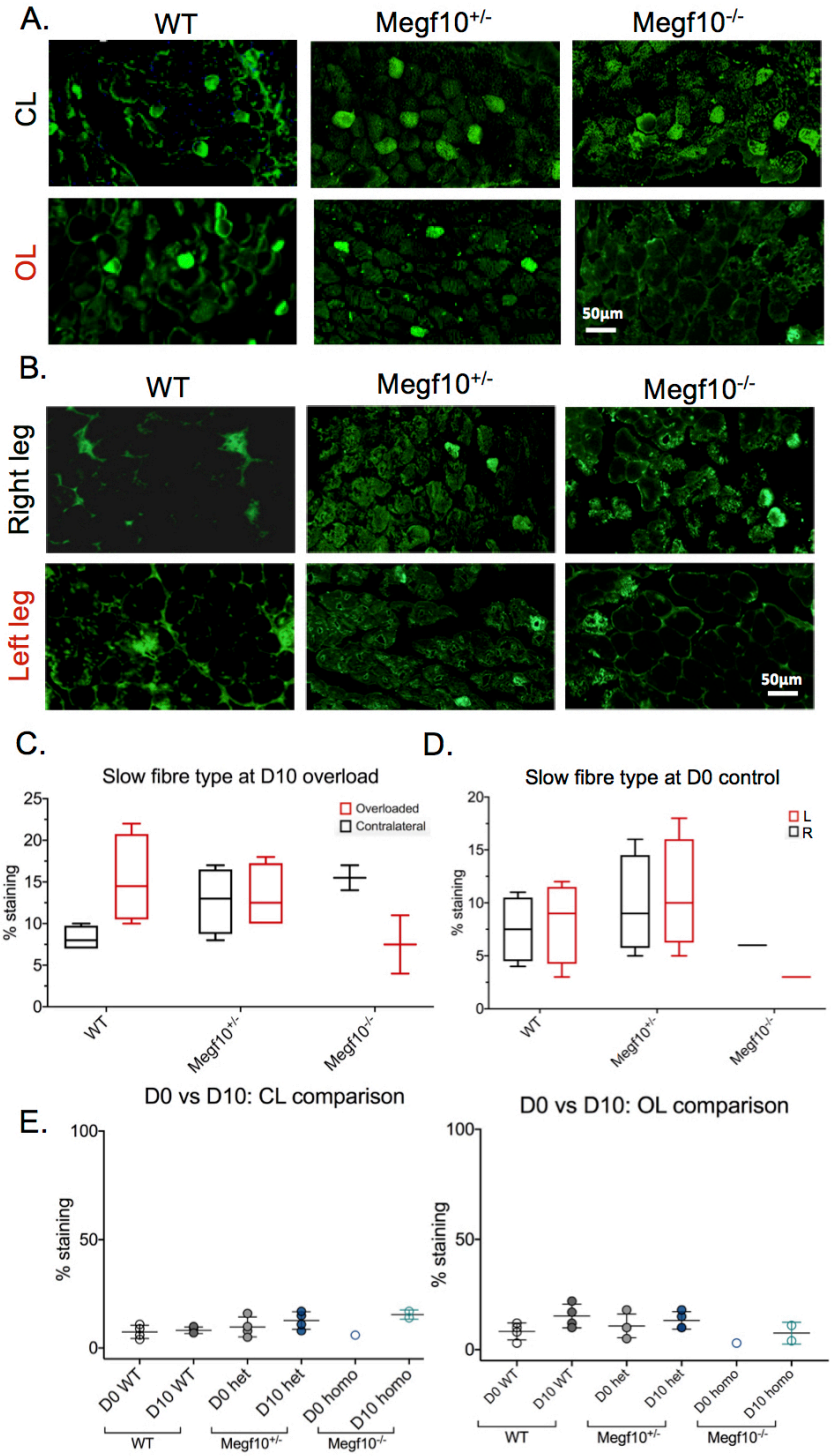

Figure 35. Distribution of slow fibre type in EDL. A. Representative images showing staining of slow fibres in D0, unloaded EDL. **B.** Representative images showing staining of slow fibres in overloaded EDL. **C.** Quantification of slow fibres in overloaded EDL muscle, averaged per mouse (n=4 for WT and Megf10$^{+/-}$, n=2 for Megf10$^{-/-}$). **D.** Quantification of slow fibres in unloaded EDL muscle, averaged per mouse (n=4 for WT and Megf10$^{+/-}$, n=1 for Megf10$^{-/-}$). **E.** Direct comparison of slow fibre staining in D0 and D10 overloaded fibres. Box plots show minimum, first quartile, median, third quartile and maximum values in each graph. Error bars represent S.D. **** p <0.0001. *** p <0.001. ** p <0.01. * p <0.05.

3.3.7 Mean fibre cross-sectional area in the diaphragm from Megf10$^{+/-}$ mice is smaller

Continuous genotyping of pups born from Megf10$^{+/-}$ x Megf10$^{+/-}$ matings indicated a surprisingly low number of Megf10$^{-/-}$ mice, lower than predicted from the expected Mendelian ratio of 1:2:1 for heterozygous breeding. This percentage of 33.3% Megf10$^{-/-}$ mice should have roughly been obtained since only the filial generation of mice were used for these experiments (Ramaley, 1912). The low numbers of Megf10$^{-/-}$ mice arose suspicion that these mice may have been dying shortly after birth, and may have been consumed by the mother, an event that commonly occurs when the offspring is deemed to be ill or too weak to survive (Klug et al., 2007). A possible reason for this early death was suspected to be related to respiratory distress, due to the mutation in the MEGF10 gene potentially causing similar issues as seen in human cases of EMARDD (Logan et al., 2011). To investigate a potential impact on respiration, we stained the diaphragm muscle from 6-week old WT and Megf10$^{+/-}$ mice for laminin, which outlines the muscle fibres, to determine if muscle fibre size and organisation is affected. Due to diaphragm sampling occurring at a relatively late stage in the investigation, no Megf10$^{-/-}$ mice were available. Analysis of diaphragm cross-sections revealed stark differences between WT and Megf10$^{+/-}$ mice (Fig. 36A). The mean fibre CSA per mouse was significantly lower in the diaphragms from Megf10$^{+/-}$ than WT mice (Fig. 36B). The same trend was observed for a comparison of the CSA of individual fibres, which additionally showed the greater range of CSA in fibres from WT mice compared to Megf10$^{+/-}$ (Fig. 36C). The thickness of the laminin between fibres was increased in the Megf10$^{+/-}$ diaphragm compared to WT (Fig. 36D). Smaller fibre size and increased laminin deposition surrounding the fibre are likely to impair the ability of the muscle to generate power and resist fatigue. In Megf10$^{+/-}$ mice, only one copy of the MEGF10 gene is defective, so this explains why the observed changes were not sufficient in reducing viability of Megf10$^{+/-}$ pups. Since Megf10$^{-/-}$ mice have two defective copies of the

MEGF10 gene, it can be hypothesised that the damage to the diaphragm is even more extensive in these animals. This may explain why the Mendelian ratio was not as expected and why Megf10$^{-/-}$ mice do not survive long after birth. Those Megf10$^{-/-}$ that were able to survive into adulthood for inclusion in this study may have been 'escapers', managing to avoid early respiratory distress or disguise their weakness from their cannibalistic mother.

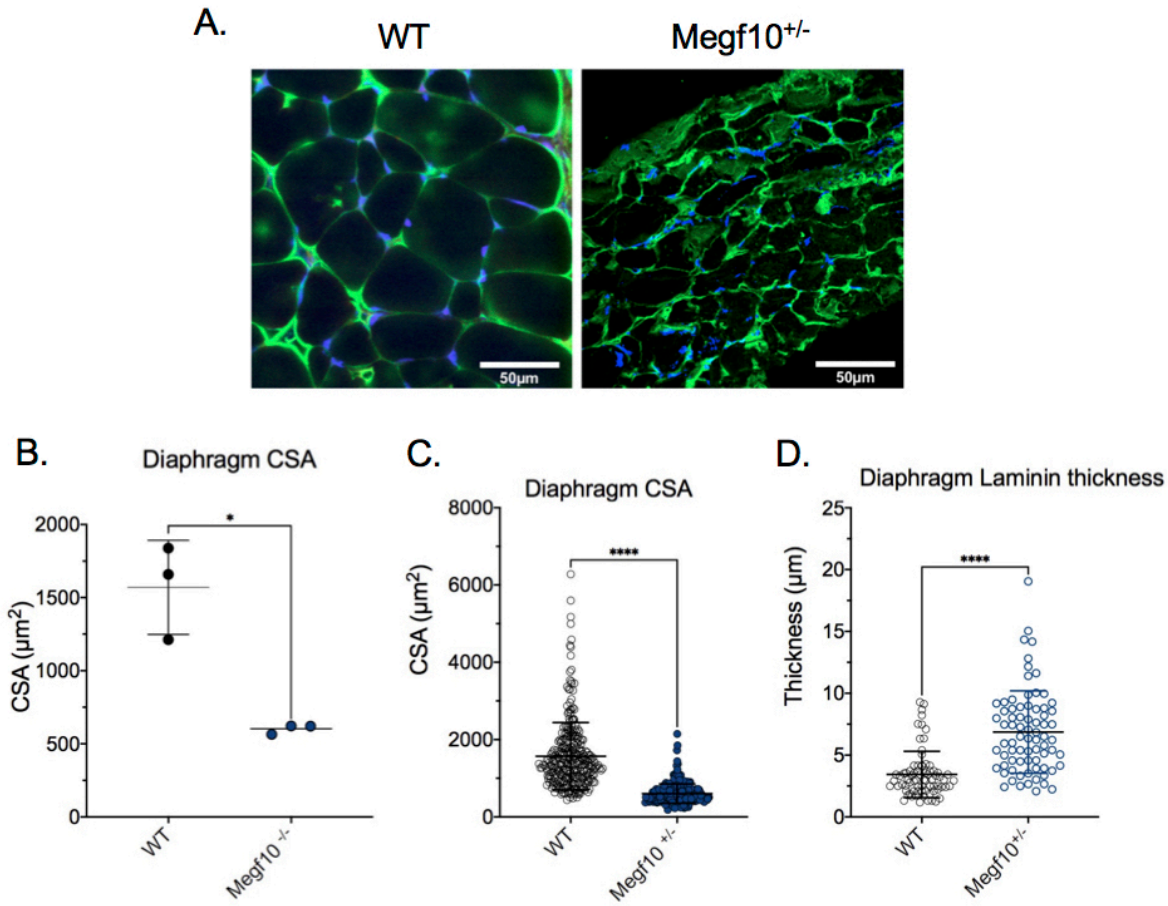

Figure 36. Comparison of WT and Megf10$^{+/-}$ diaphragm. A. Representative images of stained diaphragm cross-sections showing differences in fibre structure. Laminin outlined in green and nuclei visualised with DAPI. **B.** Measurements of CSA in diaphragm fibres, averaged per mouse (n=3 for WT and Megf10$^{+/-}$). **C.** Scatter plot showing individual measurements. **D.** Scatter plot showing thickness of laminin divisions between fibres, measured from 5 fibres per mouse. Error bars represent S.D. **** p <0.0001. *** p <0.001. * p <0.05.

3.3.8 Loss of the MEGF10 gene does not affect capillarisation of muscle tissue

Vascular endothelial cells (lectin^{+}) and Pax7 positive satellite cells were observed around the periphery of fibres in all genotypes (Fig. 37). When a 10-day overload was applied there was no significant difference in the number of endothelial cells surrounding fibres from WT, Megf10$^{+/-}$ and Megf10$^{-/-}$ EDL tissue when values were averaged to each mouse (Fig. 38A). In an unloaded control, again, there was no significant difference in the number of lectin positive cells when values were averaged to each mouse (Fig. 38B).

At D10, no significant difference in proportion of Pax7^{+} nuclei between CL and OL muscle was observed, in any of the genotypes (Fig. 38C). In both the overloaded and contralateral EDL, Pax7 expression in Megf10$^{-/-}$ mice was significantly lower than in WT and Megf10$^{+/-}$ mice. A similar trend was observed in an unloaded control. The proportion of Pax7^{+} positive nuclei in fibre cross sections was similar in the left and right EDL muscle at D0 in each of the genotypes, but significantly reduced in Megf10$^{-/-}$ mice compared to WT. This difference was observed for the mean values per mouse (Fig. 38D).

Nearest neighbour analysis (NNA) showed that the distance between Pax7 positive satellite cells and lectin positive vascular endothelial cells was similar between genotypes in a D0 unloaded control, with no significant differences between WT, Megf10$^{+/-}$ and Megf10$^{-/-}$ EDL mice (Fig. 38E). When distances were averaged to each mouse, 10-day overload did not significantly alter the proximity Pax7 and lectin positive cells to one another (Fig. 38F).

A direct comparison of lectin staining between D0 and D10 overloaded EDL showed that there was a greater number of endothelial cells surrounding fibres in control EDL, compared to contralateral EDL after 10-days overload, in Megf10$^{-/-}$ mice (Fig. 38G). This was the only significant difference found in the comparisons of unloaded EDL. Compared to control tissue, OL EDL had a significantly greater number of vascular endothelial cells in WT, but no significant change occurred in Megf10$^{+/-}$ mice between

D0 and D10 (Fig. 38H). Due to differences observed between D0 and CL tissue, the effects observed in 10-day overloaded EDL from Megf10$^{-/-}$ mice may not have been as a result of the procedure.

A direct comparison of NNA between D0 and D10 overloaded EDL showed no differences in the CL tissue (Fig. 38I). However, the distance between Pax7^{+} and lectin^{+} cells was significantly reduced at D10 compared to D0, in WT and Megf10$^{+/-}$ (Fig. 38J). This suggests that the change in proximity is likely an effect of the overload. For Megf10$^{-/-}$ mice, the reduction in distance was not significant. In general, overload appears to mildly increase vascularisation in all genotypes, however this observation is confounded by the variability within the results.

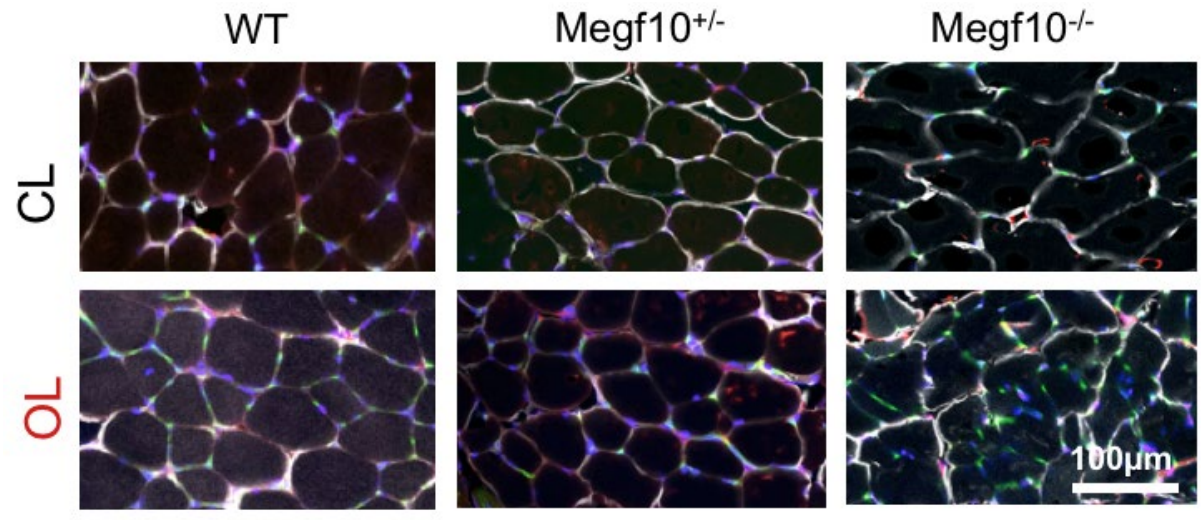

Figure 37. Capillarisation in EDL. A. Representative images of 10-day overloaded EDL tissue showing lectin (green), Pax7 (red), laminin (grey) and DAPI (blue) staining around muscle fibres.

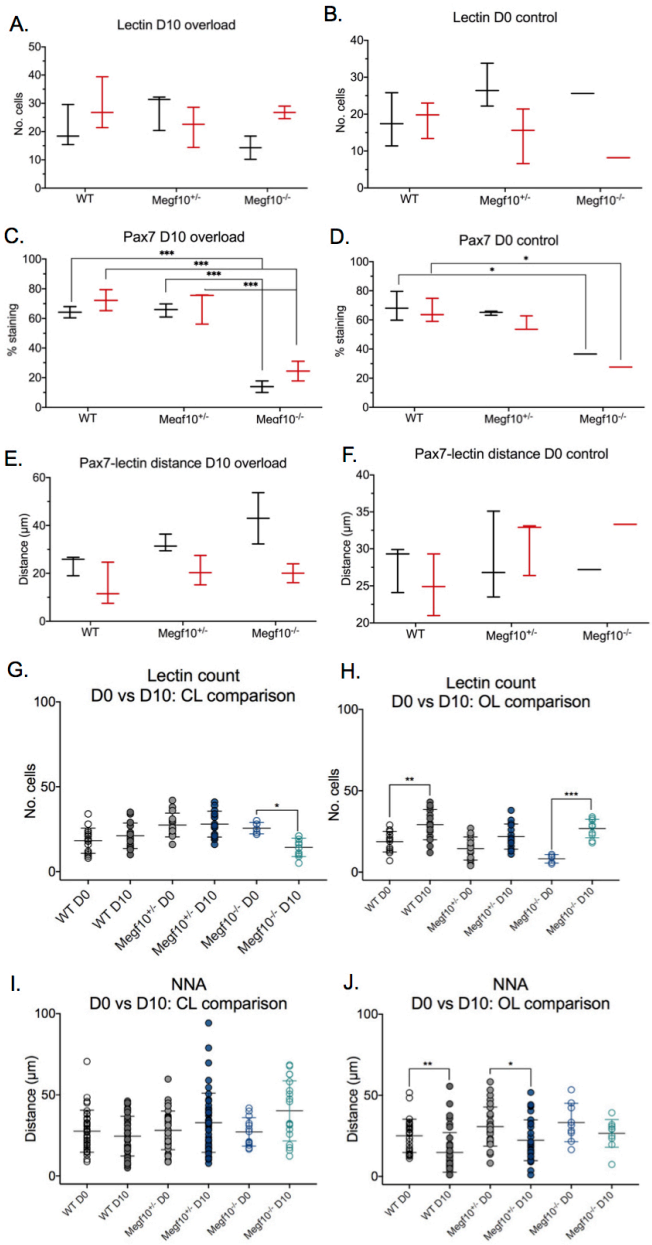

Figure 38. Analysis of capillarisation in EDL. A. Mean number of cells per mouse showing lectin staining in overloaded EDL (n=3 for WT and Megf10$^{+/-}$, n=2 for Megf10$^{-/-}$). **B.** Mean number of cells per mouse showing lectin staining in unloaded EDL (n=3 for WT and Megf10$^{+/-}$, n=1 for Megf10$^{-/-}$). **C.** Mean value per mouse for % Pax7^{+} nuclei in overloaded EDL (n=3 for WT and Megf10$^{+/-}$, n=2 for Megf10$^{-/-}$). **D.** Mean value per mouse for % Pax7^{+} nuclei in unloaded EDL (n=3 for WT and Megf10$^{+/-}$, n=1 for Megf10$^{-/-}$). **E.** Mean distance per mouse between Pax7^{+} and nearest lectin^{+} neighbours in overloaded EDL (n=3 for WT and Megf10$^{+/-}$, n=2 for Megf10$^{-/-}$). **F.** Mean distance per mouse between Pax7^{+} and nearest lectin^{+} neighbours in unloaded EDL (n=3 for WT and Megf10$^{+/-}$, n=1 for Megf10$^{-/-}$). **G.** Direct comparison of lectin staining in D0 and D10 CL fibres. **H.** Direct comparison of lectin staining in D0 and D10 OL fibres. **I.** Direct comparison of NNA in D0 and D10 CL fibres. **J.** Direct comparison of NNA in D0 and D10 CL fibres**.** Error bars represent S.D. 5 FOV for each mouse, 20 fibres counted. **** p<0.0001. *** p<0.001. ** p<0.01. * p<0.05. Black: CL, red: overloaded, or black: right leg, red: left leg.

3.4 Discussion

These data demonstrate that overload surgery induces a mild hypertrophy response as reported previously (Rosenblatt et al., 1994). Initial experiments showed that D10 overload was a suitable time point to evaluate hypertrophy as a result of overload, as while the extent of overload was similar to that at D6, the variation in hypertrophy was lower at this time point. Experiments with Megf10$^{+/-}$ and Megf10$^{-/-}$ mice showed that loss of MEGF10 impairs the hypertrophic response of overloaded EDL, as shown by the significantly lower relative hypertrophy. This observation is supported by a significantly smaller increase in fibre CSA after 10-day overload compared to WT mice, however the high level of variability in CSA values prevents a conclusion being reached regarding the effects on fibre size. The reduction in hypertrophy in Megf10$^{+/-}$ and Megf10$^{-/-}$ mice was linked to a reduction in TF^{+} stained satellite cells. We also observed that muscle fibre CSA from the diaphragm muscle was reduced in Megf10$^{+/-}$ compared to WT. These changes are not apparently linked to changes in fibre type, or vascularisation.

The response of the EDL muscle to overload in WT mice was consistent with previous reports that described an increase in EDL mass following sustained overload (Egginton et al., 2011; Johnson and Klueber, 1991). We observed an increase in mass of the overloaded tissue by ~40%. This is greater than hypertrophy reported previously in similar studies (~22%) on rodents, but has been reported to range from 9%-33% when up to 30 days overload is applied (Egginton et al., 1998; Huey et al., 2016; Seiden, 1976). Any slight differences in EDL weight between right and left legs at D0 (unoperated controls) may have occurred due to the accidental excision of EDL tissue during sampling, or failure to fully remove extraneous tissue e.g. fascia.

Although our work was unable to determine if overload increases fibre CSA, this is an effect that has been widely reported for WT rodents (Carter et al., 1995; Rosenblatt e al., 1994; Snijders et al., 2019). Following ~9 days overload, CSA has been reported to increase by 35%, with a 54% increase in myonuclei that occurs prior to fibre

hypertrophy (Bruusgaard et al., 2010). The accompanying increase in myonuclei corresponds to the effects we reported here, with the greatest increase at D10 overload. Previous work has found that while they do have a role in enhancing fibre hypertrophy, some increase in fibre size is possible without functional satellite cells (Murach et al., 2017). The means by which CSA was calculated, manually outlining fibres with ImageJ software, may have introduced bias and limited the data. An alternative method would be to calculate the minimum Feret's diameter of the fibre cross-sections, a method that measures the closest possible distance between the two parallel planes of a muscle fibre. Calculation of Feret's diameter minimizes the effects of oblique sectioning, a factor that may have contributed to the often unexpectedly large fibre CSA in certain samples, such as the D0 comparison of right and left EDL in Megf10$^{+/-}$ mice (Pertl et al., 2003). The lack of significant difference in CSA in WT or Megf10$^{-/-}$ at D0 suggests a sample sectioning error; some temporary enlargement of muscle fibres due to inflammation from surgery can occur, however, the D0 mice did not undergo any intervention so this can be ruled out (Toumo and Best, 2003). Blinding the cross-sectional images to prevent prior knowledge of the genotype and overload intervention would also have strengthened this analysis. The role of satellite cells in hypertrophy of WT mice was explored in our work, by investigating the change in expression of TFs after overload. The increase in Pax7^{+}, MyoD^{+} and myogenin^{+} satellite cells of WT mice following 10-day overload supports previous findings (Hyatt et al., 2008; Sakuma et al., 1998). Thus, the experimental data shown here shows that EDL from WT mice responds to overload as expected, and this is a suitable approach to explore the effects of overload in Megf10$^{+/-}$ and Megf10$^{-/-}$ mice following overload.

Pax7 is necessary for the activation and subsequent expansion of satellite cells in response to stimulus such as overload (Xin and Rudnicki, 2012). The reduction of Pax7 observed in Megf10$^{+/-}$ and Megf10$^{-/-}$ mice, compared to WT, may be indicative of impaired satellite cell activation in these mice. Our findings agree with a previous report that found MEGF10 deficient mice to have reduced expression of Pax7 and MyoD,

resulting in inadequate regeneration of EDL muscle, following barium chloride treatment. Reduced regeneration in Megf10$^{-/-}$ mice was characterised by the presence of atrophic fibres, highly variable fibre size and increased muscle fibrosis (Li et al., 2021).

The reduced expression of MyoD and myogenin (TFs involved in the specification and differentiation of myogenic cells) in Megf10$^{-/-}$ mice after overload suggests that MEGF10 may also be important in later stages of regeneration. MEGF10 has been suggested to interact with Notch1. A reduction of Notch1 signalling has been shown to impair proliferation and reduces the migration of committed, MyoD^{+} satellite cells along existing fibres (Holterman et al., 2007; Saha et al., 2017). Thus, when MEGF10 is absent, key myogenic transcription factors are not transcribed at quantities sufficient to drive myogenesis. This impaired interaction with Notch1 and subsequent failure of myogenic transcriptional activity may have occurred due to the knockout mutation disrupting the disulphide bonds that form between the EGF-like domains. Disruption of these bonds results in a misfolding of the MEGF10 protein, rendering it non-functional (Wouters et al., 2005). Deletion mutations of the MEGF10 gene can also disrupt the EMI domain, impacting on protein-protein interactions (Callebaut et al., 2003). High expression of MEGF10 has been previously reported in Pax7^{+} satellite cells (Holterman et al., 2007, Seale et al., 2004). It also has a close transcriptional relationship with the myogenic transcription factors that are transcribed later in myogenesis, namely Myf5, MyoD and myogenin. Previous work using a CTX injury model of muscle regeneration found that levels of MEGF10 mRNA showed a similar expression pattern to the transcription factors 3 days post injury. Additionally, four E-box binding sites have been identified on the promoter region of the MEGF10, which act as binding sites for the myogenic bHLH transcription factors (Park et al., 2014). It thus follows that impairment of MEGF10 is likely to result in the disruption of myogenic transcription factor expression in satellite cells, affecting regeneration.

Impaired satellite cell activity may help to explain the significant reduction in hypertrophy of overloaded EDL in Megf10$^{+/-}$ and to an even greater extent, Megf10$^{-/-}$

mice. The differences in the response to overload between genotypes is consistent with a role for MEGF10 in muscle regeneration. MEGF10, present in the plasma membrane of satellite cells, is able to activate satellite cells and drive the formation of new myofibres via myonuclear accretion (Holterman et al., 2007). However, myonuclear accretion occurred after overload for all genotypes, suggesting that the EDL of Megf10$^{-/-}$ mice was capable of undergoing hyperplasia, although accretion was less pronounced. Previous work using WT mice has shown that fibre type distribution changes with muscle remodelling (Green et al., 1984). Previous work using a similar overload model to this study reported a small increase in the proportion of type 2a fibres following 28-day overload (Rosenblatt and Parry, 1985). Additionally, the proportion of slow type fibres typically increases in response to overload with relatively low load, however, our study could not discern any difference in slow fibre distribution following overload, or between mouse genotypes (Ogborn and Schoenfeld, 2014).

Following overload, expression of the vascular endothelium protein lectin increased in the EDL, in both WT and Megf10$^{-/-}$, and it is possible that this new capillary growth is triggered by a transient state of hypoxia placed upon the EDL muscle, in response to increased anabolic energy demands due to removal of the synergistic TA (Hermansen and Wachtlova, 1971). The distance between satellite cells and endothelial cells around myofibres also decreased due to overload, which potentially allows enhanced communication between the two cell types. When they are in close proximity to one another, vascular cells can activate satellite cells and vice versa, via secretion of growth factors such as insulin-like growth factor-1 (IGF), hepatocyte growth factor (HGF) and vascular endothelial growth factor (VEGF) (Hendrickse and Degens, 2019). The absence of MEGF10 did not significantly alter the vascular response in overloaded tissue.

The significantly reduced number of satellite cells stained positively for myogenic markers in both Megf10$^{+/-}$ and Megf10$^{-/-}$ muscle fibres supports the hypothesis that MEGF10 is essential for the satellite cell response to drive muscle regeneration through

myogenesis. However, muscle histology analyses do not support this hypothesis and conflict with the findings from isolated skeletal muscle fibres. No significant increase in fibre CSA was observed after 10-day overload in any of the three genotypes, and lack of MEGF10 did not have a clear effect on the vascular response during muscle hypertrophy. Further experiments are required to understand if MEGF10 does have a role in the increase of CSA following overload, an event that was not observed in this study, but is widely reported in the literature (Murach et al., 2017, Blough et al., 2000, Reggiani et al., 2020, Lourenço et al., 2020). Such experiments should include a larger sample size than reported here, incorporate more reliable methods of measure fibre size (e.g. Feret's diameter), and optimise cryosectioning protocol to improve protein staining and reduce the number of oblique fibres. Crucially, sections should be stained for MEGF10 to check for its presence around the muscle fibre and observe whether levels increase following overload. Additionally, future experiments could expand on the investigation of MEGF10 mutation on vascular activity by staining for other proteins apart from lectin. Previous work has identified the presence of MEGF10 in $CD34^{-}/Pax7^{-}/MyoD^{-}$ cells on the periphery of isolated muscle fibres (Hughes, 2016). These unknown cells were suspected to be pericytes, vascular cells previously shown to have a role in myogenesis (Dellavale et al., 2011). The reduction of pericytes and subsequent impact on myogenesis because of MEGF10 knockout would be an interesting route to explore in the future.

In some cases, a small hypertrophic effect was observed in contralateral EDL muscles, despite these muscles not being subjected to overload. This phenomenon occurs because of the altered gait of the animals after surgery. Often, the mice limp and redistribute their weight so that more load is placed on the contralateral leg. This causes a small hypertrophic effect on the contralateral side and is the reason that D0 (unoperated) and sham operated EDL muscles were included in this study to provide additional controls.

The images of diaphragm from Megf10$^{+/-}$ mice closely resemble images from the diaphragm of the *mdx* mouse (Stedman et al., 1991). This established mouse model of DMD has diaphragm tissue that is functionally impaired and closely resembles the diaphragm of human sufferers of DMD. Respiratory distress as a result of weak diaphragm muscle is a severe consequence of DMD in humans, and is often the cause of death in these patients (Stedman et al., 1991). Similarly, loss of MEGF10 in humans causes respiratory distress (Logan et al., 2011). This change to structure in the diaphragm of Megf10$^{+/-}$ mice may lead to respiratory distress (Logan et al., 2011). In humans with MEGF10 mutations that lead to EMARDD, those with heterozygous mutations tend to be asymptomatic and without respiratory distress, which does not align with the damage observed in the diaphragms of Megf10$^{+/-}$ mice in this study. This is perhaps explained by the high levels of heterogeny in clinical presentation of EMARDD in humans, with symptoms varying depending on the specific type of MEGF10 mutation (Logan et al., 2011, Liewluck et al., 2016). This may also be an indication of a lack of translatability of the mouse model to human EMARDD patients, as biological differences exist between mice and humans that may allow heterozygous humans to better compensate for the lack of one copy of the MEGF10 gene. Further work is needed to confirm if the diaphragm of Megf10$^{-/-}$ mice is affected more strongly, and this would involve sampling and running analyses on diaphragm from adult Megf10$^{-/-}$ mice. A previous mouse model for MEGF10 knockout was reported to have a ‘mild’ phenotype. The model we have used here may be a better model for EMARDD given the strong effects on the diaphragm (Logan et al., 2011). The observed atrophy to the diaphragm may have been caused by impaired synthesis and increased degradation of proteins in the muscle fibres, accompanying increased release of inflammatory cytokines, imbalanced metabolic hormones, increased apoptosis and oxidative stress. Proteolysis within the diaphragm can occur via activation of the ubiquitin proteasome system and caspases (van Hees et al., 2008; van Hees et al., 2007). Mitochondrial oxidative stress activates further apoptosis within the diaphragm and causes further degradation of

diaphragmatic muscle proteins (Barbieri and Sestili, 2012). The degeneration of the diaphragm will likely activate satellite cells, and these satellite cells will proliferate then attempt fusion to aid in regeneration of the tissue. However, previous work investigating fibrotic diaphragm of COPD patients found a severe impairment of satellite cells to fuse and differentiate into myotubes (Verheul et al., 2006). Further evidence to suggest that satellite cell function in the MEGF10$^{+/-}$ mice was altered, is previous work exploring the function of satellite cells in *mdx* mice. This study found that satellite cells had elevated expression of FGF receptors, resulting in increased sensitivity to growth factors, indicative of degeneration (Crisona et al., 2004)

The investigation of the effects of MEGF10 mutation on skeletal muscle hypertrophy was limited by the small sample size MEGF10 knockout mice in relation to WT. This was especially relevant to the experiments involving analysis of the diaphragm, whereby only 3 WT and 3 MEGF10$^{+/-}$ mice were sampled with no samples from the MEGF10$^{-/-}$ mice. Thus, the effect of complete loss of MEGF10 on diaphragm structure cannot be assessed and very little can be taken from these results in the context of EMARDD, whereby the genotypic background of patients is most similar to Megf10$^{+-/-}$ mice. Additionally, inadequate sample size in other experiments within this investigation is a likely contributor to inconclusive findings e.g., the effect of MEGF10 mutation on capillarisation and CSA.

4 Characterisation of Satellite Cell Populations

4.1 Introduction

My experiments with the MEGF10 knockout mouse showed that MEGF10 deficient skeletal muscle fibres are less able to respond to overload than normal muscles. This was linked to a reduction in activation of satellite cells, as demonstrated by a reduction in staining for transcription factors such as MyoD and myogenin. While the *in vivo* studies are a useful approach to assess the effects of hypertrophy on satellite cell behaviour, a complementary approach is to isolate muscle fibres and observe changes in satellite cell activation *in vitro*. These analyses can provide supplementary data on how satellite cells behave, as cell culture provides a comparable stimulus to overload, with a transition from quiescence to activation achieved by changing medium to a higher serum content (Bischoff, 1986; Anderson et al., 2012). Additionally, isolating satellite cells and carrying out FACS allows a high-throughput investigation of a much wider pool of cells, compared to analysis of satellite cells still attached to myofibres.

Previous work has shown fibre isolation and subsequent culture to be an effective way of analysing satellite cell behaviour, as this process allows various measurements to be taken that give information about their role in myogenesis. Early experiments investigated the mitotic behaviour of satellite cells by marking dividing nuclei with bromodeoxyuridine (BdrU) and recording the length of time in each phase of the cell cycle (Schultz, 1996). These experiments determined that dividing satellite cells have a ~32hr cell cycle and that a limited number of divisions occur before fusion with other myogenic cells. The orientation of division can also be analysed with *in vitro* culture of isolated fibres. Time-lapse imaging of cultured myofibres over a 24hr time period established that satellite cells dividing asymmetrically remain in contact for a longer period of time than those that divide symmetrically. In this study it was established that

the length of cell cycle was 10hrs on average for the first and second divisions, then 8hrs on average for the third and fourth. Filming began after 24hrs in culture had elapsed to allow fibres to settle and respond to the culture environment. Divisions were not synchronous and there was a split of asymmetric and symmetric divisions, This understanding of satellite cell division timing and orientation further suggests a high level of heterogeneity within the satellite cell niche (Siegel at al., 2011). The migration of a satellite cell towards another satellite cell along the fibre, for fusion, can also be observed through filming cultured fibres. Work analysing fibres cultured fibres from 24-72hrs found that newly produced satellite cells often migrate along the fibre with sister satellite cells, and that they group together in 'clumps' prior to fusion later in the culture period (Siegel et al., 2009). Recently, MEGF10 has been implicated in the migratory behaviour of satellite cells in a study that investigated detachment of satellite cells from fibres cultured over 72hrs. Fewer satellite cells were found to detach from fibres that were isolated from $Megf10^{-/-}$ mice, suggesting that MEGF10 plays a part in the activation and migration of satellite cells to fusion targets (Li et al., 2021). The scope of measurements that can be taken using cultured fibres consolidates this technique as useful for studying satellite cells *in vitro*, whilst remaining relatively undisturbed in their original position underneath the basal lamina (Moyle et al., 2014).

Another method of analysing satellite cell behaviour *in vitro* is by isolating the cells from resident myofibres entirely. Neonatal mice tend to be used in satellite cell isolations, due to higher numbers of satellite cells compared to adults (Allbrook et al., 1971). This method has been used previously to set up primary cultures of isolated satellite cells, allowing comparison of quiescent satellite cells to activated and dividing progenitors (myoblasts) (Collins et al., 2005). Using immunofluorescence to investigate expression patterns of isolated satellite cells in adherent culture, it has been found that quiescent cells express Pax7, but those that become myoblasts go on to express MyoD, and eventually myogenin (Shefer et al., 2006).

Following isolation from muscle, the satellite cell sample can be purified and sorted into distinct populations based on protein expression using fluorescence activated cell sorting (FACS) (Gromova et al., 2015). A previously established selection scheme for satellite cells in FACS uses the surface markers CD34 and α7-integrin to separate out satellite cells, and various other endogenous markers such as CD45, CD31, CD11b and Sca1 in order to identify and separate haematopoietic and stromal cells that exist in the niche alongside satellite cells (Sacco et al., 2008; Maesner et al., 2016). CD34 and α7-integrin are useful markers as CD34 is expressed by the majority of satellite cells, quiescent or activated, and α7-integrin is a skeletal muscle specific laminin-binding surface antigen (Ziober at al., 1997; Blanco-Bose, 2001). Work using reporter mice has found that most cells within this purified population also express the ubiquitous satellite cell marker, Pax7, further validating a selection scheme using these markers (Beauchamp et al., 2001; Ziober at al., 1997; Maesner et al., 2016).

Here I investigated whether culturing myofibres *in vitro* causes satellite cells to progress through the myogenic programme similarly to *in vivo* following 10-day overload, by analysing the transcription factor expression and movement of satellite cells after set lengths of time in culture. I then determined how this behaviour *in vitro* was affected by a loss of MEGF10, and used FACS to understand what proportion of WT satellite cells contain MEGF10 and how this changes in Megf10$^{+/-}$ mice, thus, further elucidating the role of MEGF10 in muscle regeneration.

4.2 Methods

4.2.1 General procedures

All media, glassware, plastic and surgical tools were sterilised before use, either by autoclaving at 121°C for 15 min or washing thoroughly with 70% ethanol in H_2O.

4.2.2 Satellite cell isolation

Satellite cells were isolated from skeletal muscle fibres from C57BL/6Tac and Megf10$^{tm1(KOMP)Vlcg}$ mice (of Megf10$^{+/-}$ genotype) by standard proteolytic digestion methods (Pasut et al., 2013). Neonatal (1-2 days old) mice were used as they have higher numbers of satellite cells than adults. Prior to sampling, enzymatic solutions and media were prepared using ingredients listed (Table 13). A litter of neonates were removed from their mother and killed by schedule 1 as soon as possible thereafter. Heads, paws and tails were removed using dissection scissors and the remaining torso was washed with 70% ethanol in a 100mm petri dish (Nunc). It was then placed into a second 100mm petri dish filled with 20ml antibiotic-antimycotic solution (A5955, Sigma) and carefully skinned with forceps and dissection scissors, taking care not to pierce the gut. All limbs were dissected and then placed into a smaller 60mm petri dish (Nunc) filled with 6ml antibiotic-antimycotic solution.

Muscle from each limb was carefully dissected and placed into a fresh 60mm petri dish, and this was then minced thoroughly with a No. 10 scalpel blade. This process was repeated for each neonate in the litter and minced muscle was then divided into five portions and dispensed into five centrifuge tubes. 5ml pre-prepared enzyme solution was added to each tube and these were then incubated at 37°C with shaking for 15 mins. Contents of the tube were then mixed by aspirating 10 times to help release the satellite cells from the tissue. Undigested muscle tissue was allowed to settle at the bottom of the tube before supernatant was removed and placed into a sterile glass beaker (200ml). 25ml inhibition media was added to the beaker, to inhibit further digestion of the released satellite cells, and the beaker placed on ice. 5ml trypsin solution was added to each centrifuge tube containing the remaining muscle tissue and they were again incubated at 37°C with shaking for 15 mins. The suspension was again mixed by pipette, muscle tissue allowed to settle, supernatant, containing released cells, tipped into the glass beaker, and 25ml inhibition media added. This process was repeated twice more. The

mixture of supernatant + inhibition medium, containing satellite cells (~150ml) was then filtered using filters with a pore size of 45μm into a fresh 200ml glass beaker.

Filtered solution was then divided into 50ml falcons and centrifuged at 1000rpm for 10 mins. Supernatant was discarded and pellets were resuspended in 10ml culture media. The cell suspension was decanted into a T75 flask to carry out pre-plating. The flask was incubated at 37°C, 5% CO2 for 1hr to allow other cells (e.g. fibroblasts) to adhere to the flask, leaving a purer satellite cell population in the cell suspension. A 10μl sample of the cell suspension was then taken and cells were counted using a glass haemocytometer. The cell suspension was then divided for use in fluorescence activated cell sorting (FACS).

Solution	Composition	Preparation
Trypsin stock solution (6mg/ml)	402mg trypsin from porcine pancreas (Sigma T303) in warmed 67ml Ca^{2+} & Mg^{2+} free HBSS (Gibco 14170120).	Mixed at room temperature for 2hrs. Can be stored at -20°C prior to use.
Collagenase stock solution (2mg/ml)	18mg collagenase (Type 1) from *Clostridium histoyticum* (Sigma C0130) in warmed 9ml Ca^{2+} & Mg^{2+} free HBSS.	Collagenase added to HBSS immediately before digestion to ensure optimal activity of collagenase.
Enzyme solution	17ml trypsin stock solution 9ml collagenase stock solution.	Added together and mixed.
Inhibition medium	15ml FBS (Gibco) 1.5ml P/S 58.5ml Ca^{2+} & Mg^{2+} free HBSS.	Added together and mixed.
Culture medium	DMEM 20% FBS 2% CEE 1%P/S	Can be stored at -4°C but must be warmed to 37°C prior to use.

Table 13. Solutions used to isolate satellite cells, compositions and method of preparation.

HBSS: Hanks balanced salt solution.

4.2.3 Fluorescence activated cell sorting (FACS)

Live cells were purified into distinct populations based on surface protein expression using FACS. Cells from the satellite cell isolation were divided into 15ml Falcon tubes, with ~10,000 cells in each tube, and a different staining condition (Table 14). The cell suspensions were centrifuged at 1000rpm for 10 mins and supernatant discarded. Pre-conjugated primary antibodies, diluted in 200ul wash medium (1% BSA in PBS) and this was added to each falcon. To identify a purified population of satellite cells, antibodies for ubiquitous satellite cell markers CD34, and α7-integrin were chosen (Beauchamp et al., 2000; Ziober at al., 1997). CD45 was selected to identify haemopoietic cells within the niche – this protein is expressed on most vascular endothelial cells. (Montarras et al., 2005; Shaw et al., 2004). The MEGF10 antibody used for the FACS analysis was validated by previous work in the lab that compared three commercially available MEGF10 antibodies (Sigma Prestige, Millipore, Santa Cruz). Of these antibodies, only the Sigma Prestige antibody was able to recognise MEGF10 well in both immunocytochemistry and immunoblotting experiments (Hughes, 2016). This may be because the Sigma Prestige antibody recognises the ECD of MEGF10, whereas the other two antibodies recognise the intracellular domain (Kay et al., 2012, Bröhl et al., 2012). Interactions between proteins and the intracellular domain of MEGF10 may inhibit the binding of the antibodies, although this was not confirmed. These previous results informed the choice to use the Sigma Prestige antibody for the FACS investigation. The MEGF10 primary antibody was not pre-conjugated, so to conjugate it to a FITC fluorophore, a Lightning Link® kit (Abcam) was used. Briefly, 10µl MEGF10 antibody was added to the lyophilised mixture containing the FITC label, and left to incubate at room temperature for 3hrs. 1µl Lightning Link® quencher reagent was then added, and following incubation at room temperature for 30mins, the conjugated MEGF10 antibody was ready to use (Ferrara et al., 2013). The mixture containing wash medium and primary antibody was transferred to fresh centrifuge tubes and incubated at room temperature for 40 mins on a rocker. 2ml of additional wash medium was then added to

each tube and the tubes were inverted to mix. Tubes were centrifuged at 250 *x g* for 5 mins, supernatant was, discarded, and 500µl of wash medium was added. A blank sample (was medium only) and a sample containing all antibodies mixed together in the wash medium were used as controls in the sort.

Samples were loaded into and sorted by a FACSMelody™ (BD). To set up an optimal gating strategy, unstained WT cells, WT cells stained with a single antibody, and WT cells stained with multiple antibodies were analysed to identify populations with common characteristics: forward scatter (informing on cell size), side scatter (informing on cell granularity) and expression of protein markers. All samples were run and information was displayed regarding the populations that existed within the pool of satellite cells, and the percentage that each population comprised. A gating strategy was set by initially running controls with samples stained with a single antibody, and then using these initial measurements to separate out distinct cell populations in the samples stained for all four markers (CD34, α7-integrin, CD45 and MEGF10). Using this gating strategy, two more biological repeats were carried out for wild-type (WT, C57BL/6Tac) mice. Four additional sorts were carried out using satellite cells isolated using four neonatal mice from the Megf10$^{tm1(KOMP)Vlcg}$ mouse colony. Genotyping of these mice was carried out retrospectively.

Tube	Primary antibody	Conjugated fluorophore	Excitation/emission wavelength	Catalogue no.
1	None (blank control)	N/A	N/A	N/A
2	MEGF10 (Sigma)	FITC (using Lightning Link® kit (Abcam))	496/519nm	HPA026876 (MEGF10 primary), ab102884 (FITC conjugate)
3	CD34	Alexa Fluor 450®	405/446nm	RAM34
4	α7-integrin	Phycoerythrin (PE)	566/574nm	FAB3518P
5	CD45	PECy5	488/694nm	ab167004
6	All antibodies	N/A	N/A	N/A

Table 14. Controls and test antibodies used in FACS. 6 tubes were used in these experiments. One was a control, and 5 used antibodies to surface proteins.

4.2.4 Muscle fibre isolation and culture

EDL and gastrocnemius muscle were dissected from 6-week old mice, digested, and individual fibres isolated using the methods described earlier (Chapter 4). Muscle was obtained from male and female adult C57BL/6Tac (bred in-house at the University of Leeds) and Megf10$^{tm1(KOMP)Vlcg}$ mice of known genotype (final body mass approx. 25g).

Following fibre isolations, fibres were transferred to 60mm petri dishes, coated in sterile filtered 5% BSA in PBS and then filled with 6ml culture media (DMEM + 10% H/S + 0.5% CEE + 1% P/S). Muscle fibres were carefully removed from the dishes containing isolation media using a narrow-bore pipette coated with 5% BSA. No more than 30 fibres were added to each dish. Dishes were incubated at 37ºC, 5% CO_2 for 24-96hrs.

4.2.5 Fixation, staining and analysis of fibres

Fibres were fixed immediately after isolation, and following 24, 48, 72 and 96hrs in culture. After removal from the cell culture incubator, a stereomicroscope was used to transfer long, iridescent fibres into a 2ml Eppendorf tube, leaving any hypercontracted

fibres in the petri dish. Selected fibres were then fixed, stained and imaged using methods and antibodies as described (Chapter 4).

Expression of myogenic transcription factors over 96hrs in culture was investigated by staining for Pax7, MyoD and myogenin at each time point. The number of positively stained satellite cells was measured using methods as described (Chapter 4).

4.2.6 Satellite cell migration tracking

To track the movement of satellite cells on isolated fibres, fibres were filmed throughout the culture process from 0-96hrs. To prevent the fibres from freely floating during filming, Matrigel™ was used (Hughes et al., 2010). Matrigel protein matrix mixture (Corning) was defrosted at 4ºC for 1hr until it became a viscous liquid. 50µl of Matrigel™ was pipetted into the centre of nine wells in a black glass-bottomed 96-well plate (Ibidi). A narrow-bore pipette coated in 5% BSA was then used to remove 3-4 freshly isolated muscle fibres from a petri dish containing culture medium. Another layer of Matrigel™ was added on top of the fibres and the plate was placed back into the incubator at 37°C, 5% CO_2 for at least 1hr to allow the fibres to settle and the Matrigel™ to set.

Filming of satellite cells was carried out on an EVOS cell imaging system (ThermoFisher Scientific). The EVOS software was used to select 5 regions of interest per well to image. Points were selected if fibres looked healthy and unlikely to hypercontract, and if there were several satellite cells in the field of view. Fibres were imaged at 15-minute intervals over the course of 24-48hrs, 48-72hrs and 72-96 hrs. Raw images were then organised and compiled into movies and saved as .AVI files in ImageJ. ImageJ processing software (NIH) was used to manually track the positions of satellite cells in each frame. The resulting datasets (x, y positions over time) were analysed to generate distance travelled in µm and velocity in µm/min. Comparisons of satellite cell motility were made for each of the different genotypes (WT, Megf10$^{+/-}$, and Megf10$^{-/-}$).

Fibres from Megf10$^{-/-}$ mice were only filmed from 0-48hrs, due to insufficient numbers of mice.

4.2.7 Analysis of satellite cell number on fibres

The total number of satellite cells on cultured fibres was measured from single frames obtained from the EVOS filming at 24hrs, 48hrs, 72hrs and 96hrs (for WT and Megf10$^{+/-}$ mice), and at 0 and 24hrs only for Megf10$^{-/-}$ mice, due to insufficient numbers of these mice. Fibres filmed over a 24-hour time period all eventually hypercontracted, however, fibres from Megf10$^{-/-}$ mice were consistently observed to hypercontract sooner than WT or Megf10$^{+/-}$ fibres. Thus, measurements of satellite cell numbers were not possible for Megf10$^{-/-}$ fibres beyond 24hrs. Satellite cells were identified as round cells residing underneath the basal lamina of the muscle fibre. Average counts were taken from three images, each image with the full length of a muscle fibre spanning the frame. The total number of satellite cells visible per fibre within the frame was recorded. Images were analysed using ImageJ processing software (NIH).

4.3 Results

4.3.1 21% of CD34^{+} cells from WT mice are MEGF10^{+}

The gating strategy (forward and side scatter) identified that ~80% of cells were live, on average (Fig. 39A). Single cells were then identified (Fig. 39B) and then sorted further into three distinct populations based on expression of CD34 and CD45: cells that are CD34^{+}, CD45^{-} , cells that are CD34^{-}, CD45^{+} (vascular endothelial cells) and cells that are CD34^{-}, CD45^{-} (Fig. 39C). The average percentage of CD34^{+}, CD45^{-} cells was 32.8% and the average percentage of CD34^{-}, CD45^{+} haematopoietic cells was 8.7%. The rest of the cells within the population were not positive for either marker.

Within the population of CD34^{+}, CD45^{-} satellite cells, three further sub-populations were identified based on expression of MEGF10 and the focal adhesion

protein, α7-integrin. Cells were sorted based on α7-integrin expression in order to determine which of the $CD34^+$ cells were satellite cells. Although CD34 is a ubiquitous marker of satellite cells, not all $CD34^+$ cells are satellite cell (Nielson et al., 2008). The majority of $CD34^+$, $CD45^-$ cells were negative for both markers, so the presence of satellite cells within the cell population, and their potential expression of MEGF10, could not be confirmed. (Fig. 39D). On average, 2.4% of $CD34^+$ cells were $MEGF10^-$/α7-$integrin^+$ and 21% were $MEGF10^+$/α7-$integrin^-$. The extremely low expression of α7-integrin was unexpected as it is highly co-expressed with CD34 in satellite cells (Incitti et al., 2019). A possible reason for this is poor recognition of the protein by the of α7-integrin antibody, perhaps due to expired antibody or staining protocol error. MEGF10 staining was not observed in the α7-$integrin^+$ population, potentially indicating a lack of MEGF10 expression by myogenic cells within the population. Little can be derived from this finding since the α7-integrin staining was so poor, but it may suggest the presence of another non-myogenic $CD34^+$ cell type within the population that expresses MEGF10. Within the $CD45^-$, $CD34^-$ population, no $MEGF10^+$ cells were observed (Fig. 39E). With the haematopoietic cell ($CD34^-$, $CD45^+$) population (Fig. 39F), on average, only 0.3% of cells were positive for α7-integrin and 2.2% for MEGF10, suggesting that haematopoietic cells typically do not express these markers.

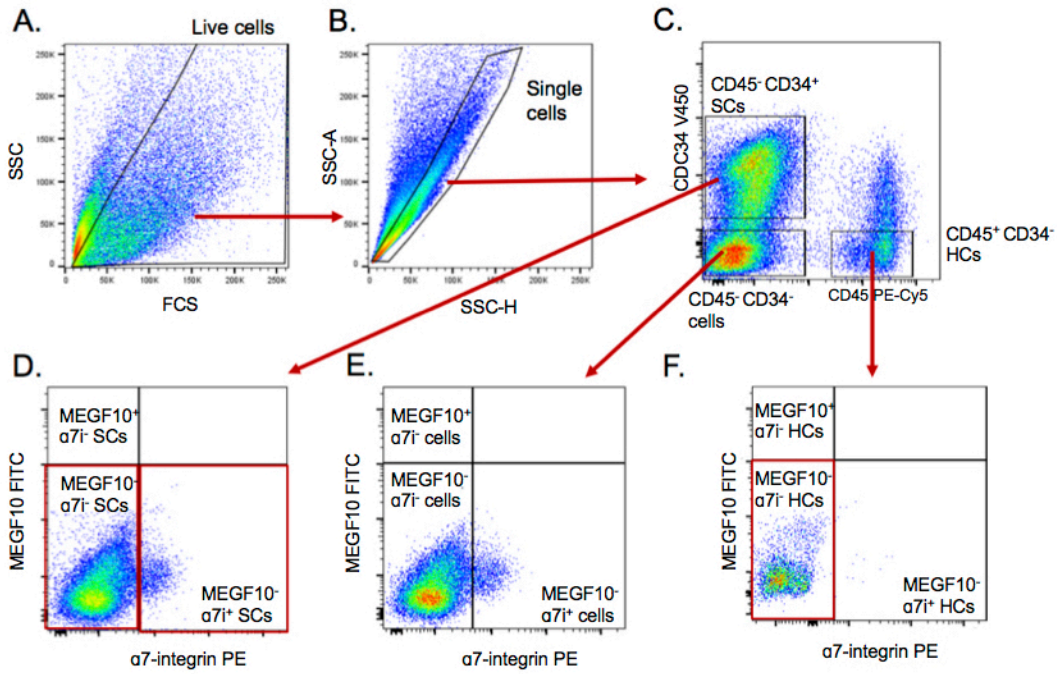

Figure 39. Gating strategies to separate distinct populations from isolated WT satellite cells: representative data from one of three sorts. A. Gate surrounding live cells, gate marked in black. **B.** Gate containing single cells, gate marked in black. **C.** Three gates containing single, live cells that are separated according to their expression of CD34 and CD35. D. Cells within the $CD45^{-}/CD34^{+}$population, divided into three gates based on their expression of MEGF10 and α7-integrin. **E.** Cells within the $CD45^{-}/CD34^{-}$ population, divided into three gates based on their expression of MEGF10 and α7-integrin. **F.** Cells within the $CD45^{+}/CD34^{-}$ population, divided into three gates based on their expression of MEGF10 and α7-integrin.

4.3.2 Numbers of $CD34^+$ cells are reduced in $Megf10^{+/-}$ mice

FACS analysis of isolated cells from neonatal $Megf10^{+/-}$ mouse muscle (Fig. 40) showed that the percentage of $CD34^+$, $CD45^+$ cells was significantly reduced compared to WT (Fig. 41). The percentage of haemopoietic cells ($CD34^-$, $CD45^+$) was not significantly different compared to WT. Within the $CD34^+$, $CD45^-$ population, the percentage of cells that were $MEGF10^+$ decreased by about 76% in cells isolated from $Megf10^{+/-}$ mouse muscle compared to WT. However, this difference was not statistically significant (Fig. 41). The percentage of α7-$integrin^+$ satellite cells was low in both WT and $Megf10^{+/-}$ cell populations and in the haematopoietic cell population, levels were also low with no significant differences (Fig. 41). Since α7-integrin was expected to be ubiquitously expressed alongside CD34 in satellite cells, it is likely that staining did not work for this marker. Since CD34 expression is not exclusive to satellite cells and the myogenic marker α7-integrin could not reliably indicate positive cells, the effect on satellite cells by reduction of MEGF10 could not be explored in this experiment. The results do, however, suggest that there is a general reduction in $CD34^+$ cells when MEGF10 expression is reduced.

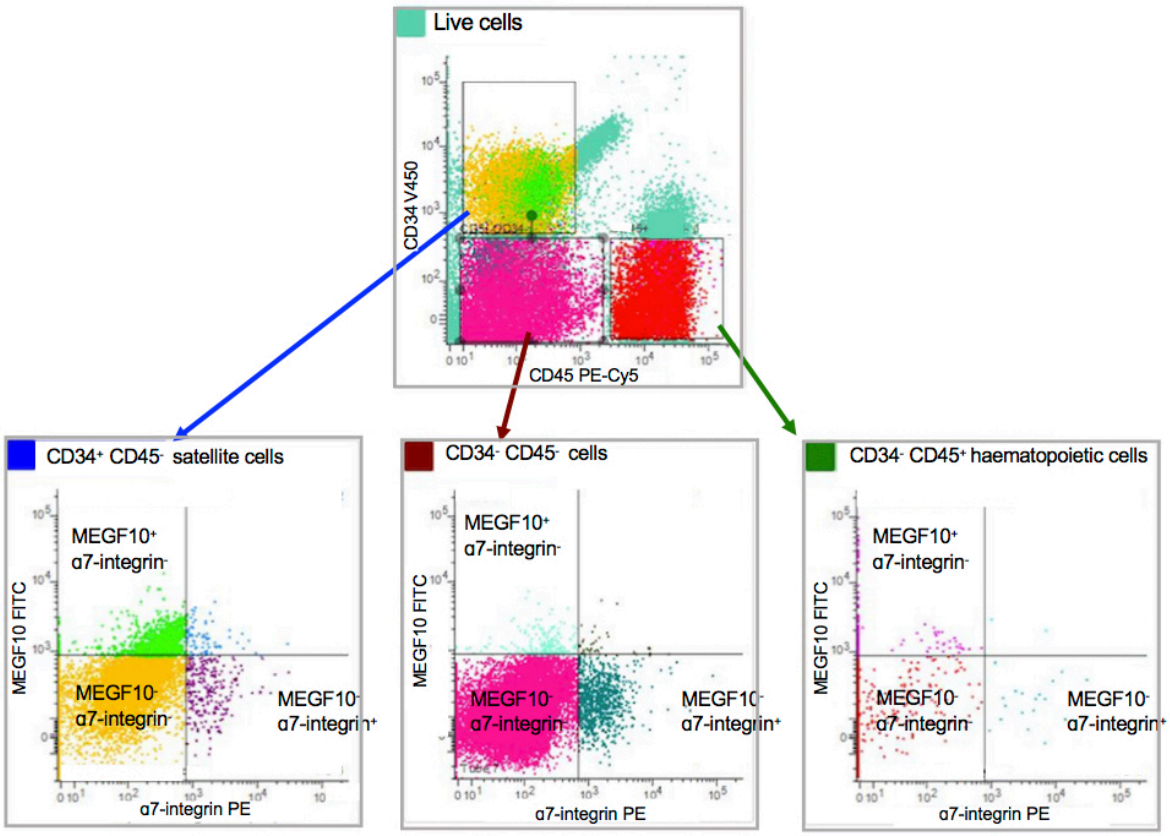

Figure 40. Populations of Megf10$^{+/-}$ cells after FACS. Representative plot showing live single cells from an Megf10$^{-/+}$ mouse, showing cells that express markers to make them fall within the parameters of the gated populations. Gates show CD34^{+}/CD45^{-}, CD34^{-}/CD45^{+} and CD34^{-}/CD45^{-} populations. Arrows point to representative plots showing the subpopulations within each gated population.

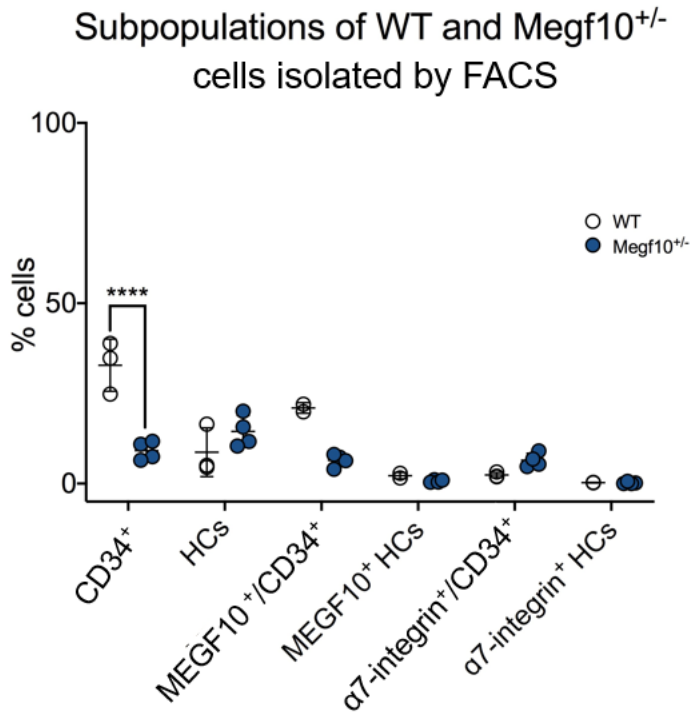

Figure 41. Plots of the percentage of cell type within isolated cell subpopulations from WT and Megf10$^{+/-}$ muscle. Comparison of the percentage of cells within the parent population of isolated cells from WT and Megf10$^{+/-}$ mice, identified as CD34^{+} cells or haematopoietic cells (HCs). n=3 biological repeats for WT, n=4 biological repeats for Megf10$^{+/-}$. Error bars represent mean ± S.D. **** p <0.0001.

4.3.3 Transcription factor (TF) expression in cultured fibres from Megf10$^{+/-}$ mice

The longest length of time that skeletal muscle fibres from all mouse genotypes could be observed in culture was 48hrs, and at this time-point staining for Pax7, MyoD and myogenin was observed in satellite cell nuclei (Fig. 42). In cultured WT fibres, the number of Pax7 positive satellite cell nuclei was highest at 24hrs (Fig. 43B). MyoD expression was highest at 48hrs (Fig. 43C), and myogenin expression was highest at 96hrs (Fig. 43C). In fibres from Megf10$^{+/-}$ and Megf10$^{-/-}$ mice, freshly isolated (0hrs) and at 24hrs, there was a significantly lower number of nuclei stained positively for Pax7. (Fig. 43A, B). This difference was most pronounced in freshly isolated fibres from Megf10$^{-/-}$ mice, whereby there was an average reduction of 27 positively stained nuclei compared to WT.

MyoD expression increased at 24hrs and continued to increase at 48-72hrs before reducing back to lower levels in fibres from WT and Megf10$^{+/-}$ mice (Fig. 43B, C, D). At 24hrs, the number of satellite cell nuclei positive for MyoD expression was lower in fibres isolated from Megf10$^{+/-}$ mice compared to WT (Fig. 43B), although there was no significant reduction for the comparison between WT and Megf10$^{-/-}$ mice (Fig. 43B). At 96hrs, there was significantly less MyoD expression in Megf10$^{+/-}$ fibres (Fig. 43E).

Myogenin expression also increased with time as expected, up to 96hrs in WT and Megf10$^{-/-}$ mice (Fig. 43A-E). However, at 24 and 72hrs, expression of myogenin appeared to be higher in Megf10$^{+/-}$ fibres than in WT (Fig. 43B, D). Expression in Megf10$^{+/-}$ mice was significantly lower at 48hrs, but significantly higher in Megf10$^{-/-}$, compared to WT (Fig. 43C). Generally, the trends in TF expression are similar for WT and Megf10$^{+/-}$, but levels of Pax7 and MyoD tend to be reduced.

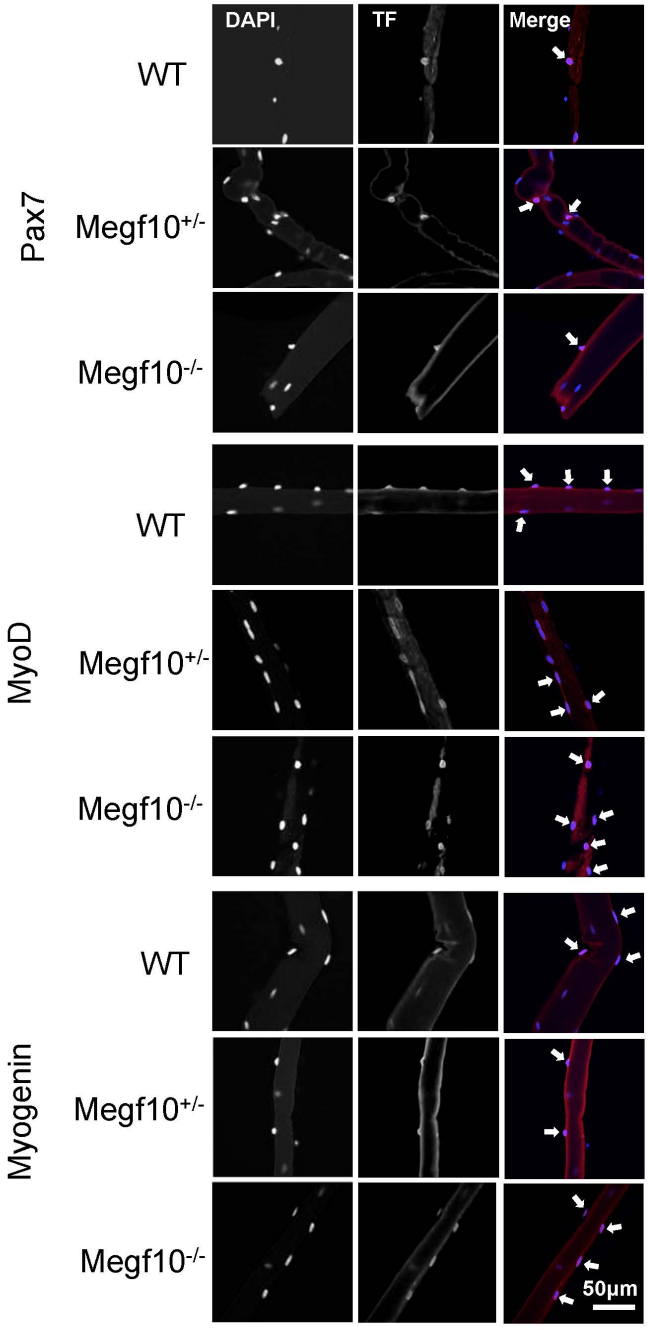

Figure 42. Immunofluorescent staining of satellite cells on cultured fibres. Single isolated fibres from EDL muscle stained for Pax7, MyoD and myogenin in red and DAPI in blue after 48hrs in culture.

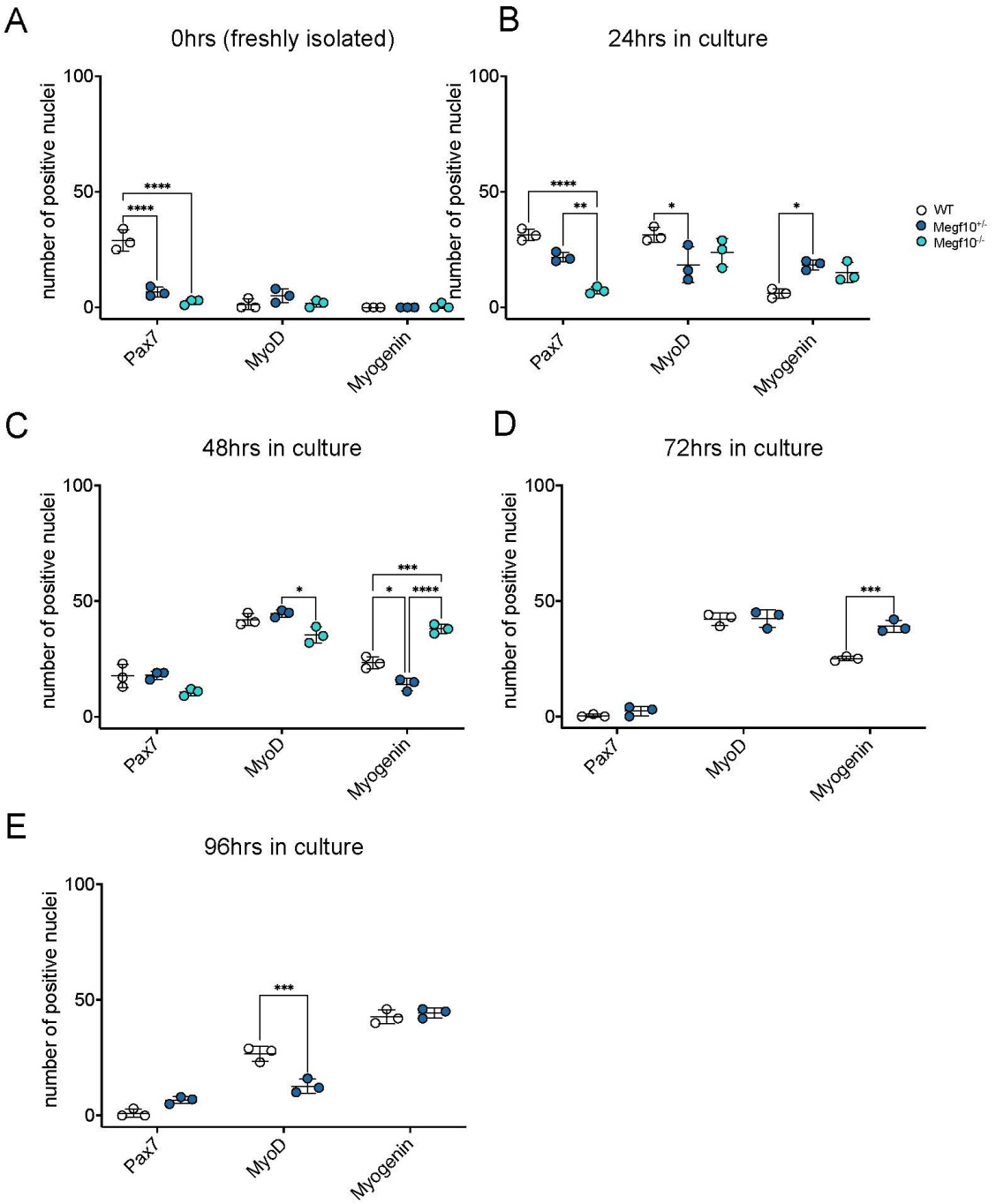

Figure 43. Expression of myogenic TFs in fibres cultured over 96 hrs. A. Number of Pax7, MyoD and myogenin positive nuclei for WT, Megf10$^{+/-}$ and Megf10$^{-/-}$ fibres at 0hrs. **B.** Number of Pax7, MyoD and myogenin positive nuclei for WT, Megf10$^{+/-}$ and Megf10$^{-/-}$ fibres at 24hrs. **C.** Number of Pax7, MyoD and myogenin positive nuclei for WT, Megf10$^{+/-}$ and Megf10$^{-/-}$ fibres at 48hrs. **D** Number of Pax7, MyoD and myogenin positive nuclei for WT, Megf10$^{+/-}$ and Megf10$^{-/-}$ fibres at 72hrs. **E.** Number of Pax7, MyoD and myogenin positive nuclei for WT, Megf10$^{+/-}$ and Megf10$^{-/-}$ fibres at 96hrs. n=3 for WT and Megf10$^{+/-}$, n=2 for Megf10$^{-/-}$. Error bars represent mean ± S.D. **** p<0.0001. *** p <0.001. ** p <0.01. * p <0.05.

4.3.4 No clear difference in satellite cell velocity when MEGF10 is reduced

The number of satellite cells on fibres filmed on the EVOS was lower for Megf10$^{+/-}$ mice compared to WT at all time points, although this difference was not found to be significant (Fig. 44A, B). Due to short survival time of Megf10$^{-/-}$ fibres in culture, quantification could only be carried out at 24hrs. At this time point, there were fewer satellite cells on the Megf10$^{-/-}$ fibres compared to WT, but again this reduction was not significant (Fig. 44A, B). The lower satellite cell numbers observed, while not statistically significant, agrees with the reduced number of satellite cells in Megf10$^{+/-}$ mice as indicated by FACS and the reduced percentage of Pax7 nuclear staining in Megf10$^{+/-}$ and Megf10$^{-/-}$ mice at various culture time-points.

Tracked satellite cells moving along cultured fibres showed a great range of velocity measurements from 24-96hrs, and at each culture time point, significant differences in velocity were observed between genotypes (Fig. 45A-C). The loss of MEGF10 did not appear to inhibit movement of satellite cells, especially early in the culture period from 24-48hrs, as mean velocity of satellite cells on Megf10$^{-/-}$ was 3.7μm/min compared to 3.6μm/min for WT and 3.4μm/min for Megf10$^{+/-}$ satellite cells (Fig. 45A). From 48-72hrs in culture, mean recorded velocity was significantly greater for Megf10$^{+/-}$ satellite cells compared to WT (Fig. 45B). From 72-96hrs this trend was reversed, with a reduction in velocity of 2.89μm/min in satellite cells from Megf10$^{+/-}$ mice compared to WT (Fig. 45C). While the expected decrease in satellite cell velocity occurred at the later stages of cell culture, the results from earlier culture time-points make it difficult to understand what effect, if any, reduction of MEGF10 had on satellite cell motility.

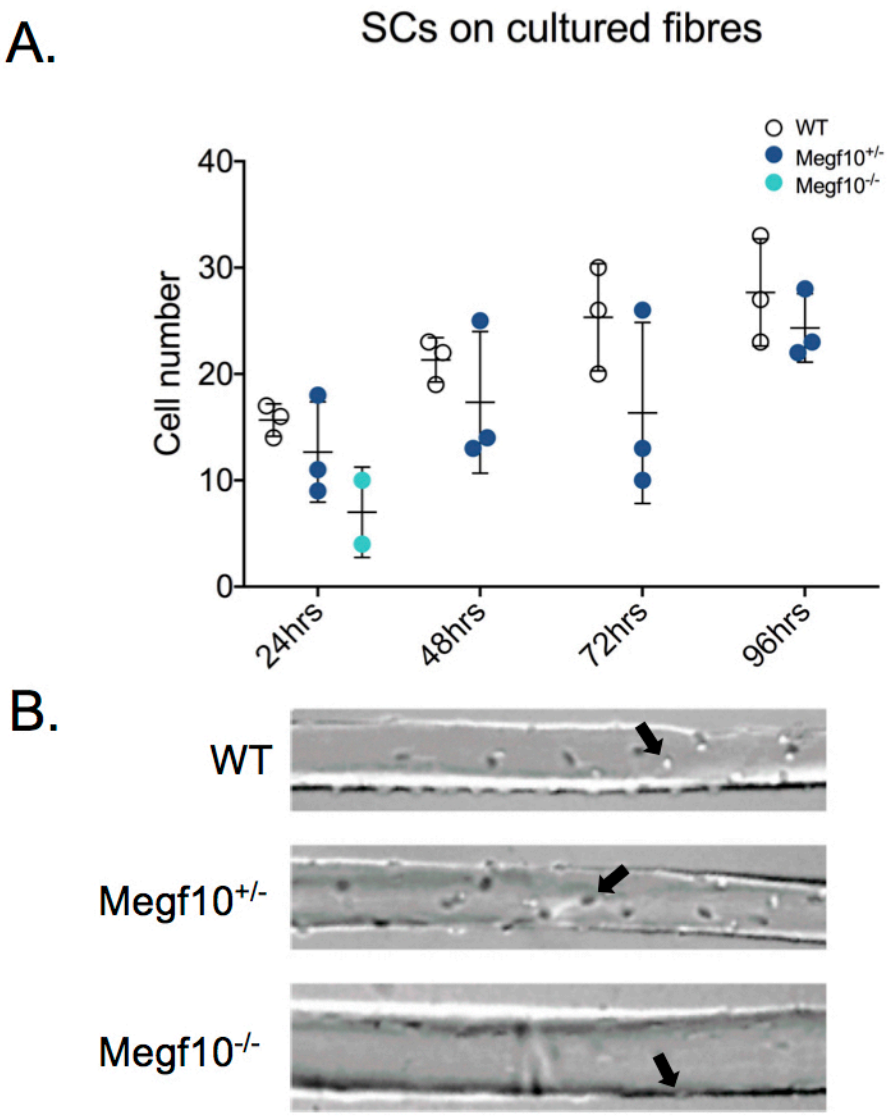

Figure 44. Analysis of satellite cell density on cultured cells. A. Plots showing the number of satellite cells counted per fibre from 24-96hrs for WT, Megf10$^{+/-}$ and Megf10$^{-/-}$ fibres. Error bars represent mean ± S.D. **B.** Representative snapshots taken from WT, Megf10$^{+/-}$ and Megf10$^{-/-}$ fibres filmed at 24hrs.

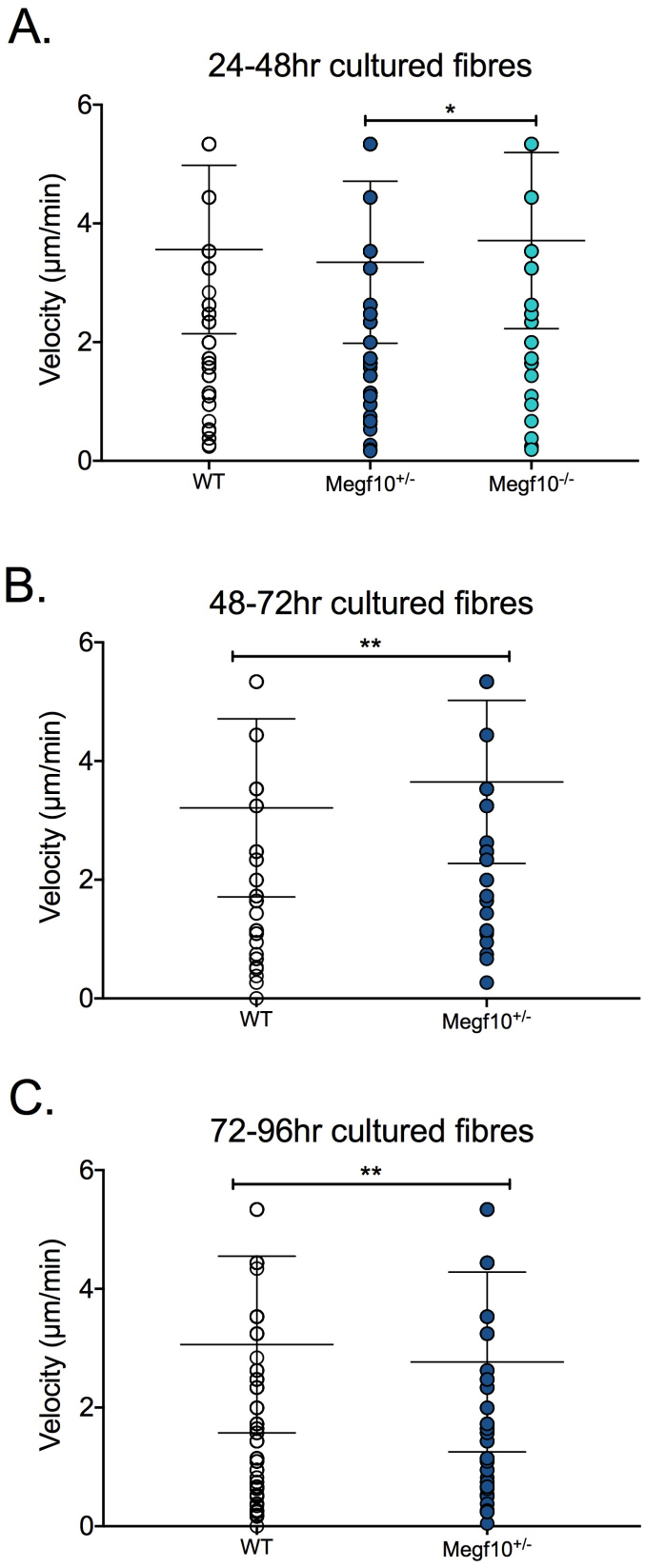

Figure 45. Velocity of tracked satellite cells over the course of 96hrs in culture. **A.** Plots showing the velocity of satellite cells from 24-48hrs. **B.** Plots showing the velocity of satellite cells from 48-72hrs. **C.** Plots showing velocity of satellite cells from 72-96hrs. Error bars represent S.D. ** p <0.01. * p <0.05.

4.4 Discussion

Isolated cells from WT and Megf10$^{+/-}$ muscle showed a similar distribution of CD34^{+}, CD45^{-} cells and CD34^{-}, CD45^{+} (haematopoietic cells), however, the population of CD34^{+} satellite cells was significantly reduced in Megf10$^{+/-}$ mice. The lower number of satellite cells in Megf10$^{+/-}$ mice agrees with previous comparisons made between genotype in *in vivo* overload experiments (Chapter 4). Within the population of CD34^{+} cells, about 21% were Megf10 positive in WT mice, and this was reduced by approximately 76% in Megf10$^{+/-}$ mice. This reduction was expected, as these mice had only one normal copy of the MEGF10 gene. Culturing fibres, which activates satellite cells, showed a similar trend in expression of Pax7, MyoD and myogenin with time in culture. However, there was some reduction in Pax7 and MyoD expression in satellite cells on Megf10$^{+/-}$ and Megf10$^{-/-}$ fibres compared to WT. Changes in myogenin expression were unexpected; a reduction was observed in Megf10$^{+/-}$ satellite cells, however there was a significant increase in percentage nuclei stained positively for myogenin in Megf10$^{-/-}$ satellite cells. The extremely low expression of Pax7 later in the culturing period (72hrs and 96hrs) was unexpected. While the number of Pax7^{+} cells was expected to decrease as satellite cells become specified for differentiation, some Pax7 staining was still expected to be found. This is due to the previously reported behaviour of satellite cells whereby a proportion withdraw from the terminal myogenic programme and return to quiescence, thus maintaining a Pax7^{+} satellite cell niche that can be drawn upon later (Zammit et al., 2004). Some differences were observed in the migration of satellite cells along the muscle fibres, although a trend based on the presence of MEGF10 was not clear.

Previously, silencing of MEGF10 in activated satellite cells by transfection with small interfering RNA (siRNA) has been shown to result in 30% less activated satellite cells on isolated myofibres (Holterman et al., 2007). Lower satellite cell numbers were observed after FACS in Megf10$^{+/-}$ mice compared to WT, although this constituted the whole population of quiescent and activated satellite cells. Notably, the satellite cell

isolation was carried out on neonatal mice, and this phase is a period of rapid satellite cell proliferation whereby most of the satellite cell pool is established (Tajbakhsh, 2009; Saha et al., 2017).

A reduction in Pax7 expression was observed when there was a loss of MEGF10, in both freshly isolated (0hrs) fibres and FACS of isolated satellite cells. Pax7 and CD34, used to indicate satellite cells in isolated fibres and in FACS respectively, are both ubiquitous markers of satellite cells, thus, it appears that the reduction of MEGF10 inhibits the expansion of the satellite cell niche (Sambavisan et al., 2011). This agreement between the two methods was expected because of previous work reporting on the importance of MEGF10 in satellite cell proliferation (Saha et al., 2017), however, a greater level of heterogeneity was expected within isolated satellite cells compared to those still attached to fibres. This is because satellite cells are not exposed to signals from interstitial and vascular tissue when they reside under an intact basal lamina in fibre isolations, but they still share a niche with these cells following satellite cell isolation (Musaro and Barberi, 2010). Both satellite cell culture methods used together allowed a more complete insight into how satellite cells are affected by a loss of MEGF10.

Megf10$^{+/-}$ satellite cells moved with a reduced velocity at 72hrs, consistent with a previous report (Li et al., 2021). In that case, distance travelled by Megf10$^{-/-}$ satellite cells that had detached from the fibres was also reduced at 72hrs. However, this reduction was found at 24hrs and 48hrs also, which challenges my findings, whereby I found no difference or increased velocity in Megf10$^{+/-}$ and Megf10$^{-/-}$ mice at these time points. Greater differences in migration velocity observed at a later time point in my study may occur because there is more attachment of cells to laminin via integrin α7β1 after a greater length of time in culture (Siegel et al., 2009). The reduced velocity of satellite cells from Megf10$^{+/-}$ mice at 72hrs, suggests that MEGF10 may be important in facilitating movement of myogenic satellite cells along the muscle fibre to their fusion targets.

The changes observed in this chapter (reduction in the number of satellite cells on cultured fibres, reduction in myogenic TF expression and reduction in velocity later in

culture) agree with previous literature that describes the effects of reduced levels of MEGF10 on satellite cell behaviour. Interestingly, the FACS analysis revealed that only ~21% of satellite cells in the WT population were positive for MEGF10, which is a relatively small population considering the overall changes observed when MEGF10 levels are decreased. Previous reports have suggested that the majority of activated and quiescent satellite cells express MEGF10 (Saha et al., 2017; Holterman et al., 2007). However, in one report (Holterman et al., 2007), an antibody generated by the lab was used, that is no longer available, and was not independently validated. In the second (Saha et al., 2017), the antibody was raised to the cytoplasmic domain of MEGF10 and has been previously shown to be unreliable at recognising MEGF10 in immunostaining and western blot (Hughes, 2016).

These *in vitro* experiments complement the *in vivo* overload studies (Chapter 4), but findings were not entirely consistent between the two investigations. Both types of experiments showed a lower percentage staining for Pax7 and MyoD on fibres from Megf10$^{+/-}$ and Megf10$^{-/-}$ compared to WT in culture, and this reduction was observed in Megf10$^{+/-}$ and Megf10$^{-/-}$ fibres following 10-day overload. Expression of myogenin was not as clearly inhibited in culture compared to after overload, and overall, the reductions in TF expression were not as severe as observed on Megf10$^{+/-}$ and Megf10$^{-/-}$ fibres stimulated by 10-day overload. This suggests that stimulation by high serum conditions in culture is a milder stimulus than activation by overload surgery. *In vitro*, satellite cells are activated by the growth factors present in the chick embryo extract and foetal bovine serum present in culture media, capable of triggering pathways such as Notch and Wnt (Yablonka-Reuveni, 1995; Le Grand and Rudnicki, 2007). It is difficult to determine what culture time point best represents 10-day overload as there are similarities and differences in trends for each culture time point compared to 10-day overload. One large discrepancy is the reduction in Pax7 that occurs later in culture for all three genotypes, compared to relatively high expression of Pax7 after 10-day overload. Thus, exploration of MEGF10 deficiency *in vitro* should be carried out in addition to, not in place of *in vivo*

overload experiments as the stimulation created by culture conditions does not completely recapitulate the effects of overload induced regeneration.

5 Discussion

5.1 Myogenic cell culture is improved by soft surfaces that mimic skeletal muscle *in vivo*

This investigation found that myoblast cells *in vitro* differentiate better and show enhanced expression of myogenic genes on soft cell culture surfaces that have a stiffness similar to that of skeletal muscle *in vivo* (~12kPa). Analysis was carried out on C1F cells, a Pax3-expressing cell line, and these showed a similar myogenic expression pattern to the more commonly used Pax7-expressing C2C12 cell line. The enhanced differentiation on soft surfaces agrees with several previous reports that myoblasts fuse and differentiate better on softer surfaces made of biomimetic materials such as gelatin methacryloyl, polyacrylamide, and the material used in this study, PDMS (Shin et al., 2017; Constantini et al., 2017; Engler et al., 2004; Kaji et al., 2010). Previous investigations using PDMS, a preferential substrate due to its tuneable elasticity and capability to undergo surface modifications such as micropatterning, have utilized the C2C12 cell line to investigate myoblast fusion and differentiation (Palchesko et al., 2012; Kaji et al., 2010; Shimizu et al., 2009; Denes et al., 2019). My investigation has contributed novel data regarding gene expression of myogenic and ECM proteins on hard and soft surfaces, which complements previous work using RNAseq on C2C12 cells (Denes et al., 2019).

In addition to Pax3, Pax7, MyoD and myogenin, the investigation could be strengthened by using immunostaining to probe for additional genes that were highlighted in RNAseq. Vascular cell adhesion molecule 1 (VCAM1), calcium activated chloride channel 3a1 (Clca3a1) and cytochrome c oxidase subunit 6B1 (COX6B) are all genes that were upregulated on PDMS compared to glass, and this could be validated with immunofluorescent staining on each surface. Each of these genes are indicative of

enhanced myogenic and metabolic activity on PDMS (Rosen et al., 1992; Choo et al., 2017; Ng et al., 2015; Duggan et al., 2011). Future advancements in myoblast culture on soft PDMS may include optimization of other aspects of the surface, such as curvature, which is already beginning to be explored (Kemkemer et al., 2018; Hild et al., 2020). Limitations within this investigation include the lack of a D5 sample on the hard surfaces, which removed the ability to make a full comparison between surfaces along the differentiation timeline. Additionally, the stiffness of the surfaces may have lacked accuracy. Although the PDMS surfaces were prepared using a ratio of polymer and curing agent reported previously, the lack of validation following preparation means that it cannot be guaranteed that these surfaces were consistently 12kPa. (Oschner et al., 2007). In future experiments, the elasticity of each surface could be tested using atomic force microscopy, which makes indentations in the surface and calculates an accurate measure of elasticity based on the magnitude of the indentation (Vinckier and Semenza, 1998).

5.2 Suitability of the mouse overload model as a model for hypertrophy

In this study I chose to investigate changes in satellite cell behaviour at 10 days overload, as I found hypertrophy was optimal at this time point. Previous studies have investigated overload at different time points for their analysis, ranging from 7 to 30 days (Armstrong et al., 1979; Rosenblatt and Parry, 1992; Johnson, 1988). Other aspects of hypertrophy such as angiogenesis may be maximally affected at different time points. For example, one study found that after 14 days, there was a greater capillary to fibre ratio and capillary beds within the muscle were more complex and tortuous for overloaded rat EDL (Zhou et al., 1998). I did not find a significant change in the vascular endothelial cell content following overload at 10 days in any of the three mouse genotypes. A future direction could be to test a range of time points in order to see changes in capillarization, as

changes in vasculature may occur after the 10-day overload time-point. The investigation may also have been limited in that sampling time-points went directly from 6 to 10, as changes in the muscle may have been occurring during the days in between, and these would not have been captured. Sampling every day would allow a fuller picture of the gradual changes that occur during hypertrophy.

Varying the type and duration of overload may be important in making rodent models of regeneration more robust, as the suitability of mice as a translational model for humans is often called into question. Previous work that compared walking muscles of mice and humans found that the fibres of mice do not stretch to the same extent as humans when walking, and that joint angles are considerably different between the species (Hu et al., 2017). While these anatomical differences are difficult to compensate for in mice, factors such as age and sex, which influence levels of hypertrophy, can be accounted for in overload models (Murach et al., 2017; Neal and Morgan, 2012). However, the inclusion of female mice in my investigation, in addition to the original choice of males, may have limited the investigation and reduced the overall responses observed after overload, since the hypertrophic response is different between the sexes (MacLean et al., 2008; Lee and Maclean, 2011; Ogawa et al., 2015). A stronger response may have been observed if I had only used one sex exclusively in my investigation. Future experiments should carry out separate sex investigations on adult mice, to understand the hypertrophic response in both males and females. This would improve translatability to all humans, whilst reducing the confounding effect of analysing both sexes together with inconsistent relative sample sizes.

Overload surgery is an established means of inducing muscle hypertrophy that is more physiological and less damaging than other methods such as freeze injury, cardiotoxin injection or barium chloride injection. However, other methods that are less invasive could be explored in the future (Hardy et al., 2016). One example is the use of treadmill running. Previous work has found this to increase mass of the EDL by 12-18%. This is less than the average hypertrophy of WT mice found in my study (~40%), but only

slightly lower than typical overload hypertrophy values reported by past overload studies (~22%) (Egginton et al., 1998; Huey et al., 2016; Seiden, 1976; Kemi et al., 2002).

5.3 MEGF10 is necessary for a normal hypertrophic response to overload

In response to overload stimulus, there were significant reductions in hypertrophy, myonuclear accretion and myogenic transcription factor expression in Megf10$^{+/-}$ and Megf10$^{-/-}$ mice, compared to WT. This is consistent with previous reports that MEGF10 is necessary for the proliferation of satellite cells in response to injury. Loss of MEGF10 reduces the level of satellite cell expansion and therefore a reduction in subsequent fusion and differentiation into multinucleated myotubes (Saha et al., 2015; Logan et al., 2011).

Previous investigations into the effects of loss of MEGF10 has used myoblast cell lines and a mouse model (Saha et al., 2015; Mitsuhashi et al., 2013; Saha et al., 2017; Li et al. 2021). Two previous key studies using a Megf10$^{-/-}$ mouse model reported that myoblasts and satellite cells derived from Megf10$^{-/-}$ mice displayed decreased proliferation and migration, skeletal muscle samples from the mice showed increased fibrosis, and muscles had impaired regeneration following injury (barium chloride injection) (Li et al., 2021; Saha et al., 2017). However, it is worth noting that the skeletal muscle from Megf10$^{-/-}$ mice only had a mild phenotype, with only a mild increase in fibrosis, similar to that found for the *mdx* mouse (Saha et al., 2017). A more severe phenotype was found when the Megf10$^{-/-}$ mice were crossed with the *mdx* (deficient for dystrophin) (Saha et al., 2017). Both of these two previous studies used the Megf10$^{tm1c(KOMP)Jrs}$ Megf10$^{-/-}$ mouse obtained using a different gene targeting approach ('gene trap') to the ones used here (Megf10$^{tm1(KOMP)Vlcg}$). In the Megf10$^{tm1c(KOMP)Jrs}$ mouse, a splice acceptor was inserted between exons 3 and 4, and exon 4 is flanked by *loxP* sites. The targeted allele serves as a gene trap in which transcription is terminated after

exon 3. In the mouse used here, insertion of Velocigene cassette ZEN-Ub1 created a deletion of size 31918bp between positions 57313561-57345478 of Chromosome 18 (Build GRCm39). This deletes exons 1-24. While in principle, both types of model should result in similar phenotypes, it is possible that our mouse model, which deletes a large proportion of the MEGF10 gene, is more efficient in reducing MEGF10 levels in the heterozygous mice. While the Megf10$^{tm1(KOMP)Vlcg}$ model has been used previously, those investigations were on the role of MEGF10 in the brain (Chung et al., 2013; Iram et al., 2016). Thus, this study is the first report on a muscle phenotype in the Megf10$^{tm1(KOMP)Vlcg}$ mouse.

My results have thus provided new evidence for the importance of MEGF10 in facilitating adequate regeneration. The Megf10$^{+/-}$ mice, which maintained one functional copy of the gene, showed a stronger phenotype compared to the previous reports using the alternative mouse model (Megf10$^{tm1c(KOMP)Jrs}$). The mice used in my study (Megf10$^{tm1(KOMP)Vlcg}$) showed that regeneration in the Megf10$^{+/-}$ mice was mildly impaired, as indicated by a reduced hypertrophy compared to wild-type mice, reduced myogenic expression and reduced myonuclear accretion. These reductions were greater in the Megf10$^{-/-}$ mice.

The CSA of fibres, percentage of slow fibres and capillary density was not significantly different between genotypes. In comparison, the Megf10$^{tm1c(KOMP)Jrs}$ mouse model has reduced fibre CSA in the EDL muscle but not in the soleus muscle, and in human patients with EMARDD, fibre diameter is reduced by ~20% (from a median value of 21.1μm to 16.7cm in patients) (Logan et al., 2011; Saha et al., 2017). Hypertrophy is expected to increase fibre CSA (Deveci and Egginton, 2002) and this was supported by my findings of a significant increase in CSA for WT and Megf10$^{+/-}$ mice after 10-day overload. However, CSA was significantly decreased in Megf10$^{-/-}$ mice. The variability of CSA values in Megf10$^{-/-}$ mice made it difficult to conclude what effects the loss of MEGF10 had on fibre CSA. Variable quality of frozen sections and the manual method of obtaining a measure of CSA may have been contributing factors in this. Future

experiments should use a refined protocol to avoid the erroneous measurement of oblique fibres. An added complexity to investigating CSA change after overload is the small increase in CSA that occurs as mice get older. The mice used in these experiments were ~6 weeks old, which is still a period of rapid EDL growth, as the muscle only stops growing when the mouse reaches ~17 weeks of age (White et al., 2010). Thus, further investigations should consider the use of more mature mice.

In addition, other markers of vascular cells, such as CD146 and CD31 could be explored (Birbrair et al., 2013; Uezumi et al., 2006). The presence of a distinct $CD45^+$ population that shares a niche with satellite cells, as evidenced by FACS isolation in this study, suggests that this may also be a useful marker of vascular endothelial cells in future experiments. Since satellite cells could not be identified in the FACS investigation due to a lack of myogenic identification via α7-integrin staining, little could be understood with regards to the effect of MEGF10 reduction on satellite cells. The $CD34^+$ cells that were identified could potentially be several other cell types e.g., endothelial cells, epithelial progenitor cells or interstitial cells among others (Sidney et al., 2014). Thus, the general observation that $CD34^+$ were reduced in $MEGF10^{+/-}$ cell populations is not particularly meaningful in the context of satellite cells. Future experiments should use fresh, validated α7-integrin antibody and confirm the identity of satellite cells isolated by FACS, by culturing the cells after the sort. Satellite cells can then be cultured and stained for specific nuclear markers e.g., Pax7.

On freshly isolated fibres from $Megf10^{+/-}$ and $Megf10^{-/-}$, the number of $Pax7^+$ satellite cells was significantly lower than WT, and in addition, the number of $CD34^+$ cells (which may include satellite cells) was shown to be lower in $Megf10^{+/-}$ by FACS isolation. As the culture period progressed to 48hrs, the number of $Pax7^+$ satellite cells increased in both mutant genotypes. This suggests that despite impairment of MEGF10, the proliferation and self-renewal of satellite cells is not completely impeded. This may be thanks to the presence of Notch signalling that is able to persist in the absence of MEGF10. Notch is able to drive the transcription of Pax7 in foetal and post-natal

myogenesis, and while MEGF10 has a synergistic relationship with this pathway, it is also able to function independently (Koch et al., 2013; Shawber et al., 1996; Holterman et al., 2007) .However, the reduced numbers of $Pax7^{+}$ satellite cells in $Megf10^{+/-}$ and $Megf10^{-/-}$ suggests that Notch signalling in the absence of MEGF10 may not allow optimal regeneration. Future endeavours to understand the requirement of MEGF10, and its relationship with Notch in self-renewing and proliferating satellite cells could involve co-staining isolated fibres with MEGF10 and Notch antibodies. The low levels of $CD34^{+}$ staining in isolated muscle cells from neonatal mice may be indicative of an early foetal defect that results in impaired muscle regeneration. This may serve in the explanation of the skewed Mendelian ratio observed.

The investigation of the change in fibre type composition after overload was limited, as only slow-type fibres were stained and the sample size of mice was small, especially with regards to $Megf10^{-/-}$ mice. To obtain a more complete understanding of how fibre type distribution following overload is changed as a result of MEGF10 reduction, the proportion of fast type 2a, 2b and 2x fibres should be measured in addition to slow type 1 fibres, particularly as slow type 1 fibres are rare in EDL (<1% in adult mice) (Rosenblatt and Parry, 1985; Johnson and Klueber, 1991). Slow (type 1) fibres are slow to fatigue due to their high oxidative energy supply, and are therefore more abundant in postural muscles (Schiaffino, 2010). Fast (type 2) fibres are quick to fatigue and more abundant in muscles that facilitate explosive movement. Type 2a rely mainly on oxidative metabolism, 2b and 2x mainly glycolytic (Talbot and Maves, 2016). Whilst similar in function, fast type 2b and 2x contain different myosin heavy chain isoforms (Schiaffino et al., 1989). A small increase in the proportion of type 2a fibres was reported following overload at day 7 and day 21 in mice (Johnson and Klueber, 1991) and at day 28 (Rosenblatt and Parry, 1985), using a similar overload model to the one reported. In $Megf10^{-/-}$ mice there was a small reduction in type 2 fibres compared to wild-type (Saha et al., 2017). However, that study did not stain for type 1 fibres, and did not study the effect of overload, so many questions still remain.

5.4 Diaphragm muscle in MEGF10 knockout mice is compromised

Analysis of diaphragm sections from Megf10$^{+/-}$ and WT mice showed significant differences between the two genotypes, as evidenced by smaller muscle fibres and greater thickness of laminin between fibres. We suspected this might explain the skewed Mendelian ratio, with fewer Megf10$^{-/-}$ mice being born, as it is possible that diaphragm impairment is even more severe in the Megf10$^{-/-}$ mice. The increased laminin thickness indicates impaired regeneration, as it indicates abnormal ECM deposition, however, additional methods to analyse diaphragm sections could be included in the future (Taetzhch et al., 2021; Zhang et al., 2021). These include using Masson's trichrome stain, a highly sensitive stain for collagen-rich areas of fibrosis, widely used in analysis of muscular dystrophies (Fanbin, et al., 2011; Wagner et al., 2002). Using laminin alone, as used here, is limiting as it is not a widely regarded marker of histopathological fibrosis. It's increased deposition in the diaphragm merely indicates increased ECM remodelling and does not inform on the degeneration that is causing the deposition (Lu et al., 2011).

This investigation was limited by insufficient animal numbers, so future experiments should include all three genotypes with a more exhaustive investigation of fibrosis. The skewed Mendelian ratio should also be confirmed by genotyping pups from a new Megf10$^{+/-}$ breeding pair, with sampling of late stage embryos (d18.5). A significant limitation of the current study is the failure to record all births and incidents of maternal cannibalism. It is suspected that Megf10$^{-/-}$ mice may have been born and either failed to thrive or displayed phenotypic deficiencies that led the mother to eat them. Acquiring data on the number and nature of these incidents would provide greater insight on the potential impact of MEGF10 mutation, and may have further validated this mouse model as a model of EMARDD.

The investigation of the effects on the diaphragm can be further expanded by a histological analysis of satellite cells in muscle sections, staining for Pax7. The

differences in satellite cell activity between genotypes may be most crucial in the diaphragm of this mouse model, and an understanding of this is lacking in the current study. Additionally, a functional comparison of diaphragm muscle could be carried out in future experiments, using electrical currents to investigate whether a lack of MEGF10 diminishes the maximal twitch force generated by the diaphragm during contraction (Bowen et al., 2015). This would provide a more complete picture of the extent of respiratory distress that occurs in this mouse model.

The original human EMARDD cases had respiratory distress, caused by diaphragmatic paralysis, and dysphagia, and it is possible that this mouse model is replicating this effect, causing early death. Thus, the effects of MEGF10 loss on the diaphragm is an exciting result to pursue further, because this is a previously unreported aspect of the Megf10$^{-/-}$ mouse phenotype, and may further validate the mice as a model of EMARDD.

5.5 How might this study impact on research into muscular dystrophies?

The hypertrophy induced by overload surgery recapitulates the regeneration that occurs in normal skeletal muscle, in response to external stimulus such as weight bearing exercise or injury (Egginton et al., 2011). Since this regeneration process is impaired in muscular dystrophies, it is a good experimental model to investigate what changes occur in dystrophic muscle (Guiraud and Chang, 2019). A well-established model of Duchenne muscular dystrophy is the *mdx* mouse, and a notable aspect of this model's phenotype is a poorly formed, fibrotic diaphragm (Burns et al., 2019). The similarity between this model and the Megf10$^{+/-}$ mouse, as evidenced by diaphragm analysis, suggests that MEGF10 knockout mice may be a good alternative model of the EMARDD subtype of muscular dystrophy. However, further experiments on EDL and diaphragm muscle taken from the MEGF10 knockout mice is required in order to better validate this.

5.6 Final conclusions

This study has shown that MEGF10 plays a role in the response of satellite cells to overload, through the proliferation of satellite cells and eventual fusion and differentiation of myotubes. This role has been demonstrated by the reduction in overall hypertrophy of EDL muscle following overload, and the reduction in myogenic transcription factor expression on muscle fibres in mice that are heterozygous or homozygous for a MEGF10 deletion mutation. The observation of some level of hypertrophy and satellite cell activity in the absence of MEGF10, as seen in MEGF10$^{-/-}$ mice, suggests that the processes can occur (to a limited extent) without MEGF10. This is likely due to the remaining availability of Notch signalling components that are able to function with or without interaction with MEGF10.Despite attempting to investigate the effect of MEGF10 knockout on muscle capillarization and fibre type distribution, no conclusions were able to be made due to sampling issues and low sample size..

Low birth numbers of mice homozygous for the MEGF10 mutation encouraged investigation into potential reasons for pre-natal or neonatal deaths of these mice. Making links to the human phenotype of EMARDD, the disease that these mice may provide a model for, the diaphragm muscle was investigated to assess whether respiratory distress may be occurring in these mice. An analysis of mice that contained a heterozygous MEGF10 mutation and thereby reduced levels of MEGF10, showed structural impairments to the diaphragm that are hypothesised to be more severe in mice that lack MEG10 completely.

This investigation also validated the use of an optimized cell culture set up for culturing myoblast cells, showing improved fusion and differentiation of cells on collagen-coated polymer surfaces with an elasticity more similar to muscle tissue *in vivo.* RNA-seq analysis of cells indicated differential expression of many key myogenic and ECM related genes on optimized vs standard surfaces throughout a 7-day differentiation period.

Through a series of *in vivo* and *in vitro* experiments, this investigation has validated soft PDMS cell culture surfaces, C1F myoblasts, and Megf10$^{-/-}$ mice as effective tools in the research of myogenesis in the context of muscular dystrophies. The investigation here has paved the way for a continuation of this research, with a view for future experiments to either build on or optimize the methods used here (Fig. 46).

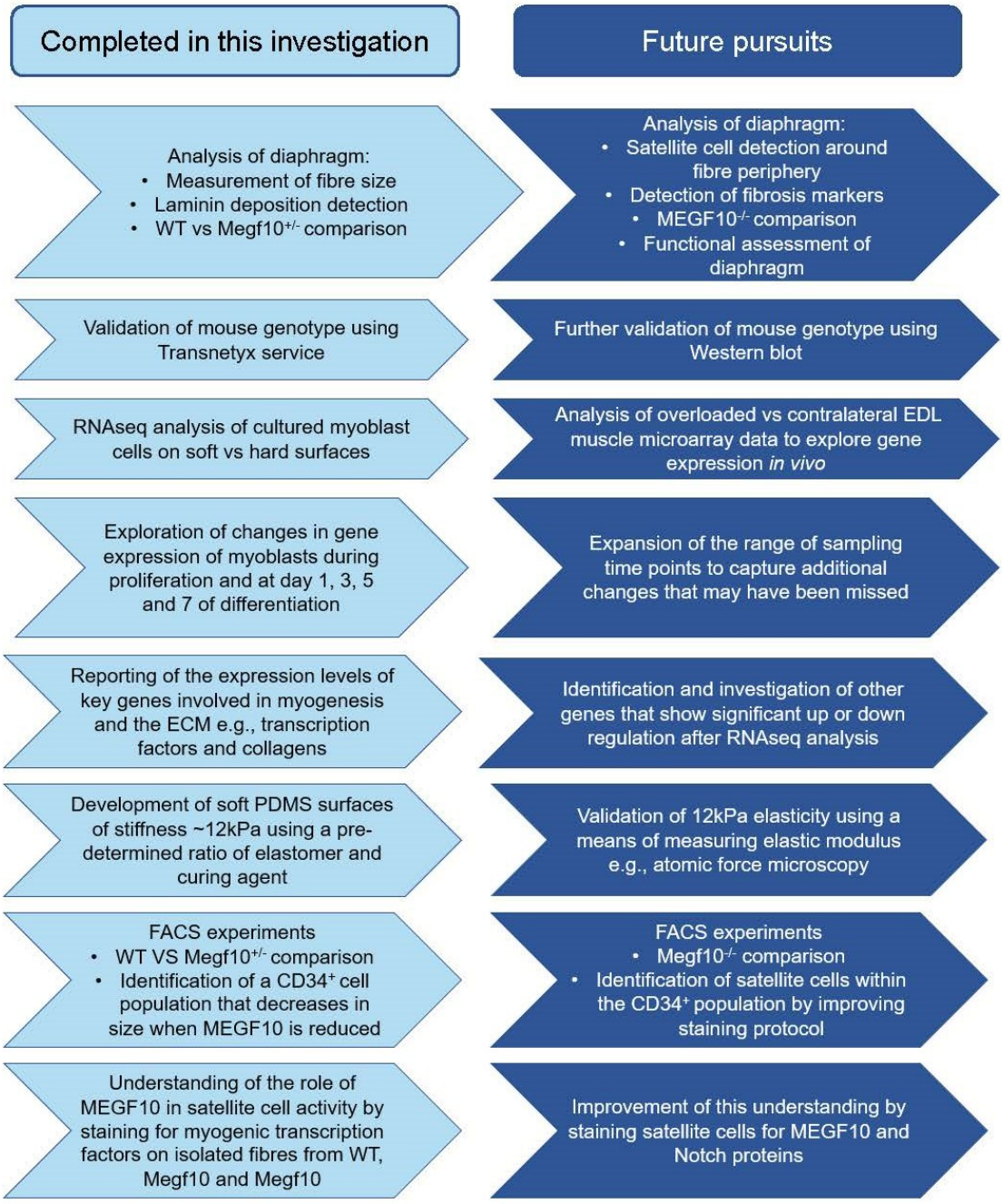

Figure 46. Schematic of experiments carried out in this investigation alongside corresponding next steps. Light blue chevrons indicate the methods carried out in this investigation that led to the key findings Darker blue chevrons describe the suggested modifications or next steps that will build upon the findings reported here.

6 Bibliography

Allamand, V., Brinas, L., Richard, P., Stojkovic, T., Quijano-Roy, S. and Bonne, G. (2011). ColVI myopathies: where do we stand, where do we go? *Skeletal Muscle.* **1(1)**, pp. 1-4.

Allbrook, D. B., Han, M. F. and Hellmuth, A. E. (1971). Population of muscle satellite cells in relation to age and mitotic activity. *Pathology*. **3(3)**, pp. 233-243.

Allen, D. G., Whitehead, N. P. and Froehner, S. (2016). Absence of Dystrophin Disrupts Skeletal Muscle Signalling: Roles of Ca2+, Reactive Oxygen Species, and Nitric Oxide in the Development of Muscular Dystrophy. *Physiological Reviews.* **96(1)**, pp. 253-305.

Anders, S. and Huber, W. (2010). Differential expression analysis for sequence count data. *Nature Precedings,* pp. 1.

Anderson, J. E., Wozniak, A. C. and Misunoya, W. (2012). Single muscle fiber isolation and culture for cellular, molecular, pharmacological, and evolutionary studies. *Methods in Molecular Biology.* **798**, pp. 85-102.

Andrews, S. (2014). FastQC: A quality-control for high-throughput sequence data. *Bioinformatics.babraham.ac.uk/projects/fastqc.*

Andrs, V. and Walsh, K. (1996). Myogenin Expression, Cell Cycle Withdrawal and Phenotypic Differentiation are Temporally Separable Events that Precede Cell Fusion Upon Myogenesis. *The Journal of Cell Biology*. **132(4)**, pp. 657-666.

Armstrong, R. B., Marum, P., Tullson, P. and Sawbert, C. W. (1979). Acute hypertrophic response of skeletal muscle to removal of synergists. *Journal of Applied Physiology.* **46**, pp. 835-842.

Ato, S. and Ogasawara, R. (2021). The relationship between myonuclear number and protein synthesis in individual rat skeletal muscle fibres. *Journal of Experimental Biology.* **224(10)**:jeb242496.

Attwaters, M. and Hughes, S. M. (2021). Cellular and molecular pathways controlling muscle size in response to exercise. *FEBS Journal.* Epub ahead of print.

Aziz, A., Liu, Q. and Dilworth, F. J. (2010). Regulating a master regulator: establishing tissue-specific gene expression in skeletal muscle. *Epigenetics*. **5(8)**, pp. 691-695.

Bachman, J. F., Klose, A., Liu, W., Paris, N. D., Blanc, R. S., Schmalz, M., Knapp, E. and Chakkalakal, J. V. (2018). Prepubertal skeletal muscle growth requires Pax7-expressing satellite cell-derived myonuclear contribution. *Development.* **145(20)**, pp. 1-13.

Baghdadi, M. B., Castel, D., Machado, L., Fukada, S., Birk, D. E., Relaix, F., Tajbakhsh, S. and Mourikis, P. (2018). Notch/CollagenV/CalcR reciprocal signalling retains muscle stem cells in their niche. *Nature.* **557(7707)**, pp. 714-718.

Baker, N. L., Morgelin, M., Peat, R., Goemans, N., North, K. N., Bateman, J. F. and Lamande, S. R. (2005). Dominant collagen VI mutations are a common cause of Ullrich congenital muscular dystrophy. *Human Molecular Genetics.* **14(2)**, pp. 279-293.

Bamman, M.M., Roberts, B.M. and Adams, G.R. (2018). Molecular regulation of exercise-induced muscle fiber hypertrophy. *Cold Spring Harbor perspectives in medicine*, **8(6)**, p.a029751.

Barbieri, E. and Sestili, P. (2012). Reactive oxygen species in skeletal muscle signaling. *Journal of signal transduction.* **2012,** pp.2-17.

Beauchamp, J. R., Heslop, L., Yu, D. S. W., Tajbakhsh, S., Kelly, R. G., Wenrig, A., Buckingham, M. E., Partridge, T. A. and Zammit, P. S. (2000). Expression of CD34 and Myf5 Defines the Majority of Quiescent Adult Skeletal Muscle Satellite Cells. *The Journal of Cell Biology.* **151(6)**, pp., 1221-1233.

Benitez, B. and Komivez, E. A. (2000). Disulfide bond plasticity in epidermal growth factor. *Proteins - Structure Function and Genetics.* **40(10**, pp. 168-174.

Bentzinger, C. F., Wang, Y, X., Maltzahn, J., Soleimani, V. D., Yin, H. and Rudnicki, M. A. (2013). Fibronectin regulates Wnt7a singalling and satellite cell expansion. *Cell Stem Cell*. **12(1)**, pp. 75-87.

Berkes, C. A. and Tapscott, S. J. (2005). MyoD and the transcriptional control of myogenesis. *Seminars in Cell and Developmental Biology.* **16**, pp. 585-595.

Bidanset, D., Guidry, C., Rosenberg, L., Choi, H., Timple, R. and Hook, M. (1992). Binding of the proteoglycan decorin to collagen type VI. *Journal of Biological Chemistry*. **267**, pp. 5250-5256.

Birbrair, A., Zhang, T., Wang, Z. M., Messi, M. L., Enikolopov, G. N., Mintz, A. and Delbono, O. (2013). Role of pericytes in skeletal muscle regeneration and fat accumulation. *Stem cells and development*. **22(16)**, pp. 2298-2314.

Bischoff, R. (1986). Proliferation of muscle satellite cells on intact myofibres in culture. *Developmental Biology.* **115(1)**, pp. 129-139.

Blanco-Bose, W. E., Yao, C., Kramer, R. H. and Blau, H. M. (2001). Purification of mouse primary myoblasts based on α7-integrin expression. *Experimental Cell Research.* **265**, pp. 212-220.

Blau, H. M. and Pavlath, G. K. (1983). Defective myoblasts identified in Duchenne muscular dystrophy. *Proceedings of the National; Academy of Sciences of the United States of America.* **80(5)**, pp. 4856-4860.

Blau, H. M., Chiu, C. P. and Webster, C. (1983). Cytoplasmic activation of human nucelar genes in stable heterocaryoris. *Cell.* **32**, pp. 1171-1180

Blau, H. M., Webster, C., Pavlath, G. K. and Chiu, C. P. (1985). Evidence for Defective Myoblasts in Duchenne Muscular Dystrophy. *Advances in Experimental Medicine and Biology.* **182**, pp. 85-110.

Blough, E.R. and Linderman, J.K., 2000. Lack of skeletal muscle hypertrophy in very aged male Fischer 344× Brown Norway rats. *Journal of Applied Physiology*, **88(4),** pp.1265-1270.

Bodine, S.C., Stitt, T.N., Gonzalez, M., Kline, W.O., Stover, G.L., Bauerlein, R., Zlotchenko, E., Scrimgeour, A., Lawrence, J.C., Glass, D.J. and Yancopoulos, G.D. (2001). Akt/mTOR pathway is a crucial regulator of skeletal muscle hypertrophy and can prevent muscle atrophy in vivo. *Nature cell biology*, **3(11),** pp.1014-1019.

Bonaldo, P., Russo, V., Bucciotti, F., Doliana, R. and Colombatti, A. (1990). Structural and functional features of the alpha 3 chain indicate a bridging role for chicken collagen VI in connective tissues. *Biochemistry.* **29**, pp. 1245-1254.

Bosutti, A., Giniatullin, A., Odnoshivkina, Y., Giudice, L., Malm, T., Sciancalepore, M., Giniatullin, R., D'Andrea, P., Lorenzon, P. and Bernareggi, A. (2021). "Time window" effect of Yoda1-evoked Piezo1 channel activity during mouse skeletal muscle differentiation. *Acta Physiologica*, p.e13702.

Boyden, S. E., Mahoney, L. J., Kawahara, G., Myers, J. A., Mitsuhashi, S., Estrella, E. A., Duncan, A. R., Dey. F., DeChene, E. T. and Blasko-Goehringer, J. M. (2012). Mutations in the satellite cell gene MEGF10 cause a recessive congenital myopathy with minicores. *Neurogenetics*. **13(2)**, pp. 115-124.

Bowen, S., Mangner, T., Werner, S., Glaser, S., Kullnick, Y., Schrepper, Y., Doenst, T., Oberbach, A., Lincke, A., Steil, L. and Schuler, G. (2015). Diaphragm muscle weakness in mice is early-onset post-myocardial infarction and associated with elevated protein oxidation. *Journal of Applied Physiology.* **118(1)**

Brack AS, Conboy IM, Conboy MJ, Shen J, Rando TA. (2008) A temporal switch from notch to Wnt signaling in muscle stem cells is necessary for normal adult myogenesis. *Cell Stem Cell*. **2(1),** pp. 50-9.

Briata, P., Lin, W. J., Pasero, M., Chou, C. F., Trabucchi, M., Rosenfeld, M. G., Chen, C. Y. and Gherzi, R. (2011). PI3K/AKT signalling determines a dynamic switch between distinct KSRP functions favouring skeletal myogenesis. *Nature*. **19**, pp. 478-487.

Bröhl, D., Vasyutina, E., Czajkowski, M.T., Griger, J., Rassek, C., Rahn, H.P., Purfürst, B., Wende, H. and Birchmeier, C., 2012. Colonization of the satellite cell niche by skeletal muscle progenitor cells depends on Notch signals. *Developmental cell*, **23(3)**, pp.469-481.

Bruusgaard, J. C., Johansen, I. B., Egner, I. M., Rana, Z. A. and Gunderson, K. (2010). Myonuclei acquired by overload exercise precede hypertrophy and are not lost on detraining. *Proceedings of the National Academy of Sciences of the United States of America.* **107(34)**, pp. 15111-15116.

Buckingham, M. (2006). Myogenic progenitor cells and skeletal myogenesis in vertebrates. *Current Opinion in Genetics and Development.* **16(5)**, pp. 525-532.

Buckingham, M. and Relaix, F. (2015). Pax3 and Pax7 as upstream regulators of myogenesis. *Seminars in Cell & Developmental Biology.* **44**, pp. 115-125.

Burattini, S., Luchetti, F. and Curci, R. (2004). C2C12 murine myoblasts as a model of skeletal muscle development: Morpho-functional characterisation. *European Journal of Histochemistry.* **48(3)**, pp. 223-234.

Burns, D. P., Drummond, D. P., Bolger, D., Murphy, K. H., Coiscaud, A. P., Edge, D. and O'Halloran, K. D. (2019). N-acetyle cystiene improves dystrophic (*mdx*) mouse diaphragm muscle quality and strength. *The Journal of the Federation of American Societies for Experimental Biology.* **33(S1)**, pp. 843.

Callebaut, I., Mignotte, V., Souchet, M. and Mornon, J.P. (2003). EMI domains are widespread and reveal the probable orthologs of the Caenorhabditis elegans CED-1 protein. *Biochemical and biophysical research communications*, **300(3)**, pp.619-623.

Carter, G. T., Wineinger, M. A., Walsh, S. A., Horasek, J., Abresch, R. T. and Fowler, W. M. (1995). Effect of voluntary wheel-running exercise on muscles of the *mdx* mouse. *Neuromuscular Disorders*. **5(4)**, pp. 323-332.

Casar, J. C., McKechnie, B. A., Fallon, J. R., Young, M. F. and Brandan, E. (2004). Transient up-regulation of biglycan during skeletal muscle regeneration: delayed fibre growth along with decorin increase in biglycan-deficient mice. *Developmental Biology.* **268(2)**, pp. 358-371.

Chal, J. and Pourquie, O. (2017). Making muscle: skeletal myogenesis *in vivo* and *in vitro*. *Development*. **144**, pp. 2104-2122.

Chang, N. C., Chevalier, F. P. and Rudnicki, M. A. (2016). Satellite Cells in Muscular Dystrophy – Lost in Polarity. *Trends in Molecular Medicine.* **22(6)**, pp. 479-496.

Charge, S. B. and Rudnicki, M. A. (2004). Cellular and Molecular Regulation of Muscle Regeneration. *Physiological Reviews.* **84(1)**, pp. 209-238.

Chen, X. and Li, Y. (2009). Role of matrix metalloproteinases in skeletal muscle. *Cell Adhesion & Migration.* **3(4)**, pp. 337-341.
Chiu, J., Tseng, L., Huang, T., Liu, C., Wang, J., Huang, C., Tsai, F. and Hsu, C. (2020). MEGF11 is related to tumour recurrence in triple negative breast cancer via chemokine upregulation. *Nature Scientific Reports.* **10**, pp. 8060.

Choo, H. J., Canner, J. P., Vest, K. E., Thomson, Z. and Pavlath, G. K. (2017). A tale of two niches: differential functions for VCAM1 in satellite cells under basal and injured conditions. *American Journal of Physiology-Cell Physiology.* **313**, pp. 392-404.

Christov, C., Chretien, F., Abou-Khalil, R., Bassez, G., Vallet, G., Authier, F., Bassaglia, Y., Shinin, V., Tajbakhsh, S., Chazaud, B. and Gherardi, R. K. (2007). Muscle Satellite Cells and Endothelial Cells: Close Neighbors and Privileged Partners. *Molecular Biology of the Cell.* **18(4)**, pp. 1397-1409.

Chronopoulos, A., Thrope, S. D., Cortes, E., Lachowski, D., Rice, A. J., Mykuliak, V. V., Rog, T., Lee, D. A., Hytonen, V. P and Hernandez, A. E. (2020). Syndecan-4 tunes cell mechanics by activating the kindlin-integrin-RhoA pathway. *Nature Materials.* **6**, pp. 669-678.

Chrzanowska, M. and Burridge, K. (1996). Rho-stimulated contractility drives the formation of stress fibres and focal adhesions. *Journal of Cell Biology.* **133(6)**, pp. 1403.

Chung, W.S., Clarke, L.E., Wang, G.X., Stafford, B.K., Sher, A., Chakraborty, C., Joung, J., Foo, L.C., Thompson, A., Chen, C. and Smith, S.J., 2013. Astrocytes mediate synapse elimination through MEGF10 and MERTK pathways. *Nature*. **504(7480)**, pp.394-400.

Ciciliot, S. and Schiaffino, S. (2010). Regeneration of Mammalian Skeletal Muscle: Basic Mechanisms and Clinical Implications. *Current Pharmaceutical Design.* **16**, pp. 906-914.

Clark, P., Coles, D. Peckham, M. (1997). Preferential Adhesion to and Survival on Patterned Laminin Organizes Myogenesis in Vitro. *Experimental Cell Research.* 283(2), pp. 275-283.

Collins, C. A, Gnocci, V. F., White, R. B., Boldrin, L., Perez-Ruiz, A., Relaix, F., Morgan, J. E. and Zammit, P. S. (2009). Integrated Functions of Pax3 and Pax7 in the Regulation of Proliferation, Cell Size, and Myogenic Differentiation. *PloS one*. **4(2)**, pp. e4475.

Collins, C. A. and Zammit, P. S. (2009). Isolation and grafting of single muscle fibres. *Methods in Molecular Biology*. **482**, pp. 319-330.

Constantini, M., Testa, S., Fornetti, E., Barbetta, A., Trombetta, M., Cannata, S. M., Gargioli, C. and Rainer, A. (2017). Engineering muscle networks in 3D gelatin methacryloyl hydrogels: influence of mechanical stiffness and geometrical confinement. Frontiers in Bioengineering and Biotechnology. **5**, pp. 22.

Cornelison, D. D. and Wold, B. J. (1997). Single-cell analysis of regulatory gene expression in quiescent and activated mouse skeletal muscle satellite cells. *Dev Biol* 191, 270-83.

Cornelison, D. D. W., Filla, M. S., Stanley, H. M., Rapraeger, A. C. and Olwin, B. B. (2001). Syndecan-3 and Syndecan-4 Specifically Mark Skeletal Muscle Satellite Cells and Are Implicated in Satellite Cell Maintenance and Muscle Regeneration. *Developmental Biology*. **239**, pp. 79-94.

Cossu, G. and Biressi, S. (2005). Satellite cells, myoblasts and other possible myogenic progenitors: Possible origin, phenotypic features and regeneration. *Seminars in Cell and Developmental Biology.* **16(4-5)**, pp. 623-631.

Cossu, G. and Tajbakhsh, S. (2007). Oriented Cell Divisions and Muscle Satellite Cell Heterogeneity. *Cell.* **5(1)**, pp. 859-861.

Cox, R. D., Garner, I. and Buckingham, M. E. (1990). Transcriptional regulation of actin and myosin genes during differentiation of a mouse muscle cell line. *Differentiation.* **43**, pp. 183-191.

Craig, R. and Padron, R. (1994). The structure of contractile filaments. *Myology*. pp. 134-175.

Crisona, N.J., Allen, K.D. and Strohman, R.C. (1998). Muscle satellite cells from dystrophic (mdx) mice have elevated levels of heparan sulphate proteoglycan receptors for fibroblast growth factor. *Journal of Muscle Research & Cell Motility*, **19(1)**, pp.43-51.

Crist, C. G., Montarras, D. and Buckingham, M. (2012). Muscle Satellite Cells are Primed for Myogenesis but Maintain Quiescence with Sequestration of Myf5 mRNA Targeted by microRNA-31 in mRNP Granules. *Cell Stem Cell.* **11(1)**, pp. 118-126.

Csapo, R., Gumpenberger, M. and Wessner, B. (2020). Skeletal Muscle Extracellular Matrix – What Do We Know About Its Composition, Regulation, and Physiological Roles? A Narrative Review. *Frotiers in Physiology*. **11**, pp. 253.

Damas, F., Libardi, C.A. and Ugrinowitsch, C. (2018). The development of skeletal muscle hypertrophy through resistance training: the role of muscle damage and muscle protein synthesis. *European journal of applied physiology*, **118(3)**, pp.485-500.

Darnell, M., Gu, L. and Mooney, D., 2018. RNA-seq reveals diverse effects of substrate stiffness on mesenchymal stem cells. *Biomaterials*, **181**, pp.182-188.

Dellavalle, A., Sampaolesi, M., Tonlorenzi, R., Tagliafico, E., Sacchetti, B., Perani, L., Innocenzi, A., Galvez, B.G., Messina, G., Morosetti, R. and Li, S., 2007. Pericytes of human skeletal muscle are myogenic precursors distinct from satellite cells. *Nature cell biology*, **9(3),** pp.255-267.

Dembo, M and Wang, Y. (1999). Stresses at the Cell-to-Substrate Interface during Locomotion of Fibroblasts. *Biophysical Journal.* **76**, pp. 2307-2316.

Denes, L. T., Riley, L. A., Mijares, J. R., Arboleda, J. D., McKee, K., Esser, K. A. and Wang, E. T. (2019). Culturing C2C12 myotubes on micromolded gelatin hydrogels accelerates myotube maturation. *Skeletal muscle.* **9(1)**, pp. 1-10.

Deveci, D. and Egginton, S., 2002. Muscle ischaemia in rats may be relieved by overload-induced angiogenesis. *Experimental physiology*. **87(4),** pp.479-488.

Dhawan, J. and Rando, T. A. (2005). Stem cells in postnatal myogenesis: molecular mechanisms of satellite cell quiescence, activation and replenishment. *Cell Press.* **15(12)**, pp. 666-673.

Dick, J. and Vrbova, G. (1993). Progressive deterioration of muscles in *mdx* mice induced by overload. *Clinical Science.* **84(2)**, pp. 145-150.

Discher, D. E. (2004a). Myotubes differentiate optimally on substrates with tissue-like stiffness: pathological implications for soft or stiff microenvironments. *The Journal of Cell Biology.* **166(6)**, pp. 877-887.

Discher, D. E., Discher, D. E., Janmey, P. and Wang, Y. (2013). Tissue Cells Feel and Respond to the Stiffness of Their Substrate. *Materials and Biology.* **310**, pp. 1139-1143.

Dobin, A., Davis, C. A., Schlesinger, F. and Drenkow, J. (2013). STAR: ultrafast universal RNA-seq aligner. *Bioinformatics.* **29(1)**, pp. 15-21.

Doliana, R., Bot, S., Bonaldo, P. and Colombatti, A. (2000). EMI, a novel cysteine-rich domain of EMILINS and other extracellular proteins, interacts with the gC1q domains and participates in multimerization. *FEBS Letters*. **484(2)**, pp. 164-268.

Dowling, P., Gargan, S., Murphy, S., Zweyer, M., Sabir, H., Swandullah, D. and Ohlendiek, K. (2021). The Dystrophin Node as Integrator of Cytoskeletal Organisation, Lateral Force Transmission, Fiber Stability and Cellular Signalling in Skeletal Muscle. *Proteomes.* **9(1)**, pp. 9.

Duan, D., Goemans, N., Takeda, S., Mercuri, E. and Aartsma-Rus, A. (2021). Duchenne Muscular Dystrophy. *Nature Reviews: Disease Primers*. **7(1)**, pp. 13.

Duggan, A. T., Kocha, K. M., Monk, C. T., Bremer, K. and Moyes, C. D. (2011). Coordination of cytochrome c oxidase gene expression in the remodelling of skeletal muscle. *Journal of Experimental Biology.* **214(11)**, pp. 1880-1887.

Dumont, N. A., Wang, Y. X., Maltzahn, J., Pasut, A., Bentzinger, C. F., Brun, C. E. and Rudnicki, M. A. (2015). Dystrophin expression in muscle stem cells regulates their polarity and asymmetric division. *Nature Medicine.* **21**, pp. 1455-1463.

Dupont, S., Morsut, L., Aragona, M., Enzo, E., Giulitti, S., Cordenonsi, M., Zanconato, F., Le Digabel, J., Forcato, M., Ciccatio, S., Elvassore, N. and Piccolo, S. (2011). Role of YAP/TAZ in mechanotransduction. *Nature*. **474**, pp. 179-183.

Egginton, S., Badr, I., Williams, J., Hauton, D., Baan, G. C. and Jaspers, R. T. (2011). Physiological angiogenesis is a graded, not physiological response. *Journal of Physiology.* **589(1)**, pp. 195-206.

Egginton, S., Brown, M. D. and Hudlicka, O. Walter, H., Weiss, J. B and Bate, A. (1998). Capillary Growth in Overloaded, Hypertrophic Adult Rat Skeletal Muscle: An Ultrastructural Study. *The Anatomical Record.* **252**, pp. 49-63.

Egginton, S., Hudlicka, O., Brown, M. D., Walter, H., Weisse, J. B. and Bate, A. (1998). Capillary growth in relation to blood flow and performance in overloaded rat skeletal muscle. *Journal of Applied Physiology.* **85(6)**, pp. 2025-2032.

Egner, I.M., Bruusgaard, J.C. and Gundersen, K. (2016). Satellite cell depletion prevents fiber hypertrophy in skeletal muscle. *Development*, **143(16)**, pp.2898-2906.

Ehebauer, M. T., Hayward, P. and Arias, A. M. (2007). Notch Signalling Pathway. *Science Signalling*. **364**, pp. 1-4.

Ehrmann, R. L. and Gey, G. O. (1956). The Growth of Cells on a Transparent Gel of Reconstituted Rat-Tail Collagen. *Journal of the National Cancer Institute*. 16, pp. 1375–1403.

Elosegui-Artola, A., Andreu, I., Beedle, A. E. M., Lezamiz, A., Uroz, M., Kosmalska, A. J., Orla, R., Kechagia, J. Z., Rico-Lastres, P., Le Roux, A. L., Shanahan, C. M., Trepat, X., Navajas, D., Garcia-Manyes, S. and Roca-Cusachs, P. Force Triggers YAP Nuclear Entry by Regulating Transport across Nuclear Pores. *Europe PMC.* **43(5)**, pp. 547-548.

Elveflow Team. (2021). PDMS: A review. *Elveflow.* Available: https://www.elveflow.com/microfluidic-reviews/general-microfluidics/the-polydimethylsiloxane-pdms-and-microfluidics/. Accessed 8th Jan 2022.

Engelhard, C., Sarsfield, S., Merte, J., Wang, Q., Li, P., Beppu, H., Kolodin, A. L., Sucov, H. M., and Ginty, D. D. (2013). MEGF8 is a Modifier of BMP Signalling in Trigeminal Sensory Neurones. *Elife.* **17(2)**, pp. e01160.

Engler, A. Bacakova, L., Newman, C., Hategan, A., Griffin, M. and Discher, D. (2004b). Substrate compliance versus ligand density in cell on gel responses. *Biophysical Journal*. **86**, pp. 617-628.

Engler, A. J., Griffin, M. A., Sen, S., Bonnemann, C. G., Sweeney, H. L. and Discher, D. E. (2004). Myotubes differentiate optimally on substrates with tissue-like stiffness: pathological implications for soft or stiff microenvironments. *The Journal of Cell Biology.* **166(6)**, pp. 877-887.

Fanbin, M., Jianghai, Juan, L., Yang, W., Yuxiong, W., Yanhua, C., Tao, L. and Zhenbing, C. (2011). Role of transforming growth factor β1 in the process of fibrosis of denervated skeletal muscle. *Journal of Huazhong University of Science and Technology [Medical Sciences].* **31(1)**, pp. 77-82.

Farrell, P. A., Fedele, M. J., Hernandez, J., Fluckey, J. D., Miller, J. L., Lang, C. H., Vary, T. C., Kimball, S. R. and Jefferson, L. S. (1999). Hypertrophy of skeletal muscle in diabetic rats in response to chronic resistance exercise. *Journal of Applied Physiology.* **87(3)**, pp. 1075-1082.

Ferguson, V.L., Ayers, R.A., Bateman, T.A. and Simske, S.J. (2003). Bone development and age-related bone loss in male C57BL/6J mice. *Bone*, **33(3),** pp.387-398.

Ferrara, F., Naranjo, L. A., D'Angelo, S., Kiss, C. and Bradbury, A. R. M. (2013). Specific binder for Lightning Link® biotinylated proteins from an antibody phage library. *Journal of Immunological Methods.* **395**, pp. 83-87.

Ferraro, E., Molinari, F. and Berghella, L. (2012). Molecular control of neuromuscular junction development. *Journal of cachexia, sarcopenia and muscle*, **3(1)**, pp.13-23.

Flucher, B.E., Takekura, H. and Franzini-Armstrong, C. (1993). Development of the excitation-contraction coupling apparatus in skeletal muscle: association of sarcoplasmic reticulum and transverse tubules with myofibrils. *Developmental biology*, **160(1),** pp.135-147.

Friedrichs, M., Wirsdoerfer, F., Flohe, S. B., Schnieder, S., Wuelling, M. and Vortkamp, A. (2011). BMP signalling balances proliferation and differentiation of muscle satellite cell descendants. *BMC Cell Biology.* **12(1)**, pp. 1-17.

Frontera, W.R. and Ochala, J. (2015). Skeletal muscle: a brief review of structure and function. *Calcified tissue international*, ***96*(3),** pp.183-195.

Fry, C.S., Lee, J.D., Jackson, J.R., Kirby, T.J., Stasko, S.A., Liu, H., Dupont-Versteegden, E.E., McCarthy, J.J. and Peterson, C.A., 2014. Regulation of the muscle fiber micro environment by activated satellite cells during hypertrophy. *The FASEB Journal*, **28(4)**, pp.1654-1665.

Fu, X., Wang, H. and Hu, P. (2015). Stem Cell Activation in Skeletal Muscle Regeneration. *Cellular and Molecular Life Sciences.* **72**, pp. 1663-1677.

Fukada, S., Uezumi, A., Ikemoto, M., Masuda, S., Segawa, M., Tanimura, M., Yamamoto, H., Miyagoe-Susuki, Y. and Takeda, S. (2009). Molecular Signature of Quiescent Satellite Cells in Adult Skeletal Muscle. *Stem Cells.* **25(10)**, pp. 2448-2459.

Gao, Q. and McNally, E. M. (2015). The Dystrophin Complex: structure, function and implications for therapy. *Comprehensive Physiology.* **5(3)**, pp. 1223-1239.

Gilbert, P. M., Havenstrite, K. L., Magnusson, K. E., Sacco, A., Leonardi, N. A., Kraft, P. Nguyen, N. K., Thrun, S., Lutolf, M. P and Blau, H. M. (2010). Substrate elasticity regulates skeletal muscle stem cell self-renewal in culture. *Science*. 329, pp. 1078-1081.

Gillies, A. R. and Liber, R. L. (2011). Structure and Function of the Skeletal Muscle Extracellular Matrix. *Muscle Nerve.* **44(3)**, pp. 318-331.

Goh, Q. and Millay, D.P. (2017). Requirement of myomaker-mediated stem cell fusion for skeletal muscle hypertrophy. *elife*, **6**, p.e20007.

Gonyea, W. J. and Antonio, J. (1993). Skeletal muscle fiber hyperplasia. *Medicine and Science in Sports and Exercise.* **25(12)**, pp. 1333-1345.

Goodman, C.A., Miu, M.H., Frey, J.W., Mabrey, D.M., Lincoln, H.C., Ge, Y., Chen, J. and Hornberger, T.A. (2010). A phosphatidylinositol 3-kinase/protein kinase B-independent activation of mammalian target of rapamycin signaling is sufficient to induce skeletal muscle hypertrophy. *Molecular biology of the cell*, **21(18),** pp.3258-3268.

Green, H. J., Klug, G. A., Reichmann, H., Seedorf, U., Wiehrer, W. and Pette, D. (1984). Exercise-induced fibre type transitions with regard to myosin, parvalbumin, and sarcoplasmic reticulum in muscles of the rat. *European Journal of Physiology.* **400**, pp. 432-438.

Griffeth, R.J., Bianda, V. and Nef, S. (2014). The emerging role of insulin-like growth factors in testis development and function. *Basic and clinical andrology*, **24(1)**, pp.1-10.

Griffin, M. A., Sen, S., Sweeney, H. L. and Discher, D. E. (2004). Adhesion-contractile balance in myocyte differentiation. *Journal of Cell Science.* **117(24)**, pp. 5855-5863.

Grohmann, K., Schuelke, M., Diers, A., Hoffman, K., Lucke, B., Adams, C., Bertini, E., Leonhardt-Horti, H., Muntoni, F., Ouvrier, R. and Pfeufer, A. (2001). Mutations in the gene encoding immunoglobulin μ-binding protein 2 cause spinal muscular atrophy with respiratory distress type 1. *Nature Genetics.* **29(1)**, pp. 75-77.

Gromova, A., Tierney, M. T. and Sacco, A. (2015). FACS-based satellite cell isolation from mouse hindlimb muscles. *Bio-protocol.* **5(16)**, e1558.

Grzelkowska-Kowalczyk, K., 2016. The importance of extracellular matrix in skeletal muscle development and function. *Composition and function of the extracellular matrix in the human body*, pp.3-24.

Guenther, U. P., Handoko, L., Varon, R., Stephani, U., Tsao, C. Y., Mendell, J. R., Lutzkendorf, S., Hubner, C., von Au, K., Jablonka, S. and Dittmar, G. (2009). Clinical variability in spinal muscular atrophy type 1 (DSMA1): determination of steady-state IGHMPB2 protein levels in five patients with infantile and juvenile disease. *Journal of Molecular Medicine*. **87(1)**, pp. 31-41.

Guiraud, S. and Chang, N. C. (2019). Regenerative biomarkers for Duchenne muscular dystrophy. *Neural Regeneration Research.* **14(8)**, pp. 1378.

Han, R., Kanagawa, M., Yoshida-Moriguchi, T., Rader, E. P., Ng, R. A., Michele, D. E., Muirhead, D. E., Kunz, S., Moorse, S. A., Iannaccone, S. T., Miyake, K., McNeil, P. L., Mayer, U., Oldstone, M. B. A., Faulkner, J. A. and Campbell, K. P. (2009). Basal lamina strengthens cell membrane integrity via the laminin G domain-binding motif α-

dystroglycan. *Proceedings of the National Academy of Sciences of the United States of America.* **106(31)**, pp. 12573-12579.

Hardy, D., Besnard, A., Latil, M., Jouvion, G., Briand, D., Thepenier, C., and Pascal, Q. (2016). Comparative study of injury models for studying regeneration in mice. *PLoS One.* **11(1)**, pp. e0147198.

Harris, E., Topf, A., Baressi, R., Hudson, J., Powell, H., Tellez, J., Hicks, D., Porter, A., Bertoli, M. and Evangelista, A. (2017). Exome sequences versus sequential gene testing in the UK highly specialised Service for Limb Girdle Muscular Dystrophy. *Orphanet Journal of Rare Diseases.* **12**, pp. 151.

Hastings, J. F.2, Skhinas, J. N., Fey, D., Croucher, D. R. and Cox, T. R. (2018). The extracellular matrix as a key regulator of intracellular signalling networks. *British Journal of Pharmacology,* **176(1)**, pp. 82-92.

Hendrickse, P. and Degens, H. (2019). The role of microcirculation in muscle function and plasticity. *Journal of Muscle Research and Cell Motility.* **40**, pp. 127-140.

Henriquez, J. P., Casar, J. C., Fuentealba, L., Carey, D. J. and Brandan, E. (2002). Extracellular matrix histone H1 binds to perlecan, is present in regenerating skeletal muscle and stimulates myoblast proliferation. *Journal of Cell Science.* **115(10)**, pp. 2041-2051.

Hermansen, L. and Wachtlova, M. (1971). Capillary density of skeletal muscle in well-trained and untrained men. *Journal of Applied Physiology.* **30(6)**, pp. 860-863.

Hernandez-Hernandez, J. M., Garcia-Gonzalez, E. G., Brun, C. E. and Rudnicki, M. A. (2017). The myogenic regulatory factors, determinants of muscle development, cell identity and regeneration. *Semin Cell Dev Biol* 72, 10-18.

Hild, C., Jahrig, M., Pecoraro, G. and Scwamborn, A. (2020). Behaviour of C2C12-cells on curved PDMS-substrates. *GROWTH*. **1(4E)**, 06.

Hinits, Y., Osborn, D. P., Carvajal, J. J., Rigby, P. W. and Huges, S. M. (2007). Mrf4 (myf6) is dynamically expressed in differentiated zebrafish skeletal muscle. *Gene Expression Patterns.* **7(7)**, pp. 738-745.

Hocking, D. C., Titus, P. A., Sumagin, R. and Sarelius, R. H. (2007). Extracellular Matrix Fibronectin Mechanically Couples Skeletal Muscle Contraction With Local Vasodilation. *Circulation Research*. **102(3)**, pp. 372-379.

Holmberg, J. and Durbeej, M. (2013). Laminin-211 in skeletal muscle function. *Cell Adhesion and Migration.* **7(1)**, pp. 111-121.

Holterman, C. E., Le Grand, F., Kuang, S., Seale, P. and Rudnicki, M. A. (2007). Megf10 regulates the progression of the satellite cell myogenic program. *Journal of Cell Biology*. **179(5)**, pp. 911-922.

Honardoost, M., Soleimani, M., Arefian, E. and Sarookhani, M. (2015). Expression Change of miR-214 and miR-135 during Muscle Differentiation. *Cell Journal.* **17(3)**, pp. 461-470.

Houang, E. M., Sham, Y. Y., Bates, F. S. and Metzger, J. M. (2018). Muscle Membrane Integrity in Duchenne muscular dystrophy: recent advances in copolymer-based muscle membrane stabilizers. *Skeletal Muscle.* **8(31)**, pp. 1-19.

Hu, X., Charles, J. P., Akay, T., Hutchinson, J. R. and Blemker, S. S. (2017). Are mice good models for neuromuscular disease? Comparing muscle excursions in walking between mice and humans. *Skeletal Muscle.* **7(26)**, pp. 2-14.

Hu, X., Margadant, F. M., Yao, M and Sheetz, M. P. (2017). Molecular stretching modulates mechanosensing pathways. *Protein Science.* **26(7)**, pp. 1337-1351.

Huang, H., Zhao, Y., Shang, X., Ren, H., Zhao, Y. and Liu, X. (2019). CAIII expression in skeletal muscle is regulated by Ca(2+)-CaMKII-MEF2C signalling. *Experimental Cell Research.* **385**, pp. 111672.

Huey, K. A., Smith, S. A., Sulaeman, A. and Breen, E. C. (2016). Skeletal myofiber VEGF is necessary for myogenic and contractile adaptations to functional overload of the plantaris in adult mice. *Journal of Applied Physiology.* **120**, pp. 188-195.

Hughes, C. S., Postovit, L. M. and Lajoie, G. A. (2010). Matrigel: a complex protein mixture required for optimal growth of cell culture. *Proteomics.* **10(9)**, pp. 1886-1890.

Hughes, R. E. (2016). The role of MEGF10 in skeletal muscle myopathy. Doctoral thesis. University of Leeds. Leeds.

Huse, S., Huber, J., Morrison, H., Sogin, M. and Welch, D. (2007). Accuracy and quality of massively parallel DNA pyrosequencing. *Genome Biology.* 8, pp. 143.

Hyatt, J. K., McCall, G. E., Kander, E. M., Zhong, H., Roy, R. R. and Huey, K. A. (2008). PAX3/7 expression coincides with myod during chronic skeletal muscle overload. *Muscle & Nerve.* **38(1)**, pp. 861-866.

Illumina TruSeq. (2014). TruSeq™ RNA and DNA Sample Preparation Kits v2. *Sequencing Methods Review.* pp. 134-137.

Incitti, T., Magli, A., Darabi, R., Yuan, C., Lin, K., Arpke, R.W., Azzag, K., Yamamoto, A., Stewart, R., Thomson, J.A. and Kyba, M., 2019. Pluripotent stem cell-derived myogenic progenitors remodel their molecular signature upon in vivo engraftment. *Proceedings of the National Academy of Sciences*, **116(10),** pp.4346-4351.

Iram, T., Ramirez-Oritz, Z., Byrne, M. H., Coleman, U. A., Kingery, N. D., Means, T. K., Frenkel, D. and Khoury, E. L. (2016). Megf10 is a Receptor that Mediates Clearance of Apoptotic Cells by Astrocytes. *Journal of Neuroscience.* **36(19)**, pp. 5185-5192.

Irianto, J., Pfeifer, C. R., Xia, Y. and Discher, D. E. (2016). Snapshot: Mechanosensing Matrix. *Cell.* 165(7), pp. 120.

Ishibashi, J., Perry, R. L., Asakura, A. and Rudnicki, M. A. (2005). *Journal of Cell Biology.* **171(3)**, pp. 471-482.

Iso, T., Kedes, L. and Hamamori, Y. (2003). HES and HERP families: multiple effectors of the Notch signalling pathway. *Journal of Cell Physiology.* **194(3)**, pp. 237-255.

James, N. T. (1973). Compensatory hypertrophy of the extensor digitorum longus muscle of the rat. *Journal of Anatomy.* **116(1)**, pp. 57-65.

Jat, P.S., Noble, M.D., Ataliotis, P., Tanaka, Y., Yannoutsos, N., Larsen, L. and Kioussis, D. (1991). Direct derivation of conditionally immortal cell- lines from an h-2kb-

tsa58 transgenic mouse. *Proceedings of the National Academy of Sciences of the United States of America.* 88(12), pp. 5096-5100.

Johnson, T. L. (1988). Physiological, morphological and histochemical analysis of skeletal muscle hypertrophy in the mouse. Doctoral thesis. Indiana University.

Johnson, T. L. and Klueber, K. M. (1991). Skeletal muscle following tonic overload: functional and structural analysis. *Medicine and Science in Sports and Exercise.* **23(1)**, pp. 49-55.

Kaji, H., Ishibashi, T., Nagamine, K., Kanzaki, M. and Nishizawa, M. (2010). Electrically induced contraction of C2C12 myotubes cultured on a porous membrane-based substrate with muscle-tissue like stiffness. *Biomaterials.* **31(27)**, pp. 6981-6986.

Kaliman, P., Vinals, F., Testar, X., Palacin, M and Zorzano, A. (1996). Phosphatidylinositol 3-kinase Inhibitors Block Differentiation in Skeletal Muscle. *Journal of Biological Chemistry.* **271(32)**, pp. 19146-19151.

Kann, A. P., Hung, M. and Krauss, R. S. (2016). Cell-cell contacts and signalling in the muscle stem cell niche. *Current Opinion in Cell Biology.* **73**, pp. 78-83.

Karalaki, M., Fili, S., Philippou, A. and Koutsilieris, M. (2009). Muscle regeneration: cellular and molecular events. *In Vivo.* **23**, pp. 779-96.

Kay, J. N., Chu, M. W. and Sanes, J. R. (2012). MEGF10 and MEGF11 mediate homotypic interactions required for mosaic spacing of retinal neurones. *Nature*. **483**, pp. 465-469.

Kaya-Copur, A., Marchiano, F., Hein, M. Y., Alpern, D., Russeil, J., Luis, N. M., Mann, M., Deplancke, B. and Habermann, B. H. (2021). The hippo pathway controls myofibril assembly and muscle fiber growth by regulating sarcomeric gene expression. *eLife.* **10**, pp. e63726.

Kemi, O. J., Loennechen, J. P., Wisloff, U. and Ellingsen, O. (2002). Intensity-controlled treadmill running in mice: cardiac and skeletal muscle hypertrophy. *Journal of Applied Physiology.* **93(4)**, pp. 1301-1309.

Kemkemer, R., Frey, K., Fischer, A. and Krastev, R. (2018). CurvChip-Chip platform for investigating cell responses to curved surface features. *Current Directions in Biomedical Engineering.* **4(1)**, pp. 453-456.

Kim, B. (2014). Biology of the Extracellular Matrix: An Overview. *Journal of Glaucoma.* S20.

Kinzel, B., Schmedt, C. and Blau, H. M. (2018). Induction of muscle stem cell quiescence by the secreted niche factor Oncostatin M. *Nature Communications.* **9(1)**. Article no. 1531.

Kirby, T.J., Patel, R.M., McClintock, T.S., Dupont-Versteegden, E.E., Peterson, C.A. and McCarthy, J.J. (2016). Myonuclear transcription is responsive to mechanical load and DNA content but uncoupled from cell size during hypertrophy. *Molecular biology of the cell*, **27(5)**, pp.788-798.

Kleinman, H. K., Klebe, R. J. and Martin, G. R. (1981). Role of collagenous matrices in the adhesion and growth of cells. *Journal of Cell Biology.* 88(3), pp. 473-485.

Klug, H. and Bonsall, M.B., 2007. When to care for, abandon, or eat your offspring: the evolution of parental care and filial cannibalism. *The American Naturalist*, **170(6),** pp.886-901.

Koch, U., Lehal, R. and Radtke, F. (2013). Stem cells living with a Notch. *Development*, **140(4)**, pp.689-704.

Konopka, A. R. and Harber, M. P. (2014). Skeletal Muscle Hypertrophy after Aerobic Exercise Training. *Exercise and Sport Sciences Reviews.* **42(2)**, pp. 53-61.

Kopan, R., Nye, J. S. and Weintraub, H. (1994). The intracellular domain of mouse Notch: a constitutively activated repressor of myogenesis directed at the basic helix-loop-helix region of MyoD. *Development.* **120(9)**, pp. 2385-2396.

Kovanen, V. (2002). Intramuscular extracellular matrix: complex environment of muscle cells. *Exercise and Sport Sciences Reviews.* **30(1)**, pp. 20-25.

Kraemer, W. J. and Zatsiorsky, V. M. (2006). Science and Practice of Strength Training. *Human Kinetics*, pp. 50.

Kuang, S., Charge, S. B., Seale, P., Huh, M. and Rudnicki, M. A. (2006). Distinct roles for Pax7 and Pax3 in adult regenerative myogenesis. *The Journal of Cell Biology.* **172(1)**, pp. 103-113.

Kuang, S., Gillespie, M. A. and Rudnicki, M. A. (2008). Niche Regulation of Muscle Satellite Cell Self-Renewal and Differentiation. *Cell Press.* 2(1), pp. 22- 31.

La Framboise, W. A., Guthrie, R. D., Scalise, D., Elborne, V., Bombach, K. L., Armanious, C. S. and Magovern, J. A. (2003). Effect of muscle origin and phenotype on satellite cell muscle-specific gene expression. *Journal of Molecular and Cellular Cardiology.* **35(10)**, pp. 1307-1318.

Labeit, S., Kolmerer, B. and Linke, W. A. (1997). The giant protein titin: an emerging role in physiology and pathophysiology. *Circulation Research.* **80(2)**, pp. 290-294.

Landfeldt, E. Lindgren, P., Bell, C. F., Guglieri, M., Straub, V., Lochmuller, H. and Bushby, K. (2016). Quantifying the burden of caregiving in Duchenne muscular dystrophy. *Journal of Neurology.* **263(5)**, pp. 906-915.

Le Grand, F. and Rudnicki, M. A. (2007). Skeletal Muscle Satellite Cells and Adult Myogenesis. *Current Opinions in Cell Biology.* **926**, pp. 628-633.

Lee, E. J., Nam, J. H. and Choi, I. (2018). Fibromodulin modulates myoblast differentiation by controlling calcium channel. *Biochemical and Biophysical Research Communications.* **503(2)**, pp. 580-585.

Lee, N.K. and MacLean, H.E., 2011. Polyamines, androgens, and skeletal muscle hypertrophy. *Journal of cellular physiology*, *226*(6), pp.1453-1460.

Levental, I., Georges, P.C. and Janmey, P.A., 2007. Soft biological materials and their impact on cell function. *Soft Matter*. **3(3),** pp.299-306.

Li, C., Vargas-Franco, D., Saha, M., Davis, R. M., Manko, K. A., Draper, I., Pacak, C. A. and Kang, P. B. (2021). Megf10 deficiency impairs skeletal muscle stem cell migration and muscle regeneration. *FEBS Open Bio.* **11(1)**, pp. 114-123.

Li, H., Handsaker, B., Wysoker, A., Fennel, T., Ruan, J., Homer, N., Marth, G., Abecasis, G. and Durbin, R. (2009). The Sequence Alignment/Map Format and SAMtools. *Bioinformatics.* **25(16)**, pp. 2078-2079.

Li, M., Andersson-Lendahl, M., Sekersen, T. and Arner, A. (2016). Knockdown of fast skeletal myosin binding protein C in zebrafish results in a severe skeletal myopathy. *Journal of General Physiology.* **147(4)**, pp. 309-322.

Li, X., McFarland, D. C. and Velleman, S. G. (2008). Extracellular matrix proteoglycan decorin-mediated myogenic satellite cell responsiveness to transforming growth factor-β1 during cell proliferation and differentiation: Decorin and transforming growth factor-β1 in satellite cells. *Domestic Animal Endocrinology***. 35(3)**, pp. 263-273.

Li, Y., Li, J., Zhu, J., Sun, B., Branca, M., Tang, Y., Foster, W., Xiao, X. and Huard, J. (2007). Decorin gene transfer promotes muscle cell differentiation and muscle regeneration. *Molecular Therapy.* **15(9)**, pp. 1616-1622.

Liao, Y., Smyth, G. K. and Shi, W. (2019). The R package Rsubread is easier, faster, cheaper and better for alignment and quantification of RNA sequencing reads. *Nucleic Acids Research.* **47(8)**: e47.

Liao, Y., Wang, J., Jaehnig, E., Shi, Z. and Zhang, B. (2019). WebGestalt 2019: gene set analysis toolkit with revamped UIs and APIs. *Nucleic Acids Research.* **47(W1)**, pp. W199-W205.

Liewluck, T., Milone, M., Tian, X., Engel, A.G., Staff, N.P. and Wong, L.-J. 2016. Adult-onset respiratory insufficiency, scoliosis, and distal joint hyperlaxity in patients with multiminicore disease due to novel Megf10 mutations. *Muscle & nerve.* **53(6),** pp.984-988.

Light, N. and Champion, N. E. (1984). Characterisation of muscle epimysium, perimysium and endomysium collagens. *Biochemical Journal.* **219**, pp. 1017-1026.

Little, A.G., Lau, G., Mathers, K.E., Leary, S.C. and Moyes, C.D., 2018. Comparative biochemistry of cytochrome c oxidase in animals. *Comparative Biochemistry and Physiology Part B: Biochemistry and Molecular Biology*, *224*, pp.170-184.

Littlefield, R. S. and Fowler, V. M. (2008). Thin filament length regulation in striated muscle sarcomeres: pointed-end dynamics go beyond a nebulin ruler. *Seminars in Cell and Molecular Biology.* 19(6), pp. 511-519.

Liu, J., Burkin, D. J. and Kaufman, S. J. (2008). Increasing alpha 7 beta 1-integrin promotes muscle cell proliferation, adhesion and resistance to apoptosis without changing gene expression. *American Journal of Physiology Cell Physiology.* **294(2)**, pp. 624-640.

Logan, C. V., Lucke, B., Caroline, P., Abdelhamed, Z. A., Parry, D. A., Szymanska, K., Diggle, C. P., Riesen, A., Morgan, J. E., Markham, G., Ellis, I., Mazur, A. Y., Markham, A. F., Shires, M., Helliwell, T., Scoto, M., Hubner, C., Bonthron, D. T., Taylor, G. R., Sheridan, E., Muntoni, F., Carr, I. M., Schuelke, M. and Johnson, C. A. (2011). Mutations in MEGF10, a regulator of satellite cell myogenesis, cause early onset myopathy, areflexia, respiratory distress and dysphagia (EMARDD). *Nature Genetics.* **43**, pp. 1189-1192.

Loov, C., Hillered, L., Ebendal, T. and Erlandsson, A. (2012). Engulfing astrocytes protect neurones from contact-induced apoptosis following injury. *PLoS One.* **7(3)**, pe33090.

Lourenço, Í., Krause Neto, W., dos Santos Portella Amorim, L., Moraes Munhoz Ortiz, V., Lopes Geraldo, V., Henrique da Silva Ferreira, G., Chagas Caperuto, É. and Florencio Gama, E., 2020. Muscle hypertrophy and ladder-based resistance training for rodents: A systematic review and meta-analysis. *Physiological Reports***, 8(17)**, p.e14502.

Love, M. I., Huber, W. and Anders, S. (2014). Moderated estimation of fold change and dispersion for RNA-seq data with DESeq2. *Genome Biology.* **15**, pp. 550.

Lovett, F. A., Gonzalez, I., Salih, D. E. M., Cobb, L. J., Tripathi, G., Cosgrove, R. A., Murrell, A., Kilshaw P. J. and Pell, J. M. (2006). Convergence of Igf2 expression and adhesion signalling via RhoA and p38 MAPK enhances myogenic differentiation. *Journal of Cell Science.* **119(23)**, pp. 4828-4840.

Lu, P., Takai, K., Weaver, V.M. and Werb, Z. (2011). Extracellular matrix degradation and remodeling in development and disease. *Cold Spring Harbor perspectives in biology*, **3(12)**, p.a005058.

MacLean, H. E., Chiu, W. M., Notini, A.J., Axell, A. M., Davey, R. A., McManus, J. F., Ma, C., Plant, D. R., Lynch, G. S. and Zajac, J. D., 2008. Impaired skeletal muscle development and function in male, but not female, genomic androgen receptor knockout mice. *The FASEB Journal*, **22(8),** pp.2676-2689.

Maesner, C. C., Almada, A. E. and Wagers, A. J. (2016). Established cell surface markers efficiently isolate highly overlapping populations of skeletal muscle satellite cells by fluorescence-activated cell sorting. **6(13)**, pp. 1-10.

Mahdy, M. A. A. (2019). Biotoxins in muscle regeneration. *Journal of Muscle Research and Cell Motility.* **40(3)**, pp. 291-297.

Martin, M. (2011). Cutadapt Removes Adaptor Sequences From High-Throughput Sequencing Reads. *EMBnet Journal*. **17**, pp. 10-12.

Matsumura, K., Ervasti, J. M., Ohlendieck, K., Kahl, S. D. and Campbell, K. P. (1992). Association of dystrophin-related protein with dystrophin-associated proteins in mdx mouse muscle. *Nature*. **360**, pp. 588-591.

Mauro, A. (1961). Satellite cell of skeletal muscle fibres. *The Journal of Biophysical and Biochemical Cytology*. **9**, pp. 493-495.

McCarthy, J.J., Mula, J., Miyazaki, M., Erfani, R., Garrison, K., Farooqui, A.B., Srikuea, R., Lawson, B.A., Grimes, B., Keller, C. and Van Zant, G., 2011. Effective fiber hypertrophy in satellite cell-depleted skeletal muscle. *Development*, **138(17)**, pp.3657-3666.

McClure, M. J., Ramey, A. N., Rashid, M., Boyan, B. D. and Schwartz, Z. (2019). Integrin-alpha7 signaling regulates connexin 43, M-cadherin, and myoblast fusion. *American Journal of Physiology Cell Physiology.* **316**, pp. C876-C887.

McCroskery, S., Thomas, M., Maxwell, L., Sharma, M. and Kambadur, R. (2003). Myostatin negatively regulates satellite cell activation and self-renewal. *Journal of Cell Biology.* **162(6)**, pp. 1135-1147.

McKee, T. J., Perlman, G., Morris, M. and Komarova, S. V. (2019). Extracellular matrix composition of connective tissues: a systematic review and meta-analysis. *Scientific Reports.* **9(1)**, pp. 10542.

Menezes de Oliveira, B.M., Matsumura, C.Y., Fontes-Oliveira, C.C., Gawlik, K.I., Acosta, H., Wernhoff, P. and Durbeej, M., 2014. Quantitative Proteomic Analysis Reveals Metabolic Alterations, Calcium Dysregulation, and Increased Expression of Extracellular Matrix Proteins in Laminin α2 Chain–deficient Muscle. *Molecular & Cellular Proteomics*, *13*(11), pp.3001-3013.

Mercuni, E. and Muntoni, F. (2013). Muscular Dystrophies. *The Lancet.* **381(9861)**, pp. 845-860.

Messina, G. and Cossu, G. (2009). The origin of embryonic and fetal myoblasts: a role of Pax3 and Pax7. *Genes and Development.* **23**, pp. 902-905.

Millay, D. P., O'Rourke, J. R., Sutherland, L. B., Bezprozvannaya, S., Shelton, J. M., Bassel-Duby, R. and Olson, E. N. (2013). Myomaker is a membrane activator of myoblast fusion and muscle formation. *Nature*. **499**, pp. 301-305.

Mitsuhashi, S., Mitsuhashi, H., Alexander, M.S., Sugimoto, H. and Kang, P.B., 2013. Cysteine mutations cause defective tyrosine phosphorylation in MEGF10 myopathy. *FEBS letters*, **587(18)**, pp.2952-295.

Miyazaki, M., Moriya, N. and Takemasa, T. (2020). Transient activation of mTORC1 signaling in skeletal muscle is independent of Akt1 regulation. *Physiological Reports*, **8(19)**, p.e14599.

Modd, F. P. and LeBlond, C. P. (1971). Satellite cells as the source of nuclei in muscles of growing rats. *The Anatomical Record*. **170**, pp. 421-436.

Molkentin, J. D., Black, B. L., Martin, J. F. and Olson, E. N. (1995). Cooperative activation of muscle gene expression by MEF2 and myogenic bHLH proteins. *Cell* 83, 1125-36.

Monclus, M. A., Young, T. J. and Di Maio, D. (2010). AFM indentation method used for elastic modulus characterisation of interfaces and thin layers. *Journal of Materials Science.* **45**, pp. 3190-3197.

Montarras, D., Morgan, J., Collins, C., Relaix, F., Zaffran, S., Cumano, A., Partridge, T. and Buckingham, M. (2005). Direct isolation of satellite cells for skeletal muscle regeneration. *Science.* **309**, pp. 2064-2067.

Morgan, J. E., Beauchamp, J. R., Pagel, C. N., Peckham, M., Ataliotis, P., Jat, P. S., Farmer, K., Noble, M. D. and Partridge, T. A. (1994). Myogenic Cell Lines Derived from Transgenic Mice Carrying a Thermolabile T-Antigen: A Model System for the Derivation of Tissue-Specific and Mutation-Specific Cell Lines. *Developmental Biology*. **162(2)**, pp. 486-498.

Morgan, J. E., Gross, J. G., Pagel, C. N., Beauchamp, J. R., Fassati, A., Thrasher, A. J., Di Santo, J. P., Fisher, I. B., Xu, S. W., Abraham, D. J. and Partridge, T. A. (2002). Myogenic cell proliferation and generation of a reversible tumorigenic phenotype are triggered by pre-irradiation of the recipient site. *Journal of Cell Biology*. **157(4)**, pp. 693-702.

Morgan, J. E., Moore, S. E., Wash, F. S. and Partridge, T. A. (1992). Formation of skeletal muscle invivo from the mouse C2 cell line. *Journal of Cell Science.* **102**, pp. 779-787.

Moriya, N. and Miyazaki, M. (2018). Akt1 deficiency diminishes skeletal muscle hypertrophy by reducing satellite cell proliferation. *American Journal of Physiology-Regulatory, Integrative and Comparative Physiology*, **314(5)**, pp.R741-R751.

Mourikis, P. and Tajbakhsh. (2014). Distinct contextual roles for Notch signalling in skeletal muscle stem cells. *BMC Developmental Biology.* **14(1)**, pp. 1-8.

Mourikis, P., Sambasivan, R., Castel, D., Rocheteau, P., Bizzarro, V. and Tajbakhsh, S. (2011). A Critical Requirement for Rotch Signalling in Maintenance of the Quiescent Skeletal Muscle Stem Cell State. *Stem Cells.* **30(2)**, pp. 243-252.

Moyle, L. A. and Zammit, P. S. (2014). Isolation, culture and immunostaining of skeletal muscle fibres to study myogenic progression in satellite cells. *Stem Cells and Tissue Repair.* pp. 63-78.

Murach, K. A., Fry, C. S., Kirby, T. J., Jackson, J. R., Lee, J. D., White, S. H., Dupont-Versteegden, E. E., McCarthy, J. and Peterson, C. A. (2017). Starring or Supporting Role? Satellite Cells and Skeletal Muscle Fiber Size Regulation. *Physiology*. **33**, pp. 26-38.

Murach, K. A., White, S. H., Wen, Y., Ho, A., Dupont-Versteegden, McCarthy, J. J. and Peterson, C. A. (2017). Differential requirement for satellite cells during overload-induced muscle hypertrophy in growing versus mature mice. *Skeletal Muscle.* **7(1)**, pp. 1-13.

Murach, K.A., Fry, C.S., Dupont-Versteegden, E.E., McCarthy, J.J. and Peterson, C.A., 2021. Fusion and beyond: Satellite cell contributions to loading-induced skeletal muscle adaptation. *The FASEB Journal*. **35(10)**, pp.e21893.

Musaro, A., McCullagh, K., Paul, A., Houghton, L., Dobrowolny, G., Molinaro, M., Barton, E.R., Sweeney, H.L. and Rosenthal, N. (2001). Localized Igf-1 transgene expression sustains hypertrophy and regeneration in senescent skeletal muscle. *Nature genetics*, **27(2)**, pp.195-200.

Musaro, A. and Barberi, L. (2010). Isolation and culture of mouse satellite cells. *Methods in Molecular Biology.* **633**, pp. 101-111.

Narici, M. V and Maffulli, N. (2010). Sarcopenia: characteristics, mechanisms and functional significance. *British Medical Bulletin.* **95(1)**, pp. 139-159.

Nayak, A. and Amrute-Nayak, M. (2020). SUMO system – a key regulator in sarcomere organization. *The FEBS Journal.* **287(11)**, pp. 2176-2190.

Neal, A., Boldrin, L. and Morgan, J. E. (2012). The satellite cell in male and female, developing and adult mouse muscle: distinct stem cells for growth and regeneration. *PLoS One*. **7(5)**, pp. e37950.

Ng, S. F. J., Dayal, A. and Grabner, M. (2015). The Calcium-Activated Chloride Channel in Zebrafish Skeletal Muscle is Activated During Excitation-Contraction Coupling. *Biophysical Journal*. **108(2)**, pp. 420a.

Nielsen, J.S. and McNagny, K.M. (2008). Novel functions of the CD34 family. *Journal of cell science*, **121(22),** pp.3683-3692.

Nishimura, D., Sakai, H., Sato, T., Sato, F., Nishimura, S., Toyama-Sarimuchi, N., Bartsch, J. W. and Sehara-Fujisawa, A. (2015). Roles of ADAM8 in elimination of injured muscle fibres prior ro skeletal muscle regeneration. *Mechnisms of Development.* **135**, pp. 58-67.

Ochsner, M., Dusseiler, M. R., Grandin, H. M., Luna-Morris, S., Textor, M., Vogel, V. and Smith, M. L. (2007). Micro-well arrays for 3D shape control and high resolution analysis of single cells. *Lab on a Chip.* **7(8)**, pp. 1074-1077.

Ogawa, M., Kitakaze, T., Harada, N. and Yamaji, R., 2015. Female-specific regulation of skeletal muscle mass by USP19 in young mice. *J Endocrinol*, *225*(3), pp.135-145.

Ogborn, D. and Schoenfeld, B. J. (2014). The role of fibre types in muscle hypertrophy: implications for loading strategies. *Strength and Conditioning Journal*. **36(2)**, pp. 20-25.

Olguin, H. C. and Olwin, B. B. (2004). Pax-7 up-regulation inhibits myogenesis and cell cycle progression in satellite cells: a potential mechanism for self-renewal. *Developmental Biology.* **257(2)**, pp. 375-388.

Orpha.net. Early-onset myopathy-areflexia-areflexia-respiratory distress-dysphagia syndrome. (2022). Available: https://www.orpha.net/consor/cgi-bin/OC_Exp.php?lng=EN&Expert=439212. Accessed Jan 15 2022.

Otis, J. S., Burkholder, T. J. and Pavlath, G. K. (2005). Stretch-induced myoblast proliferation is dependent on the COX-2 pathway. *Experimental Cell Research.* **310(2)**, pp. 417-425.

Ott, M. O., Bober, E., Lyons, G., Arnold, H. and Buckingham, M. (1991). Early expression of the myogenic regulatory gene, myf-5, in precursor cells of skeletal muscle in the mouse embryo. *Development.* **111**, pp. 1097-1107.

Palchesko, R. N., Zhang, L., Sun, Y. and Feinberg, A. W. (2012). Development of polydimethylsiloxane substrates with tunable elastic modulus to study cell mechanobiology in muscle and nerve. PLoS One. **7(12)**, e51499.

Park, S.Y., Yun, Y., Kim, M.J. and Kim, I.S. (2014). Myogenin is a positive regulator of MEGF10 expression in skeletal muscle. *Biochemical and biophysical research communications*, **450(4),** pp.1631-1637.

Parker, F., White, K., Phillips, S. and Peckham. M. (2016). *Cytotechnology.* **68**, pp. 2159-2169.

Pasut, A., Jones, A. E. and Rudnicki, M. A. (2013). Isolation and Culture of Individual Myofibres and their Satellite Cells from Adult Skeletal Muscle. *JoVE.* **73**, e50074.

Pawson, T. and Scott, J. D. (1997). Signalling through scaffold, anchoring, and adaptor proteins. *Science*. **278(5346)**, pp. 2075-2080.

Peltzer, J., Colman, L., Cebrian, J., Musa, H., Peckham, M. and Keller, A. (2008). Novel Murine Clonal Cells Either Express Slow or Mixed (Fast and Slow) Muscle Markers Following Differentiation In Vitro. *Developmental Dynamics.* 237, pp. 1412-1423.

Perez-Ruiz A., Gnocci, V. F. and Zammit, P. S. (2007). Control of Myf5 activation in adult skeletal myonuclei requires ERK signalling. *Cell Signal.* **19**, pp. 1671-1680.

Pertl, C., Eblenkamp, M., Pertl, A., Pfeifer, S., Wintermantel, E., Lochmüller, H., Walter, M.C., Krause, S. and Thirion, C., 2013. A new web-based method for automated analysis of muscle histology. *BMC musculoskeletal disorders*, **14(1),** pp.1-9.

Pierson, T. M., Markello, T., Accardi, J., Wolfe, L., Adams, D., Sincan, M., Tarazi, N. M. and Fajardo, K. F. Novel SNP array analysis and exome sequencing detect ahomozygous exon 7 deletion ofMEGF10causing early onsetmyopathy, areflexia, respiratory distress and dysphagia (EMARDD). *Neuromuscular Disorders*. **23**, pp. 483-488.

Poschl, E., Schlotzer-Schrehardt, U., Brachvogel, B., Saito, K., Ninomoya, Y. and Mayer, U. (2004). Collagen IV is essential for basement membrane stability but dispensable for initiation of its assembly during development. *Development.* **131(7)**, pp. 1619-1628.

Potthoff, M. J., Arnold, M. A., McAnally, J., Richardson, J. A., Bassel-Duby, R. and Olson, E. N. (2007). Regulation of skeletal muscle sarcomere integrity and postnatal muscle function by Mef2c. *Molecular and Cell Biology.* **27**, pp. 8143-51.

Pozzi, A., Yurchenco, P. D. and Iozzo, R. V. (2017). The nature and biology of basement membranes. *Matrix Biology.* **57**, pp. 1-11.

Prasad, V. and Millay, D. P. (2021). Skeletal muscle fibers count on nuclear numbers for growth. *Seminars in Cell and Developmental Biology.* Epub ahead of print.

Przewozniak, M., Czaplicka, I., Czerwinkska, A. M., Markowska-Zagrajek, A., Moraczewski, J., Streminska, W., Janczyk-Ilach, K., Ciemerych, M. A., Brzoska, E. (2013). Adhesion Proteins – an Impact on Skeletal Myoblast Differentiation. *PloS one.* **8(5)**, pp.e61760.

Quach, N. L., Biressi, S., Reichardt, L. F., Keller, C. and Rando, T. A. (2009). Focal Adhesion Kinase Signalling Regulates the Expression of Caveolin 3 and β1 Integrin, Genes Essential for Normal Myoblast Function. *Molecular Biology of the Cell.* **20(14)**, pp. 3169-3450.

Ramaley, F. (1912) Mendelian proportions and the increase of recessives. *The American Naturalist*, **46(546),** pp.344-351.

Rao, Z., Handford, P., Mayhew, M., Knott, V., Brownlee, G. G. and Stuart, D. (1995). The structure of the Ca2+ binding epidermal growth factor-like domain – its role in protein-protein interactions. *Cell.* **82(1)**, pp. 131-141.

Rayagiri, S. S., Ranaldi, D., Raven, A., Azhar, N. I. F. M., Lefebvre, O., Zammit, P. S., Borycki, A. (2018). Basal lamina remodelling at the skeletal muscle stem cell niche mediates stem cell self- renewal. *Nature.* **9**. Article no. 1075.

Rebbeck, R.T., Karunasekara, Y., Board, P.G., Beard, N.A., Casarotto, M.G. and Dulhunty, A.F. (2014). Skeletal muscle excitation–contraction coupling: who are the dancing partners?. *The international journal of biochemistry & cell biology*, **48**, pp.28-38.

Reggiani, C. and Schiaffino, S. (2020). Muscle hypertrophy and muscle strength: dependent or independent variables? A provocative review. *European Journal of Translational Myology*, **30(3**).

Relaix, F., Montarras, D., Zaffran, S., Gayraud-Morel, B., Rocancourt, D., Tajbakhsh, S., Mansouri, A., Cumano, A. and Buckingham, M. (2006). Pax3 and Pax7 have distinct and overlapping functions in adult muscle progenitor cells. *Journal of Cell Biology.*172(1), pp. 91-102.

Ren, X. and Kuan, P. (2020). Negative binomial additive model for RNAseq data analysis. *BMC Bioinformatics.* **21**, pp. 171.

Rhodes, S. J and Konnieczny, S. F. (1989). Identification of MRF4: a new member of the muscle regulatory factor gene family. *Genes & Development.* **3**, pp. 2050-2061.

Ridone, P., Vassalli, M. and Martinac, B. (2019). Piezo1 mechanosensitive channels: what are they and why are they important. *Biophysical Reviews.* **11**, pp. 795-805.

Rodgers, J. T., King, K. Y., Brett, J. O., Cromie, M. J., Charville, G. W., Maguire, K. K., Brunson, C., Mastey, N., Liu, L., Tsai, C. R., Goodell, M. A. and Rando, T. A. (2014). mTORC1 controls the adaptive transition of quiescent stem cells from G0 to G(Alert). *Nature*. **510(7505)**, pp. 393-396.

Romanazzo, S., Forte, G., Ebara, M., Uto, K., Pagliari, S., Aoyagi, T., Traversa, E. and Taniguchi, A., 2012. Substrate stiffness affects skeletal myoblast differentiation in vitro. *Science and technology of advanced materials*.

Rosen, G. D., Sanes, J. R., LaChance, R., Cunningham, J. M., Roman, J. and Dean, D. C. (1992). Roles for the integrin VLA-4 and its counter receptor VCAM-1 in myogenesis. *Cell*. **69(7)**, pp. 1107-1119.

Rosenblatt, J. D. and Parry, D. J. (1992). Gamma irradiation prevents compensatory hypertrophy of overloaded mouse digitorum longus muscle. *Journal of Applied Physiology.* **73(6)**, pp. 2538-2543.

Rosenblatt, J. D. and Parry, D. J. (1993). Adaptation of rat extensor digitorum longus to gamma irradiation and overload. *European Journal of Physiology.* **423**, pp. 255-264.

Rosenblatt, J. D., Yong, D. and Parry, D. J. (1994). Satellite Cell Activity is Required for Hypertrophy of Overloaded Adult Rat Muscle. *Muscle & Nerve.* **17(6)**, pp. 608-613.

Roy, F. V. and Fiers, W. (1983). Metabolic turnover of phosphorylation sites in simian virus 40 large T antigen. *Journal of Virology,* **45(1)**, pp. 442-446.

Ruilin, Z., Yang, J., Zhu, J. and Xu, X. (2009). Depletion of zebrafish Tcap leads to muscular dystrophy via disrupting sarcomere-membrane interaction, not sarcomere assembly. *Human Molecular Genetics.* 18(21), pp. 41304140.

Ruiten, H. J. A., Bettolo, C. M., Cheetham, T., Eagle, M., Lochmuller, H., Straub, V., Bushby, K. and Guglieri, M. (2016). Why are some patients with Duchenne muscular dystrophy dying young: an analysis of causes of death in North East England. *European Journal of Paediatric Neurology.* **20(6)**, pp. 904-909.

Sacco, A., Doyonnis, R., Kraft, P., Vitorovic, S. and Blau, H. M. (2008). Self-renewal and expansion of single transplanted muscle stem cells. *Nature.* **456**, pp. 502-506.

Saha, M., Mitsuhashi, S., Jones, M. D., Manko, K., Reddy, H. M., Bruels, C. C., Cho, K., Pacak, C. A., Draper, I. and Kang, P. B. (2017). Consequences of MEGF10 deficiency on myoblast function and Notch1 interactions. *Human Molecular Genetics*. **26(15)**, pp. 2984-3000.

Saha, M., Mitsuhasi, S. and Kang, P. (2015). Identification and Characterisation of Disease Mechanisms in MEGF10 Myopathy. *Federation of American Societies of Experimental Biology.* **29(S1)**, pp. 1038-1041.

Sakuma, K., Watanabe, K., Sano, M., Uramoto, I., Sakamoto, K. and Totsuka, T. (1999). The adaptive response of MyoD family proteins in overloaded, regenerating and denervated rat muscles. *Biochemica et Biophysica Acta.* **1428**, pp. 284-292.

Salimi, H., Kocaturk, N. M., Daimaguler, H., Brunn, A., Dotsch, J., Weis, J., Deckert, M. and Cirak, S. (2019). Bi-allelic mutations in *uncoordinated mutant number-45 myosin chaperone B* are a cause for congenital myopathy. *Acta Neuropathologica Communications.* **7(1)**, pp. 1-5.

Sambavisan, R., Yao, R., Kissenpfennig, A., Vanwittenmberghe, L., Paldi, A., Gayraud-Morel, B., Guenou, H., Mallisen, B. and Tajbakhsh, S. (2011). Pax-7 expressing satellite cells are indespensable for adult skeletal muscle regeneration. *Development.* **138(17)**, pp. 3647-3656.

Sampath, S. C., Ho, A. T. V., Corbel, S. Y., Millstone, J. D., Lamb, J., Walker, J., Schiaffino, S., 2010. Fibre types in skeletal muscle: a personal account. *Acta Physiologica*, **199(4),** pp.451-463.

Saxton, R.A. and Sabatini, D.M. (2017). mTOR signaling in growth, metabolism, and disease. *Cell*, **168(6)**, pp.960-976.

Schiaffino, S., Gorza, L., Sartore, S., Saggin, L., Ausoni, S., Vianello, M., Gundersen, K. and LØmo, T., 1989. Three myosin heavy chain isoforms in type 2 skeletal muscle fibres. *Journal of Muscle Research & Cell Motility*, *10*(3), pp.197-205.

Schiaffino, S., Pierobon, S. and Aloisi, M. (1976). The Fate of Newly Formed Satellite Cells during Compensatory Muscle Hypertrophy. *Virchows Archiv B Cell Pathology*. **21**, pp. 113-118.

Schmieder, R. and Edwards, R. (2011). Quality control and preprocessing of metagenomic datasets. *Bioinformatics.* **27**, pp. 863-864.

Schultz, E. (1996). Satellite Cell Proliferative Compartments in Growing Skeletal Muscles. *Developmental Biology.* **175**, pp. 84-94.

Seale, P., Ishibashi, J., Holterman, C. and Rudnicki, M.A. (2004). Muscle satellite cell-specific genes identified by genetic profiling of MyoD-deficient myogenic cell. *Developmental biology*, **275(2),** pp.287-300.

Seiden, D. (1976). Quantitative analysis of muscle cell changes in compensatory hypertrophy and work-induced hypertrophy. *American Journal of Anatomy.* **145(4)**, pp.459-465.

Shaw, J. P., Basch, R. and Shamamian, P. (2004). Hematopoetic stem cells and endothelial cell precursors express Tie-2, CD31 and CD45. *Blood Cells, Molecules and Diseases*. **32(1),** pp. 168-175.

Shawber, C., Nofziger, D., Hsieh, J.J., Lindsell, C., Bogler, O., Hayward, D. and Weinmaster, G. (1996). Notch signaling inhibits muscle cell differentiation through a CBF1-independent pathway. *Development*, **122(12),** pp.3765-3773.

Shefer, G., Mark, D. P .V., Richardson, J. B. and Yablonka-Reuveni, Z. (2006). Satellite cell-pool size does matter: defining the myogenic potency of ageing skeletal muscle. *Developmental Biology*. **294(1)**, pp. 50-66.

Shimizu, K., Fujita, H. and Nagamori, E. (2009). Alignment of skeletal muscle myoblasts and myotubes using linear micropatterned surfaces ground with abrasives. *Biotechnology and Bioengineering*. **103(3)**, pp. 631-638.

Shin, Y. C., Song, S., Hong, S. W., Jeong, S. J., Chrzanowski, W., Lee, J. and Han, D. (2017). Multifaceted Biomedical Applications of Functional Grapehene Nanomaterials to Coated Substrates, Patterned Arrays and Hybrid Scaffolds. *Nanomaterials.* **7(11)**, pp. 369.

Shore, P. and Sharrocks, A. D. (1995). The MADS-box family of transcription factors. *European Journal of Biochemistry.* **229**, pp. 1-13.

Shultz, E. (1989). Satellite cell behaviour during skeletal muscle growth and regeneration. *Medicine and Science in Sports and Exercise.* **21(5)**, pp. S181-186.

Sidney, L.E., Branch, M.J., Dunphy, S.E., Dua, H.S. and Hopkinson, A. (2014). Concise review: evidence for CD34 as a common marker for diverse progenitors. *Stem cells*, **32(6)**, pp.1380-1389.

Siegel, A. L., Atchison, K., Fisher, K. E., Davis, G. E., Cornelison, D. D. W. (2009). 3D timelapse analysis of muscle satellite cell motility. *Stem Cells.* **27**, pp. 2527-2538.

Siegel, A. L., Kuhlmann, P. K. and Cornelison, D. D. W. (2011). Muscle satellite cell proliferation and association: new insights from myofiber time-lapse imaging. *Skeletal Muscle.* **1(7)**, pp. 1-7.

Silberstein, L., Webster, G. S., Travis, M. and Blau, H. M. (1986). Developmental Progression of Myosin Gene Expression in Cultured Muscle Cells. *Cell*. 46, pp. 1075-1081.

Snijders, T. and Giannni, P. (2017). Role of muscle stem cells in sarcopenia. *Current Opinion in Clinical Nutrition.* **20(3)**, pp. 186-190.

Snijders, T., Aussiker, T., Holwerda, A., Parise, G., Van Loon, L. J. C. and Verdijk, L. B. (2019). The concept of skeletal muscle memory: Evidence from animal and human studies. *Acta Physiologica.* **229(3)**, pp. e13465.

Snow, M. J. (1978). An Autoradiographic Study of Satellite Cell Differentiation into Regenerating Myotubes Following Transplantation of Muscles in Young Rats. *Cell and Tissue Research.* **186**, pp. 535-540.

Stedman, H. H., Sweeney, H. L., Shrager, J. B., Maguire, H. C., Panettieri, R. A., Petrof, B., Narusawa, M., Leferovich, M., Sladky, J. T. and Kelly, A. M. (1991). The mdx mouse diaphragm reproduces the degenerative changes of Duchenne muscular dystrophy. *Nature.* **352**, pp.536-539.

Straughn, A. R., Hindi, S. M., Xiong, G. and Kumar, A. (2018). Canonical NF-κB signalling regulates satellite stem cell homeostasis and function during regenerative myogenesis. *Journal of Molecular Cell Biology.* **11(1)**, pp. 53-66.

Sultan, S.H., Dyer, C. and Knight, R.D. (2021). Notch Signaling Regulates Muscle Stem Cell Homeostasis and Regeneration in a Teleost Fish. *Frontiers in cell and developmental biology*, **9**.

Sun, L., Kewei, M., Wang, H., Xiao, F., Gao, Y., Zhang, W., Wang, K., Gao, X., Ip, N. and Wu, Z. (2007). JAK1-STAT1-STAT3, a key pathway promoting proliferation and preventing premature differentiation of myoblasts. *Journal of Cell Biology.* **179(1)**, pp. 129-138.

Sun, Z., Bhagwate, A., Prodduturi, N., Yang, P. and Kocher, J. A. (2017). Indel detection from RNA-seq data: tool evaluation and strategies for accurate detection of actionable mutations. *Briefings in Bioinformatics.* **18(6)**, pp. 973-983.

Suzuki, A., Miniamide, R. and Iwata, J. (2018). Wnt/β-catenin signalling plays a crucial role in myoblast fusion through regulation of nephrin expression during development. *Development*. **145(23)**, pp. 168351.

Taetzsch, T., Shapiro, D., Eldosougi, R., Myers, T., Settlage, R. E. and Valdez, G. (2021). The microRNA miR-133b fucntions to slow Duchenne muscular dystrophy pathogenesis. *Journal of Physiology.* **599(1)**, pp. 171-192.

Tajbakhsh, S. (2009). Skeletal muscle stem cells in developmental versus regenerative myogenesis. *Journal of internal medicine*. **266**, pp. 372-389.

Tajbakhsh, S. and Buckingham, M. (2000). The birth of muscle progenitor cells in the mouse: Spatiotemporal considerations. *Current Topics in Devlopmental Biology.* **48**, pp. 225-268.

Tajbakhsh, S., Rocancourt, D., Cossu, G. and Buckingham, M. (1997). Redefining the genetic hierarchies controlling skeletal myogenesis: Pax-3 and Myf-5 act upstream MyoD. *Cell.* **89**, pp. 127-138.

Takayama, K., Mitsuhashi, S., Noguchi, S., Hayashi, Y. K., Nonaka, I. and Nishino, I. (2014). A first Asian MEGF10 myopathy due to novel homozygous mutation. *Neuromuscular Disorders.* **24**, pp. 9-10.

Takayama, K., Mitsuhashi, S., Shin, J., Tanaka, R., Fuji, T., Tsuburaya, R., Mukaida, S., Noguchi, S., Nonaka, I. and Nishino, I. (2016). Japanese multiple epidermal growth factor 10 (MEGF10) myopathy with novel mutations: A phenotype-genotype correlation. *Neuromuscular.* **26(9)**, pp. 604-609.

Talbot, J. and Maves, L., 2016. Skeletal muscle fiber type: using insights from muscle developmental biology to dissect targets for susceptibility and resistance to muscle disease. *Wiley Interdisciplinary Reviews: Developmental Biology*. **5(4)**, pp.518-534

Taylor, M. V. and Hughes, S. M. (2017). Mef2 and the skeletal muscle differentiation program. *Seminars in Cell and Developmental Biology.* **72**, pp. 33-44.

Thomas, K., Engler, A. J. and Meyer, G. A. (2014). Extracellular matrix regulation in the muscle satellite cell niche. *Connective Tissue Research.* **56(1)**, pp. 1-8.

Tian, B., Ding, X., Chen, W., Liang, J., Fan, Y., Li, S. and Zhou, Y. (2019). Matrix stiffness regulates SMC functions via TGF-β signalling pathway. *Biomaterials.* **221**, pp. 119407.

Trentesaux, C., Striedinger, K., Pomerantz, J. H. and Klein, O. D. (2020). From Gut to Glutes: the Critical role of Niche Signals in the Maintenance and Renewal of Adult Stem Cells. *Current Opinion in Cell Biology.* **63**, pp. 88-101.

Uezumi, A., Ojima, K., Fukada, S. I., Ikemoto, M., Masuda, S., Miyagoe-Suzuki, Y. and Takeda, S. I. (2006). Functional heterogeneity of side population cells in skeletal muscle. *Biochemical and Biophysical Research Communications.* **341(3)**, pp. 864-873.

Urcuiolo, A., Quarta, M., Morbidoni, V., Gattazzo, F., Molon, S., Grumati, P., Montemurro, F., Tedesco, F. S., Blaauw, B., Cossu, G., Vozzi, G., Rando, T. A. and Bonaldo, P. (2013). Collagen VI regulates satellite cell self-renewal and muscle regeneration. *Nature Communications.* **4**, pp. 1964.

Van Hees, H.W., Li, Y.P., Ottenheijm, C.A., Jin, B., Pigmans, C.J., Linkels, M., Dekhuijzen, P.R. and Heunks, L.M. (2008). Proteasome inhibition improves diaphragm function in congestive heart failure rats. *American Journal of Physiology-Lung Cellular and Molecular Physiology***, 294(6),** pp.L1260-L1268.

Van Hees, H.W., Van Der Heijden, H.F., Ottenheijm, C.A., Heunks, L.M., Pigmans, C.J., Verheugt, F.W., Brouwer, R.M. and Dekhuijzen, P.R. (2007). Diaphragm single-fiber weakness and loss of myosin in congestive heart failure rats. *American Journal of Physiology-Heart and Circulatory Physiology*, **293(1)**, pp.H819-H828.

Vasyutina, E., Martarelli, B., Brakebusch, C., Wende, H. and BirchMeier, C. (2009). The small G-proteins Rac1 and Cdc42 are essential for myoblast fusion in the mouse. *Proceedings of the National Academy of Sciences of the United States of America.* **106(22)**, pp. 8935-8940.

Velocigene. (2008). Alleles produced for the KOMP project by Velocigene (Regeneron Pharmaceuticals). MGI Direct Data Submission. J:136110.

Verheul, A.J., Hafmans, T., Croes, H.J. and Dekhuijzen, P.N.R. (2006). Cytoskeletal accumulations in the diaphragm muscle of patients with COPD. *Am J Respir Crit Care Med*, **169**, p.A245.

Vigotsky, A.D., Schoenfeld, B.J., Than, C. and Brown, J.M., (2018). Methods matter: the relationship between strength and hypertrophy depends on methods of measurement and analysis. *PeerJ*, **6**, p.e5071.

Vinckier, A. and Semenza, G. (1998). Measuring elasticity of biological materials by atomic force microscopy. *FEBS letters*, **430(1-2),** pp.12-16.

Wagner, K. R., McPherron, A. C., Winik, N. and Lee, S. J. (2002). Loss of myostatin attenuates severity of muscular dystrophy in mdx mice. *Annals of Neurology: Official Journal of the American Neurological Association and the Child Neurology Society.* **52(6)**, pp. 832-836.

Wardle, F. C. (2019). Master control: transcriptional regulation of mammalian *MyoD*. *Journal of Muscle Research and Cell Motility.* **40**, pp. 221-226.

Weintraub, J. Y. and Benezram R. (1992). Overexpression of Id proteins inhibits the muscle differentiation program: *in vivo* association of Id with E2A proteins. *Genes and Development*. **6**, pp. 1466-1479.

Wen, Y., Bi, P., Liu, W., Asakura, A., Keller, C. and Kuang, S. (2012). Constitutive Notch Activation Upregulates Pax7 and Promotes the Self-Renewal of Skeletal Muscle Satellite Cells. *Molecular and Cellular Biology.* **32(12)**, pp. 2300-2311.

White, R.B., Biérinx, A.S., Gnocchi, V.F. and Zammit, P.S., 2010. Dynamics of muscle fibre growth during postnatal mouse development. *BMC Developmental Biology*. **10(1),** pp.1-11.

Williams, B. A., Ordahl, C. P. (1994). Pax-3 expression in segmental mesoderm marks early stages in myogenic cell specification. *Development.* **120**, pp. 785-796.

Winder, S. J. (2001). The complexities of dystroglycan. *Trends in Biochemical Sciences.* **26(2)**, pp. 118-124.

Wong, S. S. (1993). CRC Chemistry of Protein Conjugation and Crosslinking. *CRC Press.*

Wood, A. J., Lin, C. H., Li, M., Nishtala, K., Alaei, S., Rossello, F., Sonntag, C., Hersey, L., Miles, L. B., Krisp, C., Dudczig, S., Fulcher, A. J., Gibertini, S., Conroy, P. J., Siegel, A., Mora, M., Jusuf, P., Packer, N. H. and Currie, P. D. (2021). FKRP-dependent glycosylation of fibronectin regulates muscle pathology in muscular dystrophy. *Nature Communications.* **12(1)**, pp. 2951.

Wouters, M.A., Rigoutsos, I., Chu, C.K., Feng, L.L., Sparrow, D.B. and Dunwoodie, S.L. (2005). Evolution of distinct EGF domains with specific functions. *Protein Science*, **14(4)**, pp.1091-1103.

Wozniak, A. C. and Anderson, J. E. (2007). Nitric oxide-dependence of satellite stem cell activation and quiescence on normal skeletal muscle fibres. *Developmental Dynamics.* **236(1)**, pp. 240-250.

Wright, W. E., Sassoon, D. A. and Lin, V. K. (1989). Myogenin, a factor regulating myogenesis, has a domain homologous to MyoD. *Cell.* 56(4), pp. 607-617.

Wu, L., Brady, L., Shoffner, J. and Tarnopolsky, M.A., 2018. Next-generation sequencing to diagnose muscular dystrophy, rhabdomyolysis, and hyperCKemia. *Canadian Journal of Neurological Sciences*. **45(3),** pp.262-268.

Xin, W. Y. and Rudnicki, M. A. (2012). Satellite cells, the engines of muscle repair. *Nature Reviews Molecular Cell Biology.* **13(2)**, pp. 127-133.

Yablonka-Reuveni, Z. (1995). Myogenesis in the Chicken: the Onset of Differentiation of Adult Myoblasts in Influenced by Tissue Factors. *Basic Applied Myology.* **5(1)**, pp. 33-41.

Yaffe, D. and Saxel, O.R.A., (1977). Serial passaging and differentiation of myogenic cells isolated from dystrophic mouse muscle. *Nature*. **270(5639)**, pp.725-727.

Yin, H., Price, F. and Rudnicki M. A. (2013). Satellite cells and the muscle stem cell niche. *Physiological Reviews.* **93(1)**, pp. 23-67.

Zammit, P. S. (2017). Function of the myogenic regulatory factors Myf5, MyoD, Myogenin and MRF4 in skeletal muscle, satellite cells and regenerative myogenesis. *Seminars in Cell and Developmental Biology.* **72**, pp. 19-32.

Zammit, P.S., Golding, J.P., Nagata, Y., Hudon, V., Partridge, T.A. and Beauchamp, J.R. (2004). Muscle satellite cells adopt divergent fates: a mechanism for self-renewal?. *The Journal of cell biology*, **166(3)**, pp.347-357.

Zammit, P. S., Relaix, F., Nagata, Y., Ruiz, A. P., Collins, C. A., Partridge, T. A. and Beauchamp, J. R. (2006). Pax7 and myogenic progression in skeletal muscle satellite cells. *Journal of Cell Science.* **119(9)**, pp. 1824-1832.

Zhang, B. Kirov, S. and Snoddy, J. (2005). WebGestalt: an integrated system for exploring gene sets in various biological contexts. *Nucleic Acids Research.* 2(1), pp. 741-748.

Zhang, P., Liang, X., Shan, T., Jiang, Q., Deng, C., Zheng, R. and Kuang, S. (2015). mTOR is necessary for proper satellite cell activity and skeletal muscle regeneration. *Biochemical and Biophysical Research Communications.* **463**, pp. 102-108.

Zhang, W., Liu, Y. and Zhang, H. (2021). Extracellular matrix: an important regulator of cell functions and skeletal muscle development. Cell and Bioscience. **11(1)**, pp. 1-3.

Zhang, Y., Lahmann, I., Baum, K., Shimojo, H., Mourikis, P., Wolf, J., Kageyama, R. and Birchmeier, C. (2021). Oscillations of Delta-like1 regulate the balance between differentiation and maintenance of muscle stem cells. *Nature Communications.* **12(1)**, pp.1-16.

Zhou, A. L., Egginton, S., Brown, M. D. and Hudlicka, O. (1998). Capillary Growth in Overloaded, Hypertrophic Adult Rat Skeletal Muscle: An Ultrastructural Study. *The Anatomical Record.* **252(1)**, pp. 49-63.

Zhou, S., Chen, S., Pei, Y. A. and Pei, M. (2021). Nidogen: a matrix protein with potential roles in musculoskeletal tissue regeneration. *Genes and Diseases*

Ziober, B. L., Chen, Y. and Kramer, R. H. (1997). The Laminin-binding Activity of the α7-integrin Receptor is Defined by Developmentally Regulated Splicing in the Extracellular Domain. *Molecular Biology of the Cell.* **8**, pp. 1723-1734.

8. Annex

UD down	UD up	D1 down	D1 up	D3 down	D3 up	D7 down	D7 up
Lrrn1	Zfp566	Gba	Dusp9	Dmrta2	Ssx2ip	Pex6	Mki67
Klk4	Fn3krp	Mcts1	Sla	Pax7	Zbtb20	Wdr89	Slfn9
Lrrc15	Myo1h	Itfg3	Rorb	Kctd12	Rab27a	Hmg20b	Ifi44
Col5a3	Zfp873	Guf1	Krt33b	Zcchc5	Map1b	Pim1	Padi1
Gjb3	Snrnp35	Cst3	Nat8l	Mfap2	Rhof	Mxra7	Usp18
H2-M9	B630005N14Rik	Vrk3	Pkp1	Gpm6b	Nuak1	Col5a1	Isg15
Tnni1	Intu	Eya1	Macc1	Dtx4	Snrpd1	Parp8	Ifit1
Cntn2	Celf2	Klc4	Padi2	Plxdc2	Hip1r	H2afj	Mtus2
Mb	Tsc22d2	Dph1	Anxa8	Loxl2	Tro	Pid1	E2f7
Myh8	Zfp958	Atp2b1	Gfod1	Stc1	Lmod3	Dennd6b	Padi2
Wnt11	Ccdc93	Lpar6	Idi1	Necab1	Xrcc2	Tcea2	2810417H13Rik
G0s2	Ift80	Rnasel	Dynap	Fjx1	Stk17b	Plin2	E2f2
Spock2	Nfat5	Stk11ip	Tuba1b	Mgp	Tex15	Marcks	Cenpe
Rbfox1	Zfp60	Zfp14	Igfn1	Pamr1	Cdca7l	Manf	Padi3
Postn	Fv1	Cmpk2	Esrrb	Lama4	D3Ertd751e	Cep41	Grem1
Whrn	Echdc3	Smtn	Tmsb10	Fzd4	Pdp2	Epha3	Tgtp2
Srpk3	Lpar6	9830147E19Rik	Chil1	Syt14	Sc5d	Creld2	Kif18b
H2-M1	Fbxo48	Abhd6	Trabd2b	Gas6	Dbi	Gas1	Ifit3b
Ptpru	Kctd12b	Calr	Baalc	Plagl1	Bbs12	Mob3b	Fam71b
Trim72	Il20rb	Edem3	Cdkl5	Elfn1	Cdca5	Galnt6	Casc5
Col15a1	Plag1	Atp2c1	Murc	Lrrn1	Ahnak	Rgma	Ifit3
Mgll	Zfp951	Ppap2a	Mal	Igfbp3	Slc43a3	Mrps24	Trim30a
Jag1	C2cd5	Tlr3	Cycs	Ednra	Eme1	Abhd12	Hmmr
Hey1	Kmt2d	Tspan6	Stk32b	Sox8	Mastl	Rpl27a	Apol9a
Myom3	Klhl42	Zfp523	Gpbar1	Adgra3	Dnmt1	Sdhb	Lmo2
Htr2b	Rpusd2	Iah1	Rtl1	Gpx7	Ndufb6	Kctd13	Top2a
Cspg4	Zfhx4	Slc50a1	Tuba4a	Dcn	Wfs1	Tex264	Ckap2l

Ret	Lpp	Gdi1	Tnfaip8	Wbscr17	Mcm6	Sh3gl1	Il12a
Tmem8c	Sc5d	P2rx5	Gm4737	Cox6b2	Smc4	Ppt2	Lonrf3
Tspan18	Zfp397	Lrig1	Rrad	Scand1	Zfp850	Tmem98	Pabpn1l
Mybph	Casc5	Tlcd2	Kbtbd8	Klf12	Eepd1	Akr1b8	Ccnb1
Sp7	Idi1	Entpd6	Dhfr	Kazn	Rgs14	Echdc2	Fam107a
Ror2	Gm14326	Ccl9	Hecw2	Epb4.1l4a	Ak4	Reep4	Pole
Hhipl1	Mab21l3	Ogn	Casp1	Hic1	Cav3	Esd	Lig1
Edil3	Bbs12	Ntn4	Tuba1c	Cacna1g	Spin2c	Nt5c	Gbp7
Enpp1	Tmem79	Usp11	Ak4	Ptprn	Casp8ap2	Glb1	Ccna2
Neurl1a	Gabpb2	Mthfsd	Kctd11	Igsf10	Anln	Anxa2	Sgol2a
Hs3st3b1	Bod1l	2510039O18Rik	Gapdh	Lrrn2	Cetn4	Pofut2	Gm12185
Hs3st3a1	Zfp97	Glmp	Fndc3c1	Mdfi	Scfd2	Il3ra	Scml4
Obscn	Lhx9	Rabac1	Gnb4	Heyl	Syt1	Grhpr	Gcnt4
Atp2a1	Simc1	Josd2	Pkia	Eef2k	Cemip	Bri3	Rtp4
Slc24a4	Rpl35	Acvr2a	Mb	Lppr3	Aif1l	Nenf	AI661453
R3hdml	Arhgap28	Eva1a	AA414768	Nrep	Cdkn2d	Ifi30	3830403N18Rik
Olfm2	Cldn12	Pla2g6	Hmgn5	Lpar4	Cd274	Ppic	Cdc6
Cdh10	Kcnd1	Gdpd3	Cdv3	Rerg	Wnt4	Cobl	Slc17a7
Mfap2	Ccdc114	Myo1h	1810037l17Rik	Cebpb	Tmx4	Ubl7	Brca1
Myl1	Gm14305	Poglut1	Tnnc2	Pde10a	Dnajc28	Sil1	Hmgn5
Asic3	Zscan20	Bcl3	Hhex	Ror2	Lman1l	Tcf7l1	Sptbn2
Anxa8	Cdk6	Cpt1a	Srp54a	Ccdc8	Efnb3	Tmem150a	Kntc1
Tnnt3	Phip	Inafm1	Fam111a	Cdc42ep5	Rfx3	Unc13b	Knstrn
Cxcl14	Lypd6	Pkn3	Apobec2	Piezo2	Zfp808	Klf4	Clspn
Doc2b	Clcn3	Rnpc3	Timm8a1	Socs1	Gins2	Arpc4	Grem2
Jund	4932438A13Rik	Fam3a	Mfap1b	Scube3	Pkhd1	P2rx6	Gbp3
Klhl41	Zfp950	Smarcd3	Lmod3	Zfp580	Rfc5	Adamts10	Casp1
Sgca	Gen1	Dcbld1	Ahr	Sema6b	Alpk2	Fbln5	Oasl2
Nox4	9130008F23Rik	Slc7a8	Tubb6	Arhgdib	Ripply1	Rpl32	Irx2

Syn1	Zbtb37	Mfsd3	Tnni2	Tgfbi	Mtss1l	Fam101a	Oas1b
Cbln1	Fam131b	Jkamp	Gnao1	Rarres2	Itgb6	Slc22a17	Coro2a
Smyd1	Lcp1	Safb2	Acta1	Sfrp2	Gbp3	Cox6b1	Sim1
Fxyd6	Calcrl	Prcp	Cotl1	Thbs2	Adamtsl3	Rps3a1	Lrrc26
Hdac9	Zfp442	Sp140	Hmgcs1	Frem1	Nlrc5	Serpinh1	Dhx58
Bean1	Zfp111	Slc45a3	Tnnc1	Mamdc2	Il1r1	Dbn1	Gfod1
Apobec2	Jade2	Adamts6	Krt14	Kctd15	Tyms	Rgl1	Irf7
Tmem151a	Abcg1	Ces2e	Dclk1	P3h3	4930579G24Rik	Gtf3a	Pcdhgc4
Hfe2	Foxl1	Fbxo10	Zbtb20	Slc16a12	Atad5	Plaur	Il21r
D430019H16Rik	Nfib	Apc2	4930579G24Rik	Bmyc	Amot	P3h1	Alg13
Gprc5c	Cenpf	Gucy1a2	Plcb1	Plxnc1	Cdv3	Dos	Pola1
Filip1	Llgl2	Sec11a	Ube2g2	Podxl2	Mrpl51	Cnih2	Thrb
Myo18b	Mgat3	Hs6st2	Myog	Tmtc1	Mcm4	Tmem86a	Kcnc4
Cd244	Gsta4	Tm9sf1	Pcna	Jund	Zfp697	Clasrp	Arhgap11a
Fgf21	Zfp738	Tapt1	Smpx	Card10	Nsl1	Bmper	Fndc3c1
Adam12	Tmem88	D430042O09Rik	Sohlh2	Cntfr	Pcdhgc4	Ccdc53	Anln
Plxdc2	Zfp759	Tmem209	Xirp2	Slitrk2	Tmem37	Chst11	Mcm5
Nfatc4	Zfp26	Snx19	Nmnat2	Camk1g	Trp63	Pcdhga1	Gas2l3
Pacsin1	Slfn9	Pkmyt1	Gadl1	Zfp771	Cenph	Csnk2b	Naip2
Inpp4b	Bhlhb9	Stim1	Mrpl51	Acot1	Enkur	Egr1	Apol9b
Tnnc1	Rgs20	Pcdhb22	Cetn4	Igfbp4	Tbx15	Tusc3	Kif20b
Cacnb1	Zfp781	Neil1	Them5	Slc40a1	Apitd1	Ehd2	Dtl
Cacna1s	Zfp329	Nprl3	Tpi1	Kcnk1	Haus8	Smpdl3a	Dusp2
Cacng1	Zfp850	Lmf2	Gfra2	Trnp1	Spag5	Foxp4	Ago3
Klf9	Ankle1	Adamts4	Nanos1	Vldlr	Recql4	Pdgfa	Ncapg2
Serpine2	Rasgrp3	3110052M02Rik	Klhl34	Zfp467	Tubb2a	Rab4b	Chrne
Shisa2	Mamdc4	Hecw1	Padi3	Medag	Bub1b	Fbxo17	Ifi27l2a
Myl4	Zfp960	Tmem260	Btbd11	Serpinf1	Brca2	Atf6b	Cenpf

Synpo2l	Pbx4	Enthd2	Mylpf	Eva1a	Filip1	Bphl	Kif11
3425401B19Rik	Rps6ka6	Unc50	Pgbd5	Boc	Hhex	Gli2	Dynap
Kcnk1	Neil3	Pear1	Nfil3	Adamts17	Palm3	Hcfc1r1	Chmp4c
Pappa	Zfp160	Pam	Ngef	Scara5	Chaf1a	Bcap31	Ppp1r27
Casq2	Pou2f1	Atp2a2	Myh13	Spats2l	Myh2	Car11	Syne2
Ryr1	Lancl3	Lrch4	Lamtor2	Csf2ra	Parp14	Igfbp3	Tcf19
Myh1	Zfp595	Dhrs7b	Mctp2	Xk	Nrxn3	Fam198b	Irgm1
Tnni2	Dclre1c	Ogfod3	Ndrg1	Smpdl3a	Gfra2	Ccdc86	Foxg1
Piezo2	Gm14325	Plxnb2	Gcat	Slc22a17	Ppargc1a	Naglu	Polq
Fam167a	Zfp248	Tmc7	Tst	Serpine2	Gm14137	Kdelr2	Wdhd1
Csrp2	Otx1	Hoxa5	Hspb7	Hr	E2f7	Dusp23	Ncapg
Lmod3	Akap17b	Nxf1	Ccdc96	Nppc	Gpatch4	Fzd2	Lrrc30
Crip1	Zfp933	Tbc1d17	Prkg2	Col3a1	Tnni2	Hhat	Cdca7
Wbscr17	Magi3	Tmem165	Onecut2	Bcl7c	Aurkb	Add3	Fam111a
Lin7a	Arhgap19	Cacna1s	Snx7	Col26a1	Igfbp6	Sh3bgrl3	Lrtm1
Actn3	Tdrkh	Pih1d2	Anp32e	Rnaset2b	Slc5a3	Mdga1	Asb10

Annex 1. List of top 100 and downregulated genes at each time point for hard (T2) vs soft (T3) surfaces.